THEORETICAL STUDIES ON ENERGY AND ELECTRON TRANSFER IN SOME COMPLEX MOLECULAR SYSTEMS

A DISSERTATION SUBMITTED FOR THE DEGREE OF DOCTOR OF PHILOSOPHY (SCIENCE)

OF
JADAVPUR UNIVERSITY
2009

BY
DIPANKAR RANA

S.N.BOSE NATIONAL CENTRE FOR BASIC SCIENCES
BLOCK-JD, SECTOR-III, SALT LAKE CITY
KOLKATA-700098, INDIA

Prof. Gautam Gangopadhyay,
S.N.Bose National Centre for Basic Sciences,
Block - JD, Sector - III, Salt Lake City,
Kolkata - 700098,
INDIA
E-mail : gautam@bose.res.in

CERTIFICATE FROM THE SUPERVISOR

This is to certify that the thesis entitled **Theoretical studies on energy and electron transfer in some complex molecular systems** submitted by **Dipankar Rana** who got his name registered on **June 30, 2005** for the award of **Ph.D. (Science)** degree of **Jadavpur University**, is absolutely based upon his own work under the supervision of **Professor Gautam Gangopadhyay** and that neither this thesis nor any part of it has been submitted for any degree/diploma or any other academic award anywhere before.

Signature of the Supervisor

& date with official seal

.

To....

My family, parents, kith and kin...

And with respect and gratitude to...

All of my teachers I faced from nursery to S.N.B.N.C.B.S...

ACKNOWLEDGMENTS

This thesis entitled **Theoretical studies on energy and electron transfer through complex molecular systems** is a part of my research work in theoretical chemistry at S.N.Bose National Center for Basic Sciences since the commencement of project work under Prof. Gautam Gangopadhyay in the month of February 2000 under my Post. M.Sc. research course-work in the 1999-2000 session.

First of all I would like to express respect and gratitude to my supervisor Prof. Gautam Gangopadhyay from the depth of my heart. I owe most of my works for my Ph.D. from him. His temperate role makes my destitute mind with pretexts and pretences to a polarised mind with a minute lustre. I am also grateful to Prof. M. Sanjay Kumar whose introductory training in quantum mechanics at the beginning of my research work helped me to slacken my indulgences in quantum physics.

The completion of my thesis has left me indebted to many. I owe a considerable debt to those who studied on the related subjects before and from whose works I have benefited greatly. It is difficult to thank them all individually; the bibliography at the end is an obvious tribute to them. I would like to thank Prof. A. Mookerjee and Prof. S. Duttagupta, Prof. S. Sengupta, Prof Sreeram, Prof. R. Banerjee, Prof S.S. Manna, Prof. A. Lahiri, Prof. P. Singha Deo and all of them who enlightened the chairs of Dean and Director during this period for their supports favouring me to enjoy library and computation facilities and sometimes affording accommodation at S.N.B.N.C.B.S. for my academic purposes. I would like to acknowledge my teachers whom I met in the Post. M.Sc. course-work specifically my supervisor, Prof. G. Gangopadhyay, Prof. A. Mookerjee, Prof. S.S. Manna, Prof. R.K. Moitra, Prof. A. Mohari. I would like to convey my all respect and gratitude to Prof. B.D.R. and Prof. A.M. Jayannavar and Prof.Y. Tanimura for their stimulating discussions and making comments those facilitated our publications. I occasionally met Prof. Y. Tanimura of Kyoto University, Prof S.K. Chakraborty of S.N.B.N.C.B.S. Kolkata, Prof. B. Bagchi of I.I.Sc. Bangalore, Prof. Alok Kumar Samanta of B.A.R.C. Mumbai, and Prof. D.S. Ray of I.A.C.S. Kolkata. The feeling of their indirect-touch seems to me as the philosopher's stone. I would like to convey my all respect in the memory of Prof. Somnath Ghosh and convey my all gratitude to Prof. Abhijit Bhattacharyya whom I met at Maulana Azad College, Kolkata. Their timely advices oriented myself to love Physical Chemistry at my graduation level. I want to remember Prof. D.C. Mukherjee, Prof. R.S. Banerjee, Prof. N.G. Mukherjee, Prof. S.N. Bhattacharyya, Prof. San-

jib Ghosh, Prof S.S.Z. Adnan, Prof. Shyamal Chakraborty, Prof. S.K. Bose and Prof. C. Mukhopadhyay of Calcutta University and Prof. D.S. Ray of I.A.C.S and Prof. K.K. Kundu of J.U. for their stimulating and innovative physical chemistry classes in my post graduation.

Thanks are also due to my senior colleagues at S.N.B.N.C.B.S. Banida, Subhrada, Atishda, Indrada, Anindada, Chhandadi for their co-operation in learning physics and computations. Thanks are due to my Post M.Sc. friends Swarnali, Sumana, Rumani, Samir, Sudip. I would like to thank Santa, Anuj, Kamal, Durga, Debashish and Abhishek for their helps.

Many many thanks to Tuhin for his various helps specially issuing books and other necessary academic informations related to research. Thanks are also due to Mukul, Aftab, Kartik, Badiur, Soumendu, Masiurda, Harun, Roby, Rudra, Kingshuk, Biswajit, Hemant, Snehashish, Deba, Mainak. I would like to thank all of my well wishers of Post B.Sc. and Post M.Sc at our center during this period. I want to remember the smiling face of Mr. Sunish Deb who also encourages me for doing good academics. I would like to thank all of them who have been overseeing the CC and Library during this period for their support favouring me.

I would like to convey my absolute regards to my parents, jethu, masima, Brojoma, Swapnama, chhotomasi and heartiest love to my brother Subhankar and his friends and sister Dipanwita. Many many thanks to Dipakda, Tapas, Pradip and Hem for sending papers for me to continue my research work. I would like to thank my childhood friend Deboprosad and Maheshda, Chinmoy, Manudi, Pintu and all my well wishers for their constant encouragement and support. I want to thank Gurupada my lab partner at P.G. level and friend who encourages me to do something new. Thanks are due to my friends and colleagues in Jenkins School, CoochBehar and Hooghly Branch Govt. School, Hooghly for their support.

Finally, I wish to express my heart-felt round of applause for my wife who let me devote myself fully to this task over a rather long period of time and waited for its completion willingly.

List of publications

1. **Steady-state spectral properties of dendrimer supermolecule as a light harvesting system**
Dipankar Rana and Gautam Gangopadhyay,
Chemical Physics Letters, **334**,(2001), 314

2. **Studies on energy transfer in dendrimer supermolecule using classical random walk model and Eyring model**
Dipankar Rana and Gautam Gangopadhyay,
Journal of chemical physics,**118**,(2003), 434

3. **Theoretical studies of electron transfer through dendrimeric architecture**
Dipankar Rana and Gautam Gangopadhyay,
Journal of Chemical Physics, **124**, (2006), 044909

4. **Dynamics and spectra of dendrimer molecule**.
Dipankar Rana and Gautam Gangopadhyay,
(*in communication*)

Contents

Chapter 1

1 Introduction

1.1 Introduction

In this age of great crisis of energy, one of the biggest challenge in modern science is to convert the solar energy efficiently into more useful form, such as chemical fuel or electricity. One of the most ubiquitous processes in nature is the photosynthesis where sunlight is converted into chemical energy by the absorption of photons in a light harvesting antenna complex superimposed on a pigment called chlorophyll. Then the excitation energy on the antenna complex is transferred down to the reaction centre where it is used for charge separation which on consequent many other processes leads ultimately to convert the light energy into the form of chemical energy to run the living world. The whole process happens very efficiently in nature but it is extremely difficult to implement in its full scope of generality and effectiveness in the laboratory. However, progress in photochemistry and chemical synthesis has come to a point where light energy conversion can be attempted by artificial molecular devices.

Even from a viewpoint of simplified black-box-type block diagram, the photosynthetic machinery of a green plant is very complex one. From the the work on the X-ray crystallographic structure of photo systems of some bacterial photosynthetic reaction centres, people have got some primitive idea of this complex machine. Based on this simple viewpoint of energy conversion, the knowledge of two fundamental functions of this machine can be gathered: (i) antenna effect of the light harvesting complex and (ii) the photo-induced charge separation within the reaction center. Basically it is a scheme of an efficient charge and energy transportation problem within a magical integrity of structure and function of the reaction system in green plants. The structure of a bacterial photosynthetic reaction system is like a supra-molecular complex. The synthesis of large supra-molecular devices are the main topic of interest in organic chemistry for more than last twenty years. At the same time the achievement of an efficient photo-induced charge separation over a large distance is made possible by the optimization of several aspects

of this photochemical device, namely, (i) geometrical disposition of various molecular components over a super-molecule and (ii) the potential surface as a driving force for the thermodynamic feasibility of the energy or electron transfer or transportation and (iii) kinetic feasibility of the electron transfer even in the domain of unfavorable thermodynamic situation by a suitable conformation of structure by providing entropic advantages.

With this end in view we have primarily focused on some class of dendrimer[2, 3, 4, 5, 6, 7, 8, 9, 10, 11, 12, 13, 14, 15, 16, 17, 18, 19, 20, 21, 23, 24, 25, 26, 27, 28, 29, 30, 31, 32, 33, 231, 35, 36, 37, 38, 39, 40, 41, 42, 43, 44, 46, 47, 50, 51, 65, 53, 54, 55] molecule as artificial light harvesting system. We have thoroughly studied energy and electron transfer in dendrimer molecules of various types. We have also studied non-equilibrium steady state flow of energy and electron through the dendrimeric network. The thermodynamic and kinetic feasibility of energy or electron transfer is again studied through the spectroscopic signature of network geometry on the spectra of the dendrimer system. In all these transfer and non-equilibrium transport mechanism various irreversible decay phenomena are an integral part of the dynamic processes. We have touched upon the energy transport processes on various networks to find out the advantage of the network of cyclically disposed reaction centre chosen by the nature in photo-system over many other similar networks of synthetically made light harvesting systems.

Most of the biological electron or energy transfer processes are controlled by specific design of biological medium. In a solvent medium as well as in isolated large molecule the rate of electron transfer are explained by classical Marcus theory and its quantum mechanical variants[144]. The controlling parameters are free energy of reaction, reorganization energy and the donor - acceptor distance. However, in an intra-molecular case where the transfer takes place through a long bridge is not yet well understood. Specific design of complex molecular network as a bridging medium between the donor and acceptor makes them very much interesting to study as opto-electronic materials and molecular conductors[137].

1.2 The Scope of the Thesis:

Although the scope of research in light harvesting system and studies on the efficiency in energy and electron transfer in a molecular network is huge, we limit ourselves in the study of energy and electron transport

process in dendrimer super-molecule and similar complex networks relevant in photosynthetic system. To understand the factors governing the rate of transfer due to the various pattern of the hierarchical dispositions of the bridge groups, we have developed theories using classical random walk approach and classical and quantum statistical mechanical approaches.

One of the most studied candidates as artificial light harvesting molecular complex called, dendrimers[74], are nanometer-size macro-molecules with repeating units arranged in a hierarchical self-similar fashion around a core to give highly branched tree-like structure. They are capable of displaying unusual chemical, transport and optical properties. Among the various kinds of dendrimers, Phenyl-acetylene (DPA) dendrimer is uniquely composed of repeated structures of Diphenyle acetylene units assuming a Cayley tree geometry. Among them compact dendrimer and extended dendrimer have been studied extensively. Beside this there are also numerous kinds of photo and redox active dendrimers that have been synthesized and characterized in the laboratory to understand various photochemical properties at the molecular level.

For DPA dendrimer we have constructed a quantum mechanical model where the dendrimer is composed of two-level[35, 93, 218] systems as monomer units on the nodes of a Cayley tree. Each unit is undergoing dissipation and driving by external laser field along with nearest neighbour interaction among the monomer units. We have studied the effect of a finite Cayley tree geometry on the coherent and incoherent spectra and dynamics induced by the laser field. From the spectra and dynamics, energy transfer mechanism is also inferred for the extended and compact dendrimer.

We have also analysed the energy transfer in dendrimer supermolecule using classical random walk model and Eyring model[36]of membrane permeation. Here the energy transfer is considered as a multiple barrier crossing process by thermal hopping on the backbone of a cayley tree. It is shown that the mean residence time and mean first passage time, which involve explicit local escape rates, depend upon the temperature, size of the molecule, core branching and the nature of the potential energy landscape along the dendrimer molecule.

We have also studied the electron transfer rate at steady state between donor and acceptor through dendrimeric architecture. The difference between the linear chain and dendrimeric architecture have been demonstrated with steady state rate as main observable. Depending

upon the nature of the donor and acceptor, various damping mechanism due to environment and geometry of the dendrimeric architecture, the modification of electron transfer rate have been explored.

Furthermore we would like to understand electron and energy transfer process in general for various network of molecular geometry as bridging media. It is the special geometrical disposition of the pigment molecules in the photosynthetic reaction centre in natural photo-system which actually favours the highly efficient way of energy transfer over many other possible geometrical arrangements.

1.3 Plan of the Thesis:

After a brief discussion on the basic background topics on the dynamics and spectroscopic processes in a complex molecular system, we have elucidated on the following issues: (i) dendrimer as a model of artificial photosynthetic system; (ii) classical thermodynamic model of energy transfer; (iii) electron transfer processes through bridges; (iv) intramolecular energy transfer processes; (v) non-equilibrium steady state electron or energy transport through a network of molecular system; (vi) current conduction in the network of metal molecular junction; (vii) complex network in the energy transfer in photosynthetic reaction center and electron transfer processes; and (viii) a brief review on the dendrimer molecular systems. Classical random walk problem is considered to understand the energy transport through dendrimeric network in chapter-III. We have touched upon some complex networks mimicking biologically relevant photo-systems to compare the efficiency of energy transfer in various artificial chromophoric arrangements. In chapter-IV we have studied the effect of geometry of the dendrimeric system on strong field-induced steady state spectra. We have investigated dynamics and transient spectral properties of dendrimer super-molecule in Chapter-V. Chapter VI is devoted to show the non-equilibrium steady state transport through dendrimer molecule. A thorough analysis of intra-molecular electron transfer process in single dendrimer molecule is explored here.

Chapter 2

2 An overview of energy and electron transportation in dendrimer super-molecule

Energy transfer is one of the key features in photosynthesis[1] where the transferred solar energy from the antenna of cyclically disposed chlorophyll pairs arround the reaction centre attached through the protein bridges, produce chemical energy. Among the photosynthetic light harvesting materials, light harvesting antennas have fascinated scientists to study on artificial systems. There are plenty of naturally occurring chromophores and dyes which can transport excitation energy or a free electron or ion intra-molecularly. Most of the biological electron or energy transfer processes are controlled by specific design of biological medium. In a solvent medium as well as in isolated large molecule the rate of electron transfer are explained by classical Marcus theory and its quantum mechanical variants[144]. However, in an intra-molecular case where the transfer takes place through a long bridge is not yet well understood. Synthesis of dendrimer super-molecules with their nanometer-size structure makes them a major constituent to these field of artificial light harvesting molecule, opto-electronic nanomaterials and molecular conductor[70]. The following topics will appear to be important to understand the factors which can control the energy and electron transport process in such complex molecular structure such as dendrimer super-molecule and some other biologically important molecules.

2.1 Dendrimer as an artificial light harvesting system

Dendrimers are three-dimensional highly branched macromolecules. Their solubility, viscosity and thermal behaviour are not like the classical polymers. Structurally dendrimer molecule contains three distinct parts. The site or functional group located at the middle of the molecule is termed as **core**. The sites or groups surrounding the core are successively termed as first, second, third and higher generations. The region of the molecule from the core to the generation next to the terminal or peripheral generation is termed as **bulk**. A dendrimer molecule by virtue of containing cavities of different sizes produce varities of physical behaviour specially in presence of different solvents.

One of the most symmetric looking and widely studied example of dendrimer is phenylacetylene(DPA) dendrimer, sometimes called a cayley tree. A fundamental characteristic of phenylacetylene dendrimer is the composition of legs or spokes. The compact dendrimers (series A) are perfectly structurally symmetric molecules with each of three legs composed of many independent Diphenyle Acetylene units. The phenyl group at the end of each of these moieties have threefold co-ordination at the meta positions serving as branching point to additional phenyl acetylene groups, giving rise to an exponentially expanding structure. This molecular configuration creates two fundamental characteristics of dendrimer system. Firstly, branching pattern allows maximum structural flexibility, thus, minimizing steric hindrance. This enables the synthesis of much larger dendrimeric structure. Secondly, and more importantly, the meta branching position disrupt the local- π - electronic excitation conjugation between aromatic ring systems.

In contrast to these characteristics of the compact dendrimer, the extended dendrimer(series B) are unique in that they have sizes of unequal legs, composed of linear chains of DPA units consecutively increasing length towards the center of the molecule. Because these legs are of varying lengths these localized excitation are found to be of varying energies, interestingly with an increased correlation between chain length and excitation energy. In the photosynthesis of plants carotenoids absorb energy and transfer it to the chlorophyll. In that solar energy range the chlorophyll absorbs weakly. Transfer of excitation energy from carotenoids to the chlorophyll is an essential process in photosynthesis. The dendrimeric architecture mimics that of trees found in nature. These materials are suitable for funneling excitation energy to a single site or node. The high density of sites or nodes at the periphery may be attached to photo-responsive groups which can act as donors or acceptors. The core site or node can be linked to a luminescent group that again can act as acceptor or donor. The light-harvesting is the action of transportation of energy or excitation from the periphery to the core through the dendrimeric backbone. The collected energy at the core can be used to trigger a photochemical or other subsequent events. The light-harvesting may occur by through bond or through space mechanism. When only the peripheral groups are suitable dye that can collect light and the core group is another dye acceptor and the core is separated from the periphery by a suitable spacer such as poly(aryl)-ether then the energy transfer may occur through space mechanism. This is also Förster type energy transfer mechanism. The entire dendrimeric network may act as light collecting antenna and energy transport medium. When dendrimer backbone is synthesized with phenylacetylene(PA) units then this type of en-

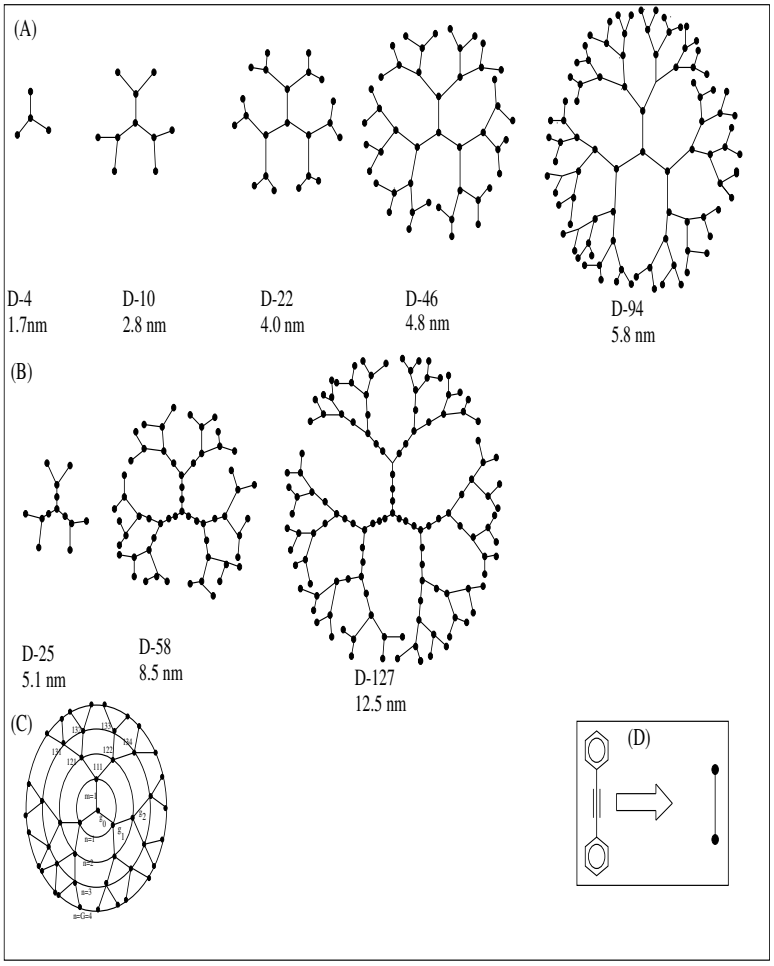

[Fig 2.1] (A) Compact dendrimer family. (B) Extended dendrimer family; (C) Schematic representation of compact dendrimer molecule of fourth generation $(G = 4)$. Each circle indicates a generation; (D) This part shows each node is a benzene ring and between two nodes there are two single bonds and a triple bond.

ergy transfer mechanism is operative. Moore and co-workers[89, 90, 183] showed first the gradient of excitation energy was inbuilt in a nanostar where phenylacytelene units are used as skeletons. The levels of localized electronic states decrease smoothly from the periphery to the core. This creates a directional energy flow from the periphery to the core. To understand the natural biological[132, 133] systems, models with dendrimeric architectures are really helpful. The light-harvesting properties of dendrimers containing metal atoms [134, 135, 136] are also important. The variation of ligands around the core creates new environment. Then various metal ions incorporated into the core feel unique environment and show different photo-physical properties. Another important property in dendrimer light-harvesting is the involvement of poly(aryl)-ether skeleton in concentrating the IR photons. Jiang and Aida used this skeleton to show that a low intensity of photon is sufficient to make a photochemical isomerization of an azo group attached to the core provided the branching of the molecule is large. For lower generation dendrimer molecules a high intensity of photon is necessary to convert the cis-azobenzene to the trans-azobenzene. Recently Chen and co-workers[55] have shown that light-harvesting ability of dendritic molecules increases with increasing generation as evidence by the enhanced rate of valence isomerisation of norbornadiene group to the quadricyclane group attached to the core.

2.2 A thermodynamic model of classical energy transport

We consider here an ideal dendrimer with a superimposed energy funnel descending from the periphery to the centre [76, 78] where a localized energy exciton follows a classical random walk to transfer energy from the periphery to the core. Here two-dimensional Cayley tree geometry is transformed into an effective one-dimensional form. It is considered that the energy transfer takes place from an initially excited state on a peripheral node of a dendrimer to a trap of finite depth which can be a mechanism to control the preferred location of excitation by monitoring the temperature. This opens the possibility of a controlled drive of photochemical processes in this super-molecule. Let us consider an excitation that migrates by nearest neighbor jumps on a dendrimer with a irreversible trap at origin with linear excitonic energy funnel. Let U be the energy descended from periphery towards trap at each generation: the funnel is characterized by the excitation energies as

$$E_0 = \epsilon$$

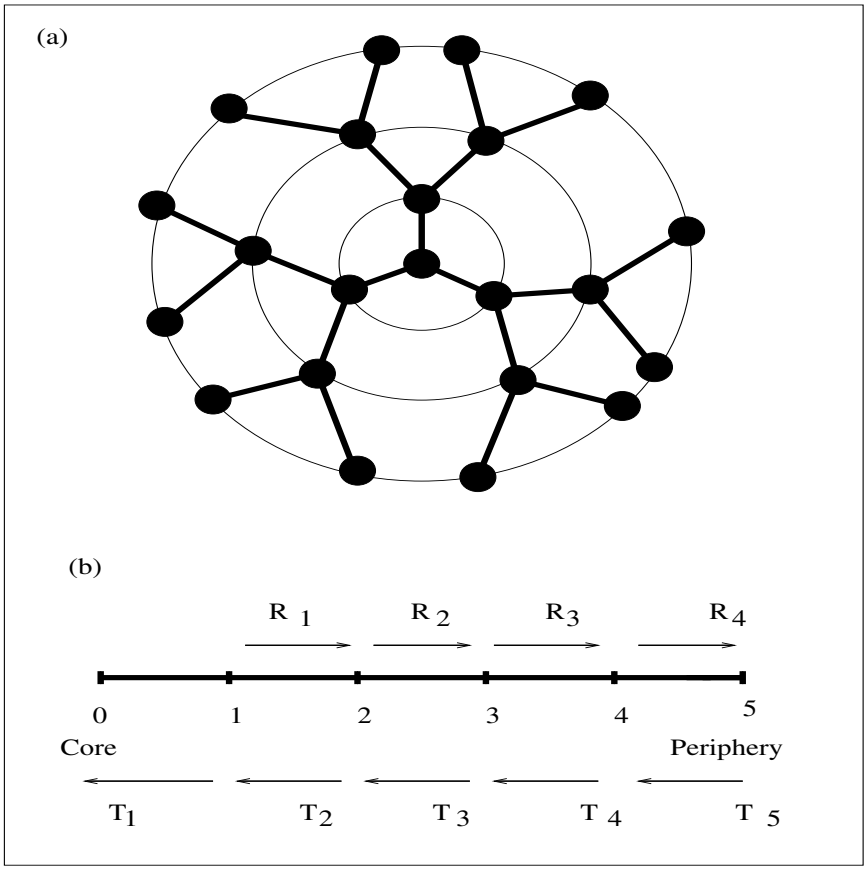

[Fig 2.2] (A)Schematic representation of dendrimer molecule of 4-th generation. (B) One dimensional equivalent of part (A).

$$E_n = \epsilon + \Delta + (n-1)U, \tag{2.1}$$

where E_0 is the excitation energy of the trap and Δ is the difference between the excitation-energy of the trap and first generation with n is the generation number. Excitation energy at periphery is $\epsilon+\Delta+(g-1)U$ and degeneracy at each generation is given by $f_n = C.(Z-1)^{(n-1)}$ where Z is branching at each node and $C = Z-1$.

The partition function is given by

$$Q = \sum_{n=0}^{g} f_n e^{\frac{-E_n}{k_B T}}$$

$$= e^{\frac{-\epsilon}{k_B T}} + Ce^{\frac{(-\epsilon-\Delta)}{k_B T}} \sum_{n=1}^{g} [(Z-1)e^{\frac{-U}{k_B T}}]^{n-1}. \tag{2.2}$$

The equilibrium occupation probabilities of the various generations are :

$$P_0 = \frac{1}{Q} e^{\frac{-\epsilon}{k_B T}},$$

$$P_n = P_0.C.e^{-\frac{\Delta}{k_B T}}[(Z-1)e^{\frac{-U}{k_B T}}]^{n-1} \tag{2.3}$$

where $1 \leq n \leq g$. Free energy, F_n as a function of generation is given by

$$F_n = -k_B T ln(P_n Q) = E_n - k_B T ln f_n \tag{2.4}$$

or, equivalently,

$$F_n = \epsilon + \Delta - k_B T ln C + (n-1)ln(Z-1)[\frac{U}{ln(Z-1)} - k_B T]. \tag{2.5}$$

From the above expression of the free energy of a particular generation one can arrive at the following conclusions about the energy transport.

- (a) When $k_B T \to 0$ the situation is such that the maximum of free energy is at the periphery and minimum of free energy is at the core. So excitation prefers to be mainly at the core.
- (b) When $k_B T = \frac{U}{ln(Z-1)}$; free energy as a function of generation gives a straight line which corresponds to the case where there is no preference of the system to be in any specific generation for $n \geq 1$.
- (c) When $k_B T > \frac{U}{ln(Z-1)}$ there is a second minimum in the free energy indicating preferred site of excitation at periphery. So in this case energetic funnel becomes less efficient relative to geometric one.

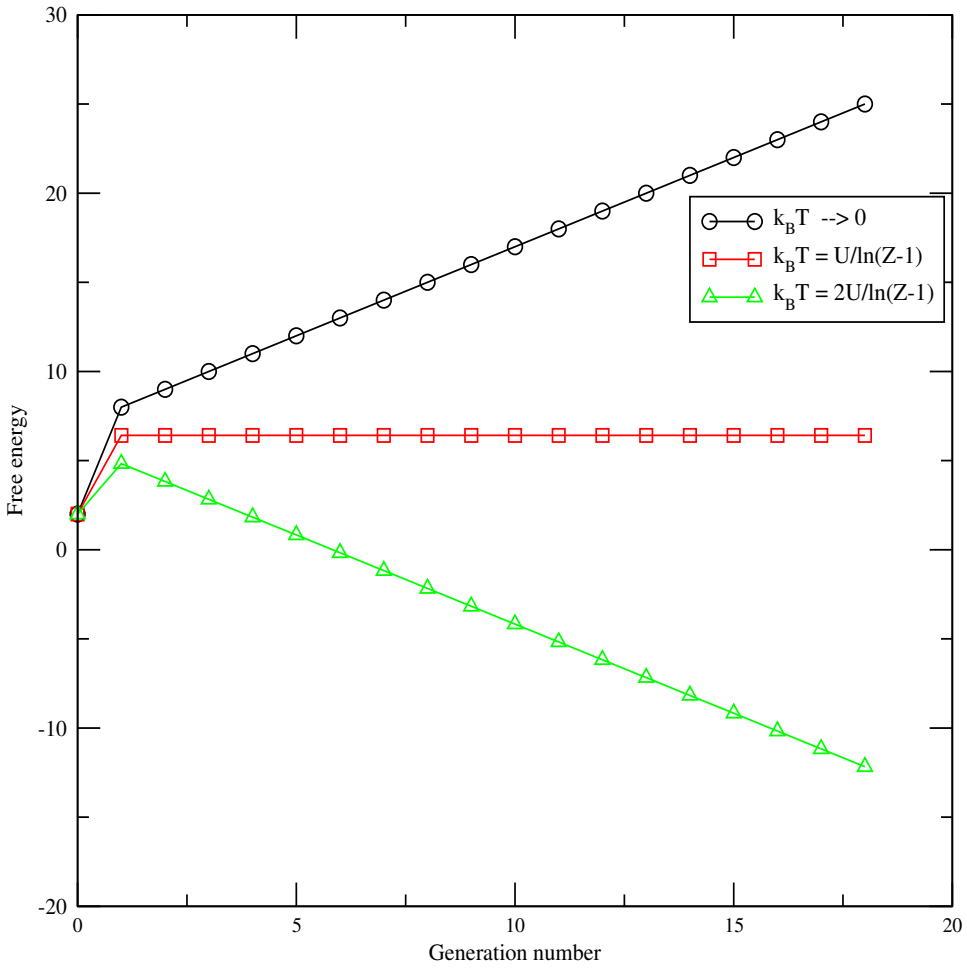

[Fig 2.3] Free energy at three different temperatures for a large dendrimer molecule

2.3 Electron transfer and steady state electron transport through a molecular bridge

Electron transfer(ET) is one of the most important basic mechanisms of chemical reactions. In biological systems, ET process is a basic step of enzymatic activity in the living cell of bacteria, plants and animals. ET is an essential process in cell metabolism, energy balance, production of ATP. In the reaction centre of purple bacteria ET occurs in a femtosecond time scale. ET reaction proceeds in such a manner that the transferred electron remains in a bound state with respect to the particular molecule or molecular system.

The nonadiabatic ET can be understood as a particular type of spatial charge redistribution on the molecular system where a coupling between the reactant and the product states exist. When the donor and acceptor belong to the same molecule the ET reaction is called intramolecular ET or alternatively unimolecular ET. If two distinct molecules are involved the reaction is called intermolecular ET or bimolecular ET. If the ET is not too fast the solvent molecules influence on the ET. This is called outer-sphere type ET. In inner-sphere type ET the intra-molecular nuclear motions are dominant. In quantum mechanical expression for the transition probability between different electronic states, Fermi Golden rule is often used to treat non adiabatic electron transfer rate. In the high temperature limit, when the energy of each vibration is considerably less than the thermal energy, $\hbar\omega << k_BT$, the rate constant can be written [37,38] as $k_{ET} = (2\pi/h)V^2(4\pi\lambda k_BT)^{1/2}exp(-G^{\#}/k_BT)$ with $G^{\#} = (\lambda+G^0)^2/4\lambda$ where V is the matrix element for electronic coupling, λ is the reorganization energy, k_B is the Boltzmann constant, and $G^{\#}$ is the activation free energy. In the expression for $G^{\#}$, G^0 is the standard free energy change for the reaction. The rate expression predicts that the rate of electron transfer increases with a more negative G^0 until the reaction is activationless, i.e, when $-G^0$ is equal to the reorganization energy, λ. At this point the rate of electron transfer will be at its maximum. When $-G^0 > \lambda$ the reaction will be in the inverted region and the rate will decrease again. The reorganization energy, $\lambda = \lambda_{in} + \lambda_{out}$ is the sum of the inner, λ_{in}, i.e, vibrational or other structural rearrangement within the molecule, and outer, λ_{out}, i.e, solvent or due to other external rearrangement of the surrounding molecules to solvate the new charge situation. λ_{out} can be estimated from a dielectric continuum model for the solvent, and give the largest contribution to λ in many electron transfer reactions in polar media. λ_{in} can be calculated with the knowledge of the vibrational modes involved in the electron transfer reaction, and

the equilibrium bond lengths of the reactant and product states.

Various types of molecules or molecular building blocks can bridge the donor and the acceptor. If DA distance is less than 20 Angstrom the ET proceeds directly from donor to the acceptor in spite of the intermediate bridging units. This is called through-space transfer. If some LUMOs participate in the ET the reaction is called through-bond transfer. The long-range ET is typical for conducting polymer or for the ET in proteins. Through bond ET is called bridge-assisted ET. The ET is super-exchange ET when LUMOs of the donor and the acceptor is off-resonant with respect to the bridging units. In this case the probability of the bridging units to be populated by the transferred electron is very low. In this case an extended electronic wave function is formed and a definite phase relation between the electronic state of different bridge units as well as the bridge and the donor exists. Thus super-exchange ET is associated with the presence of electronic coherences. Since bridging units are in off-resonant condition a small energetic fluctuations of the levels due to weak coupling to vibrational mode should have a minor effect. However a large energetic fluctuations of the levels will have a large effect. When the electronic charge jumps stepwise from one part to the other part of the DBA moiety the ET is sequential ET. Here the vibrational modulation of the electronic states and their mutual coupling can become predominant such that an extended wave function can not be formed. The electron jumps from bridge level to bridge level and one has a sequential ET.

In a bridging media where N bridge sites are present with donor and acceptor then H_S may be given by

$$H_S = \omega_A \mid A\rangle\langle A \mid + \omega_D \mid D\rangle\langle D \mid + \sum_{i=1}^{N} \omega_i \mid i\rangle\langle i \mid + V_{A1} \mid A\rangle\langle 1 \mid + V_{1A} \mid 1\rangle\langle A \mid +$$

$$V_{DN} \mid D\rangle\langle N \mid + V_{ND} \mid N\rangle\langle D \mid + \sum_{i=1}^{N-1} (V_{i,i+1} \mid i\rangle\langle i+1 \mid + V_{i+1,i} \mid i+1\rangle\langle i \mid) \tag{2.6}$$

where $\mid A\rangle$, $\mid D\rangle$ are the acceptor and donor state respectively and bridge states are from $\mid 1\rangle$ to $\mid N\rangle$.

The effective coupling between the donor and acceptor when the intra-bridge transfer coupling is weak and within the limitation of perturbation formulation and in the absence of any vibrational relaxation is given by,

$$V_{DA}^{eff} = \frac{V_{D1}}{E_D - E_1} \frac{V_{12}}{E_D - E_2} \cdots\cdots \frac{V_{N-1,N}}{E_D - E_N} V_{N,A}. \tag{2.7}$$

For identical bridge units with energy E_B and including only nearest-neighbor coupling V_B the effective coupling is

$$V_{DA}^{eff} = \frac{V_{D1}(V_B)^{N-1}V_{NA}}{(E_D - E_B)^N}. \tag{2.8}$$

The effective coupling between the donor and acceptor when the intra-bridge transfer coupling is strong can be given by

$$V_{DA}^{eff}(N) = V_{DA}^{(eff)}(1)\left(\frac{1-\sqrt{1-4\zeta^2}}{2\zeta}\right)^{(N-1)} \tag{2.9}$$

with the effective super-exchange coupling for the case of a single bridge unit $V_{DA}^{(eff)} = -V_{D1}V_{NA}/(E_0 - E_D)$ and with $\zeta = V_B/(E_0 - E_D)$.

2.4 Energy transfer process through a molecular bridge

In chemical reactions and in various photo-physical[57] processes energy transfer, between excited and ground states of two molecular chromophores, is a key phenomenon in chemistry, biology and in physics. Energy transfer occurs at a distance ranging from 1Å to 20Å. There are two types of energy transfer processes, namely, radiative transfer and non-radiative transfer. In the radiative transfer the two energy states are coupled by the radiation field. In the theory of radiative transition, the dipole moment operator $\hat{\mu}$ couples the two electronic energy states and the Franck-Condon overlap integral determines the vertical transfer probability $(\int \psi_f \hat{\mu} \psi_i d\tau)^2$ between the vibronic wave functions of the two states. In the case of non-radiative transfer the two states are coupled by an operator called the kinetic energy operator J_N and the Franck-Condon overlap integral determines the probability of horizontal transfer which is as follows

$$\text{Probability} \simeq \left(\int \psi_f \hat{J}_N \psi_i d\tau\right)^2;$$

or equivalently,

$$\text{Probability} \simeq \left(\int \psi_f \hat{J}_N \psi_i d\tau_e \int \chi_f^{\nu'} \chi_i^{\nu''} d\tau_\nu \int S_f S_i d\tau_s\right)^2$$

where $d\tau_e$, $d\tau_\nu$ and $d\tau_s$ are in the configuration spaces for electronic, vibrational and spin motion, respectively. The radiation-less transition depends upon three factors:(1) Density of states, (2) Energy gap, ΔE

betweeen the interacting electronic states; and (3) Vibronic overlap or the Franck-Condon factor.

According to Robinson and Frosch[58, 59]the rate of transfer, $k_{D^\star \to A}$ is given by the time-dependent perturbation theory,

$$k_{D^\star \to A} = \frac{4\pi^2}{h}\rho_E V^2 = \frac{4\pi^2}{h}\rho_E {\beta_{el}}^2 F, \tag{2.10}$$

$$F = \sum \left(\int \chi_{D^\star}\chi_D d\tau_\nu \int \chi_{A^\star}\chi_A d\tau_\nu \right)^2 \tag{2.11}$$

where $\chi_{D^\star}$, χ_D, $\chi_{A^\star}$, χ_A are vibrational wave functions of $D^\star$, D, $A^\star$, A, respectively with the summation is over all the vibrational states. Here ρ_E is the initial density of states of donor states; F is the vibrational overlap part and the electronic part due to the to the overlap between absorption and emission spectra is,

$$\beta_{el} = \int \Psi_i \mathcal{H} \Psi_f d\tau = \int \psi_{D^\star}\psi_A \mathcal{H} \psi_D \psi_{A^\star} d\tau. \tag{2.12}$$

However, with proper anti-symmetrization for two electronic orbitals one can write,

$$\Psi_i = \frac{1}{\sqrt{2}}\{\psi_{D^\star}(1)\psi_A(2) - \psi_{D^\star}(2)\psi_A(1)\} \tag{2.13}$$

$$\Psi_f = \frac{1}{\sqrt{2}}\{\psi_D(1)\psi_{A^\star}(2) - \psi_D(2)\psi_{A^\star}(1)\}, \tag{2.14}$$

whereby the overlap between the spectra becomes

$$\beta_{el} = \int \left(\psi_{D^\star}(1)\psi_A(2) - \psi_{D^\star}(2)\psi_A(1)\right) \mathrm{H} \left(\psi_D(1)\psi_{A^\star}(2) - \psi_D(2)\psi_{A^\star}(1)\right) d\tau \tag{2.15}$$

$$\beta_{el} = \int \psi_{D^\star}(1)\psi_A(2)\mathrm{H}\psi_D(1)\psi_{A^\star}(2)d\tau - \int \psi_{D^\star}(1)\psi_A(2)\mathrm{H}\psi_{D^\star}(2)\psi_A(1)d\tau \tag{2.16}$$

$$= \text{coulomb term} \qquad + \qquad \text{exchange term.}$$

Energy transfer by coulombic interaction considering only dipolar interaction[62, 63, 64] is given by

$$k_{ET}^{d-d} = \frac{2\pi}{\hbar}\left[\frac{M_D.M_A}{\epsilon R^3}\Gamma(\theta_D, \theta_A)\right]^2 \times \sum_{\nu'}\sum_{\nu''}\{\prod_j \mid \langle \chi_{i_{\nu' j}} \mid \chi_{f_{\nu'' j}} \rangle \mid\}^2 \delta(E_{i_{\nu'}} - E_{f_{\nu''}}) \tag{2.17}$$

where $M_D = \sqrt{2}(\langle \phi_D \mid er_D \mid \phi_{D^\star} \rangle)$ and $M_A = \sqrt{2}(\langle \phi_A \mid er_A \mid \phi_{A^\star} \rangle)$ are the transition dipole moments of $D \to D^\star$ and $A \to A^\star$ transition

respectively, ϕ is the electronic wavefunction and χ is the vibrational wave-function, ν is the vibrational quantum numbers, $\Gamma(\theta_D, \theta_A)$ is an orientational factor for the two dipoles, ϵ represents the dielectric constant of the medium. Final form of the expression for the rate constant is as derived by Förster[60] is

$$k_{ET}^{d-d} = \frac{9000 \ln 10 \Gamma^2 \Phi_D}{128\pi^5 n^4 N_A \tau_D R^6} \int_0^\infty \frac{\bar{F_D}(\bar{\nu})\epsilon_A(\bar{\nu})d\bar{\nu}}{\bar{\nu}^4} \tag{2.18}$$

where n = refractive index of the medium, Φ_D = fluorescence quantum yield, τ_D=fluorescence lifetime, $\bar{F_D}(\bar{\nu})$ = normalized donor emission, $\epsilon(\bar{\nu})$ = extinction coefficient of acceptor in units of litre mole^{-1} centimeter^{-1}, $\bar{\nu}$ = average transition frequency in centimeter^{-1}, N_A = Avogadro number. In terms of Förster critical transfer radius R_0 the rate is given by

$$k_{ET}^{d-d} = \frac{1}{\tau_D}(\frac{R_0}{R})^6 \tag{2.19}$$

where

$$R_0 = \frac{9000 \ln 10 \Gamma^2 \Phi_D}{128\pi^5 n^4 N_A} \int_0^\infty \frac{\bar{F_D}(\bar{\nu})\epsilon_A(\bar{\nu})d\bar{\nu}}{\bar{\nu}^4}.$$

Dexter[61] considered the sensitization of an impurity atom in a host crystal. The energy transfer may occur from host crystal or from another impurity atom. The exchange interaction occurs when the electronic transition is forbidden. The rate constant is given by

$$k_{ET}^{ex} = \frac{2\pi}{\hbar}\{\langle \phi_{D^\star}(1)\phi_A(2) \mid \frac{e^2}{r_{12}} \mid \phi_D(2)\phi_{A^\star}(1)\rangle\}^2 \sum_{\nu'}\sum_{\nu''} P_\nu \{\prod_j \mid \langle \chi_{i_{\nu' j}} \mid \chi_{f_{\nu'' j}}\rangle \mid\}^2 \delta(E_i - E_f) \tag{2.20}$$

The final expression for energy transfer rate in the Dexter formulation is given by

$$k_{ET}^{ex} = \frac{2\pi}{\hbar} K J_{ex} exp(-2R/L) \tag{2.21}$$

where $J_{ex} = \int_0^\infty \bar{F_D}(\bar{\nu})\bar{\epsilon_A}(\bar{\nu})$ is the exchange interaction integral of the spectral overlap between donor fluorescence and acceptor absorption spectra, L = average van der Waals radius for the initial and final molecular orbitals of the donor-acceptor system, K is a parameter that can not be evaluated from measured spectroscopic data.

Significant modifications of Förster-Dexter theory is needed to describe long-range excitation energy transfer. This works well within 10$\mathring{A}$ to 10 nm. In fluid solution and in the gas phase diffusion process may

affect the rate. In rigid polymer matrix and in random distribution of R and in pulse excitation the normalized fluorescence signal $P(t)$ is given by

$$p(t) = exp(-t/\tau_D)exp\{-4/3\pi^{4/3}[A]{R_0}^3(t/\tau_D)^{1/2}\}.$$

Similar averaging in Dexter process will give

$$P(t) = exp[-t/\tau_D - \frac{\Omega g(z)}{\beta^3}]$$

where $\Omega = \frac{[A]}{[A_0]}$ with $[A_0] = \frac{3}{4\pi {R_0}^3}$, $g(z) = g[(exp\beta)(t/\tau_D)]$, β is a constant. A clear discrimination between Förster and Dexter type excitation energy transfer can be made with dynamical studies and fitting the results with equation for $P(t)$. In diffusion controlled cases or in gas phase inter molecular excitation energy transfer occurs. For this limit the theory needed was extended by Lin[63, 64].

Intra-molecular excitation energy transfer is devoid of such complexities to some extent. Here $D^\star$ and A are linked through the same molecular architecture. Both long-range Förster type and short range Dexter type excitation energy transfer can be studied in specially designed[65] bichromophoric or multichromophoric systems. In this case through-bond, super-exchange and sometimes photo-induced electron transfer may affect the rate.

The intervening bridging media connecting the donor and acceptor greatly influence the excitation energy transfer rate. The bridge serves as a molecular spacer unit which does not influence the basic electronic structure of the two chromophores while preventing intrachromophore interaction in their ground state. At small R_0 the exchange interaction dominates and the exchange integral Z remains unaffected by the distance R. If $R_0 \rangle 3$Å Z falls off exponentially with increasing R. At D and A separations much larger than the sum of their van der Waals radii and when selection rules exclude possibility of dipole-dipole interaction the proposed mechanism is super-exchange mechanism. McConnell showed that excitation energy transfer should decrease exponentially with the σ-bonded bridge length. The main experimental observations are (i) the through-bond excitation energy transfer efficiency depends upon R in such a way that does not follow either Förster or Dexter mechanism. (ii) for rigid bridge with $R\rangle 10$Å excitation energy transfer occurs efficiently even if the d-d process is forbidden. (iii) for flexible bridges through-space Dexter-type excitation energy transfer occurs. The donor-acceptor

coupling matrix element is

$$V_{DA}^{(n)} = (\frac{\beta_{DB_1}\beta_{B_nA}}{E_{AD} - E_{B_1}})(\prod_{i=1}^{n-1} \frac{\beta_{i,i+1}}{E_{AD} - E_B i + 1}) \tag{2.22}$$

where β_{ij} is the tunneling integral between the orbitals i and j, and E_{AD} is the degenerate D and A orbitals energy; E_{B_i} is the energy of the ith bridge orbital; n is the number of bridge orbitals. This expression is based on tight-binding approximation and time and vibrationally independent. For weakly coupled chromophores those are also coupled to interchromophore bridge electronic states the rate is expressed in more explicit[66, 67] way as

$$k_{ET} = \frac{2\pi}{\hbar} \sum_i \sum_f P_i | \langle \Psi_i \mid \hat{T} \mid \Psi_f \rangle |^2 \delta(E_f - E_i) \tag{2.23}$$

where $\hat{T}$ denotes the transition operator

$$\hat{T} = V + T^{(2)} = V + V \frac{1}{E_i - H + i\epsilon} V$$

where ϵ is dephasing parameters of the system. The matrix element describing the interchromophore bridge electronic states $\mid m\rangle$ is

$$T^{(2)} = \sum_m \frac{V_{fm} V_{mi}}{E_i - E_m + i\epsilon_{mi}}$$

In presence of rapid vibrational relaxation involving through-bond interaction among donor, acceptor through bridge the intra-molecular excitation energy transfer[68] is given by

$$k_{ET} = \frac{2\pi}{\hbar} \sum_{\nu'} \sum_{\nu''} P_{i\nu'} | V_{f\nu'',m\nu} + \sum_{m\nu} \frac{V_{f\nu'',m\nu} V_{m\nu,i\nu'}}{E_{i\nu'} - E_{m\nu} + i\epsilon_{m\nu,i\nu'}} |^2 \times \delta(E_{f\nu''} - E_{i\nu'}). \tag{2.24}$$

2.5 Non-equilibrium steady-state energy and electron transport

When a system is kept in contact with two heat reservoirs at different temperatures or with two matter reservoirs with different chemical potentials the system can asymptotically reach a non-equilibrium steady state. A quantum mechanical model is considered here to serve the purpose of steady flow of energy or charge in a molecular conductor.

Let us consider a single level $\mid 1\rangle$ is coupled to a continuous manifolds $\{\mid l\rangle\}$. The general solution of the time-dependent Schrodinger equation for wave function $\Psi(t) = C_1(t) \mid 1\rangle + \sum_l C_l(t) \mid l\rangle$ follows

$$\frac{d\Psi(t)}{dt} = -\frac{i}{\hbar}H\Psi(t) = -\frac{i}{\hbar}H\{C_1(t) \mid 1\rangle + \sum_l C_l(t) \mid l\rangle\}, \tag{2.25}$$

$$\hbar\frac{dC_1}{dt} = -iE_1C_1 - i\sum_l V_{1,l}C_l, \tag{2.26}$$

$$\hbar\frac{dC_l}{dt} = -iE_lC_l - i\sum_l V_{l,1}C_l \qquad \text{for each l.} \tag{2.27}$$

With the initial condition $C_1(t = 0) = 1$, $C_l(t = 0) = 0$ for all l, the probability that the system is still in state 1 at time t is given by $P_1(t) = \mid C_1(t) \mid^2$. If population in state $\mid 1\rangle$ remains always to be constant i.e, $C_1(t) = c_1 exp(-\frac{i}{\hbar}E_1t)$, and

$$\hbar\frac{dC_l}{dt} = iE_lC_l - iV_{l,1}C_1(t) - \frac{\eta}{2}C_l or$$

$$\hbar\frac{dC_l}{dt} = iE_lC_l - iV_{l,1}c_1 exp\{-\frac{i}{\hbar}E_1(t)\} - \frac{\eta}{2}C_l \tag{2.28}$$

where

$$C_l(t) = c_l(t)exp\{-\frac{i}{\hbar}E_1t\} = \frac{V_{l,1}c_1}{E_1 - E_l + i\frac{\eta}{2}}exp\{-\frac{i}{\hbar}E_1t\}.$$

Here the driving term $V_{l,1}C_1 exp\{-\frac{i}{\hbar}E_1t\}$ pumps the amplitude of l and other term $\frac{\eta}{2}c_l$ damps it. The total flux through the system in this steady state can be calculated by observing that it must be equal to the rate at which population disappears, i.e, the flux becomes

$$J = \frac{\eta}{2}\sum_l \mid C_l \mid = \mid C_1 \mid^2 \sum_l \mid V_{l,1} \mid^2 \frac{\frac{\eta}{\hbar}}{(E_1 - E_l)^2 + (\frac{\eta}{2})^2} \tag{2.29}$$

$$\rightarrow \lim_{\eta\rightarrow 0} \mid C_1 \mid^2 \frac{2\pi}{\hbar}\sum_l \mid V_{l,1} \mid^2 \delta(E_1 - E_l). \tag{2.30}$$

Due to this flux the steady state rate is given by

$$k = \frac{J}{\mid C_1 \mid^2} = \frac{2\pi}{\hbar}\sum_l \mid V_{l,1} \mid^2 \delta(E_1 - E_l) = \frac{2\pi}{\hbar}(\overline{\mid V_{l,1} \mid^2}\rho_L)_{E_l=E_1} = \frac{\Gamma_1}{\hbar} \tag{2.31}$$

When the level $\mid 1\rangle$ is coupled to two continua, $L = \{l\}$ and $R = \{r\}$ the steady-state flux out of the system through the continuum (channel) R/L is given by

$$k_{0\to K} = \frac{J_{0\to K}}{\mid C_0 \mid^2} = \frac{\mid V_{1,0} \mid^2}{(E_0 - E_1)^2 + (\Gamma_1(E_0)/2)^2} \frac{\Gamma_{1K}(E_0)}{\hbar} \qquad (\mathrm{K} = \mathrm{L/R}). \tag{2.32}$$

Studies of non-equilibrium effects on rate of excitation energy transfer is important when we consider excitation energy transfers from donor to an acceptor. These effects are not so effective when the rate of excitation energy transfer is slow. When the rate of excitation energy transfer is faster then other loss processes, in donor state the processes like for example, vibrational relaxation etc may affect the excitation energy transfer rate and in that case the excitation energy transfer occurs from a non-equilibrium steady-state. In solution these effects are much more prominent since donor excited states undergo charge redistribution.

2.6 Current in metal-molecule-metal junction

The important transfer processes in molecular physics can be classified as: (i) transfer between a donor and an acceptor species, (ii) transfer between two sites on the same molecule and (iii) transfer between a molecular species in solution and a metal or a semiconductor electrode. Electronic conduction of a molecule connecting two metal or semiconductor electrodes, is widely studied after the development of tunneling microscope. Experimentally a molecule is connected between two metal leads or electrodes sometimes termed as "source" or "drain". There is an extra electrode "gate" which does not carry current but can affect the junction energetics by imposing an external potential.

For the unbiased junction, two electrodes have equal Fermi energy i.e, $E_{FL} = E_{FR} = E_F$ and for a biased junction, the potential bias Φ may be defined as $e\Phi = e(\Phi_L - \Phi_R) = E_{FR} - E_{FL}$ where e is the magnitude of electronic charge. The magnitude of current flow in the system when the potential bias is lower than the threshold is needed by super exchange mechanism in the form of tunneling current.

The simplest molecular wire structure comprises a molecularly bonded (by sulfur-gold, carbon-carbon or silicon-carbon etc) through a single atom to electrodes at the two molecular terminals. Rolf Landauer proposed that charge can move through such structure by elastic scattering. He has defined conductance as a scattering process. Mathematically, the

Landauer formula is

$$g = \frac{2e^2}{h} \sum_{ij} T_{ij} \tag{2.33}$$

where g is the conductance; e is the electron charge, h is Planck's constant, and T_{ij} is the scattering probability from incoming channel i to outgoing channel j. If there is one open channel without scattering, then $g = \frac{2e^2}{h} = (12.8k\Omega)^{-1}$, is the quantum of conductance. The generalized form of Landauer approach to molecular wire conductance is

$$g = \frac{2e^2}{h} Tr_M\{\Gamma^R G_M \Gamma G_N\}. \tag{2.34}$$

Here G_M is the Green's function that characterizes electron scattering between ends of the molecule. The spectral densities Γ^R and Γ^L describe the effective mixing strength between molecule and electrode at the left and right ends, respectively. Electronic structure theory permits actual calculation of g once the geometries are known.

2.7 Complex network in the photosynthetic unit

Recently the atomistic picture of proteins involved in bacterial photosynthetic light harvesting complex have been understood by a combination of x-ray crystallography, electron microscopy and molecular modeling. Hundreds of chlorophyll are required to reduce one molecule of CO_2 in presence of high intensity sunlight. In the primary reaction site (RC) very few chlorophyll are present. The other large amount of chlorophylls take part as antenna. They capture sunlight and transfer electronic excitation in a co-operative way. The photosynthetic bacterial membrane contains two types of light-harvesting complexes. LH-I and LH-II. LH-I is in direct contact with RC. LH-II antenna surrounds the LH-I. These antennae are a superior example of nanoscale engineering of nature. The complexes are formed in a specialized way within the protein scaffold. Several chromophores collect photons and transfer it in hundreds of steps over a sequence of hierarchical time-scale. The efficiency of the transfer is nearly accurate. The previous studies[71, 72] showed that the dimension of the photosynthetic complexes are optimum for light harvesting. Generally chro mophores are separated at a distance that are large with respect to their size. In photosynthetic complexes the chromophores are densely packed. The electronic interactions between the chromophores are different from most of the other model complexes. Instead of one average separation between donor and acceptor there are practically many

length scales over which the various parts of the donor and acceptor electron densities interact. The chromophores those are widely spaced such as B800 in LH-II complex form simple donors. But the chromophores those are densely packed as are B850 in LH-II act as complex acceptor. Spectroscopically each donor or acceptor behave as electronically delocalized states. The antenna arrangements are such that the interactions not only transport electronic excitations in a nearly perfect way but it can also help to dissipate extra energy that may damage the molecule.

In all bacterial light-harvesting systems the slowest step is the trapping excitation energy from any of the light-harvesting pigments to the RC. The trapping efficiency will be highest when maximum number of antenna pigments will be able to transfer their excitation energy to the RC. This process is optimized when the pigments are arranged in a ring. In PS1 the band of pigments are surrounding the electron transfer chain in such a way that the number of contact sites is maximum. RC directly take part in photochemical reactions. Light-harvesting antenna increases the absorption cross-section for collecting sunlight. In diffused or dim light the rate of absorption of photons is 100 times slower than the rate of absorption of photons in direct sunlight. The turn-over rate of chemical reaction at RC is 100 times faster than the rate of absorption of photons in the direct sunlight. This high rate of chemical reaction occurs in direct sunlight as well as in dim light. The arrangements of the chromophores around the RC are such that the rate of photochemical reaction at RC remains fixed.

2.8 A general survey on the studies of dendrimer molecules

One of the earliest synthesis of dendrimer was reported by Vögtle and co-workers[73]. Dendrimers are prepared generally by divergent or convergent methods[82]. In divergent method dendrimers are synthesized stepwise from the monomer unit starting at core to proceed towards the peryphery. The steps of the reactions are iterated to build the dendrimer layer after layer. This layer leads to generation of dendrimers. In convergent method the synthesis starts at the peryphery and proceeds toward the core. First the polymeric arms or dendrons are synthesized. These dendrons are then accumulated using the reactions of the core.

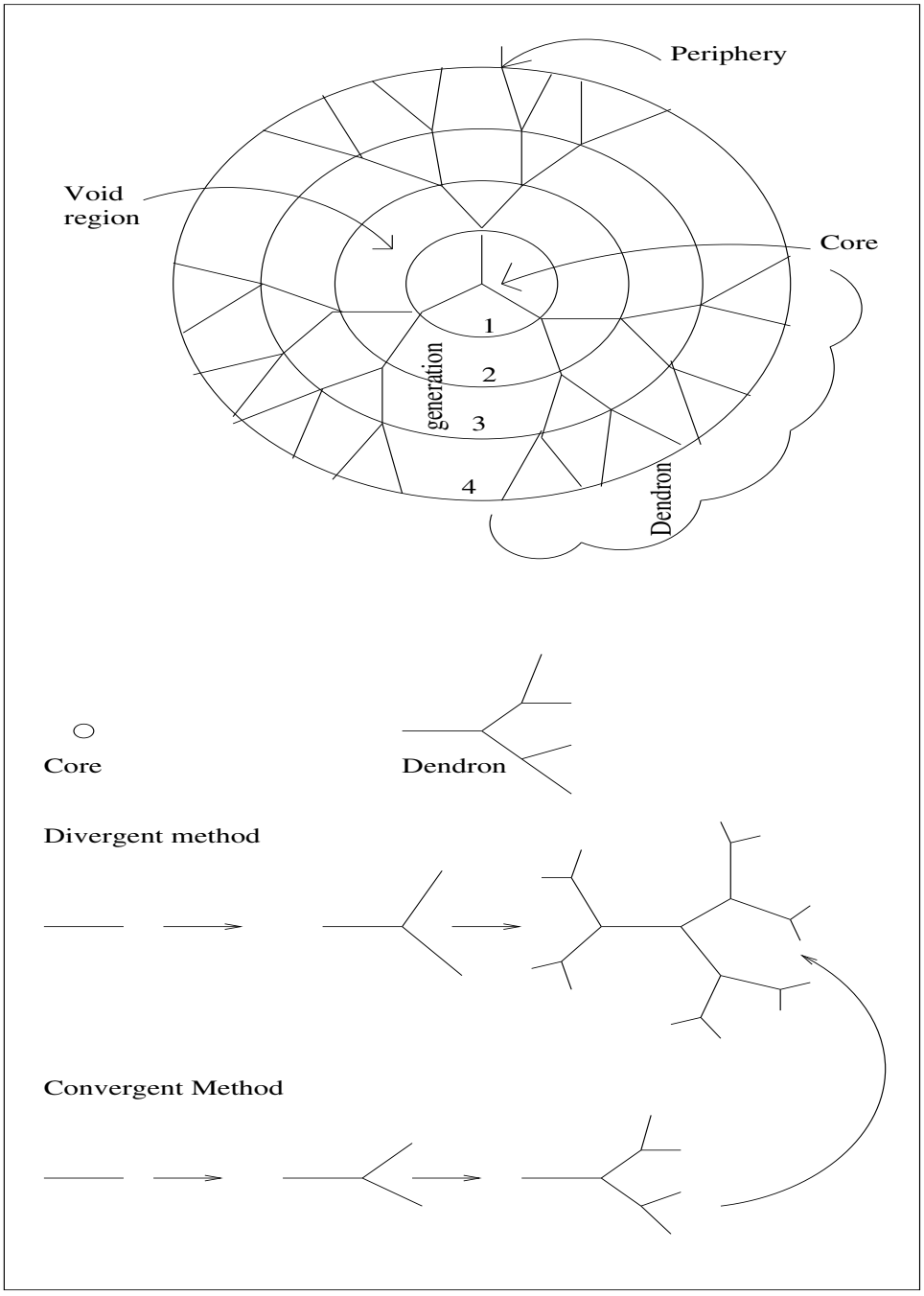

[Fig 2.4]: Top-Schematic representation of dendrimer molecule of 4th generation. Bottom-Schematic representation of divergent and convergent routes of synthesis of dendrimer..

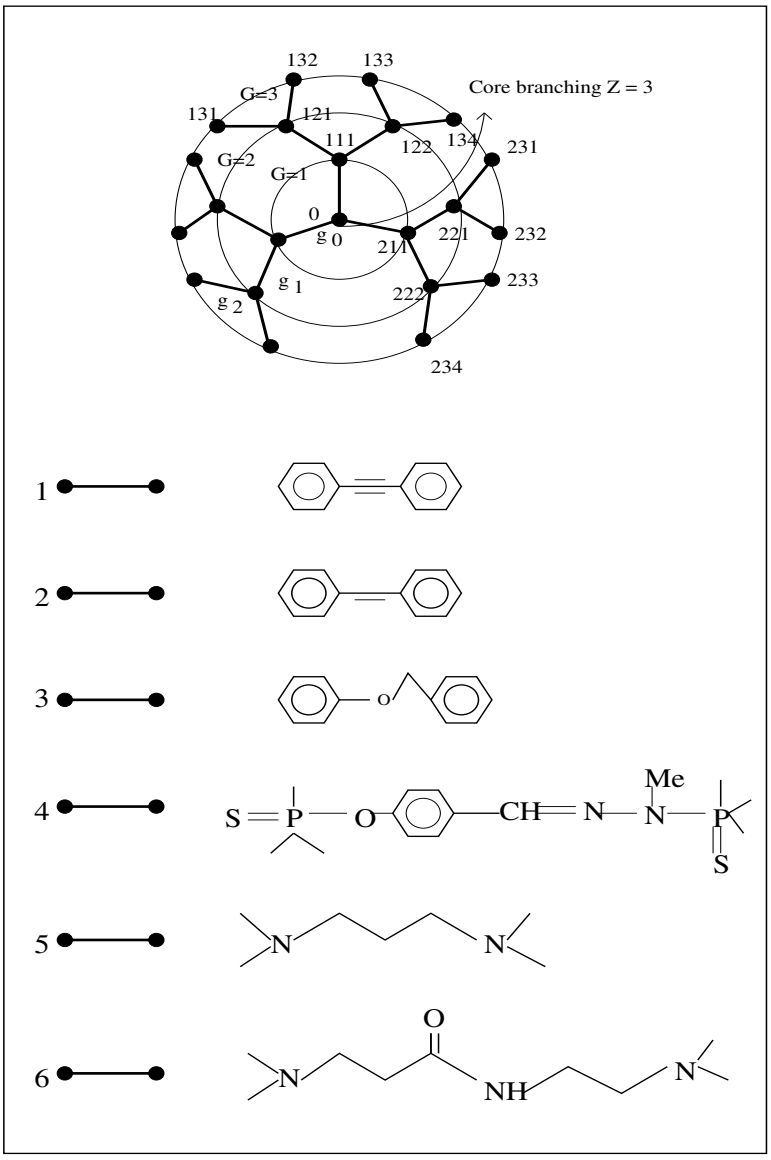

[Fig 2.5]Schematic representation of various types of dendrimeric molecules depending on the nature of the monomer units. Examples are shown for 3rd generation (G=3) as follows. (1) Poly phenylacetylene dendrimer (called PPA dendrimer), (2) Oligo phenylenevinylene dendrimer (called OPV dendrimer), (3) Poly (aryl ether) dendrimer (called Frechet-type dendrimer), (4) Phosphorous containing dendrimer (dendrimer containing hetero-atom), (5) Poly propelene imine dendrimer (called PPI dendrimer), (6) Poly (amido-amine) dendrimer (called PAMAM dendrimer).

2.8.1 Types of dendrimer

After some pioneering works[83, 84, 85, 86] the entity become a highly interesting macromolecule in various fields. They are now of various types due to the synthetic routes developed by chemists as shown in the Fig.(1). When monomer unit is phenylacytelene [24, 25, 28, 29, 30, 31, 32, 33, 35] the dendrimer is polyphenylacytelene (PPA) (type-1), when monomer unit is oligo phenylene vinylene[38, 39, 40, 41] the dendrimer is called OPV dendrimer(type-2), when monomer unit is aryl ether the dendrimer is called Frechet-type dendrimer[42] (type-3), when it contains P or N atom the dendrimer is called hetero atom[43] containing dendrimer (type-4), when monomer unit is propelene imine[44] the dendrimer is called PPI dendrimer (type-5) and when monomer unit is amido-amine[231] unit the dendrimer is called PAMAM dendrimer(type-6).

2.8.2 Use of dendrimer

The area of dendrimer research is growing very rapidly. This supermolecule has unique property of showing various micro-environments depending upon the nature of bonding and functional groups. Their unique cayley tree geometry makes them potential candidates for a wide variety of application. They are now essentially used in medicinal purposes, as catalyst, as patterned poly-redox materials, molecular-scale devices, films for communications besides their promising role in artificial light harvesting property.

Medicinal application: The cavity of dendrimer molecule can trap several small molecule. The cavity can trap ions. They can not diffuse. Thus it is possible to use the dendritic macromolecule as carrier for drug delivery[97]. Most dendrimers containing hydrocarbon entity are inert and non-toxic to human. They can be eliminated as urine[98]. Synthetic dendrimers can be tailored to bind ions[99] in a regulated manner within their larger structure to offer new route to drug delivery. Yamamoto[100] et al examined complexation of tin (Sn^{2+}) ions in a dendrimer of 4th generation with the building material as imine monomer that contains nitrogen as binding atom. Surprisingly the ions binds to imines closest to the core first although they come across the peripheral imines first. The complexation process continues generation by generation until the outermost generation is reached.

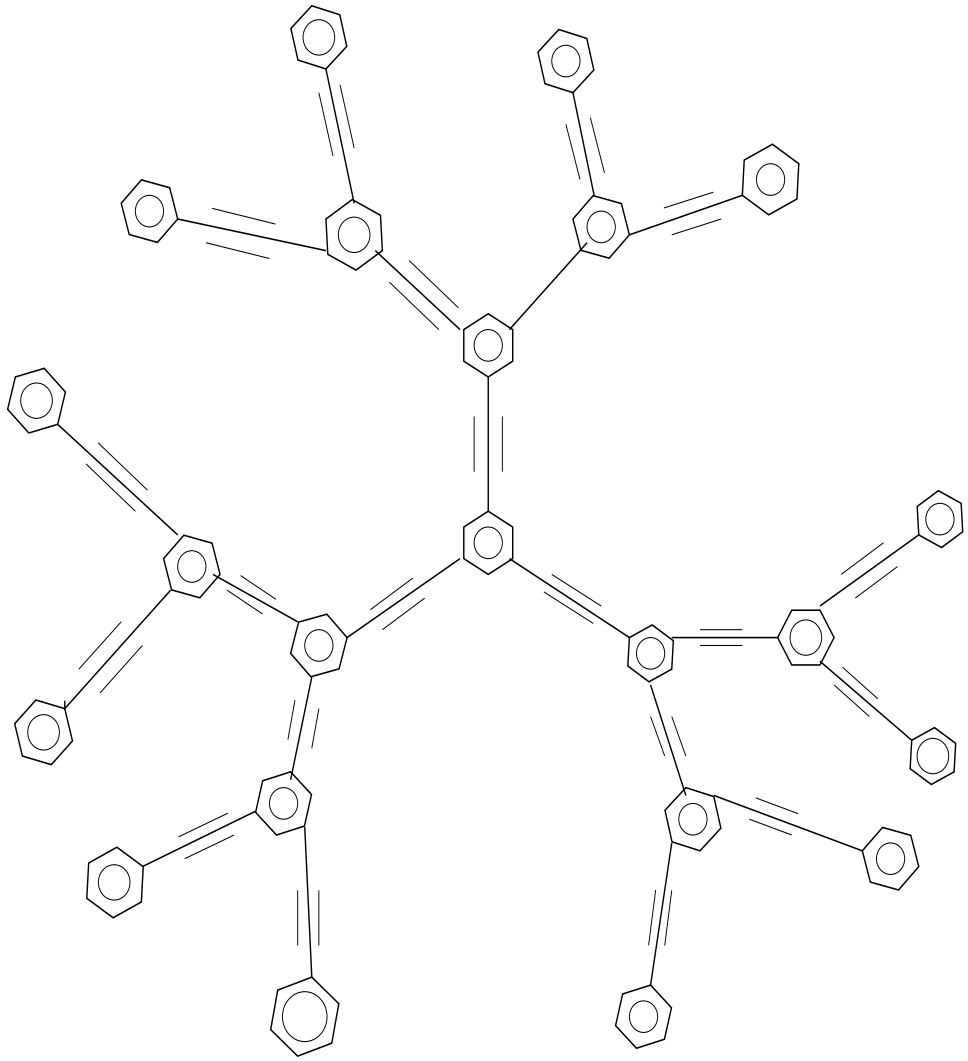

[Fig 2.6] Compact phenylacetylene dendrimer of third generation.

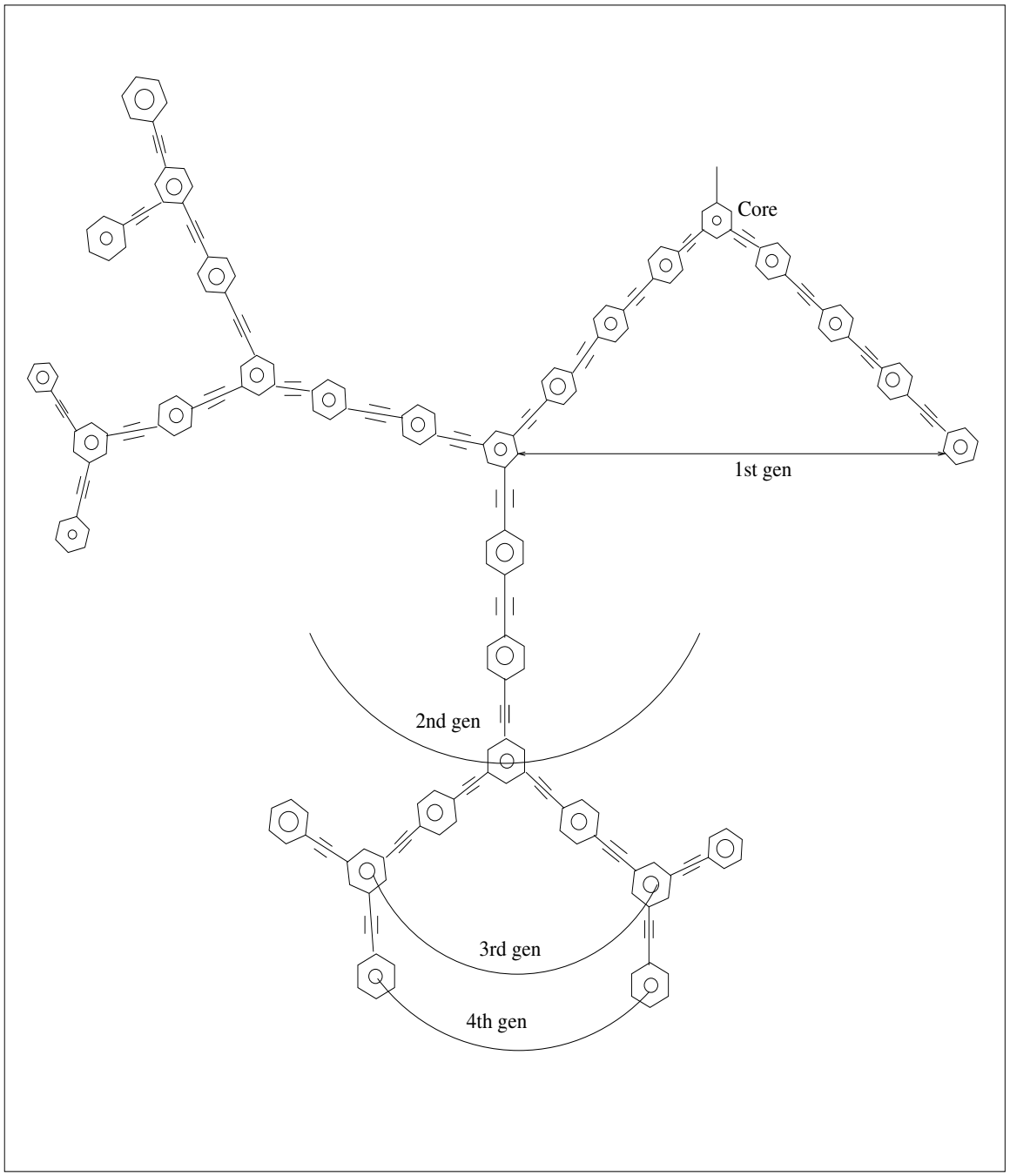

[Fig 2.7] Extended phenylacetylene dendrimer of fourth generation.

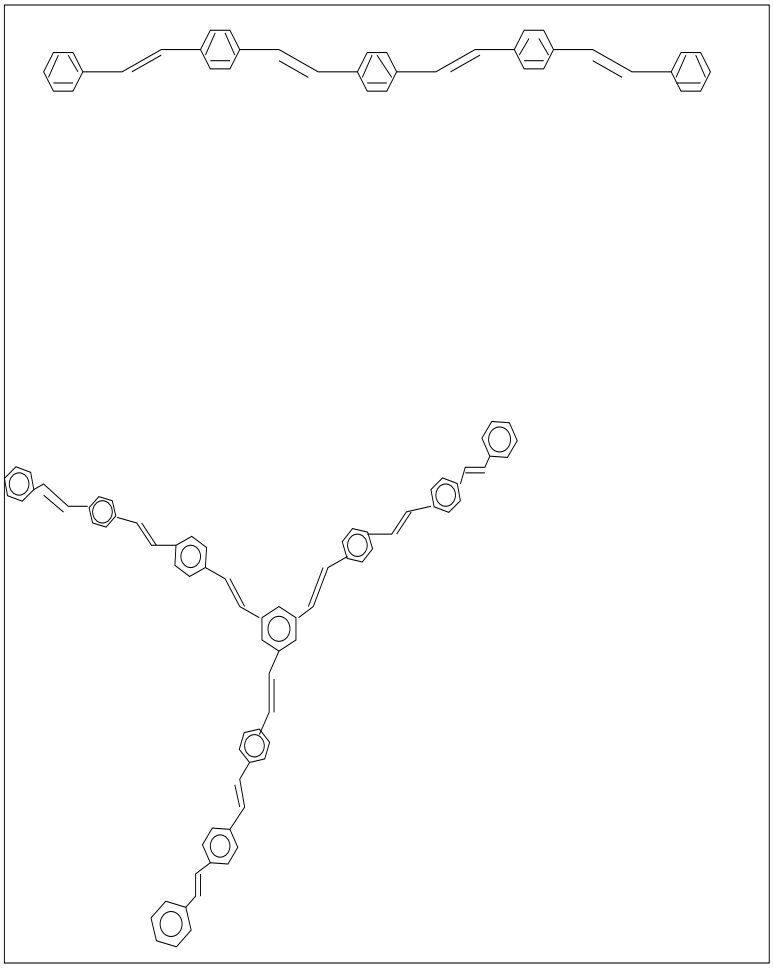

[Fig 2.8] Oligo phenylenevinylene chain and dendrimer of third generation .

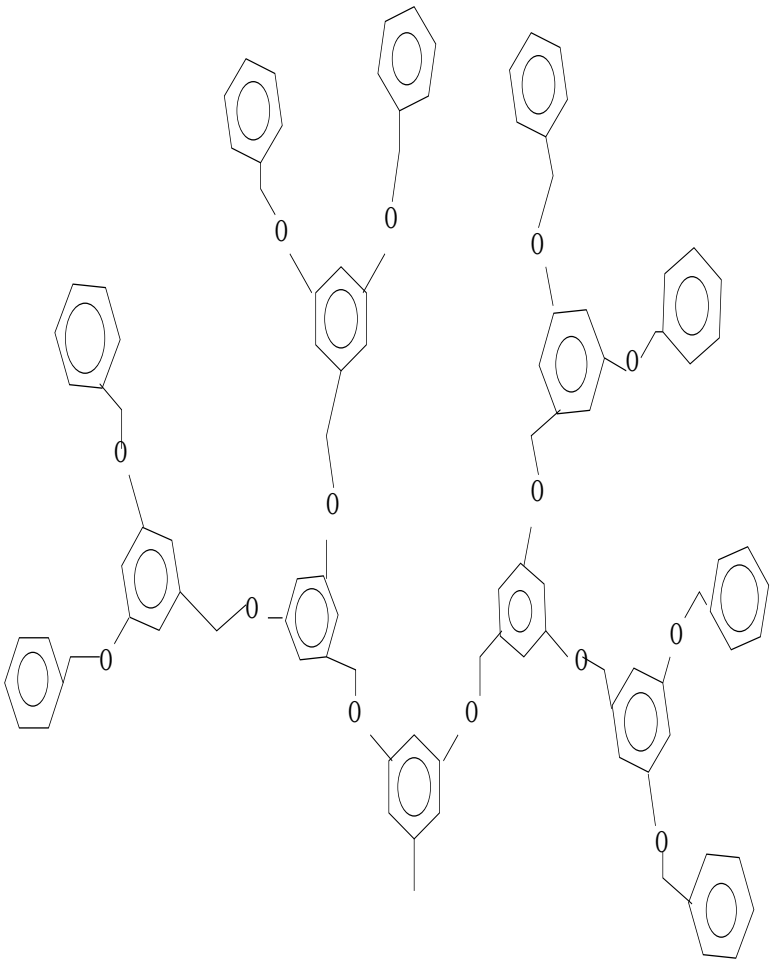

[Fig 2.9] A part of aryl-ether dendrimer (sometimes called Frachet-type dendrimer) .

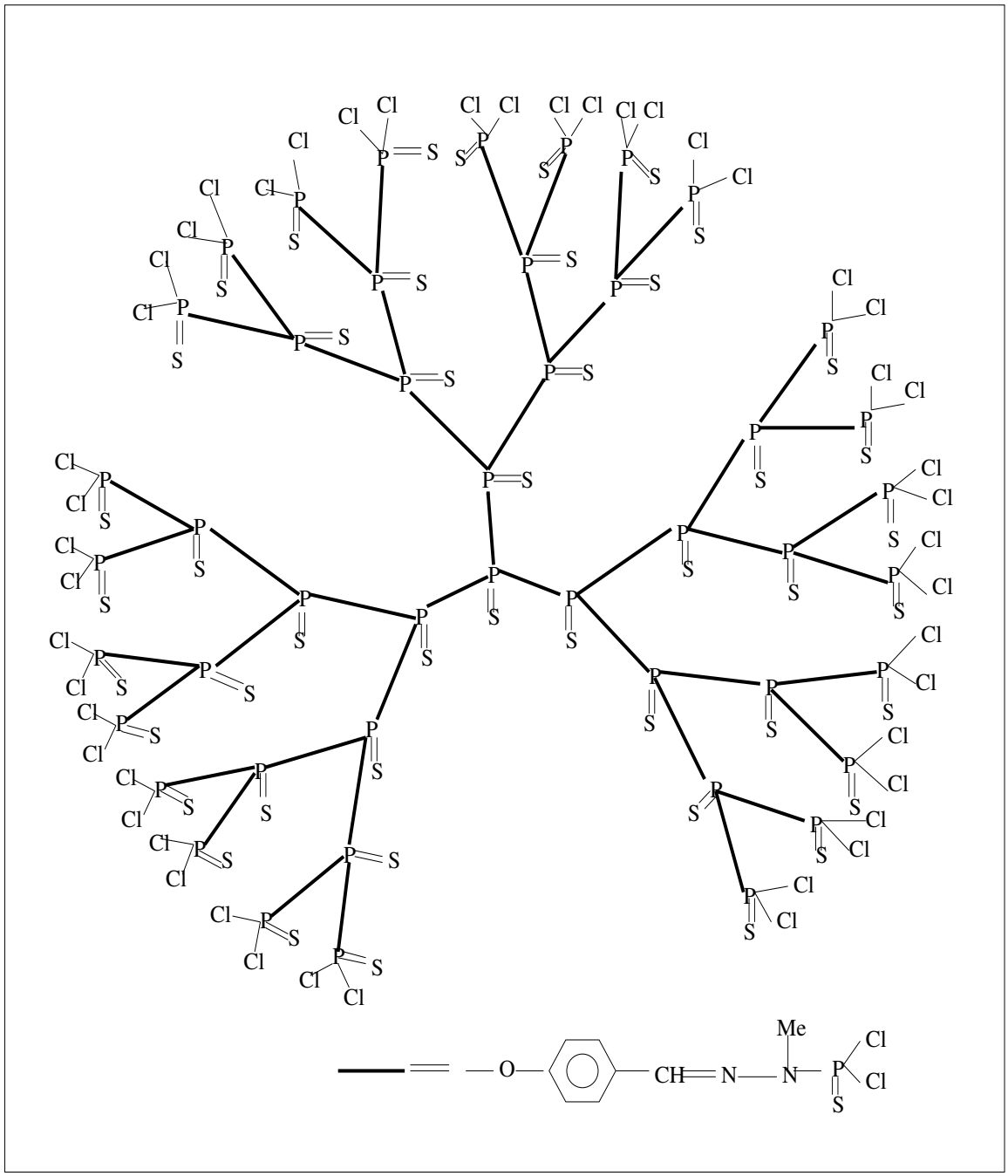

[Fig 2.10] Phosphorous containing dendrimer having p(s)cl$_2$ at the end. It has dipole moment of 8.43 D and 258 D at generation G =1 and G = 10 respectively.

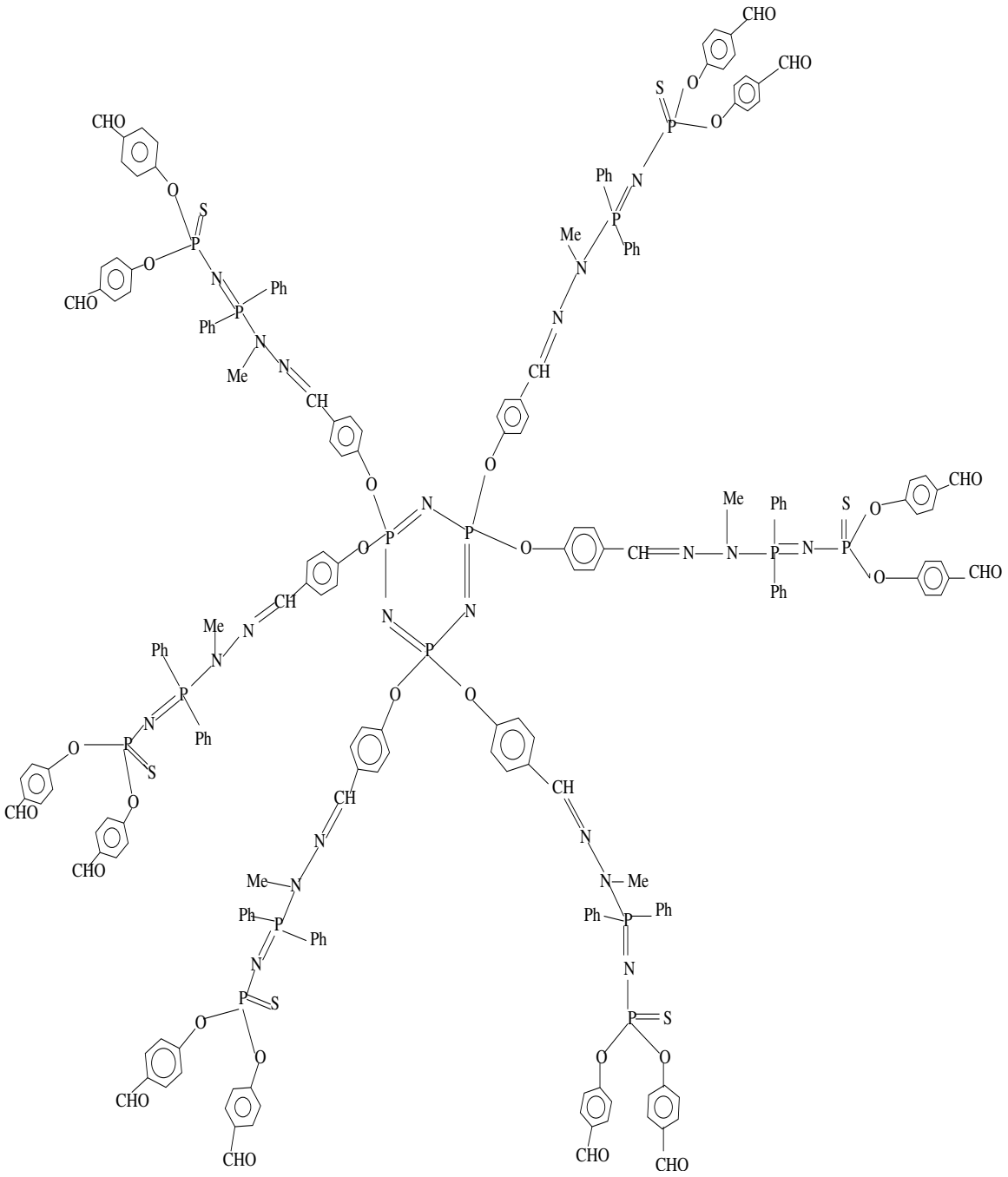

[Fig 2.11] Phosphorous containing dendrimer having aldehyde groups in the peripheral position. This dendrimer has dipole moment 8.27 D at generation G=1 and 328 D at G=11 .

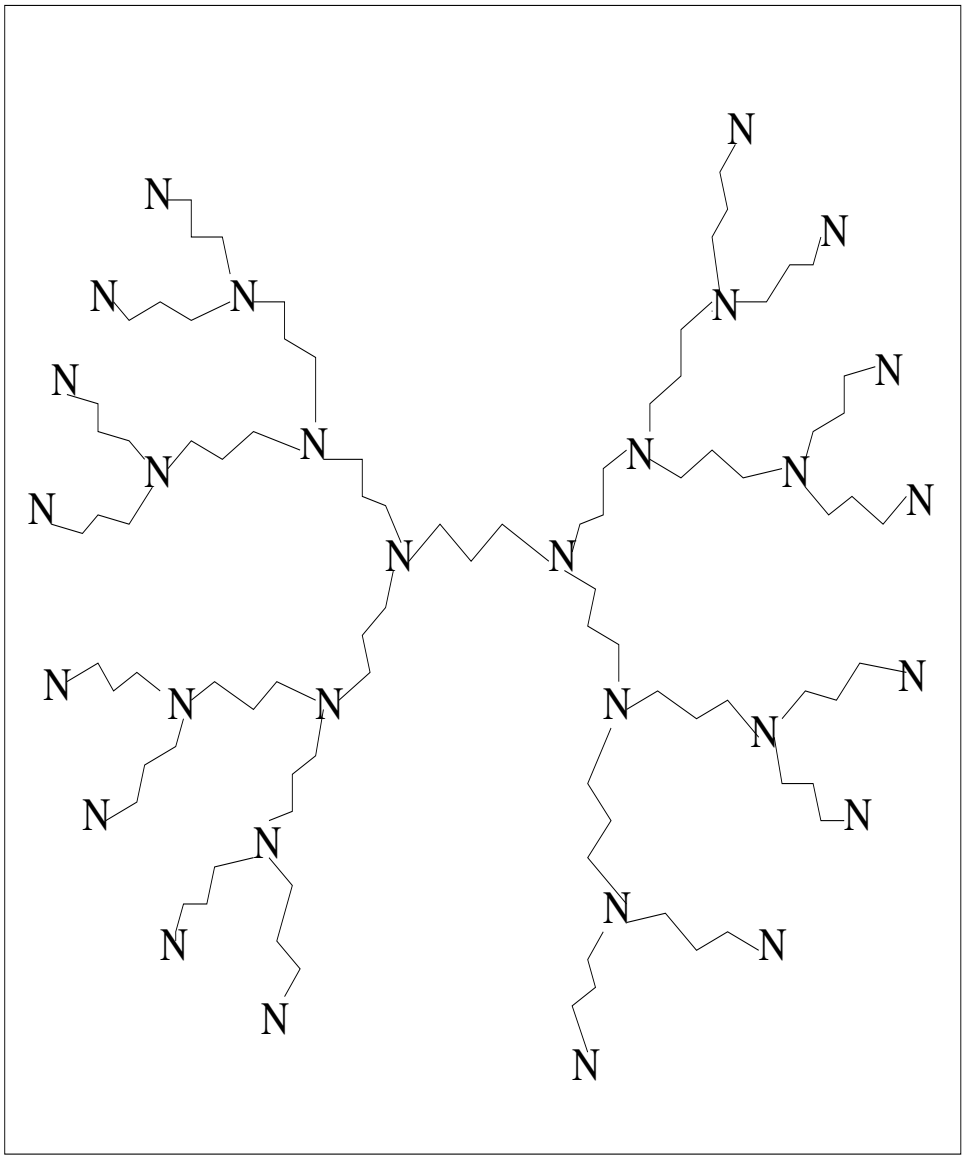

[Fig 2.12]Poly propylene imine dendrimer (called PPI dendrimer) .

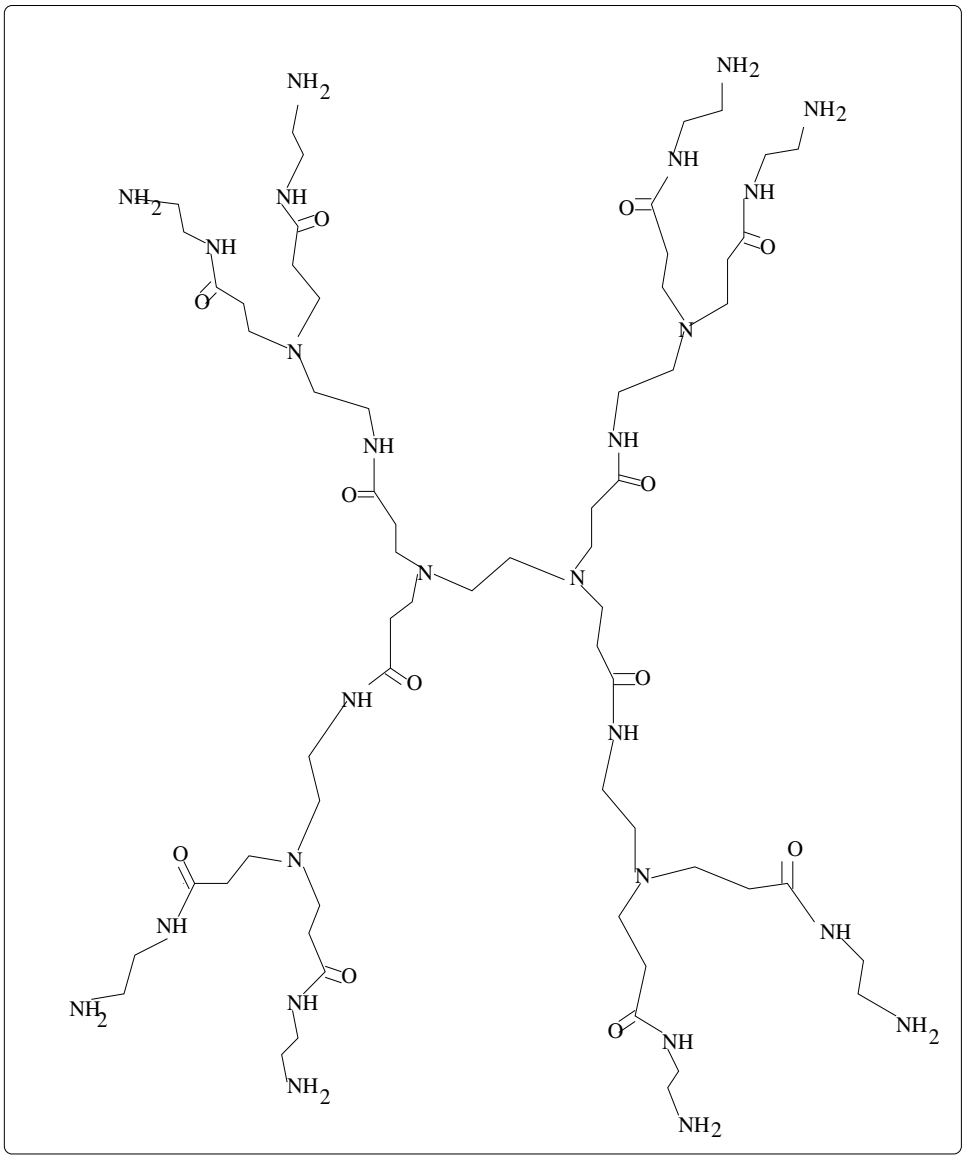

[Fig 2.13] Poly amido-amine dendrimer (called PAMAM dendrimer)

.

Dendrimer as catalyst: Fre′chet and co-workers[101] demonstrated the use of special high-polarity environment of the inner cavity of a dendrimer to catalyze a reaction. This internal polarity of dendrimer enables simple nucleophilic substitution or elimination in catalytic fashion. Their nanoscopic cavities act like micro-environment for molecular reaction[102]. The catalysts can perform their activities in two ways. The large macromolecule can produce many active sites. Their architecture can act as an intermediate between homogeneous and heterogeneous catalysts [103] in a bulk of dendrimeric sample. Again they can encapsulate[104] single catalytic site. The dendritic superstructure can modulate the activity and selectivity of the catalytic site. There are various results[104, 105, 106, 107, 108] where dendrimer can perform catalytic actvities with its numerous active sites those are designed in such a way that facile recycling or cooperativity between the catalytic centers are mentained. Dendritic branching can induce steric inhibition in catalysis. Suslick and co-workers[109] reported the epoxidation of sterically demanding alkenes catalysed by dendrimer containing manganese porphyrins. The branching inhibits the catalysis and enhance the selectivity of the catalyst. Mak[111] and Chow[112] observed the Diels-Alder reaction of smaller dienophile is less hindered by dendrimeric branching and hence have higher initial reaction velocities than the reaction of a larger dienophile.

Dendrimer as patterned poly-redox materials: The dendron may contain groups with oxidising and reducing properties[114, 113, 190] in an orderded geometry. This property is useful for electron transport and charge storage application. Diederich[115, 116, 117] and co-workers showed that dendritic iron porphyrins acts in a similar way as heme-containing electron transfer proteins Cytochrome c. They provided the quantitative measurement of micro-environment effect inside the dendrimer. The micro-environment inside the dendrimer was changed by varying the generation number of the dendrimer. The redox potential of Fe(III)/Fe(II) couple became more positive in higher generation. ion. The transformation from Fe(III) to Fe(II) become much easier. This situation is similar to the strong positive shift of Fe(III)/Fe(II) redox potential in densely packed protein shell in Cytochrome c enzyme in respiratory chain. Gorman[118, 119] and co-workers studied with poly(aryl ether) dendrons to show the shift of reduction potential to negative values with increasing generation. Fre′chet[120] and co-workers demonstrated this with zinc porphyrin as core to show the decrease in electron transfer kinetics at higher generation of the dendrimer molecule.

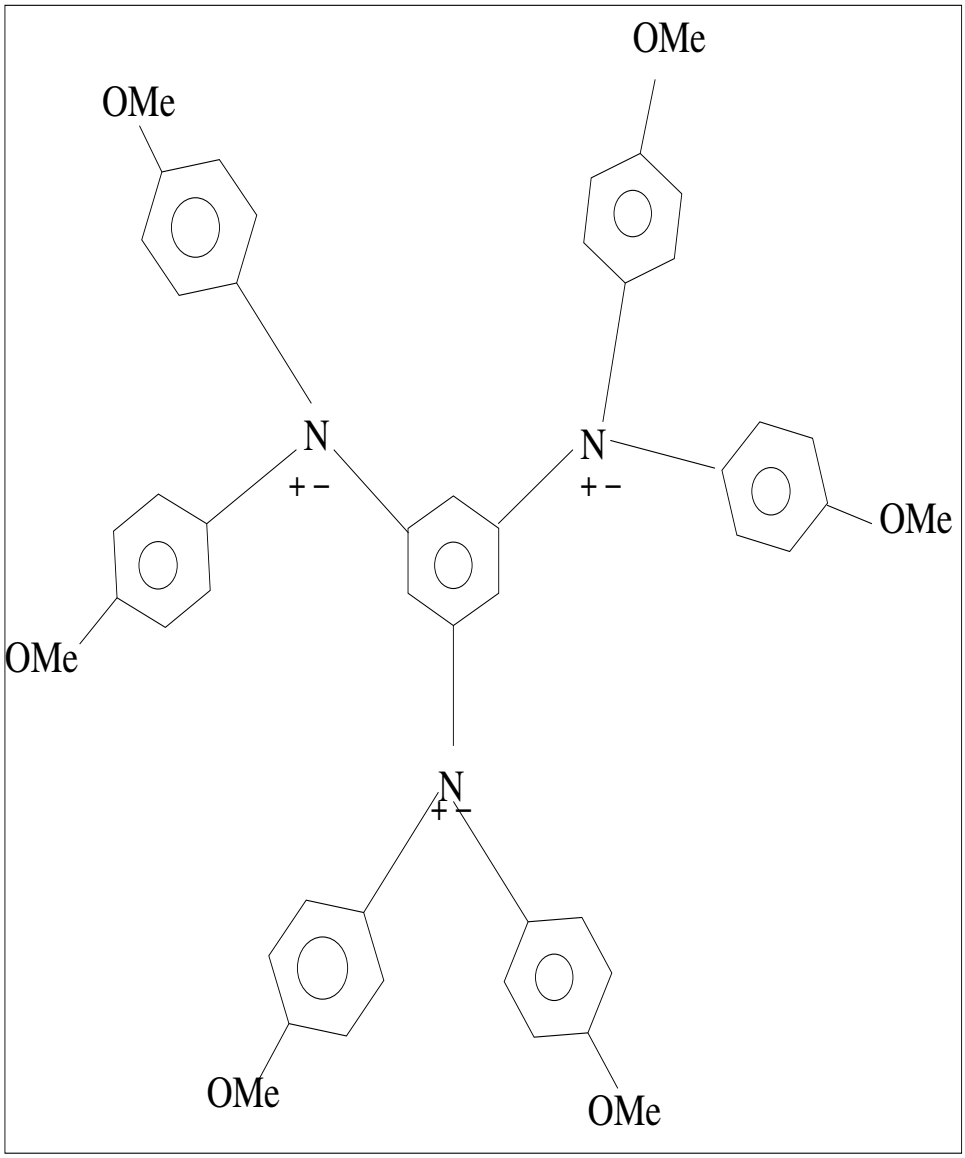

[Fig 2.14] A dendrimer that can accommodate positive or negative ions.

Information storage at the molecular scale: Blending of organic, polymer and photochemicel research are developing new strategy to synthesize nano-scale materials. The organic molecule may be patterned for the production of computer chips or it may function as a bits of information or it may function as the basis of ultra-high resolution memory or nanoprocessor devices[121]. Dendrimer with redox-gradient bulk materials are good candidate for such storage devices. In some dendrimers poly aryl amine units are arranged in such a way that a redox-gradient is developed for one-way electron and charge capture[122]. Triazine as a magnetic coupling[123] unit in dendrimer may open some other perspectives in this area.

Dendrimer Films: They are useful for signal-amplification[124] in fibre-optics communication technology. The dendrimer thin film can isolate metal ions. The dendrimer film can act as sensing interfaces between ions used for sensing application. Arrangement of multiple chromophores around core and their relative orientations within a molecular distance makes these films promising candidates for organic light-emitting diode[125, 126, 127, 129](LED). Economic fabrication of LED devices is mentained by spin casting with formation of single layer that may contain functional groups. Phenylacetylene[125, 183] dendrimers are widely used as a building materials for the dendrimeric scaffolds that can transport electron through its network. The hole transporting agent used for those purposes are amine groups and core used for this purpose is a luminescent anthracene, coumarin or pentathiophene. In many cases the efficiency of the device is very low due to self-quenching due to formation of aggregates

2.9 Some relevant experimental results on dendrimer super-molecule

2.9.1 Spectroscopic results on phenylacetylene dendrimer

A fundamental characteristic of phenylacetylene dendrimers is the composition of legs or spokes. The compact dendrimers (series A) are perfectly structurally symmetric molecules with each of three legs composed of many independent Diphenyle Acetylene units. The phenyl group at the end of each of these moieties have threefold co-ordination at the meta positions serving as branching point to additional phenyl acetylene groups, giving rise to an exponentially expanding structure. This molecular configuration creates the following fundamental characteris-

tics of these dendrimer system. First, branching pattern allows maximum structural flexibility minimizing steric hindrance and enables the synthesis of much larger dendrimeric structure. Secondly, and more importantly, the meta branching position disrupts the local- π - electronic excitation conjugation between aromatic ring systems.

In contrast to these characteristics of the compact dendrimer the extended dendrimer(series B) are unique in that they have unequal legs, composed of linear chains of DPA units consecutively increasing length towards the center of the molecule. Because these legs are of varying lengths these localized excitations are found to be of varying energies. Two kinds of dendrimers have been studied extensively. (A) Compact dendrimers : perfectly symmetric molecules with each of three legs composed of many independent Diphenyle Acetylene units (DPA); branching occurs at meta position of each benzene ring. (B) Extended dendrimers : Molecule with in-equal legs which are composed of linear chains of DPA units with increasing length towards the center of the molecule. Detailed spectroscopic[77] observational studies have been made with two kinds of dendrimers mentioned as A and B. They showed the direct experimental evidence for localized excitations[87][79][80][81] on fractal super-molecular system.

The following spectral features are found for the compact and extended dendrimers as follows. (a) At about 320 nm the vibronic optical absorption spectra of the compact dendrimer series all show a common vibration-less (0-0) transition. The lowest energy peaks are plotted versus the number of benzene rings. They got a horizontal line indicating energy pinning in the compact series. (b) Another interesting feature was monotonic increase of absorption height (intensity) with size of optical absorption. We also see the extended dendrimer has different absorption spectra. Here (a) intensity increases monotonically, (b) (0-0) peak was red shifted like other organic conjugated molecules. The energetic coincidence of all the excitations of the excitations of the compact dendrimer(from D-4 - D-94) were interpreted that the nodes of Cayley tree even in large dendrimer (D-94) had the same local electronic environment as that of (D-4) unit (even like D -2 unit). This was explained as the effect of decoupling of the resonative conjugation due to branching at meta position; the bulk D-4 excitation were also localized. The red shift in (0-0) peak of extended dendrimer was believed to be the effect of delocalization of the electronic excitation energy. Though there were still evidence of localized excitation due to peripheral nodes of approximately D-4 size.

2.9.2 Isomerization of the azobenzene at the core of aryl-ether dendrimer

Jiang and Aida observed the phenomena of harvesting low energy photons in dendrimers to trigger a photoisomerization reaction at the core. Generally infrared radiation can induce low-frequency molecular vibrations and it is dissipated rapidly through molecular collisions. In dendrimeric architectures the exterior part is crowded with high branch density and hence this part is conformationally frozen. The interior part is not constrained and is free to move. They motivated to see intra-molecular energy transfer experimentally within the unimolecular dendrimeric matrices. A series of aryl-ether dendrimers cis- and trans-L1AZO, cis- and trans-L2AZO, cis- and trans-L3AZO, cis- and trans-L4AZO and cis- and trans-L5AZO and cis- and trans-mono-L6′AZO were taken for consideration where L1AZO is an aryl-ether dendrimer of first generation having an azobenzene core, L5AZO is an aryl-ether dendrimer of fifth generation with an azobenzene core and trans-mono-L6′AZO is an aryl-ether dendron of sixth generation with an azobenzene core. They found the infrared-radiation-induced isomerization reaction was greatly affected by the variation of the dendrimer size. The IR induced isomerization of azobenzene group from cis- to trans- form present at the core is 23 times faster than thermal isomerization for cis-L4AZO dendrimer and 260 times faster for cis-L5AZO dendrimer. The lower generation cis-L1, L2, and L3AZO dendrimer was unaffected by the infrared radiation. The molecular weight of cis- and trans-L4AZO and trans-mono-L6′AZO was comparable to each other. Although the dendron trans-mono-L6′AZO was not facilitated by the IR radiation. They again found that the 1597 cm^{-1} which is the stretching vibrational band for aromatics rings facilitated the isomerization reaction. Each of the benzene ring can be excited into a stretching vibration by an infrared photon. The dendrimer backbone stops the IR excitation from dissipation by virtue of its conformationally frozen exterior. Thus a single photon can excite all the benzene rings.

On selective excitation of dendrimeric framework at the characteristic of 280 nm absorption acceleration of the cis to trans isomerization for L4AZO and L5AZO were observed but L1,L2,L3 and L6, were not affected. This part proved that internal convesrion of the singlet-excited state to the vibrational mode of the ground state accelerated the isomerisation. Thus there must be contribution from the dendrimer backbone-to-core intramolecular energy transfer.

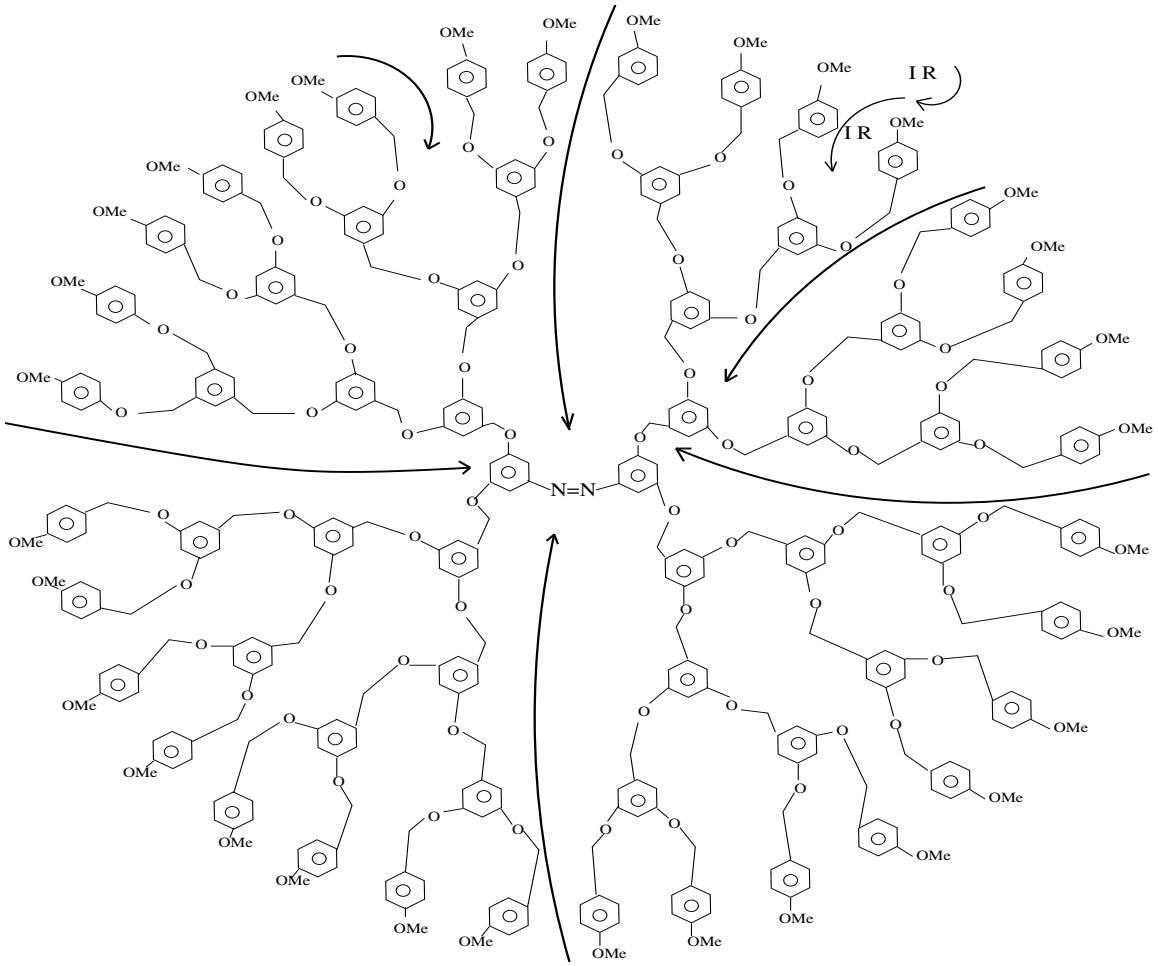

[Fig 2.15] Aryl ether dendrimer of 5th generation. The arrows indicate the motion of the IR light.

2.9.3 Isomerization of NBD group to QC group at the core of aryl-ether dendrimer

Recently J. Chen and co-workers has shown that the light-harvesting ability of the dendritic molecules enhances the rate of valence isomerization of norbornadiene (NBD) group to Quadricyclane group attached to the core. To study the effect of generation number on the isomerization of NBD group to QC group attached to the poly-aryl-ether dendrimer (Gn-NBD dendrimer) they took Gn-OH as models for dendrimer backbone donor and MNBD as model acceptor. They studied the absorption spectrum of all these components in different solvents. No significant interaction between the NBD group and dendrimer backbone of Gn-NBD was observed. The intensity of absorption of dendrimer backbone was hogher than the absorption of the NBD group. The π to π^* transitions of the aromatic rings are responsible for the absorption of the dendrimeric backbone. In G1-OH the intensity of absorption is not exactly proportional to the number of aromatic rings. The effect of aryl ether groups are prominent. So intensity is to some extent greater than the benzyl group. The dendrimer backbone at 280 nm absorbs maximum of the light energy (more than 94%) in the molecule Gn-NBD dendrimer for n=3-4.

On measurement of the fluorescence spectrum of Gn-NBD and Gn-OH molecule it has been observed that the shape and peak positions are identical but the intensities of Gn-NBD dendrimeric backbones of 1st, 2nd, 3rd and 4th generations are quenched. The presence of NBD groups are responsible for the quenching. Comparing the emission of G3-OH, absorption of G3-OH and absorption of MNBD spectrum it was observed that overlap of dendrimeric backbone donor emission with the acceptor MNBD absorption was very small. This small spectral overlap between the fluorescence of the dendrimer backbone and the absorption of the NBD group indicated the singlet-singlet energy transfer from the dendrimer backbone to the NBD group should not be very efficient. Again the fluorescence quenching phenomena suggested that there must be some sort of energy transfer from the dendrimer backbone to the NBD group. Now the question is how this energy transfer is occurring ? They investigated that intra-molecular singlet-singlet electron transfer should also be responsible for the fluorescence quenching.

Model Gn-OH showed phosphorescence but Gn-NBD dendrimers did not show any phosphorescence. The intra-molecular triplet energy transfer was found to be very inefficient in comparison to singlet-singlet energy transfer. The triplet state of the dendrimeric backbone cannot

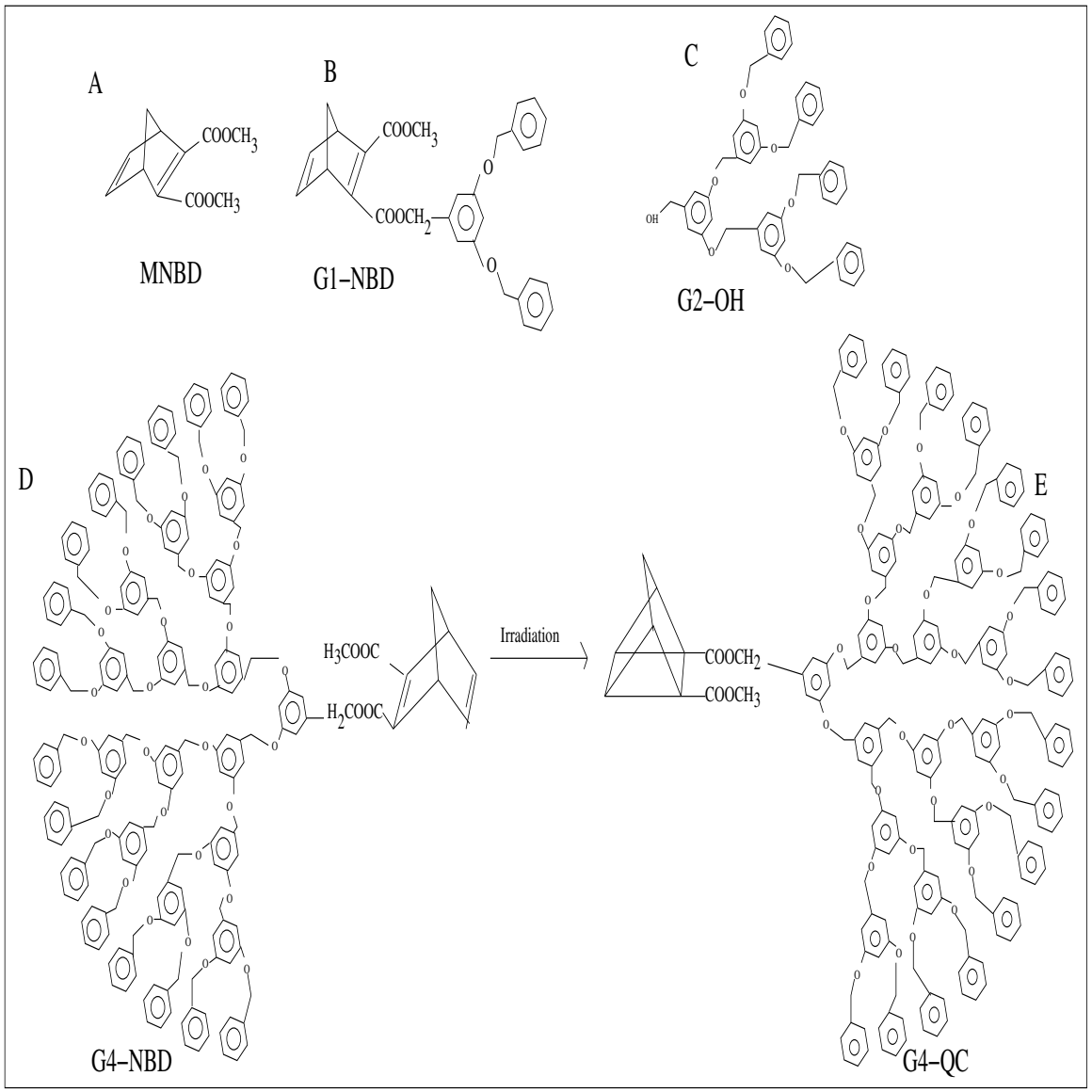

[Fig2.16](A)Dimethylbicyclo[2.2.1]hepta-2,5-diene-2,3-dicarboxylate (MNBD); (B)Norbornadiene (NBD) group attached to the core of a first generation poly(aryl ether) dendrimers: G1-NBD; (C)Hydroxyl group attached to the core: G2-OH dendrimer; (D)G4-NBD isomerizes to G4-QC on irradiation.

be formed efficiently. The electron and energy transfer efficiency ϕ_F decrease with the increase in generation. As the donor-acceptor separation increases with the increase in dendrimer generation the efficiency of the transfer decreases. They did not rule out the involvement of other decay channels. They used above mentioned accessory experimental phenomena to study the photo-sensitized isomerization of the norbornadiene group to the Quadricyclane group in the Gn-NBD dendrimer. Intramolecular photo-sensitized isomerization of the NBD group in Gn-NBD may provide evidence of the intra-molecular electron and energy transfer from the dendrimer backbone to NBD. At room temperature irradiation at the wave length 260 nm - 300 nm the valence isomerisation of NBD group to the QC group occurs in THF solution. The experiment was performed with MNBD and Gn-NBD separately at same concentration at the same wave length regime. The spectrum for MNBD and Gn-NBD were much different. Since within this wavelength regime the most of the light was absorbed by the dendrimer backbone the differences between the Gn-NBD and MNBD were due to the photoinduced intra-molecular singlet electron transfer and energy transfer process from the dendrimer backbone to the NBD group. The isomerization rate of G4-NBD is 3.8 fold higher than the G1-NBD. This higher rate is due to greater light harvesting ability of the dendrimer backbone itself. The proposed mechanism involves the electron transfer from the sensitizer to the norbornadiene to generate the singlet-state radical-ion pair, intersystem crossing to its triplet state (RIPISC), and the recombination of the triplet radical-ion pair to give the triplet nonbornadiene (RIPRC), followed by a rearrangement to the Quadricyclane. They gave the following scheme for the isomerization of Gn-NBD dendrimers to Gn-QC.

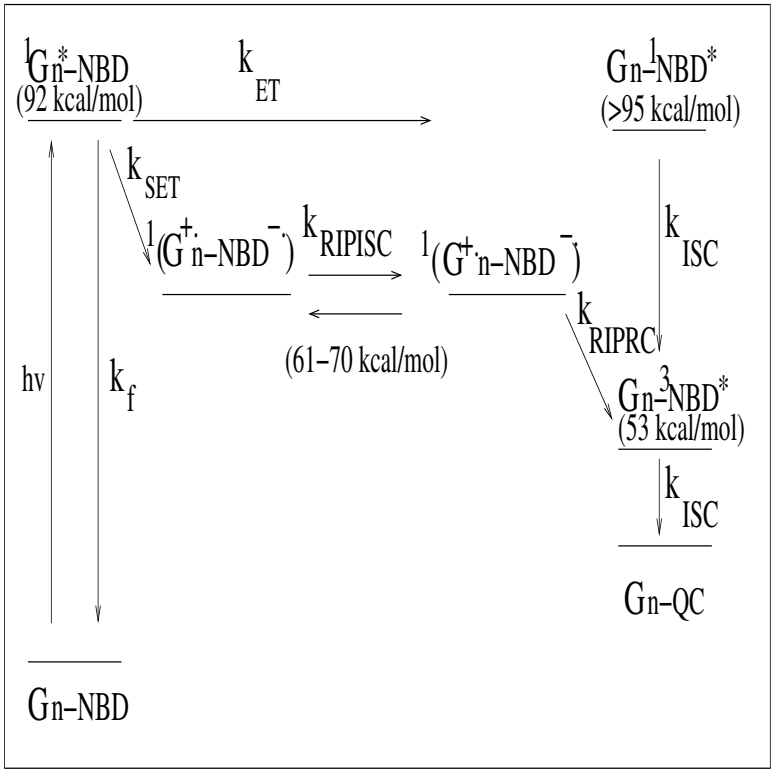

[Fig 2.17]Primary photophysical and photochemical processes in Gn-NBD

Chapter 3

3 Classical energy transport

In this chapter we have discussed about our work on the energy transfer in the dendrimer molecule as a classical random walk problem where the core unit is a trap. The problem and motivation of transient and steady flow of energy transport is described in section 3.1 and in section 3.2 we have described flow of energy in some model related to the arrangements of pigment molecule around RC. Then we have introduced the various construction of potential energy landscape on dendrimer backbone in 3.1.2. In section 3.1.3 we have given the formalism of calculation of mean first passage time(MFPT) from the local escape rates. We have explored the numerical results and discussion about the MFPT rates in section 3.1.4. Section 3.1.5 is devoted to the calculation of steady state rate through Eyring model of membrane permeation. The numerical results of the steady state rate is discussed in section 3.1.6. In section 3.2.1 we have described the equations of motion and formulation of matrices for calculation of MFPT in models decribing the arrangements of antenna[222] pigments in photosynthetic unit(PSU). In section 3.3 we have summarised the results of classical energy transport features in and through dendrimer network and conclude about our investigation.

3.1 Energy transport in dendrimeric arrangement

3.1.1 Introduction

Klafter and co-workers [76, 78] have given the mechanism of energy transfer in the dendrimer molecule as a classical random walk problem where the core unit is a trap see Fig.2.2(a) and Fig.2.2(b) in previous chapter. They have observed that the energy transfer process will be dominated by two trends (a) an entropic one, which stems from the branching at each generation, and (b) an energetic one, which is due to an energy funnel that directs the excitation towards the trap. Then they have shown with a superimposed energy funnel towards core one should be able to control the preferred location of excitation by monitoring the temperature relative to the energy funnel [78]. Raychoudhury et al have

considered the core bound excitonic diffusion on dendrimers subjected to several types of non-homogeneous funneling potential for an extended dendrimer model[92][94].

In our work we would like to understand the energy funneling effect in some other way by considering a statistical description of the flow of excitation energy on a backbone of dendrimer geometry. Let us consider that the energy transport in dendrimer super-molecule is a multi step thermal barrier crossing process. Here each node is behaving as a potential well and the connection between two successive nodes is behaving as a barrier height (see Fig.3.1 and Fig.3.2). The local escape rates again depend upon the geometry i.e. local potential well and barrier height and temperature. Then we have calculated mean first passage time and mean residence time explicitly with the local escape rates. The inverse of MFPT is equivalent to rate at which energy is transferred. For the MFPT calculation the random energy hopping over the barriers is considered on the cayley tree. Here two-dimensional process is cast into an effective one-dimensional process where the core is an absorbing boundary and the periphery is the reflecting boundary. This is described in Fig.2(b).

We have considered that the mechanism of energy transfer hinges on the potential energy landscape along the dendrimer backbone from the core to the periphery. Though for dendrimeric geometry the monomers units grows exponentially with increase in generation but the actual local environments are determined by the nodes and legs(bonds). Therefore, the local environment of a node of a phenyleacetylene compact dendrimer from that of a phenylacetylene extended dendrimer and both are different from dendrimer containing hetero atoms. In other words, the energy funneling from generation to generation depends on the specificity of the dendrimer molecule. Therefore, a general picture of the variable parameters of the potential energy landscape is very essential. Here we restrict ourself to some specific classes of potential surfaces to have some qualitative understanding about the dependence of well depth and barrier heights on the energy transport.

Next we have applied Eyring Model of Membrane Permeation[96] for energy transfer through this multiple barrier crossing way in dendrimeric geometry. For this model we have calculated flux towards core at the steady state. Unlike the formalism of mean first passage time calculation, here the system is considered as an open system. In this consideration, at the one end, say in the peripheral nodes, an external energy is contineously injected into the system and with time energy is

uniformly passed through different generations and absorbed at the core completely or partially and thereby a steady flow of energy is maintained. So an energy occupation probability in the periphery (say,1) and in the core (say,0) is maintained at the steady state. Now the question is how the steady flux of energy is governed by the barrier configurations, a two-dimensional cayley tree geometry and other parameters of the system. Therefore, one can understand the issues of kinetic and thermodynamic controllability of the energy transport process, influenced by the various parameters of the system, using both approaches.

The first approach may be relevant with the case where the core is behaving as absorbing unit/or a photo-chemical sensor group which reacts with gain of light which is being transferred from periphery to core. The second approach of rate calculation may be relevant to the case where there is no absorbing unit at core. Otherwise the later approach may be relevant with the case where every node is behaving as a sensor group. The choice of a particular method will depend upon the actual situation of the dendrimeric system. Here we have given a comparative study using both the approaches.

3.1.2 Construction of potential energy landscape on dendrimer

In the potential energy landscape on the dendrimer geometry, the nature of well and barrier height will dictate whether the superimposed funnel (or slanting of potential surface) is descended towards core or towards periphery or how the flow of energy takes place. Adopting the symmetry of each node in a particular generation, we consider an one dimensional description (Fig 2.2(b) of the system (Fig 2.2(a)) such that a node in a particular generation is situated in a potential well and connection between the nodes is behaving as a barrier. We have assigned that the first barrier height from the core well is of energy E. The next barrier height may be higher by an amount v_n i.e. $E + v_n$ or may be lower by an amount v_n i.e. $E - v_n$. The potential well at each node from the bottom of the core well has height of u_n where n is the generation number. Thus we have the parameters $\{E\ ,u\ ,v\}$ to be considered to obtain the detail structure of the one dimensional potential surface extended from the core to the periphery. Again since the dendrimer has highly symmetric structure the wells situated at a certain generation have same nature and so is the case for barrier height between same successive generation.

In Fig.3.1 and in Fig.3.2 we describe two major classes of potential surfaces. **Class-1** defines the cases where the bottom of each well are

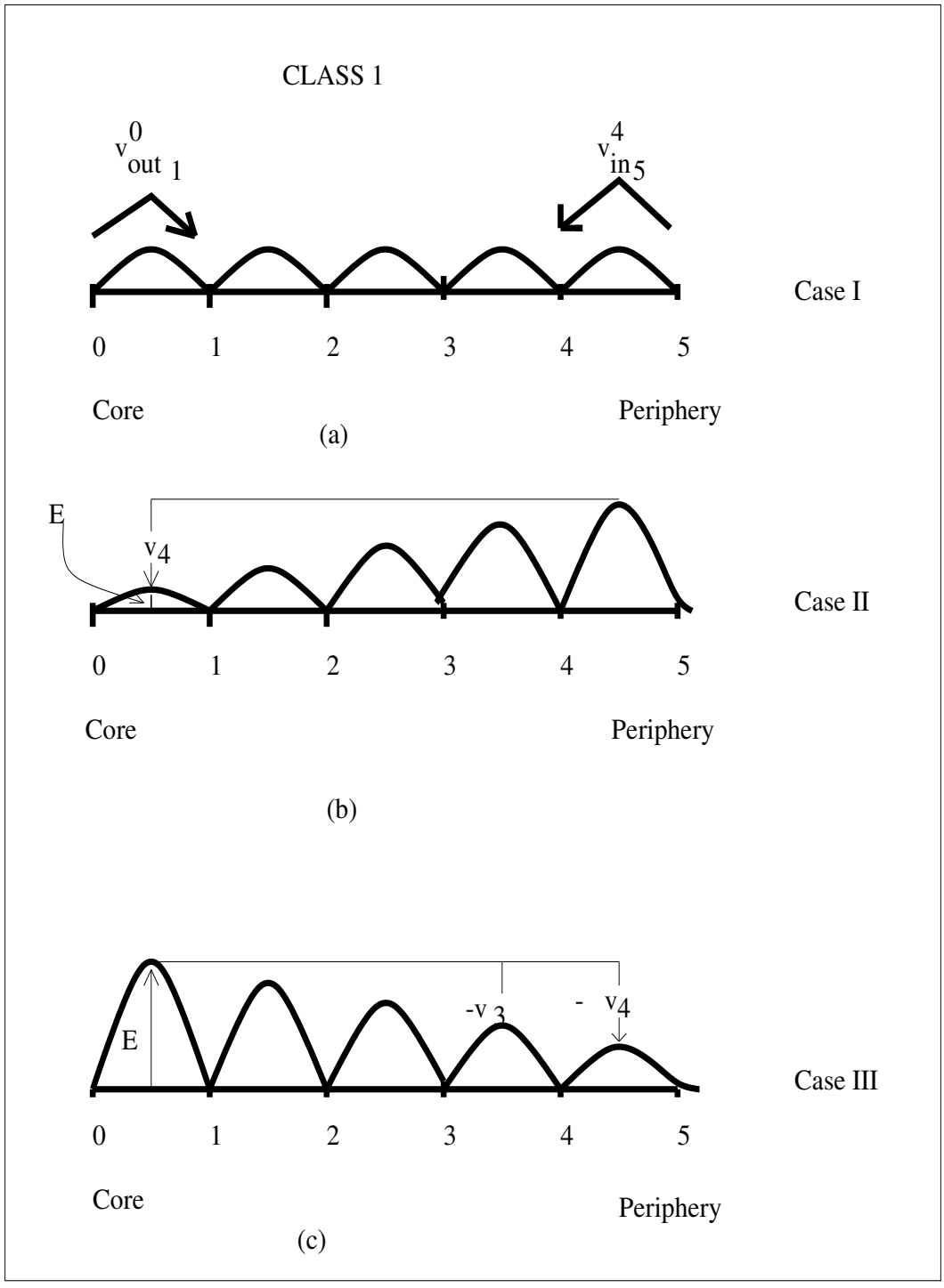

[Fig 3.1] CLASS 1: The potential energy landscape on dendrimer geometry keeping the potential well at zero level. (a). The barrier height remain constant. (b). The barrier height increases from core to periphery. The bias of the funnel towards core. (c). The potential barrier is decreasing from core toperiphery.

at a height $u_n = 0$ i.e. all wells are at zero level case(I-III). Now if the barrier heights are of same height as that of the first barrier height (E) then that is the case-I. Again if the barrier height increases after each generation with a value v_n (the increment of barrier height from top of first barrier) then that is the case-II where the barrier height increases from core to periphery. When the barrier height decreases by an amount v_n the situation is described in case-III.

Class-2 defines cases with non-zero u values in case-IV and case-V. i.e. each well have definite height. For case-IV the barrier height arises due to the positive values of v_n and u_n. Hence the effective barrier heights are $(E + v_n - u_n)$ and $(E + v_n - u_{n+1})$ at the time of outward and inward movement respectively. For case-V with v_n negative, the effective barriers are $(E - v_n - u_n)$ and $(E - v_n - u_{n+1})$ for outward and inward movement respectively. Note that case I-III we have considered that there is no superimposed energy funneling. In case IV and case V we consider the situation where the peripheral node is always above the core well but the intermediate well depths are consequently on increasing and decreasing order from the first generation node to the peripheral node. In each study of cases of IV and V the set of u_i and v_i are chosen in such a way that all the intermediate local rates of inward transitions are of the same magnitude. Similarly, all the outward transition rates are of the same value. But in case IV the barrier are much higher than in case V. We consider that the local rate of outward and inward escape from a particular well follow a Kramer's type of escape rate so that the equilibrium detailed balance picture remains valid. The escape rate can be given by

$$k_{in_g}^{g-1} = \dot{K}_{in_g}^{g-1} \frac{k_B T}{h} exp[-\frac{\{E \pm v_{g-1} - u_g\}}{k_B T}] \tag{3.1}$$

$$k_{out}{}_{g-1}^{g} = \dot{K}_{out_{g-1}}^{g} \frac{k_B T}{h} exp[-\frac{\{E \pm v_{g-1} - u_{g-1}\}}{k_B T}] \tag{3.2}$$

with a condition $u_0 = v_0 = 0$. Here a negative sign in front of v_n signifies that the barrier height is decreasing from core to the periphery. In Eq.(3.1) $k_{in}{}_g^{g-1}$ defines inward rate from a node at g-th generation to a node at $(g-1)$-th generation and in Eq.(3.2) $k_{out}{}_{g-1}^{g}$ define outward rate from a node at $(g-1)$-th generation to a node at g-th generation respectively. $\dot{K}_{in_g}^{g-1}$ is the transmission coefficient towards core for the transfer process g-th generation to $(g-1)$-th generation and $\dot{K}_{out_{g-1}}^{g}$ is the transmission coefficient towards periphery for the transfer process $(g-1)$-th generation to g-th generation. k_B is the Boltzmann's constant.

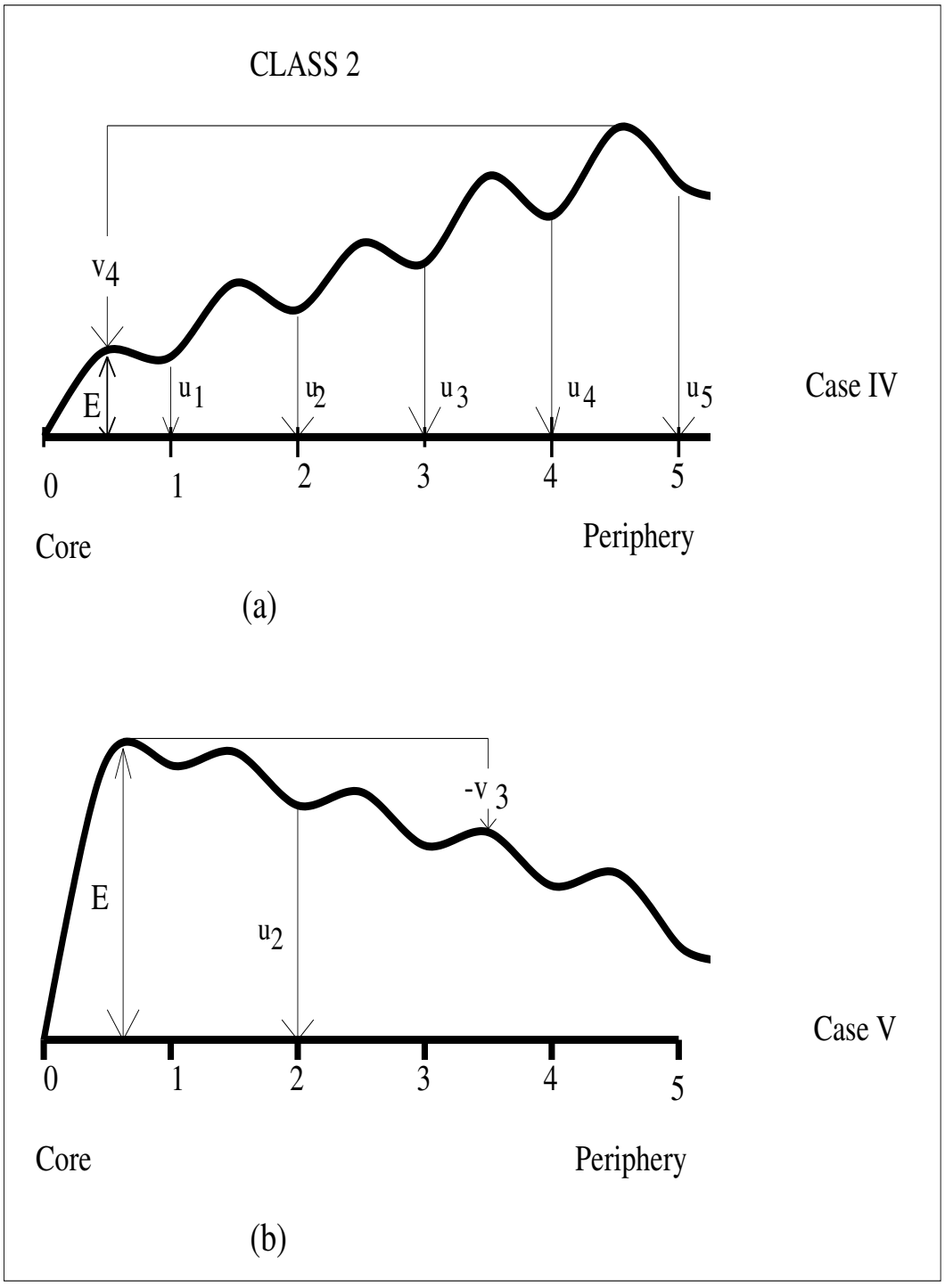

[Fig 3.2] CLASS 2: The potential energy landscape on dendrimer geometry kepping the potential well depth at different hights such that slanting is towards core in (a) and towards periphery in(b).

3.1.3 Calculation of MFPT from local escape rates

Let us calculate Mean First Passage Time (MFPT) and Mean Residence Time (MRT) in a finite one dimensional system. The MFPT is the mean time a random walker takes which starts at site n, to get trapped, and it is directly related to $\Phi(t,n)$, the survival probability of the system at time t when starting at site n,

$$\tau(n) = \int_0^\infty \Phi(t,n)dt \tag{3.3}$$

$$\Phi(t,n) = \sum_{m \neq trap} P(m,t \mid n) \tag{3.4}$$

where $P(m,t \mid n)$ is the probability to be at site m at time t, starting from site n. Mean residence time is the average time spent in a given site prior to being trapped. The MRT of site m starting from n is

$$\tau(m,n) = \int_0^\infty P(m,t \mid n)dt. \tag{3.5}$$

So MFPT for starting at site n,$\tau(n)$, is the sum of the MRTs

$$\tau(n) = \sum_{m \neq trap} \tau(m,n). \tag{3.6}$$

In (Fig 2.2(b)) we consider a random walker which moves by a nearest neighbour jumps on a one dimensional system with rates R_i towards the reflecting point (equivalent to periphery for dendrimer) and with rates T_i towards trap(equivalent to core for dendrimer). The rate equations are given by

$$\dot{P}_0 = T_1 P_1 \quad \text{(for core)} \tag{3.7}$$

$$\dot{P}_1 = T_2 P_2 - (T_1 + R_1)P_1 \tag{3.8}$$

$$\dot{P}_i = T_{i+1}P_{i+1} + R_{i-1}P_{i-1} - (T_i + R_i)P_i \qquad (1 < i < n) \tag{3.9}$$

$$\dot{P}_N = R_{N-1}P_{N-1} - T_N P_N \quad \text{(for reflecting boundary)} \tag{3.10}$$

In matrix notation we can write

$$\frac{d\hat{P(t)}}{dt} = \hat{A}\hat{P(t)} \tag{3.11}$$

where $\hat{A}$ has the form

$$\hat{A} = \begin{bmatrix} -(T_1+R_1) & T_2 & 0 & 0 & 0 & \cdots & 0 \\ R_1 & -(T_2+R_2) & T_3 & 0 & 0 & \cdots & 0 \\ 0 & R_2 & -(T_3+R_3) & T_4 & 0 & \cdots & 0 \\ 0 & 0 & R_3 & -(T_4+R_4) & T_5 & \cdots & 0 \\ \cdots & \cdots & \cdots & \cdots & \cdots & \cdots & T_N \\ 0 & 0 & 0 & 0 & 0 & R_{N-1} & -T_N \end{bmatrix}$$

where the equation of the core element is neglected.

The general solution for the survival probability at the m-th site at time t, starting from the n-th site , is

$$P(m,t \mid n) = \hat{Q}exp(\hat{A}t)\hat{P}(0), \tag{3.12}$$

where $\hat{P}(0)$ is the column vector with n-th element is 1 and other elements are zero. Therefore the mean residence time at the m-th site starting from the n-th site is

$$\tau(m,n) = \int_0^\infty \hat{Q}exp(\hat{A}t)\hat{P}(0)dt = -\left[\hat{A}^{-1}\right]_{mn}. \tag{3.13}$$

Here the existence of $\hat{A}^{-1}$ is guaranteed since there is no stationary solution in the case of a trap and so the matrix will not have a zero eigenvalue. From the property of the inverse matrix $\hat{A}^{-1}$ one can obtain the mean residence times

$$\tau(1,n) = \frac{1}{T_1} \quad \text{(m=1)} \tag{3.14}$$

$$\tau(m,N) = \tau(m-1,N)\frac{R_{m-1}}{T_m}, ...(1 < m \leq N). \tag{3.15}$$

Now we shall use eqn(3.1) and eqn(3.2) for the local escape rate from a node to a node of next higher generation or vice verse to calculate MRT and MFPT. We can relate local escape rates with T and R in the following way

$$T_i = c(z-1)^{(i-1)}{k_{in}}_i^{\,i-1} \tag{3.16}$$

$$R_{i-1} = c(z-1)^{(i-1)}{k_{out}}_{i-1}^{\,i} \tag{3.17}$$

where Z is branching at each node and $C = Z - 1$. In this way we have taken into account the degeneracy factor of nodes of ith generation. Substituting the values of T_i and R_i in equations (3.14) and (3.15) we get MRT of site m starting at N (Periphery).

$$\tau(m,n) = \frac{1}{c(\frac{k_BT}{h})\dot{K}_{in_m}^{\;m-1}}\left[\sum_{n=1}^{m-1}\frac{1}{(z-1)^{n-1}}\prod_{i=n}^{m-1}\frac{\dot{K}_{out_i}^{i+1}}{\dot{K}_{in_i}^{i-1}}exp\left[\frac{E \pm v_{m-1} - u_m}{k_BT}\right]+\right.$$

$$\frac{1}{(z-1)^{m-1}} exp\Big[\frac{E \pm v_{m-1} - u_m}{k_B T}\Big]\Big] ...(u_0 = v_0 = 0) \tag{3.18}$$

and MFPT starting at periphery N

$$\tau(N) = \sum_{m=1}^{N} \tau(m,N) = \frac{1}{c(z-1)^0(\frac{k_B T}{h})\dot{K}^0_{in_i}} exp\Big[\frac{E-u_1}{k_B T}\Big] +$$

$$\sum_{m=2}^{N} \frac{1}{c(\frac{k_B T}{h})\dot{K}_{in_m}^{m-1}} \Big[\sum_{n=1}^{m-1} \frac{1}{(z-1)^{n-1}} \prod_{i=n}^{m-1} \frac{\dot{K}^{i+1}_{out_i}}{\dot{K}^{i-1}_{in_i}}$$

$$exp\Big[\frac{E \pm v_{n-1} - u_m}{k_B T}\Big] + \frac{1}{(z-1)^{m-1}} exp\Big[\frac{E \pm v_{m-1} - u_m}{k_B T}\Big]\Big] ..(u_0 = v_0 = 0) \tag{3.19}$$

3.1.4 Discussion:

This method of calculation of MRT and MFPT involves basically the standard method of calculation of MFPT on a linear chain. Then we have taken into account the of dendrimeric geometry by Eq.(3.16) and Eq.(3.17). In this way the two-dimensional geometry has been taken into account.

Here we have investigated the effect of the set of parameters E, u_i, v_i, c, $k_B T$ on the energy transfer rate and mean residence time on the nodes of the dendrimer molecule. In the situations where the other parameters have not been specified in the figures, we have taken the values of the parameters as $E = 1.0$, for linear increase $u_n = 0.2 + 0.04(n-1)E$ and $v_n = 0.2 + 0.04(n-1)E$. For a linear decrease we have taken $v_n = -0.2 + 0.04(n-1)E$ and $u_n = 0.80 - 0.04nE$. Where the temperature is not specified we have taken $k_B T = 0.3E$ and for simplicity all transmission coefficients have been taken as 1.0 in units of E^{-1}/Time, where Time is in an arbitrary unit.

In Fig.3.3(a) we have shown the dependence of MRT,$\tau(m, G)$ on m, starting at periphery G, on the generation number and core branching. Here we see that in Fig.4(a), case I, case II and case III have more or less same nature of variation with generation number, whereas case IV and case V have many dissimilarities. For cases I-III, MRT at a certain generation increases with an increasing distance of that site(m) from trap. This is because the excitations need to cross more number of potential

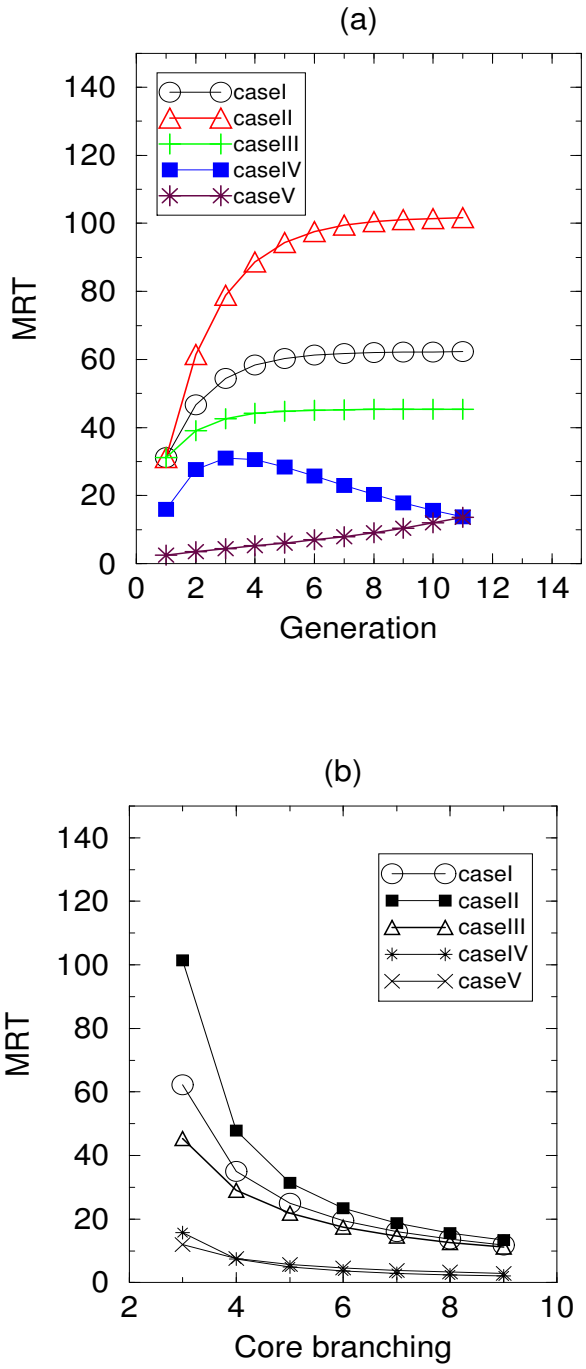

[Fig 3.3] (a)The variation of MRT with generation at which MRT is being measured for cases I-III, where MRT increases with generation and then gets saturated. The saturation of MRT occurs at a higher generation for case IV and case V. (b) The variation of MRT at the tenth generation with core branching are shown for all cases. The MRT decreases since the number of pathways towards the core increases. Due to a superimposed energy funnel in cases IV-V, MRT values are lower than in cases I-III.

barriers. This increase of MRT ceases at sites after generation 8. The MRT values get saturated. The branching effect(through the degeneracy factor) makes the environment of site equivalent after a certain generation from trap. Thus it matters very little for which site the MRT is being measured. Again, case IV is giving the similar increase upto generation 4 (a slow increase); after that there is a decrease in MRT. We have seen that for case IV at a sufficiently high generation ($G > 20$), the MRT values get saturated with a very low MRT value, which is not shown in the figure. The situation may be explained in the following manner. Here potential surface descended towards trap. The small values of MRT near trap signifies that the excitation is descended very easily following imposed funnel with a relatively lower number of barriers. The branching effect always tries to equalize the MRT values and superimposed energy funneling with its increasing height tries to decrease MRT values. These two effects compete each other in such a way that there is a decrease in MRT values. After generation 15 the branching effect overcomes superimposed funneling effect. In case V there is a slow and steady increase of MRT with generation. In summary, an increase in values of u makes MRT values smaller. It is the competetion between the combined effect of barrier height and slanting of well depth that determine the value of MRT in an identical other parameter regime.

In Fig.3.3(b) We have shown the dependence of MRT at the peripheral node on core branching. Core branching has a greater effect upon cases I-III than the effect on cases IV-V. With an increase in core branching, the number of pathways for being trapped at the core. In cases I-III the effect of core branching is seen in the presence of different barrier heights although there is no energy slanting. In cases IV-V there is effective energy funneling from the periphery to the core, so MRT values are less than in case I-III, and the effect of barrier heights is also very small.

The rate, $\frac{1}{MFPT}$, value also decreases with the size of the dendrimer molecule, which is shown in Fig.3.4(a) and Fig.3.4(b). As the system size increases the rate decreases, which is generally obsereved in all cases of Fig.3.4(a) and Fig.3.4(b). This picture is also seen in MRT cases where with an increase in generations the excitations are localized over the nodes near the periphery. But the magnitude of the rate in cases IV-V are much more than in cases I-III, which is due to the energy funneling from the periphery to the core. As the barrier heights are much higher in case IV than in case V, the rate is lower in case IV than in case V for a fixed size of the dendrimer.

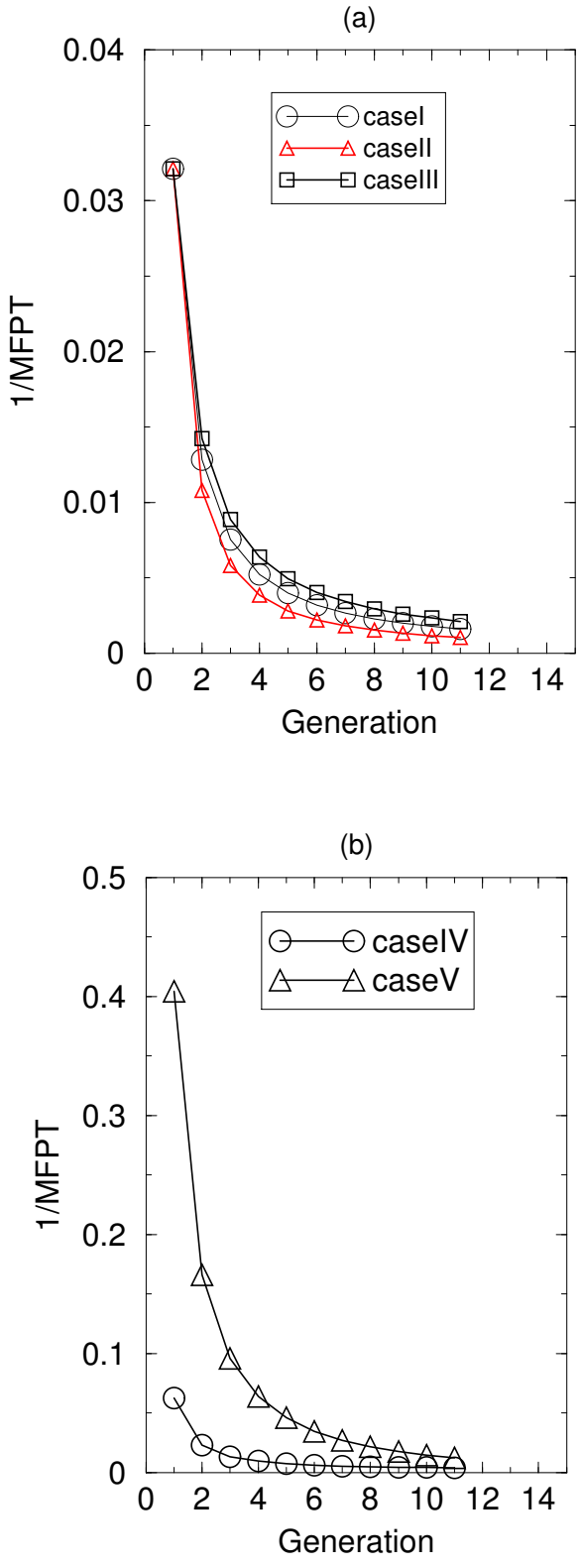

[Fig 3.4] The variation of inverse of MFPT is displayed with the size (G) of the dendrimer molecule for (a) class 1 and (b) class 2.

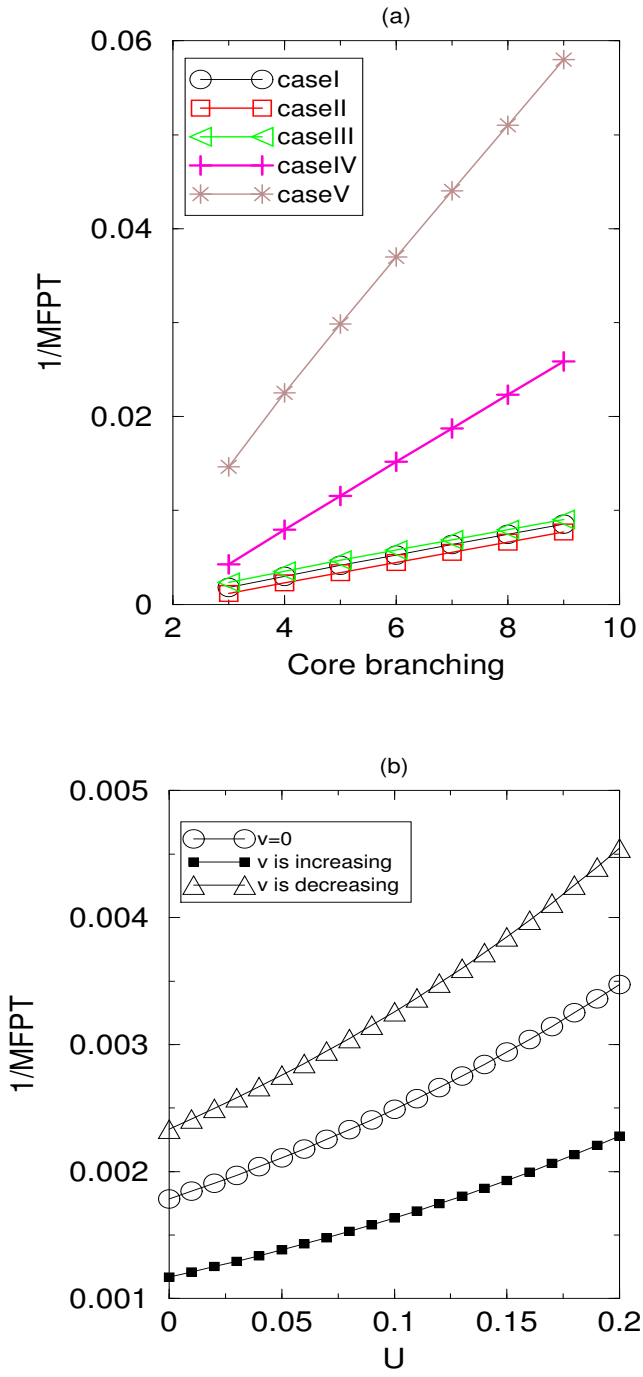

[Fig 3.5] (a) The inverse of MFPT is plotted with core branching for a dendrimer of size G = 10. (b) The inverse of MFPT is plotted with u (in units of E) for three special cases of dendrimer of size, G = 10.

In Fig.3.5(a) we have displayed the effect of core branching on the rate for a particular dendrimer. This increase in rate with core branching is expected from the fact that as the number of pathways increases the rate increases. This is also in accordance with the behaviour MRT in Fig.3.3(b). Again, cases IV-V are of much higher magnitude than in cases I-III because of the energy funneling from the core to the periphery. Internal potential surfaces, the distribution of barrier heights and well depth, are also reflected in cases I-V.

If we assume a picture of a potential surface with all $u_1 = u_2 = u_3 \ldots\ldots = u_G = u$ and all $v_1 = v_2 = v_3 = \ldots\ldots v_{G-1} = v$. For a positive value of u, i.e., when there is a slanting of the potential surface from the periphery to the core, we consider three different situations: (i) $v = 0$, barrier heights will successively decrease from the core side to the periphery side; (ii) $v = positive$, the barrier height will successively increase from the core side to the periphery side; (iii) $v = negative$, barrier heights will also successively decrease from the core side to the periphery side. In Fig.3.5(b), the competition between the effect of well depth and barrier heights on the rate is displayed. For three different values of v, 0, positive and negative depending on the barrier heights, the rates appear accordingly as expected.

In photochemical isomerization experiment, Jiang and Aida have shown that low-energy infrared photons can induce a photochemical isomerization at the core. The photons explore much time in the dendrimeric architecture when generation is high. This is in accordance with the higher MRT and MFPT for higher generation in our model.

For a compact dendrimer family of a phenyl-acetylene dendrimer the funneling is like case I for electronic excitation energy. That means that there is no bias for electronic excitation energy towards the core. So the extended dendrimer is of the case IV or case V type. Our results suggest that the transfer of excitation energy is according to the random walk model in cases IV-V, where excitation will spend little time on dendrimeric architecture, as reflected by the lower values of MRT.

3.1.5 Eyring model of steady energy transport

In above section we have taken into account the standard method of Calculating MRT and MFPT for one dimensional random walk problem and have applied them to dendrimer molecular geometry. For that we have to assume the core as a trap and the peripheral generation as reflecting

point. The Erying model for Membrane Permeation [96] considers the membrane as a series of potential energy barriers existing one behind the other, across which material must pass to cross the membrane. According to this model the flux over every barrier is same at the steady state. Again, this flux at steady state depends only on the first and last separation of barrier height and on each local rate constant for crossing the barrier height. Unlike the formalism of mean first passage time calculation, here the system is considered as an open system. In this consideration, at the one end, say in the peripheral nodes, an external energy is continuously injected into the system and with time energy is uniformly passed through different generations and absorbed at the core completely or partially and thereby a steady flow of energy is maintained. So an energy occupation probability in the periphery (say, 1) and in the core (say, 0) is maintained at the steady state. We have applied the Eyring model in this case, where each node is a potential well and each link is a barrier height, as assumed in an earlier section.

So the velocity of outward flow of any property from $(g-1)$-th generation to g-th generation can be given as

$$V^g_{out_{g-1}} = k^g_{out_{g-1}} P_{g-1} f_{g-1} w^g_{g-1} \tag{3.20}$$

where P_{g-1} is the population on $(g-1)$th node(well), f_{g-1} is numbers of such nodes in that $(g-1)$th generation, w^g_{g-1} Number of ways the property can go out towards the periphery from $(g-1)$th to gth generation.

The velocity of inward flow can be given as

$$V^{g-1}_{in_g} = k^{g-1}_{in_g} P_g f_g. \tag{3.21}$$

Thus the flux over barrier between$(g-1)$-th and g-th generation is given by

$$J^g_{g-1} = V^g_{out_{g-1}} - V_{in}{}^{g-1}_{g}. \tag{3.22}$$

Here we have assumed that outward direction of movement is positive.

Now we have

$$J^1_0 = k_{out}{}^1_0 P_0 f_0 w^1_0 - k_{in}{}^0_1 P_1 f_1 \tag{3.23}$$

$$J^2_1 = k_{out}{}^2_1 P_1 f_1 w^2_1 - k_{in}{}^1_2 P_2 f_2 \tag{3.24}$$

$$J^3_2 = k_{out}{}^3_2 P_2 f_2 w^3_2 - k_{in}{}^2_3 P_3 f_3 \tag{3.25}$$

$$J^4_3 = k_{out}{}^4_3 P_3 f_3 w^4_3 - k_{in}{}^3_4 P_4 f_4 \tag{3.26}$$

$$\cdots\cdots = \cdots\cdots - \cdots\cdots$$

$$J_{g-1}^{g} = k_{out_{g-1}}^{g} P_{g-1} f_{g-1} w_{g-1}^{g} - k_{in_g}^{g-1} P_g f_g. \tag{3.27}$$

From equations (23) and (24) eliminating values of $P_1 f_1$ we get

$$J_0^1 = k_{out_0}^{1} P_0 f_0 w_0^1 - \frac{k_{in_1}^{0}}{k_{out_1}^{2} w_1^2} [J_1^2 + k_{in_2}^{1} P_2 f_2]. \tag{3.28}$$

Again, eliminating value of $P_2 f_2$ from equations (25) and (28) we have

$$J_0^1 = k_{out_0}^{1} P_0 f_0 w_0^1 - \frac{k_{in_1}^{0}}{k_{out_1}^{2} w_1^2} [J_1^2 + \frac{k_{in_2}^{1}}{k_{out_2}^{3} w_2^3} [J_2^3 + k_{in_2}^{3} P_3 f_3]]. \tag{3.29}$$

Similarly eliminating value of $P_3 f_3$ from equations (26) and (29) we have

$$J_0^1 = k_{out_0}^{1} P_0 f_0 w_0^1 - \frac{k_{in_1}^{0}}{k_{out_1}^{2} w_1^2} [J_1^2 + \frac{k_{in_2}^{1}}{k_{out_2}^{3} w_2^3} [J_2^3 + \frac{k_{in_3}^{2}}{k_{out_3}^{4} w_3^4} [J_3^4 + k_{in_3}^{4} P_4 f_4]]]. \tag{3.30}$$

At steady state one can have $J_0^1 = J_1^2 = J_2^3 = \cdots = J$.

So J can be given as

$$J = \frac{k_{out_0}^{1} P_0 f_0 w_0^1 - \frac{k_{in_1}^{0} k_{in_2}^{1} k_{in_3}^{2} k_{in_4}^{3}}{k_{out_1}^{2} w_1^2 k_{out_2}^{3} w_2^3 k_{out_3}^{4} w_3^4} P_4 f_4}{1 + \frac{k_{in_1}^{0}}{k_{out_1}^{2} w_1^2} + \frac{k_{in_1}^{0} . k_{in_2}^{1}}{k_{out_1}^{2} . k_{out_2}^{3} . w_1^2 . w_2^3} + \frac{k_{in_1}^{0} k_{in_2}^{1} k_{in_3}^{2}}{k_{out_1}^{2} k_{out_2}^{3} k_{out_3}^{4} w_1^2 w_2^3 w_3^4}}. \tag{3.31}$$

For dendrimer of generation G, J can be given as

$$J = \frac{\left[k_{out_0}^{1} P_0 f_0 w_0^1 - \frac{\prod_{n=1}^{G} k_{in_n}^{n-1}}{\prod_{n=1}^{n} k_{out_n}^{n+1} w_n^{n+1}} P_G f_G \right]}{\left[1 + \sum_{n=1}^{G-1} \prod_{i=1}^{n} \frac{k_{in_i}^{i+1}}{k_{out_i}^{i+1} w_i^{i+1}} \right]}. \tag{3.32}$$

Substituting the values of local escape rates taking from equations(1)

and equations(2) into the equation (32) we get

$$J = \frac{\dot{K}^1_{out_0}(\frac{k_BT}{\hbar})exp\Big(\frac{-E}{k_BT}\Big)P_0f_0w_0^1 - (\frac{k_BT}{h})exp\Big[-\frac{(E-u_G)}{k_BT}\Big]\frac{\prod_{n=1}^{G}\dot{K}^{n-1}_{in_n}}{\prod_{n=1}^{G-1}\dot{K}^{n+1}_{out_n}w_n^{n+1}}P_Gf_G}{1+\sum_{n=1}^{G-1}exp\Big[\frac{\pm v_n}{k_BT}\Big]\prod_{i=1}^{n}\frac{\dot{K}^{i-1}_{in_i}}{\dot{K}^{i+1}_{out_i}w_i^{i+1}}} \tag{3.33}$$

From equation (33) it is clear that irrespective of the structure of the of the intermediate well the flux depends only on u_G. On the other hand every barrier height(v_i) affects the flux. Population at core P_0 and population at periphery P_G appear in the equation. So J will also depend upon these two populations. Again, degeneracy of core (f_0) and degeneracy at the peripheral generation (f_G) are also the determining factor to control the value of J. Flux towards core is just the negative as that of flux towards periphery.

3.1.6 Discussion

Here the energy transfer processes have been studied with the Eyring model at the steady state. We consider that the dendrimer is an open system and the method of calculation involves steady state thereby the expression of the flux is different from MFPT. Although the nodes of the dendrimer grows exponentially from the core, the actual local environment of the nodes and external driving, if any, will dictate the nature of the steady state. As in the previous cases we have chosen the similar parameter regimes, i.e., unless otherwise specified regarding the values of the parameters, we have taken the values of E, u_i, v_i, c, k_BT in exactly the way we did in previous section.

In cases where specific parameters have not changed they have fixed set of values as $E = 1.0$, $u = 0.001E$ to $0.1E$ for increasing (case-IV) and $0.1E$ to $0.001E$ for decreasing (case-V) cases, $v = 0.11E$ to $2.1E$ for increasing (case-II and caseIV) cases and $-0.01E$ to $-0.77E$ for decreasing (case-III and case-V) cases. $k_BT = 0.3E$ for the cases studied at fixed temperature and for simplicity all transmission coefficients have been taken as 1.0.

Fig.3.6(a) and Fig.3.6(b) show the nature of variation of flux towards the core with an increase in size of the dendrimer molecule. The flux in all cases decrease with an increase in size of the dendrimer and

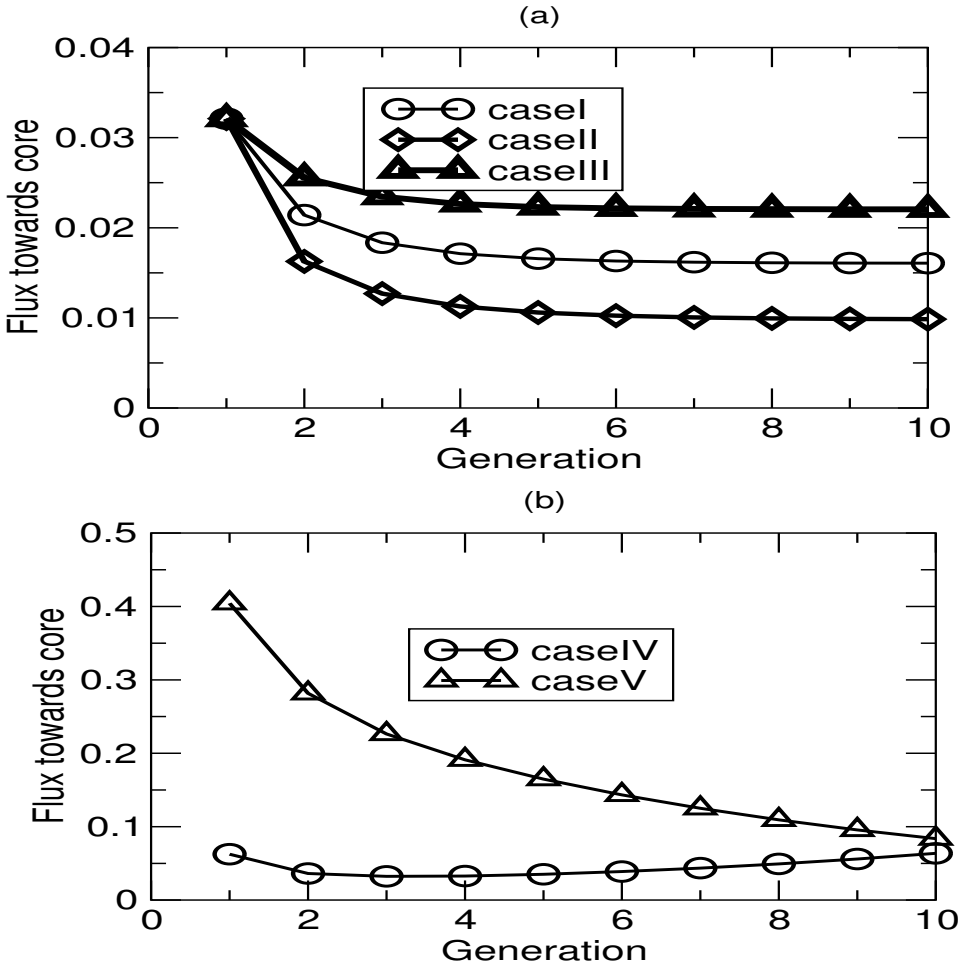

[Fig 3.6] The change of flux towards the core is shown with the size (G) of the dendrimer for (a) cases I-III, (b) cases IV-V. In case IV of (b), the flux passes through a minima. The interplay of barrier heights and well depth is reflected here.

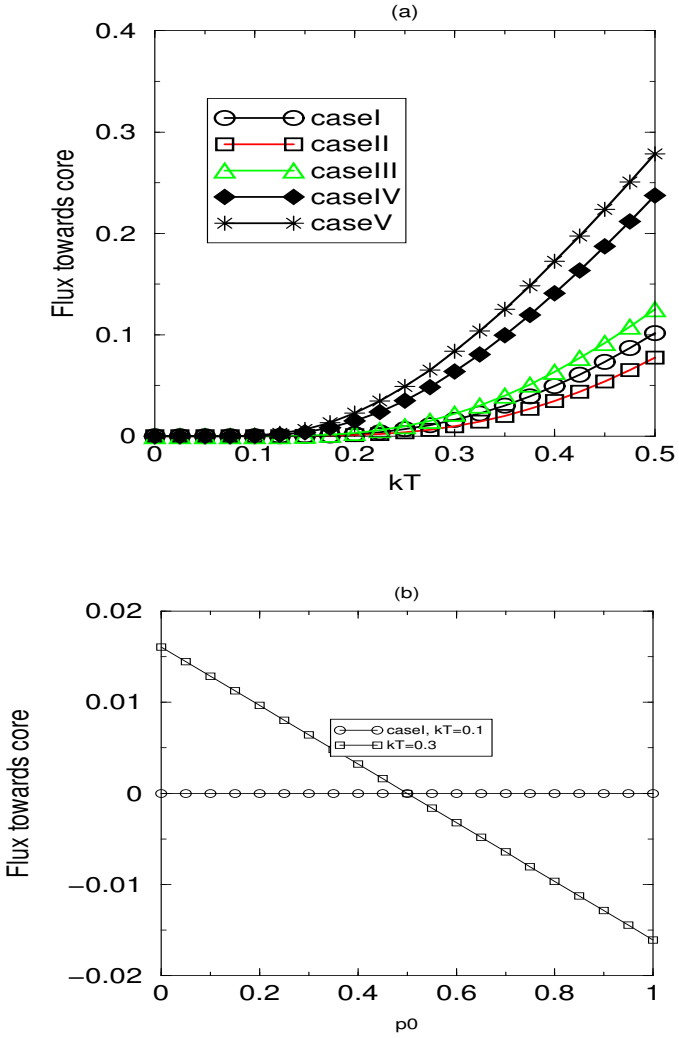

[Fig 3.7] (a) The variation of flux toward the core is shown with temperature (in units of E) for different cases of dendrimer of size (G=10). (b) The nature of variation flux towards the core is displayed with the population at the core well P_0, at two different temperatures (in units of E). When the core absorbs energy only partially at the steady state, there is a possibility of reversal of flux when $P_0 \geq 0.5$ in case I at $k_BT = 0.3E$.

attain a steady value after a critical size of the molecule. The rate of the decrease of flux with size and the steady value of the flux after a certain size depends clearly on the potential surface and local barrier heights. As in the MFPT calculation, cases (IV-V) are of a larger magnitude than in cases I-III due to superimposed energy funneling. In case IV, the local barrier heights are more than in case V and so the flux is less in case IV than in case V. The flux passes through a minimum in case IV is due to the interplay of barrier heights and superimposed energy funneling. This is because in case IV, although the barrier heights are of large magnitude, the energy difference between the core and the peripheral node is also of quite a high value.

The temperature dependence on the flux towards the core is depicted in Fig.3.7(a). The flux as usual increases with temperature non-exponentially in all cases (I-V). As in cases IV-V there is a slanting in the potential energy, cases IV and V are above cases I-III. Again, in case V the flux is higher than that in case IV because the local barrier heights are less in the former case. The effect of the barrier heights on the rate in cases I-III are also reflected in the figures where case I is above case II and below case III, which is quantitatively very similar to the result of the MFPT calculation. Again, one can find that below $k_BT = 1E$, flux is almost ten times larger than the rate from the MFPT method.

We have consider $P_0 = 0$ in all figures of flux calculation. In Fig.3.7(b) the dependence of the value of P_0 is shown on the flux. It is found that depending on the value of P_0 at a particular temperature the flux can also be negative, which is displayed for case I at two different temperatures. Depending on the other parameters of the potential surfaces and temperature, the flux can be negative for a range of nonzero values of P_0. At $k_BT \approx E$ the funneling towards core is most effective but at higher temperature when the system has enough thermal energy even to cross the the last barrier, the flux towards periphery become positive and increases due to increase in number of well and pathways (w_i^{i+1}) a near the periphery. When we control the situation in such a way that funneling effect is towards periphery (case-III and case-V) then flux towards periphery decreases with k_BT and approaches zero but remains positive for $P_0 = 0$. With some population at the core well the value at higher k_BT become negative indicating a reversal of direction of flux. Thus we can conclude that with a nonzero value of P_0 there is a possibility of reversal of direction of flux at higher temperature and direction of slanting of potential surface become ineffective.

Fig.3.8(a) and Fig3.8(b) show that with increase in the value of u_G,

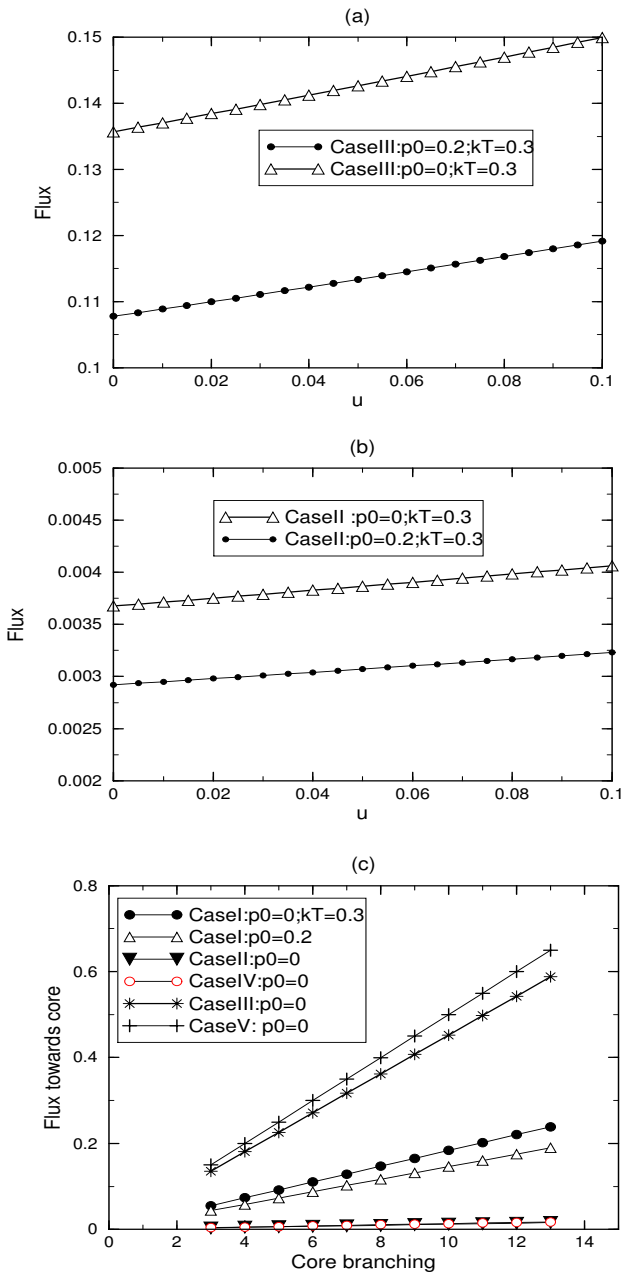

[Fig 3.8] (a) Plot of flux with $u = u_G$ the height of potential well of last generation or periphery for case III. (b) Same plot as of (a) for case II. (c)Plot of flux with core branching of dendrimer molecule of fixed generation(20). The flux towards core increases with core branching due to increase number of pathways towards core.

the flux towards the core increases which is evident from the structure of the potential surface. Fig.3.8(c) shows the nature of variation of flux with core branching when all other parameters are kept fixed. Here case-II and case-IV have similar behavior with very very slow increase of flux with increase in core branching. On the contrary, case-III and case-V have similarity with rapid increase of flux with core branching. Nevertheless, case-I has an intermediate behavior. Increase in core branching signifies an enhanced number of pathways to go towards the core. In general, it may be expected that flux towards the core will be increased with core branching. For case-II and case-IV the potential is descended towards the core. So higher core branching can not rectify the flux for these two cases so easily. For case-III and case-V the imposed slanting of potential energy are towards the periphery and thus the larger core branching is rectifying the situation more prominently. All these explains once the steady state situation is achieved.

In Fig.3.9 we have compare the flux at steady state with inverse of MFPT. Though they are quantities of two different experimantal situations the values are to some extent comparable below $k_BT = 1$. At higher temperature the flux become saturated.

In Fig.3.10 we have plotted MFPT versus core-branching. This calculation has been achieved without any approximation of 2D geometry into an effective 1D geometry. As core-branching increases the MFPT also increases exponentially. This proves that our approximation is realistic. Here all local escape rates have been set equal to unity.

3.2 Dependence of energy transport on the arrangement of pigments in Photosynthetic Unit

Pigmented algae or bacteria suspended in a liquid medium are exposed to light of known intensity and frequency to measure the rate of production of oxygen. The time lapse between the excitation procedure and the production of final product is the actual time taken by the excitation for exploration on and along the antenna molecule before being trapped. Our motivation here is to study excitation transfer by classical random walk or a first passage time problem[56]. We shall give a comparative study of excitation energy transfer in linear, square planner and circular arrangements of sites which are connected to reaction centre(RC) that is in turn connected to a trap. The trap may be considered as a charge separated state. The arrangements of nodes or sites are different than

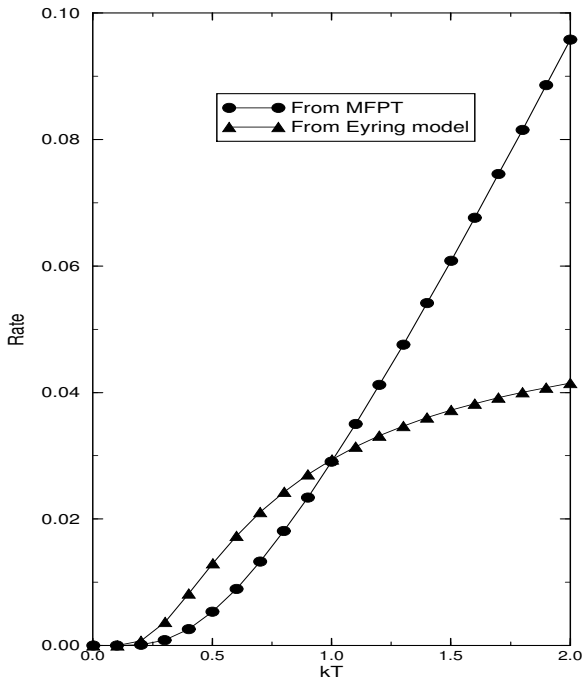

[Fig 3.9] Comparison of inverse of MFPT with flux. The two approach gave comparable results upto $k_BT = 1$ and flux at steady state become saturated at higher temperature with low value.

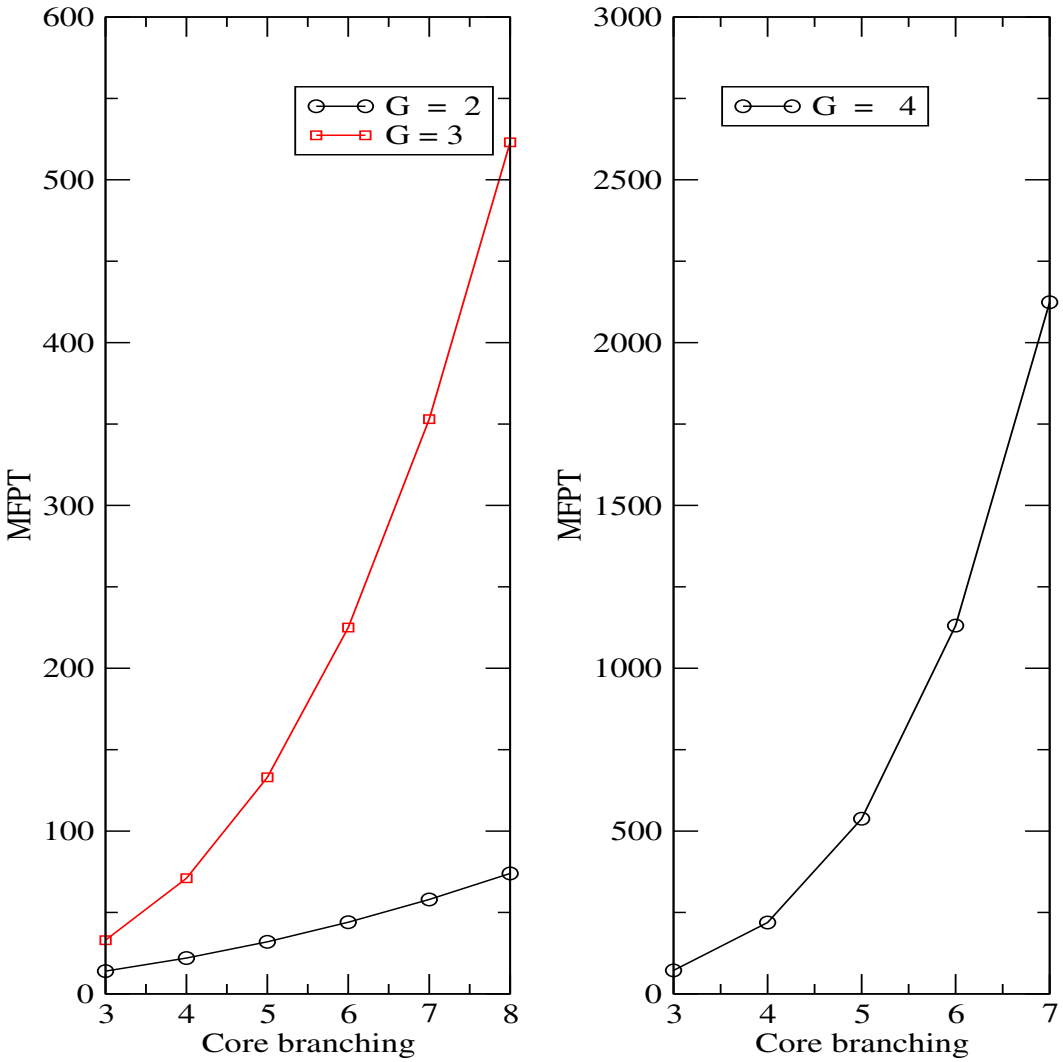

[Fig 3.10] MFPT versus core branching in actual geometry. All local escape rates are equal(=1.0).

those previously considered. Here all nodes except RC are degenerate; energy level of RC is lowered than the other nodes. An excitation can go to trap from RC at a rate of τ irreversibly. The rate of excitation transfer from pigment to RC and from RC to pigment is given by the following equation:

$$\frac{\mathrm{Rate_{inward}}}{\mathrm{Rate_{outward}}} = \exp\left(\frac{\Delta \mathrm{E_{RC}}}{\mathrm{k_B T}}\right)$$

All other local escape rates and τ are set equal to unity. The value of $\Delta E_{RC} \approx 5$ nm. We have seen how MFPT changes with size of the aggregate and temperature.

3.2.1 Equations of motion and formulation of matrices

A schematic picture of arrangements of chromophores in square planner and circular way around RC has been shown in Fig.3.11. These arrangement has been compared with a linear one. From equation of motion we have formulated the matrices for linear, square planner and circular arrangements of sites according to the theory discussed in the earlier section and we have considered the motion of excitation from RC and towards RC according to the above mentioned equation. The following are the dynamical equations and matrices:

- Case A : For the linear chain the trap is situated at end opposite to the reflecting boundary. The MFPT has been calculated for an excitation that starts at reflecting boundary. We have seen how MFPT depends upon the length of the chain.

$$\dot{P_0}(t) = \tau_1 P_1(t)$$

$$\dot{P_1}(t) = R_{21} P_2(t) - (R_{12} + T_1) P_1(t)$$

$$\ldots\ldots = \ldots\ldots + \ldots\ldots$$

$$\dot{P_i}(t) = R_{i+1\ i} P_{i+1}(t) - (R_{i\ i-1} + R_{i\ i+1}) P_i(t) (1 < i < g)$$

$$\ldots\ldots = \ldots\ldots + \ldots\ldots$$

$$\dot{P_g}(t) = R_{g-1\ g} P_{g-1}(t) - R_{g\ g-1} P_g(t) \qquad (3.34)$$

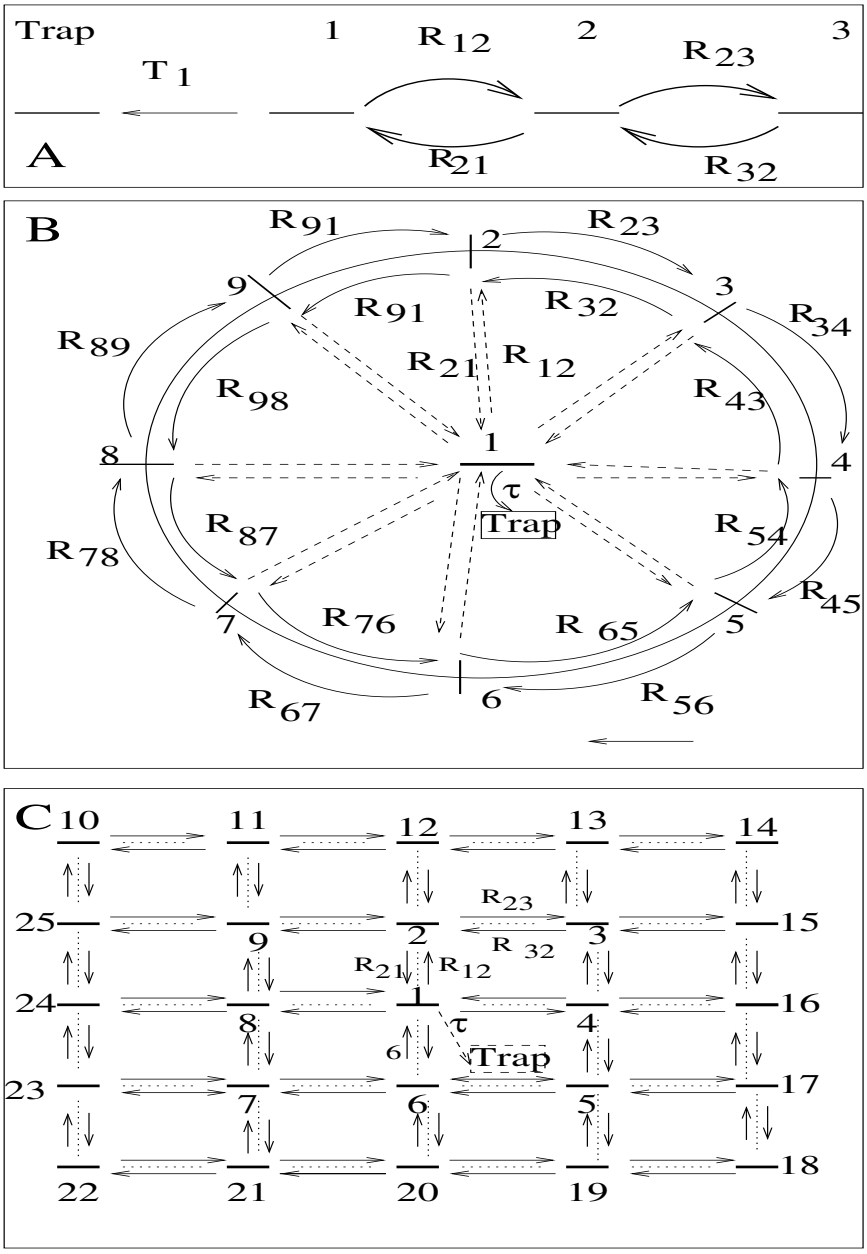

[Fig 3.11] Different arrangements of pigments in the PSU. A is for linear arrangement, B is for circular arrangement of chromophore around RC and C is for the square planner arrangement around RC.

In matrix notation we can write

$$\frac{d\hat{P(t)}}{dt} = \hat{A}\hat{P(t)}$$

where $\hat{A}$ has the form

$$\hat{A} = \begin{bmatrix} -(\tau_1 + R_{12}) & R_{21} & 0 & 0 & 0 & \cdots & 0 \\ R_{12} & -(R_{21} + R_{23}) & R_{32} & 0 & 0 & \cdots & 0 \\ 0 & R_{23} & -(R_{32} + R_{34}) & R_{43} & 0 & \cdots & 0 \\ 0 & 0 & R_{34} & -(R_{43} + R_{45}) & R_{54} & \cdots & 0 \\ \cdots & \cdots & \cdots & \cdots & \cdots & \cdots & R_{i+1\,i} \\ 0 & 0 & 0 & 0 & 0 & R_{g-1\,g} & -R_{g\,g-1} \end{bmatrix}$$

- Case B: In the case of square planner arrangement the starting point is the corner of the plane and trap is situated at the middle of the square planner unit. The form of the matrix is similar but there are four ways an excitation can move from a site. So instead of three terms there will be four R_{ij} terms.

$$\dot{P_1(t)} = -\tau_1 P_1(t) - (R_{12} + R_{14} + R_{16} + R_{18})P_1(t) + R_{21}P_2(t) + R_{41}P_4(t) + R_{61}P_6(t) + R_{81}P_8(t)$$

$$\dot{P_2(t)} = R_{12}P_1(t) + R_{32}P_3(t) + R_{92}P_9(t) + R_{122}P_{12}(t) - (R_{21} + R_{23} + R_{29} + R_{212})P_2(t)$$

$$\dot{P_3(t)} = R_{2\,3}P_2(t) + R_{13\,3}P_{13}(t) + R_{15\,3}P_{15}(t) + R_{4\,3}P_4(t) - (R_{3\,2} + R_{3\,13} + R_{3\,15}R_{3\,4})P_3(t)$$

$$\ldots\ldots\ldots = \ldots\ldots\ldots + \ldots\ldots\ldots \qquad (3.35)$$

In matrix notation we can write

$$\frac{d\hat{P(t)}}{dt} = \hat{A}\hat{P(t)}$$

where $\hat{A}$ has the form

$$\hat{A} = \begin{bmatrix} -(\tau_1 + R_{12} + R_{14} + R_{16} + R_{18}) & R_{21} & 0 \\ R_{12} & -(R_{21} + R_{23} + R_{29} + R_{212}) & R_{32} \\ R_{13} & R_{23} & -(R_{3\,15} + R_{32} + R_{34} + R_{3\,13}) \\ \cdots & \cdots & \cdots \\ \cdots & \cdots & \cdots \end{bmatrix}$$

- Case C: In the case of circular arrangement with RC in the centre the RC act as trap while the excitation starts at any equivalent site on the ring.

$$\dot{P_0}(t) = \tau_1 P_1(t)$$

$$\dot{P_1}(t) = -\tau_1 P_1(t) - \sum_{i=2}^{N} R_{1i} P_1(t) + \sum_{i=2}^{N} R_{i1} P_i(t)$$

$$\dot{P_2}(t) = R_{12} P_1(t) + R_{N2} P_N(t) + R_{32} P_3(t) - (R_{21} + R_{2N} + R_{23}) P_2(t)$$

$$\ldots\ldots = \ldots\ldots + \ldots\ldots$$

$$\dot{P_i}(t) = R_{i+1\ i} P_{i+1}(t) + R_{i-1\ i} P_{i-1}(t) + R_{1\ i} P_1(t) - (R_{i\ i-1} + R_{i\ i+1} + R_{i1}) P_i(t) (1 < i < g)$$

$$\ldots\ldots = \ldots\ldots + \ldots\ldots$$

$$\dot{P_N}(t) = R_{N-1\ N} P_{N-1}(t) + R_{2\ N} P_2(t) + R_{1\ N} P_1(t) - (R_{N\ N-1} + R_{N\ 1} + R_{N\ 2}) P_N(t) \quad (3.36)$$

In matrix notation we can write

$$\frac{d\hat{P(t)}}{dt} = \hat{A}\hat{P(t)}$$

where $\hat{A}$ has the form

$$\hat{A} = \begin{bmatrix} -(\tau_1 + \sum_{i=2}^{N} R_{1i}) & R_{21} & R_{31} & \cdots & R_{N1} \\ R_{12} & -(R_{2N} + R_{21} + R_{23}) & R_{32} & \cdots & R_{N2} \\ R_{13} & R_{23} & -(R_{31} + R_{32} + R_{34}) & \cdots & 0 \\ R_{14} & 0 & R_{34} & \cdots & 0 \\ \cdots & \cdots & \cdots & \cdots & R_{i+1\ i} \\ R_{1\ N} & R_{2\ N} & 0 & R_{N-1\ N} & -(R_{N2} + R_{N1} + R \end{bmatrix}$$

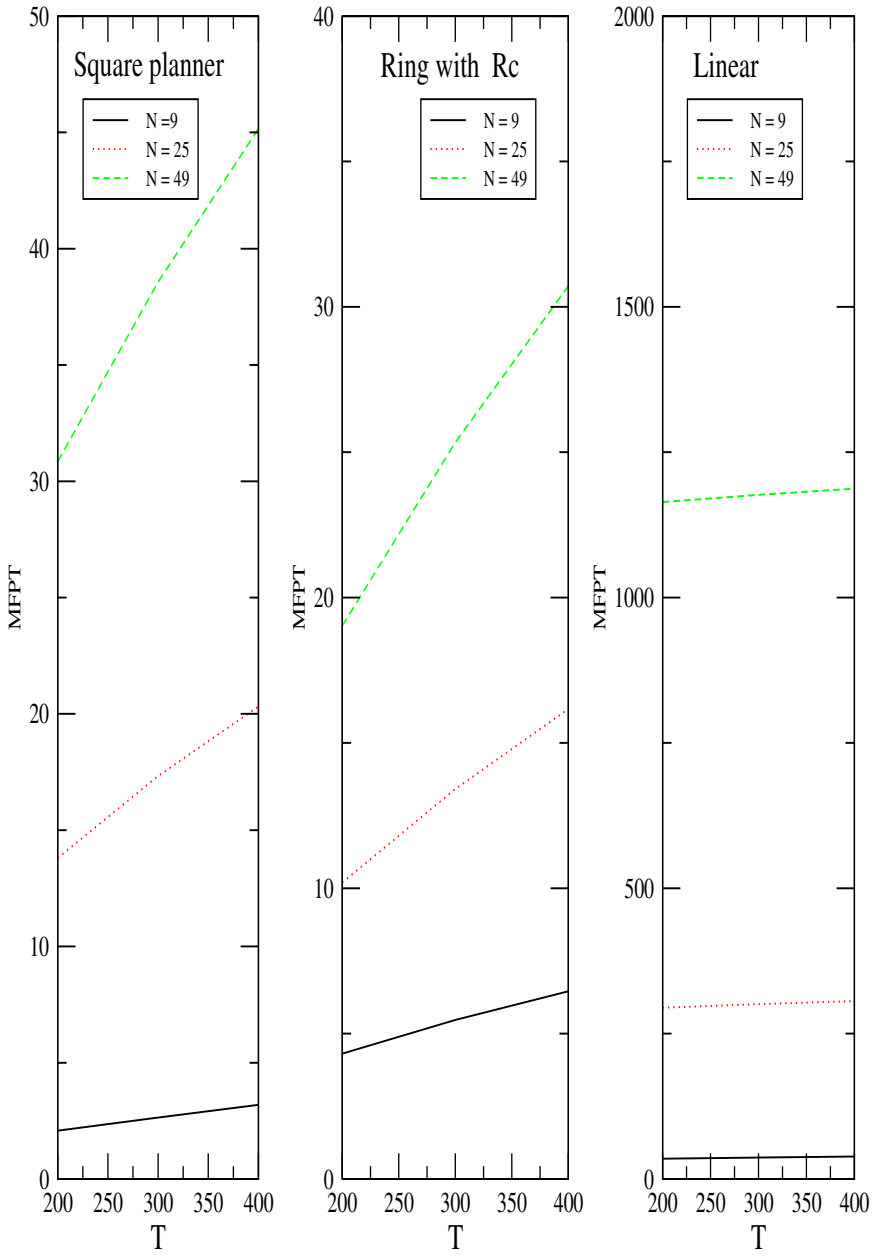

[Fig 3.12] Dependence of MFPT on size of the aggregate and temperature.

3.2.2 Discussions

We have shown the changes of MFPT with size and temperature in the Fig.3.12 on linear chain, circular arrangements with RC and on square planner arrangement of the pigment molecule. In a linear arrangement an excitation can explore on the chain for a longer time. In square planner arrangement the time for exploration is much lower and MFPT is very low. In circular arrangement with RC the MFPT is still lower. The excitation energy can transfer from peripheral sites to trap through RC in a circular arrangement very very rapidly. On increasing temperature $\text{Rate}_{\text{inward}}$ become lower. The excitation can explore for a longer period of time on and along the antenna arrangement. Thus MFPT increases with temperature. From this simplified approach we can say that excitation transfer is efficient in circular arrangement. In natural system RC is surrounded by the circular arrangement of sites presumably for efficient transfer of excitation energy.

3.3 Summary and Conclusions :

Here a statistical mechanism of energy transport in a treelike dendrimer molecule is simulated, where the variety of the local environment of the real molecule is taken into account through a gross potential energy landscape, where the thermal energy of excitation hops randomly to transport energy from periphery to the core. In this work we have assumed that each node of the dendrimer molecule is behaving as a potential well and each link between nodes is behaving as a barrier height. Then we have considered that energy is moving from one generation to other generation through thermal hopping. Then we have disposed the barrier height and potential well on and along the dendrimeric geometry in such a way that there is (i) no superimposed funneling; (ii) superimposed funneling towards core and (iii) superimposed funneling towards periphery.

We have extended the one dimensional random walk problem to dendrimeric geometry using its symmetry and we have calculated MRT and MFPT by explicit use of local escape rates and their dependence upon temperature, generation, core branching and the relative nature of potential energy landscape with classical random walk model. Eyring model of membrane permeation have been used to calculate flux of any property/energy moving from periphery to core. The dependence of flux upon temperature, generation, surface potential and core branching has been studied. From all numerical studies we find that the temperature

and branching effect have similar impact upon rate and superimposed energy funneling competes with branching. Here we have been able to compare the rates obtained from two methods of calculation viz from classical random walk model and Eyring model. We have seen that at lower temperature the rates obtained from both methods are more or less comparable though rate from MFPT has higher values at higher temperature. Out of these two methods apparently it is very difficult to conclude which one is more accurate. But if we give closure look upon individual expression of J (flux) and $\frac{1}{MFPT}$ it can be observed that in the expression of $\frac{1}{MFPT}$ each barrier height (v_i) and height of each well from core well (u_i) appear. On the other hand, in the expression of J only height of last well (u_G) appears. With this view point it may be concluded that rate from MFPT calculation is much more accurate. Although actual situation of the dendrimeric system will dictate which method is applicable. If there is only absorbing unit at the core then rate from MFPT calculation is authentic and if not then rate from Eyring model is applicable.

While the method of calculations and the physical relevance of the two approaches are quite different, it is found that the rates have a similar qualitative dependence on the parameters of the potential surfaces, the nature of the molecule, and temperature. The steady state flux calculation is a special case of the random walk problem, which can be understood as follows. If we consider a random walk problem in one dimension, the probability distribution at a different lattice point can be written as

$$\dot{P}_n = (k^n_{in_{n+1}} P_{n+1} - k^{n+1}_{out_n} P_n) - (k^{n-1}_{in_n} P_n - k^n_{out_{n-1}} P_{n-1}) = J^n_{n+1} - J^{n-1}_n.$$

When $J^n_{n+1} = J^{n-1}_n = J$, a steady state arises, i.e., $\dot{P}_n = 0$. This is a situation of steady one way flux J towards the center, $n = 0$. This steady one way flow is different from thermodynamic equilibrium, where also $\dot{P}_n = 0$, but in equilibrium there will be no one way flow of energy, i.e., all $J = 0$ to maintain the microscopic reversibility. This one way flow system is a driven open system far away from equilibrium. On the other hand, in the MFPT calculation, where the system has no influx of energy, because of the reflecting and absorbing boundary at the two ends, thereby total energy drains out of the system and no steady state can arise. For a linear lattice this drainage of energy is approximately exponentially decaying in nature but, in the driven open system, the result will be, in general, very different. A dynamical comparison between the two approaches is a little difficult because it is not an exact transformation to cast a two dimensional cayley tree geometry into an effective one dimensional

picture and the transition processes are taken in a little different way in two different approaches, in spite of the fact that the nearest neighbor interactions are only taken into account. This made us to suspect that the nearest neighbor transition process in linear dynamics is the key ingredient for this qualitative resemblance between the two results.

We have discussed some possible relations of photon localization in the different generations of the dendrimer molecule with the mean residence time and their dependence on the parameters of the system. The rate through MFPT calculations and the Eyring model and their parametric dependence on the system can be systematically explored through experiments. We think whenever there is a pulsed excitation on the periphery of the molecule, the rate from the MFPT method may be suitable. While there is a continuous supply of energy in the periphery to be used up in the center, a steady-state flow can be established and Eyring model is useful.

Excitation transfer from peripheral chlorophyll pigments to RC is very important process. In all bacterial light-harvesting systems the slowest step is the trapping excitation energy from any of the light-harvesting pigments to the RC. The trapping efficiency will be highest when maximum number of antenna pigments will be able to transfer their excitation energy to the RC. This process is optimized when the pigments are arranged in a ring. Our results also support this.

Naturally the Bchl units are arranged in a hierarchical arrangements. The Bchls that absorb at higher energy are situated far from the RC. If we go towards the RC from the outside we should come across the carotenoid, B800, B850 and B875 stepwise. So there is a gradient of energy with its direction towards the RC. So the excitation energy transfers as B800 $\rightarrow$ B850 $\rightarrow$ B875 $\rightarrow$ RC.

The gradient of the energy levels from periphery to the RC facilitate the excitation energy transfer. This gradient is created due to the arrangements of chromophores with higher excitation energies towards the periphery. Slanting of energy levels is an important aspects in energy transfer mechanism in natural as well as in artificial synthetic system.

Chapter 4

4 Dendrimer under intense laser field : a steady state study

We have considered the dendrimer super-molecule is comprised of two-level systems as monomer units on the nodes of a Cayley tree. Each unit is undergoing dissipation and driving by external laser field along with nearest neighbour interaction among the monomer units. We have studied the coherent and incoherent dynamics in the dendrimer system for the strong and weak laser field. The effect of Cayley tree geometry on the spectral properties are investigated through the intensity and width of the spectra. The origin of enhanced energy transfer mechanism of extended dendrimer in comparison to the compact one is explained.

In section 4.1 we have given an introduction of the problem. In section 4.2 we have described the model Hamiltonian and equations of motion of creation and annihilation operators of the TLS. In section 4.3 we have casted 2d dendrimeric geometry into an effective one dimensional chain for simplifying the solutions and in section 4.5 we have given the results and discussions. In section 4.6 we have given a heuristic argument to show the enhanced energy funnel type structure of the extended dendrimer. In section 4.7 and 4.8 we have given results and discussions in actual 2d geometry and outlined how dendrimer network may relevant to complex photosynthetic molecular system by showing the smooth gradient excitation from periphery to core with some manipulations of branching and also a primitive one to understand the single-molecule spectral properties. Here we have discussed only the steady-state properties.

4.1 Introduction

Dendrimers [1-8] are phenyl-acetylene units arranged in a hierarchical self-similar fashion around a core to give highly branched tree-like structure (see Fig. 1). Two kinds of dendrimers have been studied extensively. (A) Compact dendrimers : perfectly symmetric molecules with each of three legs composed of many independent Diphenyle Acetylene units (DPA); branching occurs at meta position of each benzene ring.

(B) Extended dendrimers : Molecule with un-equal legs which are composed of linear chains of DPA units with increasing length towards the center of the molecule.

Both kinds of dendrimers show the common feature of monotonic increase in intensity of absorbance with the size of dendrimer molecule since the number of units increase exponentially with increase in generation number [77]. For the extended dendrimers a shift of the lowest energy peak is observed with increase in generation number. With this observation Kopelmann et al [77] have conjectured that a superimposed energy funnel from the periphery to the core is inbuilt in the extended dendrimer. This make the extended dendrimer as a good candidate of artificial energy antenna [89]. Klafter and co-workers [76, 78] have given the mechanism of energy transfer in the dendrimer molecule as a classical random walk problem where the core unit is a trap. They have observed that the energy transfer process will be dominated by two trends (a) an entropic one, which stems from the branching at each generation, and (b) an energetic one, which is due to an energy funnel that directs the excitation towards the trap. In our work we would like to understand the experimental features from a quantum mechanical model of the dendrimer molecule. We have considered each monomer unit is a two-level system and they are interacting with the nearest neighbours. Each unit is attached with an individual bath. A laser light interacts with each unit near resonance. We have studied here how the Cayley tree geometry affects on the intensity and width of the total absorption of the dendrimer molecule. Secondly, we have studied in the steady state how the excitation energy is distributed on the various lattice points from the periphery to the core of the dendrimer molecule. The steady state we have studied here is an open system far from equilibrium. For the compact dendrimer we have found a pattern is formed on the energy profile of the various lattice points when we take the generation number very large. We have heuristically attached a special feature in the extended dendrimer model by which one can explain the energy funneling effect in the steady state situation.

4.2 Formalism : Model and the Steady state equations

Considered the schematic representation of dendrimer super-molecule as given in Fig.2.1. We have assigned each node as a two-level system. We have considered only the nearest neighbour interaction among the

nodes. Thus a node in n-th generation can only interact with one node in $(n-1)$-th generation and $(Z-1)$ nodes in $(n+1)$-th generation. The node in the zeroth generation can only interact with Z nodes of the 1st generation. The Hamiltonian of such a system can be given as

$$H = \frac{\hbar\omega_0}{2}\sigma_z^0 + \hbar g_0(\sigma_+^0 \sum_{m=1}^{Z} \sigma_-^{m11} + \sigma_-^0 \sum_{m=1}^{Z} \sigma_+^{m11}) + \sum_{m=1}^{Z}\sum_{n=1}^{G}\sum_{i=1}^{(Z-1)^{n-1}} \frac{\hbar\omega_0}{2}\sigma_z^{mni}$$

$$+ \sum_{m=1}^{Z}\sum_{n=1}^{G-1}\sum_{i=1}^{(Z-1)^{n-1}}\sum_{j=i(Z-1)-(Z-2)}^{i(Z-1)} \hbar g_n(\sigma_+^{mni}\sigma_-^{m\ n+1\ j} + \sigma_-^{mni}\sigma_+^{m\ n+1\ j}). \quad (4.1)$$

In the node index $(m\ n\ i)$, m is the index of branching of the core which varies from 1 to Z; n is the index of generation which varies from 1 to G; i is the index of the node in n-th generation of the core-branch m. g_n is the coupling coefficient between the nodes of n-th generation and $(n+1)$-th generation. We have used g for the coupling coefficients and G for generation and Z for core-branching. The second and fourth terms are the interaction energy terms between the two nodes where we have neglected the non-conserving energy terms using rotating wave approximation. ω_0 is the frequency of each two-level system.

The Hamiltonian for the interaction of a two-level system with radiation field under dipole approximation can be given by $H_{int} = -\mu.E(t)$ where μ is the dipole moment operator and $E(t)$ is the electric field. The dipole moment operator is a matrix that has off-diagonal element. If ω be the frequency of the electric field then under rotating wave approximation, $H_{int} = \frac{\hbar E_0}{2}(\sigma_+ e^{-i\omega t} + \sigma_- e^{i\omega t})$. To consider the decay of a two level system we have taken into account the master equation for reduced density operator of the two-level system as

$$\frac{d\rho}{dt} = -\frac{\gamma}{2}(1+\bar{n})(\sigma_+\sigma_-\rho - 2\sigma_-\rho\sigma_+ + \rho\sigma_+\sigma_-) + \frac{\gamma}{2}\bar{n}(2\sigma_+\rho\sigma_- - \sigma_-\sigma_+\rho - \rho\sigma_-\sigma_+) \quad (4.2)$$

where γ is the damping rate and the temperature, T is related to the thermal average photon number of the bath, $\bar{n}$ as $\bar{n} = \frac{1}{e^{\frac{\hbar\omega_0}{kT}} - 1}$. To obtained the equations of motion here we have used semi-classical approximation whereby we put $\langle\sigma_+^i\sigma_-^j\rangle = \langle\sigma_+^i\rangle\langle\sigma_-^j\rangle$. The equations of motion for the nodes attached to the core and the core itself are given by

$$\frac{d\langle\sigma_z^0\rangle}{dt} = -2ig_0[\langle\sigma_+^0\rangle \sum_{m=1}^{Z}\langle\sigma_-^{m11}\rangle - \langle\sigma_-^0\rangle \sum_{m=1}^{Z}\langle\sigma_+^{m11}\rangle]$$

$$-iE_0(\langle\sigma_+^0\rangle e^{-i\omega t} - \langle\sigma_-^0\rangle e^{i\omega t}) - \gamma(1+2\bar{n})(\langle\sigma_z^0\rangle + 1), \tag{4.3}$$

$$\frac{d\langle\sigma_+^0\rangle}{dt} = i\omega_0\langle\sigma_+^0\rangle - ig_0\langle\sigma_z^0\rangle \sum_{m=1}^{Z}\langle\sigma_+^{m11}\rangle - \frac{iE_0}{2}\langle\sigma_z^0\rangle e^{i\omega t}$$

$$-\frac{\gamma(1+2\bar{n})}{2}\langle\sigma_+^0\rangle, \tag{4.4}$$

$$\frac{d\langle\sigma_z^{m11}\rangle}{dt} = -2ig_0[\langle\sigma_+^{m11}\rangle\langle\sigma_-^0\rangle - \langle\sigma_-^{m11}\rangle\langle\sigma_+^0\rangle]$$

$$-2ig_1[\langle\sigma_+^{m11}\rangle \sum_{j=1}^{Z-1}\langle\sigma_-^{m2j}\rangle - \langle\sigma_-^{m11}\rangle \sum_{j=1}^{Z-1}\langle\sigma_+^{m2j}\rangle]$$

$$-iE_0[\langle\sigma_+^{m11}\rangle e^{-i\omega t} - \langle\sigma_-^{m11}\rangle e^{i\omega t}] - \gamma(1+2\bar{n})(\langle\sigma_z^{m11}\rangle + 1) \tag{4.5}$$

and

$$\frac{d\langle\sigma_+^{m11}\rangle}{dt} = i\omega_0\langle\sigma_+^{m11}\rangle - ig_0\langle\sigma_z^{m11}\rangle\langle\sigma_+^0\rangle - ig_1\langle\sigma_z^{m11}\rangle \sum_{j=1}^{Z-1}\langle\sigma_+^{m2j}\rangle$$

$$-\frac{iE_0}{2}\langle\sigma_z^{m11}\rangle e^{i\omega t} - \frac{\gamma(1+2\bar{n})}{2}\langle\sigma_+^{m11}\rangle. \tag{4.6}$$

The equations of motion for the bulk nodes and the nodes of the periphery are as follows :

$$\frac{d\langle\sigma_z^{pmk}\rangle}{dt} = -2ig_m[\langle\sigma_+^{pmk}\rangle \sum_{j=k(Z-1)-(Z-2)}^{k(Z-1)}\langle\sigma_-^{p\ \ m+1\ \ j}\rangle -$$

$$\langle\sigma_-^{pmk}\rangle \sum_{j=1}^{Z-1}\langle\sigma_+^{p\ \ m+1\ \ j}\rangle]$$

$$-2ig_{m-1}[\langle\sigma_+^{pmk}\rangle(\langle\sigma_-^{p\ \ m-1\ \ \frac{k+(Z-2)}{Z-1}}\rangle - \langle\sigma_-^{pmk}\rangle\langle\sigma_+^{p\ \ m-1\ \ \frac{k+(Z-2)}{Z-1}}\rangle]$$

$$-iE_0[\langle\sigma_+^{pmk}\rangle e^{-i\omega t} - \langle\sigma_-^{pmk}\rangle e^{i\omega t}] - \gamma(1+2\bar{n})(\langle\sigma_z^{pmk}\rangle + 1) \tag{4.7}$$

and

$$\frac{d\langle\sigma_+^{pmk}\rangle}{dt} = i\omega_0\langle\sigma_+^{pmk}\rangle - ig_{m-1}\langle\sigma_+^{p\ \ m-1\ \ \frac{k+(Z-2)}{Z-1}}\rangle\langle\sigma_z^{pmk}\rangle$$
$$-ig_m\langle\sigma_z^{pmk}\rangle\sum_{j=k(Z-1)-(Z-2)}^{k(Z-1)}\langle\sigma_+^{p\ \ m+1\ \ j}\rangle$$
$$-\frac{iE_0}{2}\langle\sigma_z^{pmk}\rangle e^{i\omega t} - \frac{\gamma(1+2\bar{n})}{2}\langle\sigma_+^{pmk}\rangle. \tag{4.8}$$

For the nodes in the periphery we put $g_m = 0$, where the generation number, m can have the maximum value i.e. $m = G$. By introducing the slowly varying quantity $s^i_{\pm z}$ defined by $\langle\sigma_+^{pmk}\rangle = s_+^{pmk}e^{i\omega t}, \langle\sigma_-^{pmk}\rangle = s_-^{pmk}e^{-i\omega t}$, and $\langle\sigma_z^{pmk}\rangle = s_z^{pmk}$ and substituting these quantities into the above equations of the core and the nodes attached o the core and putting $\Delta = \omega_0 - \omega$ we obtain

$$\frac{ds_z^0}{dt} = -2ig_0[s_+^0\sum_{m=1}^{Z}s_-^{m11} - s_-^0\sum_{m=1}^{Z}s_+^{m11}]$$
$$-iE_0(s_+^0 - s_-^0) - \gamma(1+2\bar{n})(s_z^0+1), \tag{4.9}$$
$$\frac{ds_+^0}{dt} = i\Delta s_+^0 - ig_0 s_z^0\sum_{m=1}^{Z}s_+^{m11} - \frac{iE_0}{2}s_z^0 - \frac{\gamma(1+2\bar{n})}{2}s_+^0, \tag{4.10}$$

$$\frac{ds_z^{m11}}{dt} = -2ig_0[s_+^{m11}s_-^0 - s_-^{m11}s_+^0] - 2ig_1[s_+^{m11}\sum_{j=1}^{Z-1}s_-^{m2j} - s_-^{m11}\sum_{j=1}^{Z-1}s_+^{m2j}]$$
$$-iE_0[s_+^{m11} - s_-^{m11}] - \gamma(1+2\bar{n})(s_z^{m11}+1). \tag{4.11}$$

$$\frac{ds_+^{m11}}{dt} = i\Delta s_+^{m11} - ig_0 s_z^{m11}s_+^0 - ig_1 s_z^{m11}\sum_{j=1}^{Z-1}s_+^{m2j}$$
$$-\frac{iE_0}{2}s_z^{m11} - \frac{\gamma(1+2\bar{n})}{2}s_+^{m11}. \tag{4.12}$$

The equations of motion for the bulk and periphery are as follows :

$$\frac{ds_z^{pmk}}{dt} = -2ig_m[s_+^{pmk}\sum_{j=k(Z-1)-(Z-2)}^{k(Z-1)}s_-^{p\ \ m+1\ \ j} -$$
$$s_-^{pmk}\sum_{j=k(Z-1)-(Z-2)}^{k(Z-1)}s_+^{p\ \ m+1\ \ j}$$

$$-2ig_{m-1}[s_+^{pmk}(s_-^{p\ \ m-1\ \ \frac{k+(Z-2)}{Z-1}} - s_-^{pmk}s_+^{p\ \ m-1\ \ \frac{k+(Z-2)}{Z-1}}]$$
$$-iE_0[s_+^{pmk} - s_-^{pmk}] - \gamma(1+2\bar{n})(s_z^{pmk}+1) \tag{4.13}$$

and

$$\frac{ds_+^{pmk}}{dt} = i\Delta s_+^{pmk} - ig_{m-1}s_+^{p\ \ m-1\ \ \frac{k+(Z-2)}{Z-1}}s_z^{pmk}$$
$$-ig_m s_z^{pmk}s_+^{pmk}\sum_{j=1}^{Z-1} s_+^{p\ \ m+1\ \ j}$$
$$-\frac{iE_0}{2}s_z^{pmk} - \frac{\gamma(1+2\bar{n})}{2}s_+^{pmk}. \tag{4.14}$$

For the steady state we have put $\frac{ds_{\pm z}{}^{pmk}}{dt} = 0$. Here we have solved the steady state and time dependent equations without resorting to any simplification as in our earlier work. As the core node has a very important role to play an exact solution shall have some nontrivial features with respect to the antenna property of the system.

The steady state solution for the core node is

$$s_+^0 = \frac{ig_0\sum_{m=1}^{Z} s_+^{m11} + \frac{iE_0}{2}}{i\Delta - \frac{\gamma(1+2\bar{n})}{2}}s_z^0 \tag{4.15}$$

with

$$s_z^{0\,2} + s_z^0 + 2s_+^0 s_-^0 = 0. \tag{4.16}$$

For the first generation node the equations become

$$s_+^{m11} = \frac{ig_0 s_+^0 + ig_m\sum_{j=1}^{(Z-1)} s_+^{m2j} + \frac{iE_0}{2}}{i\Delta - \frac{\gamma(1+2\bar{n})}{2}}s_z^{m11}, \tag{4.17}$$

$$s_z^{m11\,2} + s_z^{m11} + 2s_+^{m11}s_-^{m11} = 0. \tag{4.18}$$

For the bulk and the peripheral nodes the equations become

$$s_+^{pmk} = \frac{ig_{m-1}s_+^{pm-1\frac{k+(Z-2)}{(Z-1)}} + ig_m\sum_{j=k(Z-1)-(Z-2)}^{k(Z-1)} s_+^{pm+1j} + \frac{iE_0}{2}}{i\Delta - \frac{\gamma(1+2\bar{n})}{2}}s_z^m, \tag{4.19}$$

$$s_z^{pmk2} + s_z^{pmk} + 2s_+^{pmk} s_-^{pmk} = 0. \tag{4.20}$$

where for the peripheral nodes $m = G$, $g_m = g_G = 0$. The equations were solved without any simplification.

4.3 Casting Two Dimensional Arrangements Into Effective One Dimension

Now from the symmetry of the dendrimer molecule it can be considered that the property exhibited by a node is the same as the other nodes in a particular generation. In other-words we cast these equations of two dimensional arrangement into an equivalent one dimensional interactions of nodes. Under this condition the generalised equation of motion becomes :

$$\dot{\langle\sigma_z^0\rangle} = -6ig_0[\langle\sigma_+^0\rangle\langle\sigma_-^1\rangle - \langle\sigma_-^0\rangle\langle\sigma_+^1\rangle] - iE_0[\langle\sigma_+^0\rangle e^{-i\omega t} - \langle\sigma_-^0\rangle e^{i\omega t}] - \gamma(1+2\bar{n})[\langle\sigma_z^0\rangle + 1], \tag{4.21}$$

$$\dot{\langle\sigma_+^0\rangle} = i\omega_0\langle\sigma_+^0\rangle - 3ig_0\langle\sigma_z^0\rangle\langle\sigma_+^1\rangle - \frac{iE_0}{2}\langle\sigma_z^0\rangle e^{i\omega t} - \frac{\gamma(1+2\bar{n})}{2}\langle\sigma_+^0\rangle, \tag{4.22}$$

$$\begin{aligned}\dot{\langle\sigma_z^m\rangle} = &-4ig_m[\langle\sigma_+^m\rangle\langle\sigma_-^{m+1}\rangle - \langle\sigma_-^m\rangle\langle\sigma_+^{m+1}\rangle] - 2ig_{m-1}[\langle\sigma_+^m\rangle\langle\sigma_-^{m-1}\rangle - \langle\sigma_-^m\rangle\langle\sigma_+^{m-1}\rangle] \\ &-iE_0[\langle\sigma_+^m\rangle e^{-i\omega t} - \langle\sigma_-^m\rangle e^{i\omega t}] - \gamma(1+2\bar{n})[\langle\sigma_z^m\rangle + 1],\end{aligned} \tag{4.23}$$

and

$$\begin{aligned}\dot{\langle\sigma_+^m\rangle} = &i\omega_0\langle\sigma_+^m\rangle - ig_{m-1}\langle\sigma_+^{m-1}\rangle\langle\sigma_z^m\rangle - 2ig_m\langle\sigma_z^m\rangle\langle\sigma_+^{m+1}\rangle - \frac{iE_0}{2}\langle\sigma_z^m\rangle e^{i\omega t} \\ &-\frac{\gamma(1+2\bar{n})}{2}\langle\sigma_+^m\rangle.\end{aligned} \tag{4.24}$$

At the boundary $g_G = 0$. Here $\langle\sigma_{+,-,z}^m\rangle$ corresponds to the property $\langle\sigma_{+,-,z}\rangle$ of the jth generation.

Next we have calculated the steady state solution; the solution that is valid long after the transients associated with the turn on of the driving field have been died out. By introducing the slowly varying quantity $s_{\pm_z}^i$ defined by $\langle\sigma_+^i\rangle = s_+^i e^{i\omega t}$, $\langle\sigma_-^i\rangle = s_-^i e^{-i\omega t}$, and $\langle\sigma_z^i\rangle = s_z^i$ and substituting these quantities into the above equations and putting $\dot{s}_+^i = 0$, $\dot{s}_z^i = 0$ and $\dot{s}_-^i = 0$ we have

$$s_+^0 = \frac{3ig_0 s_+^1 + \frac{iE_0}{2}}{i\Delta - \frac{\gamma(1+2\bar{n})}{2}} s_z^0, \tag{4.25}$$

$$s_z^{0\,2} + s_z^0 + 2s_+^0 s_-^0 = 0. \tag{4.26}$$

For the bulk and the boundary the equations become

$$s_+^m = \frac{ig_{m-1}s_+^{m-1} + 2ig_m s_+^{m+1} + \frac{iE_0}{2}}{i\Delta - \frac{\gamma(1+2\bar{n})}{2}} s_z^m, \tag{4.27}$$

$$s_z^{m\,2} + s_z^m + 2s_+^m s_-^m = 0, \tag{4.28}$$

where for $m = G$, $g_m = g_G = 0$.

4.4 Steady State Absorption Spectra

To obtain the absorption line shape, E of a monomer unit, we need to calculate the rate at which quanta are absorbed from the external field (EF). This can be expressed as

$$E = \frac{1}{(\epsilon_2 - \epsilon_1)}\{\epsilon_2[\dot{W}_2(t)]_{EF} + \epsilon_1[\dot{W}_1(t)]_{EF}\} = \langle\dot{\sigma_z}(t)\rangle \tag{4.29}$$

where $[\dot{W}_2(t)]_{EF}([\dot{W}_1(t)]_{EF})$ and $\epsilon_2(\epsilon_1)$ are the rate of change of occupation probabilities and energies of levels 2(1), respectively induced by the external field. Now in the Schrödinger picture

$$[\langle\dot{\sigma_z}(t)\rangle]_{EF} = iE_0\{\langle\sigma_+(t)\rangle e^{-i\omega t} - \langle\sigma_-(t)\rangle e^{i\omega t}\}. \tag{4.30}$$

Thus E becomes

$$E = -2|\ E_0\ |^2 Im(\frac{\langle\sigma_+(t)\rangle}{E_0}e^{-i\omega t}). \tag{4.31}$$

The steady state limit of $\langle\sigma_+(t)\rangle$ is

$$\langle\sigma_+(t)\rangle = s_+ e^{-i\omega t}. \tag{4.32}$$

Thus the steady state absorbance is

$$E = 2|\ E_0\ |^2 Im(\frac{s_+}{E_0}). \tag{4.33}$$

Now if E^m is the absorbance of a monomer unit of the m-th generation the total absorbance A is calculated as

$$A = E^0 + \{\sum_{m=1}^{G} 3.2^{(m-1)}E^m\} \tag{4.34}$$

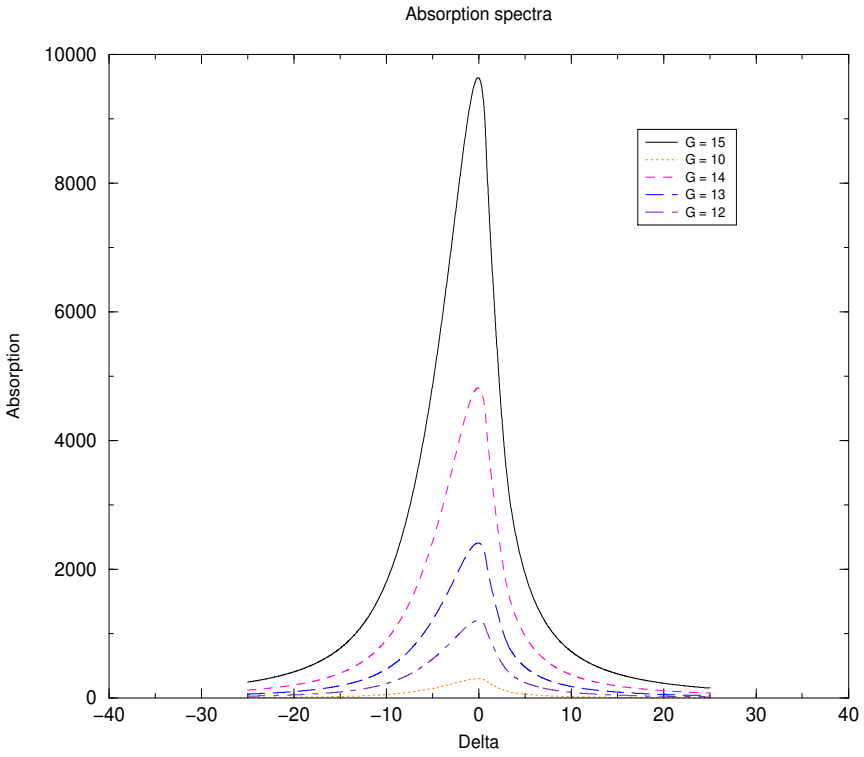

[Fig 4.1] : Variation of intensity of total absorption spectra for different generations.

4.5 Results and Discussions :

When the interaction terms (g) are zero the curve have purely Lorentzian shape and it is symmetric about $\Delta = 0$. When the g values are increased the curve much more deviate from its symmetric nature (see Fig.4.1). In all numerical plots we have taken $\bar{n} = 0$; because if $\omega_0 \simeq 320$ nm at normal temperature $\bar{n} \simeq 10^{-10}$. In all figures we have shown $\gamma = 1.0$, which means all frequency parameters taken in the plots g,E_0, and Δ are dimensionless scaled quantity to represent $\frac{g}{\gamma}$, $\frac{E_0}{\gamma}$, $\frac{\Delta}{\gamma}$ respectively.

The change in the set of values of g and E_0 changes the width and intensity of absorption spectra. For fixed values of g and E_0 the intensity of the total absorption curve increases with increase in the generation number (see Fig.4.1). This is due to exponential increase of number of nodes (or absorbing units) with increase of generation number. This result is consistent with the experimental result [77]. It was observed spectroscopically that optical absorbance increase monotonically with size of dendrimer molecule. The full-width at half maxima (FWHM) was calculated using XMGR software package with non-linear curve fitting

with tolerance = 1e-13. Since large values of g largely deviates the curve from Lorentzian we confine ourselves to that region of g values where the error become minimum. For fixed values of E_0 and for a dendrimer molecule of fixed generation (G) the FWHM vary with g following the equation

$$FWHM(g) = A_0 exp[A_1 g^{A_2}] \tag{4.35}$$

where A_0 , A_1, A_2 constant for fixed generation (see Fig.4.2). All g values (g_0, g_1, g_3.. $= g$) are taken as equal. These values become generation independent when generation $G \geq 5$. For large generation the values are $A_0 = 7.14178$, $A_1 = 0.0210268$ and $A_2 = 2.5141$ become fixed.

The variation of FWHM with generation (G) has been observed keeping E_0 and interaction terms (g) fixed. The curve follows the equation

$$FWHM(G) = A_0 - A_1 exp(-A_2 G) \tag{4.36}$$

where A_0 , A_1, A_2 are constant dependent on interaction term (g) (see Fig.4.3). Here also we have taken $g_0 = g_1 = \ldots = g_n = g$. The remarkable feature is that after certain generation, width becomes saturated. Fig.4.2 shows that the dependence of FWHM with interaction terms (g) are unaltered after $G = 5$. Fig.4.3 shows that FWHM saturates after some large generation. The coupling constants (g) are playing the same role as the damping mechanism for absorption spectra for a two-level system. For a particular node assigned as two-level system, other nodes are acting as a bath. Here for higher generation $G \geq 5$ the number of nodes are so large that any further increment in generation (G) remains the damping mechanism unaltered. This is also supported from Fig.4.2 of variation of FWHM vs generation where width becomes saturated after certain G value.

The s_z values of a two-level system signifies population inversion or it is a measure of excitation. This means by plotting s_z^i values versus generation number we can study the excitation energy distribution at steady state (see Fig.4.5 and Fig.4.6). For very large generation we have found a pattern in excitation energy is formed (see Fig.4.4). This is a co-operative self organization phenomenon which has been found in the steady states of enumerable open systems.

Our previous calculation for studying variation of FWHM involved all g values (g_1, g_2....g_G) same. This may not be the ideal situation. The size of dendrimer molecule and its diameter vary non-linearly as we go, for example, from D-4 to D-94. The distance between zeroth generation and 1st generation =0.85 nm, between 2nd and 3rd generation 0.55 nm, 3rd and 4th generation 0.4 nm, 4th and 5th generation is 0.50 nm. So

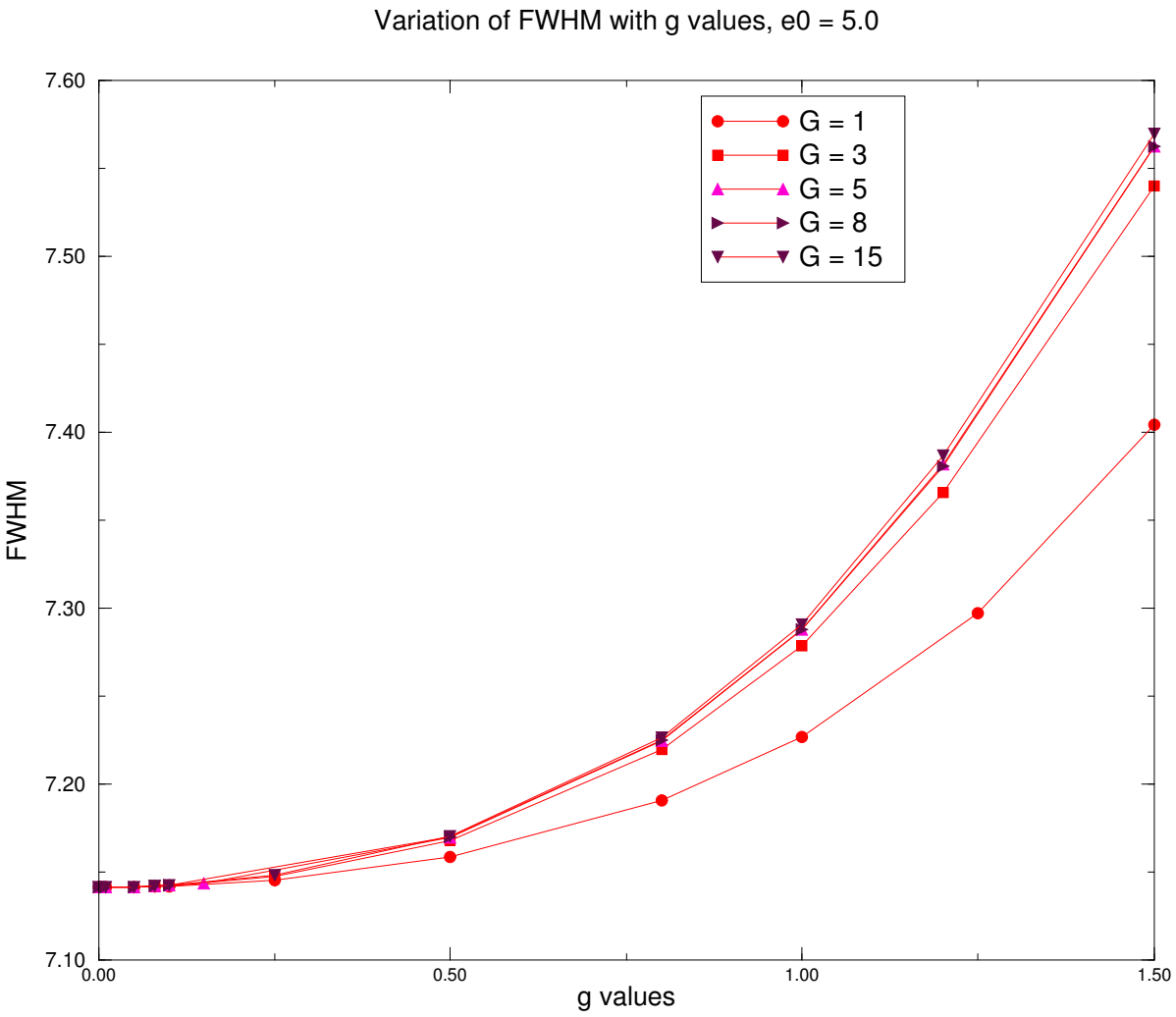

[Fig 4.2] : Variation of FWHM vs coupling constants; the curve follows the equation $FWHM(g) = A_0 exp(A_1 g^{A_2})$. A_0, A_1, A_2 are constants depending upon G. After $G \simeq 5$, these values become independent of G.

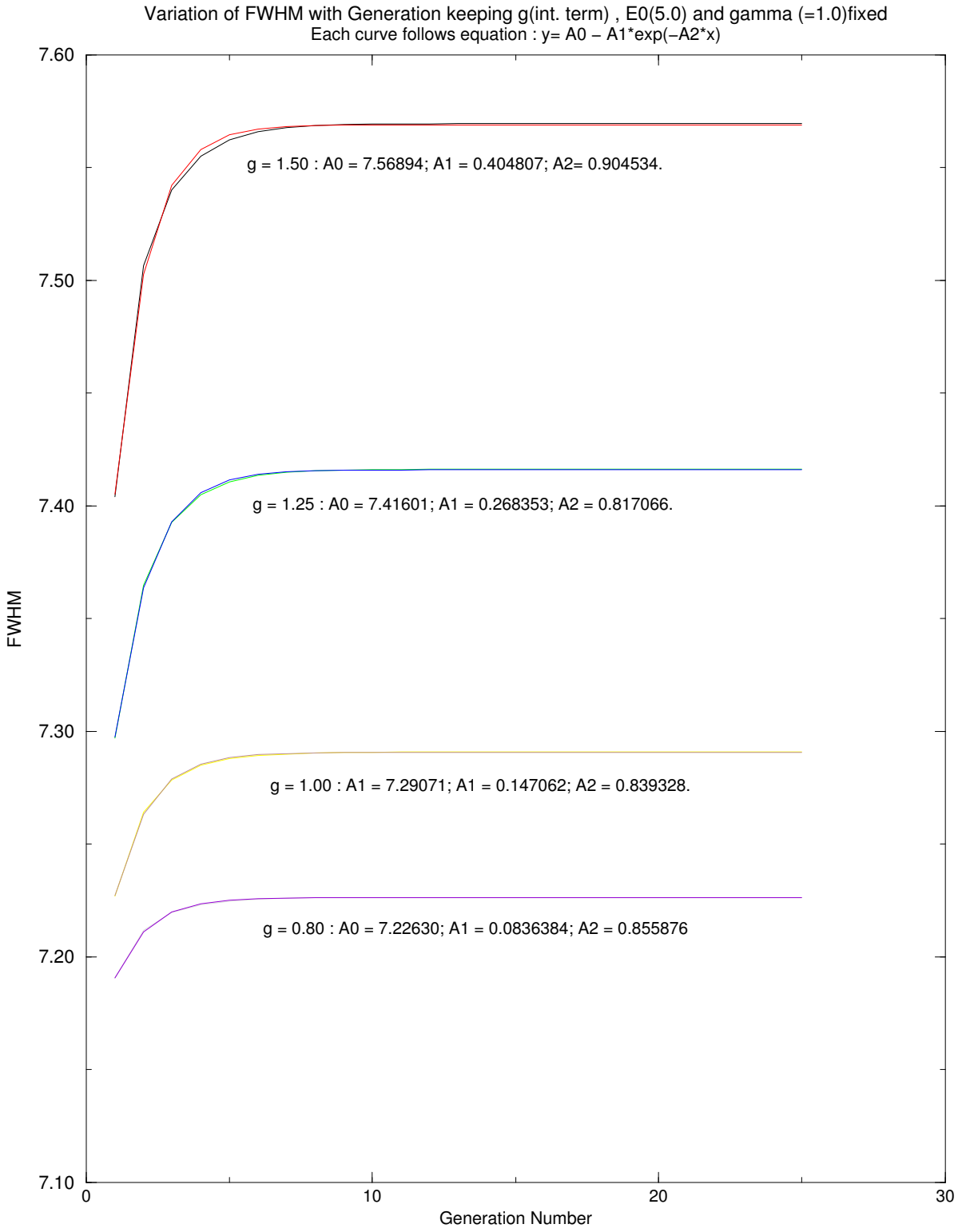

[Fig 4.3] : Variation of FWHM vs Generation; each curve fits with $FWHM(G) = A_0 - A_1 exp(-A_2 G)$. A_0, A_1, A_2 are constants. These are dependent upon g.

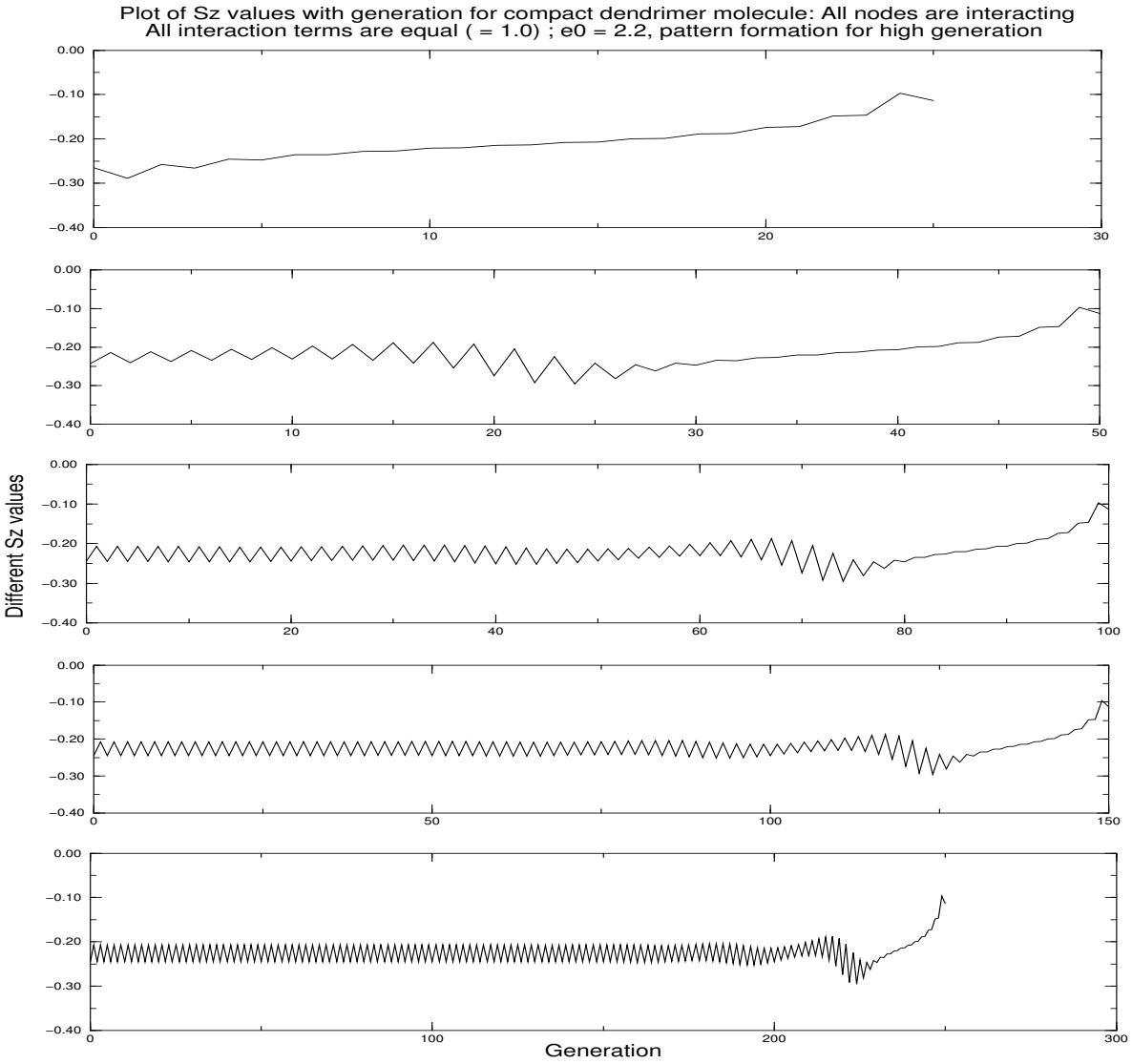

[Fig 4.4] : Pattern formation for higher generation

the distances between successive generation decreases as we go towards periphery. This means the interaction should increase between the nodes of successive generation as we go towards the periphery. This should be the realistic situation. Since we have taken only nearest neighbour interaction we have taken into account the geometrical effect in-terms of number of interactions. So variation of interaction terms will reflect the changes of local environment of a specific node. So g will carry some sense about local electrical environment with geometrical informations. We have made observation by two ways.

(1) By interacting all the nodes of the dendrimer molecule with light.

(2) By interacting only the peripheral nodes with light.

For each of the above processes we have changed the coupling constants in specific ways : (a) keeping all g values ($g_0 = g_1 = \ldots = g$) same, (b) decreasing g exponentially ($g_0 \ldots$ to $\ldots g_G$) with generation number, (c) increasing g exponentially ($g_0 \ldots$ to $\ldots g_G$) with generation number.

In the behaviour of excitation energy s_z^i at a particular generation, i (say), the general behaviour is the interplay between interaction terms (g) and the intensity of the external electric fields. In other-words, the energy and geometry (in terms of dipolar interaction terms) are the key factors to control the preferred node for absorption of maximum energy at steady state. We have listed the figures in [Fig 4.5] to demonstrate the following features.

1. When all nodes are interacting with light :

   In this case we have observed that for $E_0 \gg g$ the s_z values are almost same. Again within short range of values of s_z it has been observed that periphery is the preferred position. Under this situation the s_z values are approximately g independent. When $E_0 \simeq g$ the preferred position for excitation energy fluctuates and the trends are difficult to generalise. When $E_0 \ll g$ core and bulk are positions for maximum excitation when g are same or decreased exponentially. $(G-1)$-th generation is the preferred position when g are increased exponentially. Here a smooth increase of excitation energy from core to $(G-1)$-th generation is observed.

2. Only peripheral nodes are interacting with light :

   In this case all figures indicate that the dependence of excitation energy distribution on E_0 value is comparatively less. When coupling

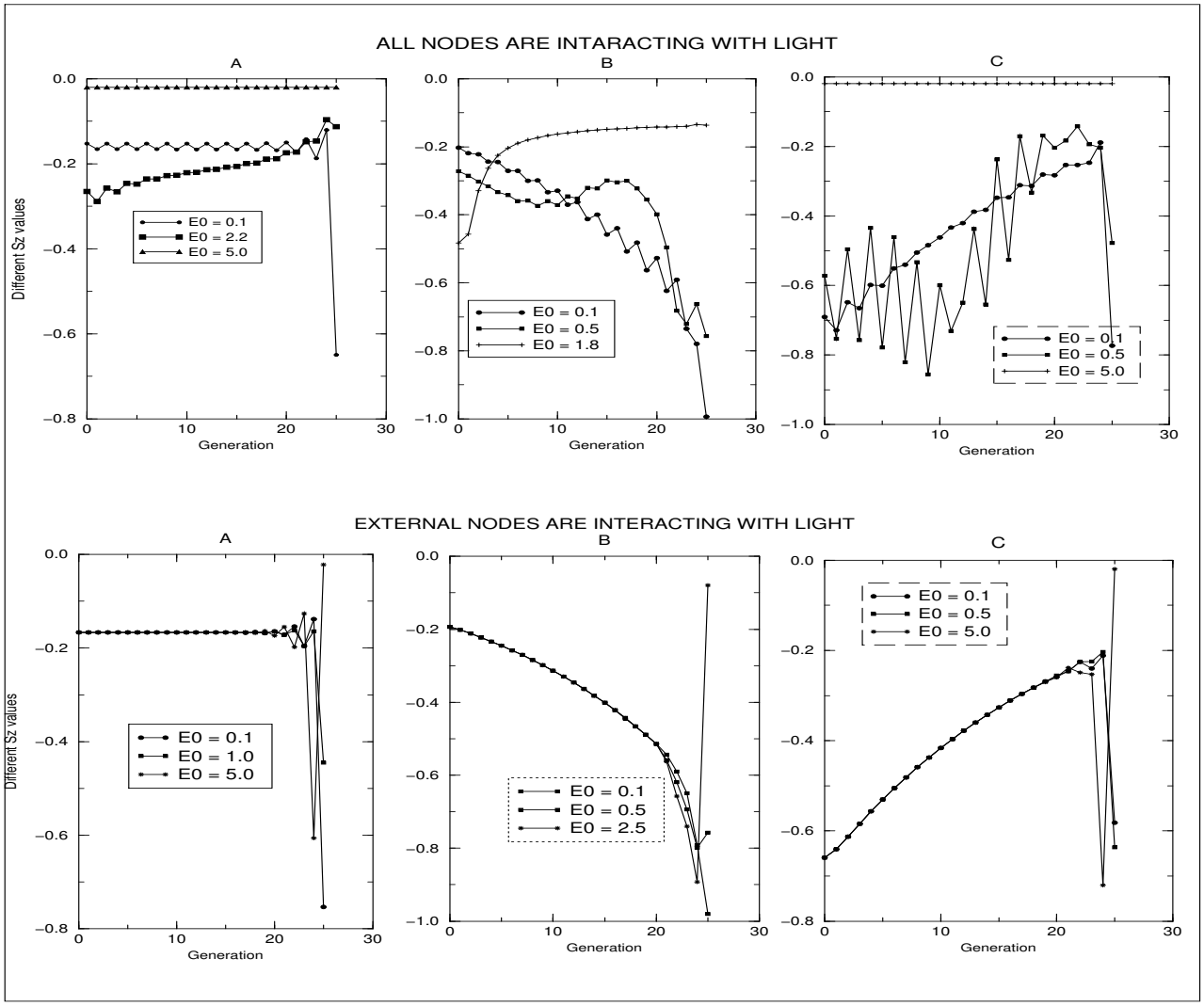

[Fig 4.5] : Changes of S_z values under different conditions for compact dendrimer. In both upper part and lower part (A) All g values are kept fixed. (B) g are $(g_0 \dots g_n$) decreased exponentially. (C) g are $(g_0 \dots g_n$) increased exponentially. **Upper part :** all nodes are interacting with light. At $E_0 \gg g$ almost all nodes are equally excited. At $E_0 \simeq g$ intermediate bohaviour (in (B) core and in (A),(C) periphery are preferred position for excitation). At $E_0 \ll g$, in (A) core and bulk, in (B) core, and in (C) $(G-1)$ th generation are absorbing maximum energy. **Lower part :** only peripheral nodes are interacting with light. At $E_0 \gg g$, $E_0 \ll g$ and $E_0 \gg g$ in all the curve it is observed that s_z are almost same. Peripheral nodes shows different behaviour when$E_0 \gg g$ only. In (B) when $E_0 \ll g$, the steady increase of s_z values shows compact dendrimer can act as energy antenna!

constants are kept fixed the s_z values remains fixed throughout the entire generation. When g's are decreased exponentially from core to the periphery the s_z values decrease towards the peripheral node and the s_z values increase towards the periphery when coupling constants are increased exponentially to that direction. This means for compact dendrimer if we somehow expose only peripheral nodes towards light (introducing some photochemical sensor group) the excitation will remain in the periphery provided interactions between nodes increase towards periphery ($g_0 < g_1 < g_2 \ldots < g_G$). This result is more realistic for localized excitation.

4.6 A heuristic argument to show the enhanced energy funnel type structure of the Extended Dendrimer:

For extended dendrimer the legs are formed by increasing number of monomer units as we go from periphery to the core. So we can simply assume that the extra monomer units are just increasing the strength of the interaction between nodes of two successive generations. The strength of the interaction is maximum at core legs and minimum at periphery. We have just multiplied the original coupling constants with the number of interactions present between the nodes of two successive generation. Any other complicated behaviour are not considered here. Under this circumstances the steady state equations become :

$$s_+^0 = \frac{3iG_0g_0s_+^1 + \frac{iE_0}{2}}{i\Delta - \frac{\gamma(1+2\bar{n})}{2}}s_z^0 \tag{4.37}$$

$$s_z^{0\,2} + s_z^0 + 2s_+^0 s_-^0 = 0 \tag{4.38}$$

For the bulk and the boundary the equation becomes

$$s_+^m = \frac{iG_{m-1}g_{m-1}s_+^{m-1} + 2iG_mg_ms_+^{m+1} + \frac{iE_0}{2}}{i\Delta - \frac{\gamma(1+2\bar{n})}{2}}s_z^m \tag{4.39}$$

$$s_z^{m\,2} + s_z^m + 2s_+^m s_-^m = 0 \tag{4.40}$$

and $G_m = \{G - (m+1)\}$, is the extra interactions between m and $(m+1)$ generation with the condition $G_m \geq 1$. Note that $g_G = 0$. We

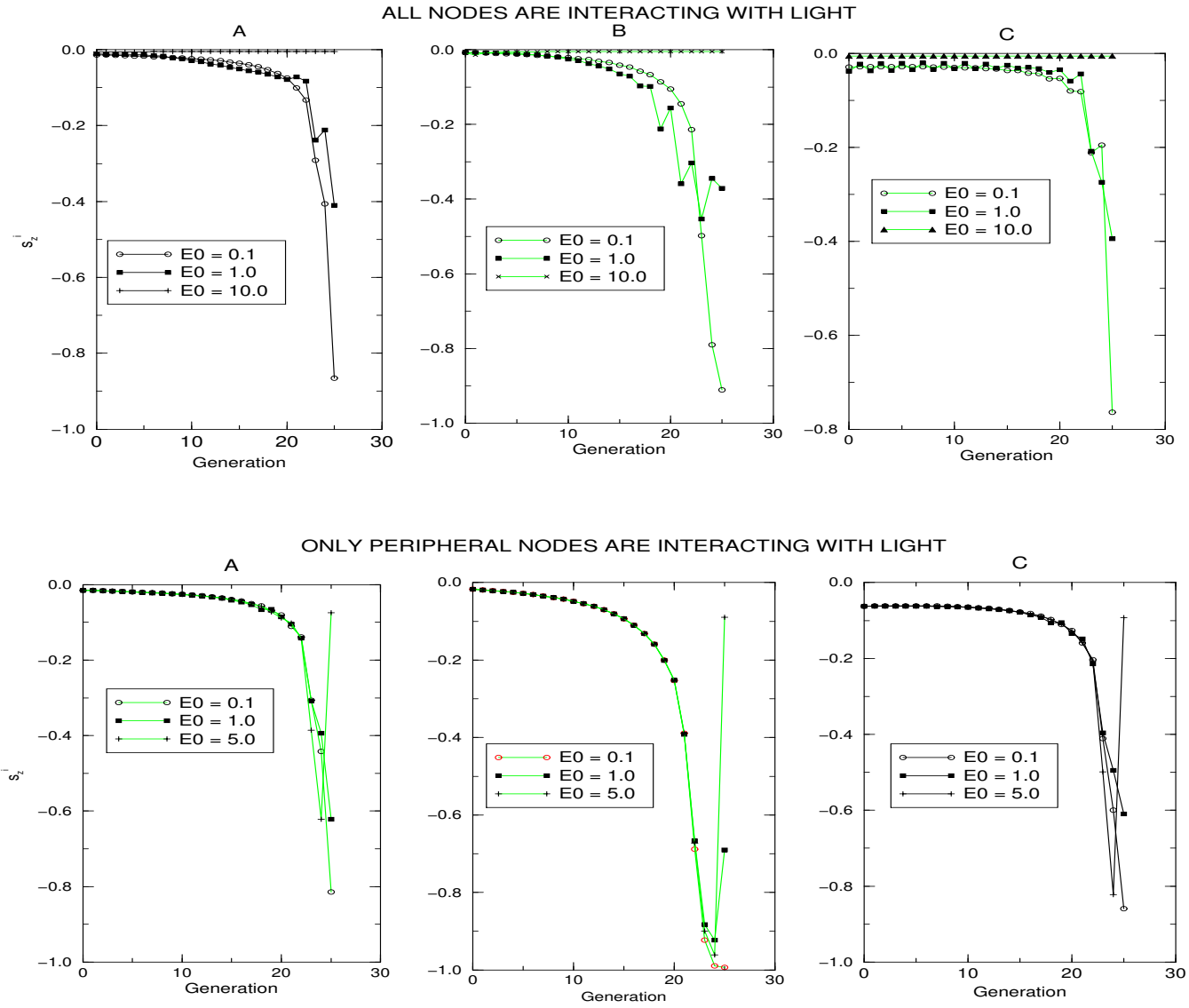

[Fig 4.6]: Changes of S_z values under different conditions for extended dendrimer. In both upper and lower cases (A) all g values are kept fixed. (B) g are $(g_0 \dots g_n)$ decreased exponentially. (C) g are $(g_0 \dots g_n)$ increased exponentially. **Upper part :** all nodes are interacting with light. In all figures core is always preferred position for absorption of maximum energy. When $E_0 \ll g$, the core is preferred and a steady increase of excitation energy from periphery to core is observed. The situation is ideal for **Energy Antenna**. When $E_0 \gg g$ almost all nodes are equally excited. At $E_0 \simeq g$ the trend is same with some intermediate fluctuations. **Lower part :** Only peripheral nodes are interacting. All curve follow the same behaviour except at peripheral node at $E_0 \gg g$. In (B) there is a fluctuation of s_z at node $(G-1)$ generation when $E_0 \simeq g$.

have calculated the s_z values. Here also we have made observation by two ways : (i) by interacting all nodes with light, (ii) by interacting only peripheral nodes with light. We have kept all the coupling constants and other parameters same as that of compact dendrimer of same generation.

(i) All nodes are interacting with light :

The general behaviour is such that core is the fovoured position for absorption of maximum excitation energy at steady state (see Fig.4.6 upper panel). Again from periphery to core there is a smooth increase of distribution of excitation energy when $E_0 \simeq g$ or $E_0 \ll g$. When $E_0 \gg g$ all nodes are equally excited. This smooth increase of excitation energy distribution from periphery to core indicates it will behave as energy antenna.

(ii) Only peripheral nodes are interacting with light :

Here the situation is such that irrespective of the values of E_0 ($E_0 \simeq g$, $E_0 \gg g$, $E_0 \ll g$) the distribution of excitation energy is always maximum at the node nearer to core (see Fig.4.6 lower panel). All the curves more or less overlap with each other. The situation is to some extent different at periphery when all nodes are saturated ($E_0 \gg g$). We consider only the peripheral nodes are interacting with light, though the maximum absorption of energy is occurring at core. So extended dendrimer are the ideal candidates for energy funneling.

By the introduction of this model we have predicted the increase of intensity of absorption spectra with increase in generation. We have shown the variation of FWHM of total absorption curve with coupling constants (when $g_0 = g_1 = g_2 \ldots g_n = g$). We have also noted the saturation of FWHM after a certain generation for a fixed coupling constants. Lastly we have shown how the variation of s_z values can predict the preferred location of excitation energy, periphery, core, or bulk. The smooth gradient of excitation energy from periphery to core with increased absorption of energy towards core can predict the energy funneling. This dendrimeric property mimics RC in photosynthetic unit. During this observation we have found that the interaction terms and the intensity of external fields are key factors. The interaction terms are representative for local electro-chemical environment of a node. This environment is a consequence of the inherent geometry of the dendrimer molecule. For a single node the number of nearest neighbour interactions reflects the inherent geometry.

In the extended dendrimer there is an increment of number of

monomer units between two successive nodes of the two successive generations while going from the periphery to the center on the Cayley tree geometry. To account for this effect in extended dendrimer we have assumed that the legs between successive generations just increase the strength of interactions with a specific rule. That means interaction parameters g_i increases from periphery to core according to the number of monomer units added between two nodes of the Cayley tree. With this heuristic model of extended dendrimer, we have found that for various parameters and ranges of parameters, there is always an enhanced increase of absorption of energy from the periphery to the core.

For very long generations this open system, the driven damped two-level-dipoles on the Cayley tree geometry, shows a pattern formation of excitation energy . This co-operative far from equilibrium phenomenon is much of academic interest nowadays and is beyond the interest of present context of dendrimer supermolecules.

4.7 Spectral features on two-dimensional geometry

4.7.1 Steady state absorption properties when all nodes are interacting with light

We have studied the absorption profiles both for dendrimeric and linear architecture. The increase in absorption intensity due to increase in generation number was demonstrated in previous section. Here we have made a detailed investigation to show that the effect of increase in core branching not only enhances the intensity (in Fig.4.10) but also the width of the absorption plot (in Fig.4.8). It is inferred that the broadening is due to the increase in effective coupling and the effective damping due to interaction of other nodes acting as bath. For a linear chain the absorption curve is considerably narrower. The occurrence of hole burning is another interesting phenomenon (in Fig.4.10). This spectral hole burning occurs at lower external field strength E_0 and due to the development of intrinsic inhomogeneity of distribution of nodes in the molecule. It again stems from the fact that each representative node suffers an unique environment with respect to the other nodes.

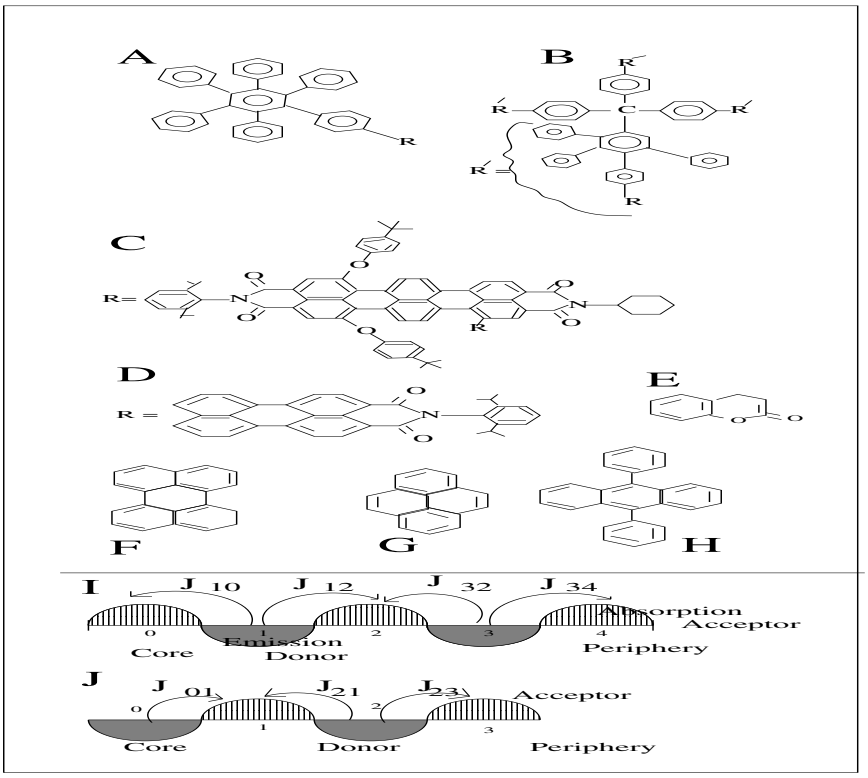

[Fig 4.7] (A) and (B) are model dendrimeric architecture used in single-molecule experiment. Various types of donor or acceptor that can be attached to the periphery or the core to control the chosen photo-physical process: (C) Perryleneimide Donor (PI), (D) Terryleneimide Acceptor (TI), (E) Coumerine, (F) Perrylene, (G) (H) Diphenyl anthracene. (I) Schematic representation of sequential absorption and emission from core to the periphery.

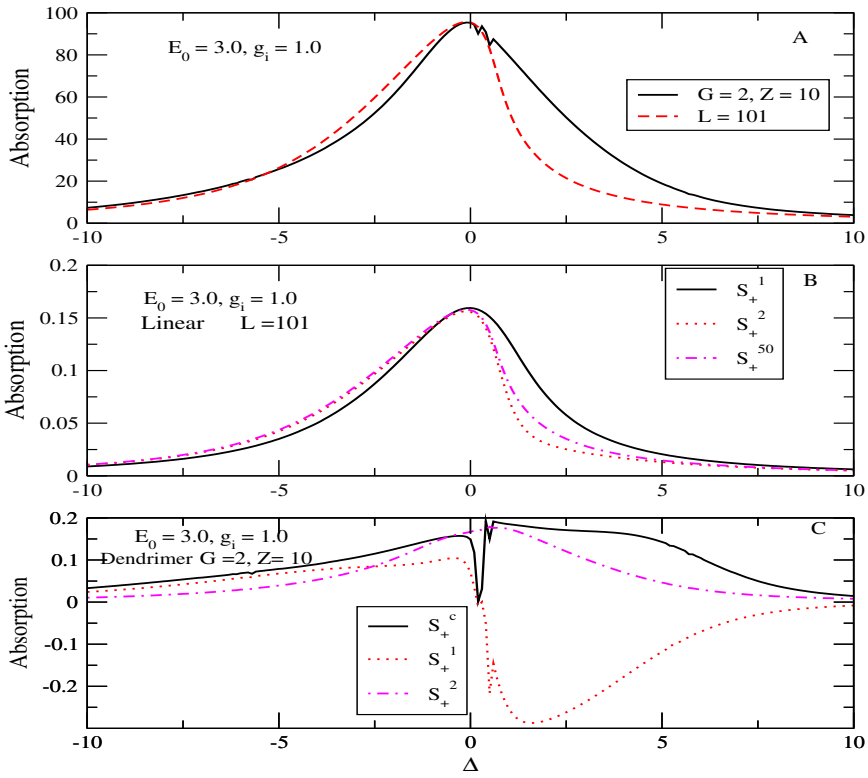

[Fig 4.8] (A) Total absorption spectra of a dendrimeric architecture(solid lines) having generation $G = 2$ and core-branching $Z = 10$ and that of a linear chain(L) (dashed lines) having equal nodes with all coupling g_i = 1.0 and field strength E_0 = 3.0. The dendrimeric network has broader absorption curve than the linear. The dendrimeric network shows hole-burning. (B) Absorption of specific node for a linear chain. Here $S_+^i \equiv$ Imag(S_+^i). The curve for the 50th node is much symmetric and broader than the 2nd node. The former one faces equivalent environment around it since this is situated at the centre of the chain. (C) Absorption of representative node for various generations of dendrimeric architecture. Here $S_+^i \equiv$ Imag(S_+^i). Core and 1st generation node shows hole burning. In the peripheral nodes this phenomena is not observed. This proves that hole-burning occurs at some node that faces different types of interactions with at least two different nodes. These interactions make the population low at the upper level or high at the lower level at that specific frequency by manifestation of the sudden decrease of absorption.

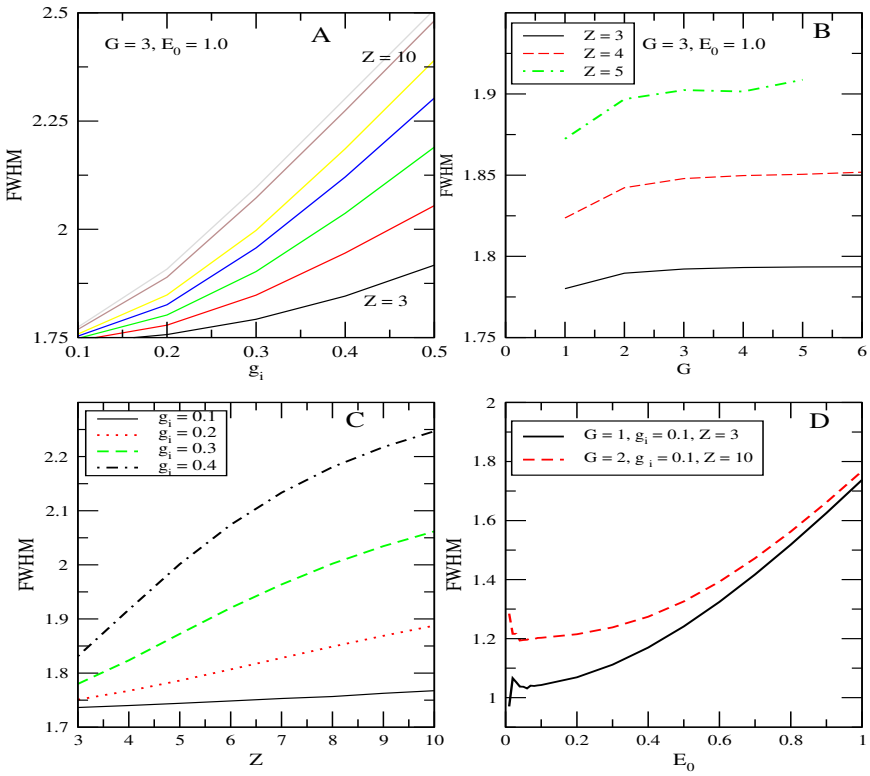

[Fig 4.9] Variation of FWHM of a dendrimer molecule with various system parameters. (A)Plot of FWHM versus coupling g_i: the curves follow, FWHM = $A_0 exp(A_1 {g_i}^{A_2})$. (B) Plot of FWHM versus generation G: the curves follow, FWHM = $A_0 - A_1 exp(-A_2 G)$ where the FWHM saturates at some higher G. (C) Plot of FWHM versus core-branching Z: the curve follow, FWHM = $A_0 exp(A_1 Z^{A_2})$ for $g_i \leq 0.30$ and $A_0 exp(-A_1 Z + A_2)$ for $g_i \geq 0.40$, where at higher values of Z the FWHM saturates. (D)Plot of FWHM versus field strength E_0 : the curves follow, $A_0 exp(A_1 {E_0}^{A_2})$ where at lower E_0 the FWHM versus E_0 is irregular because of the occurrence of hole-burning. At higher E_0 the FWHM does not change with the change of other system parameters. In all cases A_0, A_1 and A_2 are constant dependent on the dendrimer size and other parameters.

4.7.2 Full Width at Half Maxima (FWHM): effect of coupling g_i, generation G, core-branching Z and intensity E_0

In our previous work we have considered a simplified model for dendrimeric architecture where actual geometry was approximated by a one dimensional chain of connecting nodes. The degeneracy of a specific generation was accounted for by the nature of interactions of a node with its neighbouring nodes[35].

In this work we have studied the effect of actual geometry, where the core branching and generation are the key parameters. Here we have seen that the increase in intensity is due to increase in core branching. The curves at higher core branching are broadened. In Fig.4.8 we have shown the absorption profile of dendrimer and linear chain molecule. Fig.4.8A shows dendrimeric network has broad absorption profile compared to the linear chain (dashed line). Fig.4.8B shows the absorption due to contribution of individual nodes of a linear chain. The 1st and 50th node have symmetric absorption profile than the 2nd node. The 1st node feels only one interaction, 50th node feels equal environment in both side and the 2nd node feels unequal environment in its two sides. Fig.4.8C predicts that the core node and the node of 1st generation have absorption curve with hole-burning while the peripheral nodes have smooth Lorentzian (with a shift towards positive Δ) profile. The core node and a node of 1st generation can interact with at least two other nodes and a peripheral node can interact with only its previous node. Since there are different environments around the core and the periphery they have different absorption spectra. At higher core branching with increase in coupling strength, g_i we observe broadening of the profile.

We have studied the full width at half maxima (FWHM) versus various system parameters as shown in Fig.4.9. Broadening of absorption band depends on core-branching Z, coupling strength g_i, intensity of laser field E_0 and damping γ. Here all parameters are scalled with respect to γ. We have displayed the systematic variation of Z and g_i by keeping E_0 and γ fixed as shown in Fig.4.9A, Fig.4.9B and Fig.4.9C. At fixed core branching with a fixed generation dendrimer, increase in g_i obeys the following equation as shown in Fig.4.9A:

$$\text{FWHM} \;=\; A_0 exp(A_1 {g_i}^{A_2}) \tag{4.41}$$

where A_0, A_1 and A_2 are constants dependent upon Z and G. The curves are straight lines at higher Z and at higher G. The exponential nature is prominent at lower Z and at lower G. At a fixed core branching Z and

at a fixed g_i the FWHM varies with generation G as shown in Fig.4.9B:

$$\text{FWHM} \;=\; A_0 - A_1 exp(-A_2 G) \tag{4.42}$$

where A_0, A_1 and A_2 are constants dependent upon Z and g_i. The variation of FWHM with Z for fixed G and g_i is shown in Fig.4.9C:

$$\text{FWHM} \;=\; A_0 exp(A_1 Z^{A_2}) \;\text{ for } g_i \leq 0.30 \tag{4.43}$$

and

$$\text{FWHM} \;=\; A_0 - exp(-A_1 Z + A_2) \text{ for } g_i \geq 0.40. \tag{4.44}$$

At lower values of g_i the FWHM exponentially increases with Z and at higher values of g_i the FWHM exponentially increases to saturate at a fixed value as shown in Fig4.9C.

We have seen that the variation of FWHM versus E_0 is a straight line for higher values of E_0. The FWHM does not change significantly with G or Z. At lower values of E_0 ($E_0 \leq 1.0$) the FWHM versus E_0 curve shows a slow exponential increase. The nature of the curve is (see Fig.4.9D) is given by

$$\text{FWHM} \;=\; A_0 exp(A_1 {E_0}^{A_2}) \tag{4.45}$$

where A_0, A_1 and A_2 are constants dependent upon G, Z, g_i.

4.7.3 Hole burning

We have noted the feature of hole burning in total spectra and we have analysed the total spectrum from the contributions of the individual nodes in each generation in Fig.4.8 and in Fig.4.10. At a particular frequency when the hole appears the parameters are adjusted in such a way that the population at the upper level increases than that in the ground state. So from the absorption plot or from the plot of population inversion it has been observed that decrease or increase of absorption plot of individual nodes at successive generation is not uniform at the frequency of a hole. Since the total absorption curve is the collective effect of all representative nodes we find that some sort of intrinsic inhomogeneity arises due to the interplay of various system parameters. The increase in the number of holes on increasing Z actually proves the transfer of excitations to or from the nearest nodes since a node faces higher number of nodes around it as core-branching Z increases. With increase

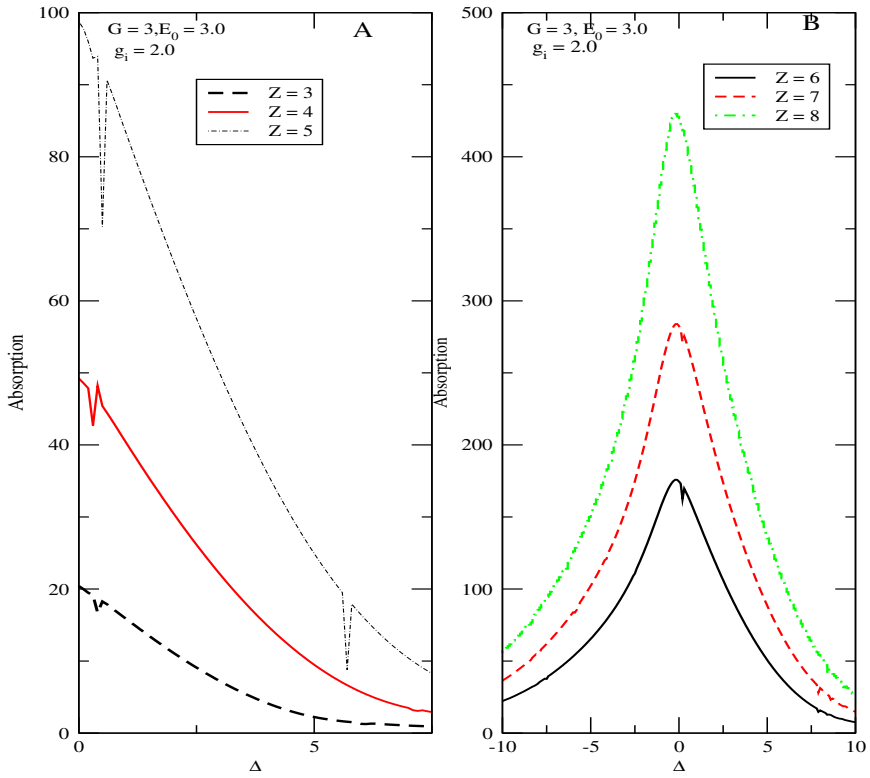

[Fig 4.10] Absorption spectra showing hole burning of a dendrimer having $G = 3$ at various core branching, (A) for Z = 3,4,5, (B) for Z = 6,7,8. The hole-burning starts at $Z = 3$, maximizes at $Z = 5$ and disappears at $Z = 8$. We have seen that at some specific Δ value $Imag(S_+)$ decreases abruptly. The S_z values also decreases at that specific Δ value. This means the population at higher level decreases or it increases at the lower level by transferring excitation energy to or from the other nodes respectively. At lower E_0 values the possibility of hole-burning increases. The increase of holes on increasing Z actually proves the transfer of excitations to or from the nearest nodes since a node faces higher number of nodes around it as core-branching Z increases. On increasing the core-branching Z much more the depth of the hole decreases due to the attainment of equivalent environment.

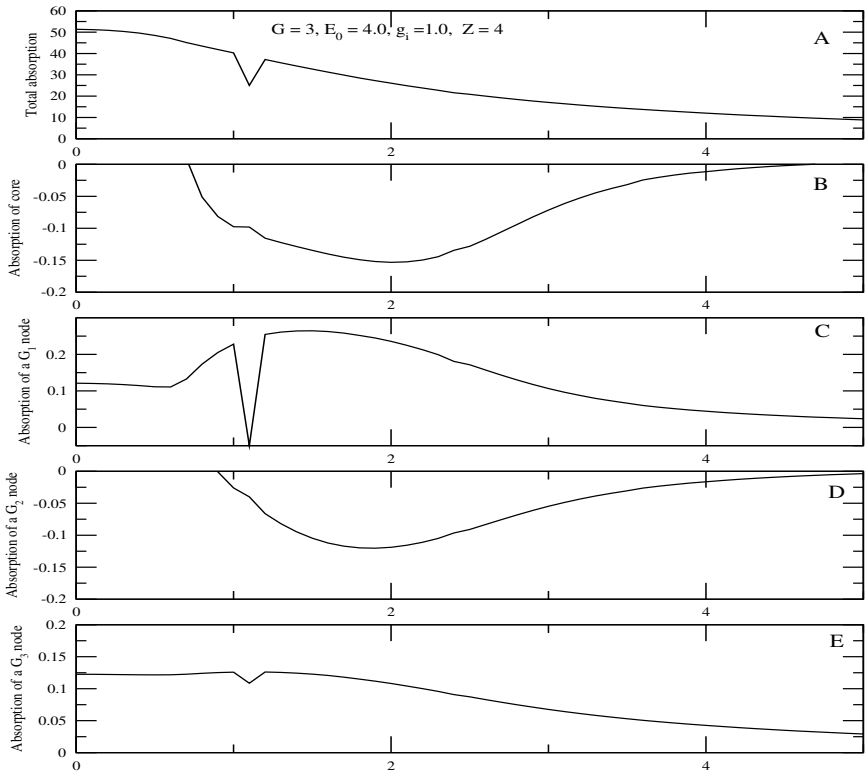

[Fig 4.11] Absorption spectra of a $G = 3$ dendrimer molecule : (A) The total absorption of the dendrimer The total absorption is the sum of the absorption of the nodes in each generation. The absorption of the representative node of each generation starting from the core to the periphery are plotted in Figs from (B) to (E) where the nodes of successive generation show a sequential absorption and emission. The peripheral nodes always show absorption while the core node shows emission or absorption depending upon the number of generation G.

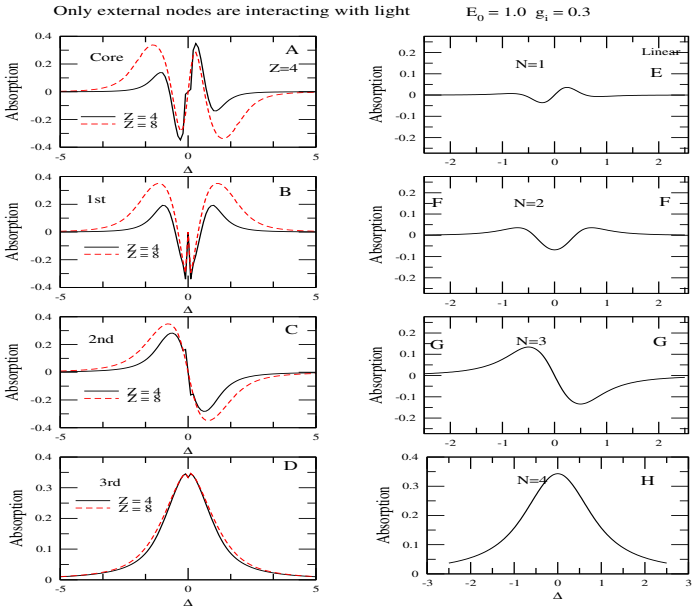

[Fig 4.12] Here only external nodes are interacting with light. Pannel (A), (B), (C) and (D) are absorption spectra of a representative node in each generation i.e, core, 1st generation, 2nd generation and periphery respectively of a $G = 3$ with two different core-branching parameters $Z = 3$ and $Z = 8$. Panel (E), (F), (G), (H) are the same for the core-branching $Z = 4$ and $Z = 8$. Panel (I), (J), (K), (L) are absorption plot for $N = 1, 2, 3, 4$ respectively for linear chain containing four nodes. The absorption profiles are splitted in case of dendrimeric architecture. In case of linear chain this kind of splitting is not observed.

in core-branching, the depth and number of holes decreases due to the attainment of equivalent environment of the individual nodes. Width of a hole again depends on the strength of the coupling between the nodes. Physically hole-burning at a specific frequency means there is no or very low absorption in the absorption curve. This study may be a primitive step to understand mechanism involved in single molecule[47, 49, 65, 54] experiment. We have assumed all nodes as two-level systems and these are equivalent. In this simple model we have seen these properties. A more sophisticated model is necessary to understand hole-burning[53] or imaging to detect the single dendrimeric architecture[49]

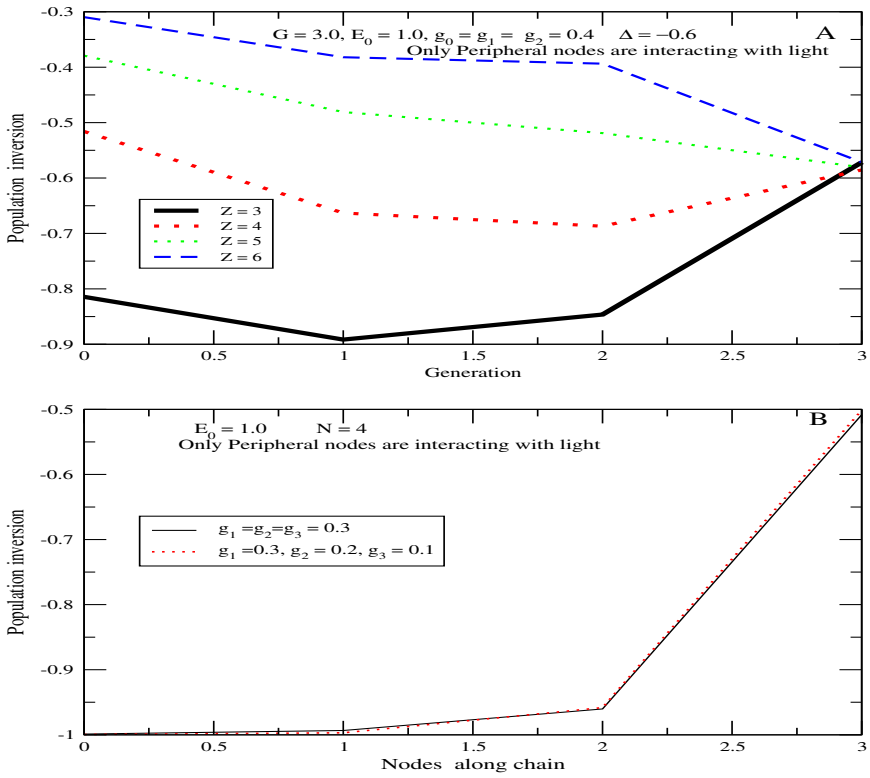

[Fig 4.13] When only the external (peripheral) nodes are interacting with light, population inversion of the nodes are plotted from core to periphery for (A) Dendrimer and (B) for linear chain. Population inversion directly increases from the external node to the core node. The case of dendrimer reflects the effect of branching. At higher Z the core become the most excited node.

4.7.4 Inter-generation excitation energy transfer mechanism

From the analysis of the theoretical absorption spectra of individual nodes of each generation we have seen sequential absorption and gain when we proceed from the core to the periphery as shown in Fig.4.1.

In Fig.4.11 panel A, B, C, D and E are absorption plot for whole molecule, for core, for a node of 1st, 2nd and 3rd generation, respectively. In panel B and C we see that while core node shows gain, the 1st generation node shows absorption in the same frequency region. We have calculated the region of overlap between nodes of two successive generations. It has been observed that there is always absorption in the peripheral nodes. There is gain in core when G is odd and absorption in core when G is even. We have shown this schematically in Fig.4.7I and in Fig.4.7J.

We have defined a quantity $J_{i\,j}$ which is the overlap region between two neighbouring generations i and j and normalized with respect to gain region. If we assign a gained node, say i as a donor it can transfer its excitation energy to the neighbouring nodes, $i \pm 1$ where absorption occurs, with a transfer rate proportional to $J_{i\,i\pm1}$ where $J_{i\,i+1}$ ($J_{i\,i-1}$) is towards the periphery (core). For various ranges of dendrimeric parameters we find $J_{i\,i+1} < J_{i\,i-1}$, which means out of two directions an excitation transfer rate towards core is greater than the peripheral direction and a consequent development of an inward bias to the core. The magnitude depends upon the various parameters where the parameters of core-branching dominates over all other parameters to act the dendrimer as an antenna system. Since this effect of biasing results for low E_0 values, it reminds the F*ö*rster energy transfer[11] in the incoherent regime although it is intra-molecular or through-bond-type-excitation transfer. Table II and Table III show that bias of excitation transfer rate towards core from the periphery is greater. This bias towards core has been shown theoretically[23, 26] by classical models and experimentally[24]. Here we have seen this with the help of a simple quantum model. Generally molecular network, long polymer chain or crystal containing photosensitive chromophores may exhibit this behaviour during single molecule experiment.

4.8 Steady state spectral properties when only external nodes are interacting with light

4.8.1 Spectral properties of successive generation

When only external nodes are interacting with light, steady state spectral properties are analysed in terms of the successive generation in Fig.4.12. There is always absorption in the external node. The main feature in the spectral profiles of the successive generation are very interesting. While the peripheral node gives an absorption curve the next node gives a dispersion curve and so on alternately upto the core node. In Fig.12 (A - D) the 3rd generation dendrimer is plotted. Similar results is obtained for the linear case (Fig.12 (E - H)).

4.8.2 Smooth gradient of excitation energy from periphery to core

Taking an example of third generation dendrimer, we have plotted the population inversion of the node in successive generations in Fig.4.13A. For low core-branching, $Z = 3$, only the peripheral nodes are excited. But with increase in core-branching the population inversion increases in the inward nodes. For high core-branching the population inversion smoothly increases towards the core. This is an ideal situation for an efficient antenna that will harvest the absorbed light energy like a photosynthetic reaction center. This property is also useful for artificial energy transport device. Fig.13B shows the case for a linear chain. Here no significant gradient of excitation energy occurs. Thus branching is the important aspect for transport processes.

Geometry, field, coupling	Frequency regime	$J_{01} : J_{21} : J_{23}$
G=3, Z=3,E_0 =3,g_i =1.0	$\Delta \approx$ 0.6-3.0	1.24 : 1.57 : 1.00
G=3, Z=3, E_0 =3 , g_i =2.0	$\Delta \approx$ 0.2-8.2	1.37 : 1.39 : 1.00
G=3, Z=4, E_0 =4, g_i =1.0	$\Delta \approx$ 1.0-4.8	1.03 : 1.03 : 1.00
G=3, Z=4, E_0 =3, g_i =1.0	$\Delta \approx$ 0.5-5.0	1.29 : 1.29 : 1.00
G=3, Z=4, E_0 =3, g_i =2.0	$\Delta \approx$ 0.0-8.5	1.50 : 1.60 : 1.00
G=3, Z=5, E_0 =3, g_i =1.0	$\Delta \approx$ 0.2-7.0	1.51 : 1.59 : 1.00
G=3, Z=5, E_0 =3, g_i =2.0	$\Delta \approx$ 0.0-10.0	1.38 : 1.75 : 1.00
G=3, Z=6, E_0 =3, g_i =1.0	$\Delta \approx$ 0.0-6.8	1.63 : 1.78 : 1.00
G=3, Z=6, E_0 =3, g_i =2.0	$\Delta \approx$ 0.0-12.0	1.24 : 1.57 : 1.00

Table 1: Sequential absorption and gain at various nodes. For this case $i = 2$ is the gained node acting as a donor. Here it is clear that $J_{2\,1} > J_{2\,3}$ for various parameter ranges and particularly important for higher core-branching, Z which means excitation transfer rate is biased towards the core.

Geometry, field, coupling	Frequency regime	$J_{10} : J_{12} : J_{32} : J_{34}$
G=4, Z=3, E_0 =3, g_i =1.0	$\Delta \approx$ 0.7-3.0	1 :1 : 1 :1
G=4, Z=4, E_0 =3, g_i =1.0	$\Delta \approx$ 0.5-5.0	1.29 : 1.29 : 1.29 :1
G=4, Z=4, E_0 =3, g_i =2.0	$\Delta \approx$ 0.3-8.8	1.64 : 1.48 : 1.59 : 1.00
G=4, Z=5, E_0 =3, g_i =1.0	$\Delta \approx$ 0.4-6.9	1.59 : 1.51 : 1.59 : 1.00
G=4, Z=5, E_0 =3, g_i =2.0	$\Delta \approx$ 0.2-10.6	1.70 : 1.38 : 1.60 : 1.00
G=4, Z=6, E_0 =3, g_i =1.0	$\Delta \approx$ 0.3-4.0	1.79 : 1.57 : 1.74 : 1.00
G=4, Z=6, E_0 =3, g_i =2.0	$\Delta \approx$ 0.1-3.0	1.62 : 1.23 : 1.59 : 1.00

Table 2: Sequential absorption and gain at various nodes. For this case i = 1,3 and the gained node acting as a donor. Here it is clear that $J_{i\,i-1} > J_{i\,i+1}$ for various parameter ranges and particularly important for higher core-branching, Z

4.9 Summary and conclusion

Our main aim is to find out the relation between the geometry of complex network of dendrimer with its spectral properties with special reference to the position of maximum absorption or excitation. We have predicted the increase of intensity of absorption spectra with increase in generation number. The variations of FWHM of total absorption curve are shown with uniform coupling constants and the saturation of FWHM beyond a certain generation. We have also numerically analysed the hole-burning and sequential emission and absorption of successive generations. The occurrence of hole-burning is found to be caused by the developement of intrinsic inhomogeneity because of the interplay of the field strength, E_0 and coupling arising due to the nodes attached to the core which subsequently modifies the damping mechanism of the nodes of the complex network. This study may be a primitive step to understand mechanism involved in single molecule[47, 49, 65, 54] experiment. We have assumed all nodes as two-level systems and these are equivalent. In this simple model we have qualitatively seen these properties. A more sophisticated model is necessary to compare in detail with the hole-burning[53] or imaging to detect the single dendrimeric architecture[49]

When only external nodes are interacting with light we have compared the absorption curve of individual nodes of the dendrimer with its linear chain counterpart. High core branching first increases the effective coupling and beyond a certain higher value of core branching absorption curves are broadened which indicates the enhancement of effective damping mechanism[35, 37]. The other interesting point is the position of maximum excitation with increase in core branching. Here we have seen the population inversion in the core node becomes maximum with increase in core branching. At large core branching excitation increases from periphery to the core. This smooth gradient of excitation energy from the periphery to the core with increased absorption of energy towards core can predict the energy funneling. During this observation we have found that the interaction terms and the intensity of external fields are the key factors. The interaction terms are representative of local electro-chemical environment of a node. This environment is a consequence of the inherent geometry of the dendrimer molecule. In the case of linear chain we have not seen this effect within the same parameter regime due to the lack of dendrimeric neighbourhood of the nodes.

We have also observed the inter generation excitation energy transfer. Table II and Table III show that bias of excitation transfer rate towards core from the periphery is always greater. This bias towards core has been shown theoretically[23, 26] by classical models and experimentally[24]. Here we have seen this with the help of a simple quantum model. Generally molecular network, long polymer chain or crystal containing photosensitive chromophores may exhibit this behaviour during single molecule experiment.

In comparison to the absorption profile with the linear chain we have noted that broadening of the absorption curve and hole-burning are the key features at steady state that makes a branched structure different from a linear one. Again smooth gradient of excitation energy from periphery to core with increase in the core-branching is also an important feature. The branching makes an environment in such a way that a node feels an enhanced interaction with its neighbouring nodes. Consequently a high core branching can introduce an effective mean field environment for a node which feels the other nodes acting as a bath. Here an effective coupling and an effective damping mechanism[35, 36, 37] is operative to control the steady-state and time dependent spectral properties. In this context one can find the experimental observation of Glazier et al[231] that at higher generation dendritic backbone acts as a solvent in affecting photo-physical properties.

Chapter 5

5 Dynamics and transient spectra of Dendrimer molecule

On the basis of the theory developed in the previous chapter here we have investigated the dynamics and transient spectra of dendrimer molecule. We have seen the variation of full width at half maximum(FWHM), hole-burning, smooth gradient of excitation, Förster-type energy transfer in the steady state behaviour of dendrimeric architecture in the previous section. In this section we shall see the time-dependent spectral phenomena. We shall see how absorption and population inversion or excitation depends upon the branching as time progresses. We shall see the changes occur in the representative node of a specific generation. We shall see how the dendrimeric network can retain excitation for a longer period of time. As a result of this a highly branched dendrimer can induce a photochemical transformation at the core even with a low intensity of photons. We shall also see the transient spectra to predict some important spectral shifts and splitting due to the dendrimeric architectute. It is shown that the transient absorption we obtained mostly support the previous experimental result[77].

In section 5.1 we have given the starting equations of motion of the creation and annihilation operators for the two-level nodes along the dendrimeric network obtained in the previous chapter. Euler method has been used for the numerical solution of the equations of motion. In section 5.3 we have given results where all nodes are interacting with light and in section 5.4 we have discussed results when only external nodes are interacting with light. In section 5.5 we have outlined transient absorption property. In this section we have also studied the molecule in two ways:(i) interacting all nodes with light and (ii) interacting only external nodes with light. We have concluded in section 5.6.

5.1 Equation of motion

For the exact evaluation of the dynamical solution of the equation of motion corresponding to damped-driven dendrimeric system is outlined in previous chapter 4 with the Hamiltonian given in equation (4.1). We

have started with the following equation of motion (with $\Delta = \omega_0 - \omega$)

$$\frac{ds_z^0}{dt} = -2ig_0[s_+^0 \sum_{m=1}^{Z} s_-^{m11} - s_-^0 \sum_{m=1}^{Z} s_+^{m11}]$$

$$-iE_0(s_+^0 - s_-^0) - \gamma(1+2\bar{n})(s_z^0 + 1), \tag{5.1}$$

$$\frac{ds_+^0}{dt} = i\Delta s_+^0 - ig_0 s_z^0 \sum_{m=1}^{Z} s_+^{m11} - \frac{iE_0}{2} s_z^0 - \frac{\gamma(1+2\bar{n})}{2} s_+^0, \tag{5.2}$$

$$\frac{ds_z^{m11}}{dt} = -2ig_0[s_+^{m11}s_-^0 - s_-^{m11}s_+^0] - 2ig_1[s_+^{m11} \sum_{j=1}^{Z-1} s_-^{m2j} - s_-^{m11} \sum_{j=1}^{Z-1} s_+^{m2j}]$$

$$-iE_0[s_+^{m11} - s_-^{m11}] - \gamma(1+2\bar{n})(s_z^{m11} + 1). \tag{5.3}$$

$$\frac{ds_+^{m11}}{dt} = i\Delta s_+^{m11} - ig_0 s_z^{m11} s_+^0 - ig_1 s_z^{m11} \sum_{j=1}^{Z-1} s_+^{m2j}$$

$$-\frac{iE_0}{2} s_z^{m11} - \frac{\gamma(1+2\bar{n})}{2} s_+^{m11}. \tag{5.4}$$

The equation of motion for bulk and boundary are as follows :

$$\frac{ds_z^{pmk}}{dt} = -2ig_m[s_+^{pmk} \sum_{j=k(Z-1)-(Z-2)}^{k(Z-1)} s_-^{p\ m+1\ j} -$$

$$s_-^{pmk} \sum_{j=k(Z-1)-(Z-2)}^{k(Z-1)} s_+^{p\ m+1\ j}$$

$$-2ig_{m-1}[s_+^{pmk}(s_-^{p\ m-1\ \frac{k+(Z-2)}{Z-1}} - s_-^{pmk} s_+^{p\ m-1\ \frac{k+(Z-2)}{Z-1}}]$$

$$-iE_0[s_+^{pmk} - s_-^{pmk}] - \gamma(1+2\bar{n})(s_z^{pmk} + 1), \tag{5.5}$$

$$\frac{ds_+^{pmk}}{dt} = i\Delta s_+^{pmk} - ig_{m-1} s_+^{p\ m-1\ \frac{k+(Z-2)}{Z-1}} s_z^{pmk}$$

$$-ig_m s_z^{pmk} s_+^{pmk} \sum_{j=1}^{Z-1} s_+^{p\ m+1\ j}$$

$$-\frac{iE_0}{2}s_z^{pmk} - \frac{\gamma(1+2\bar{n})}{2}s_+^{pmk}. \tag{5.6}$$

For transient absorption we have put ${S_z}^{pmk}(t) = -1$. Therefore the linear equations of $\hat{S_\pm}(t)$ can be solved numerically to obtain the susceptibility. At the long time limit the absorption spectra has been studied here.

Euler's method has been used for the numerical evaluation of solution of these set of equations. In a first order equation

$$\frac{dy}{dx} = f(x, y) \tag{5.7}$$

with $y = y_0$ at $x = x_0$, the slope at x_0 is $f(x_0, y_0)$; call this f_0. The value of y at $x_1 = x_0 + h$ is approximately $y_1 = y_0 + f_0.h$. The slope at x_1 is $f(x_1, y_1) = f_1$. The estimated value of y at $x_2 = x_1 + h = x_0 + 2h$ is $y_2 = y_1 + f_1 h$. This procedure is repeated giving the general expression

$$y_{n+1} = y_n + f_n h \tag{5.8}$$

$$y_{n+1} = y_n + h(\frac{dy}{dx})_{x=x_n}. \tag{5.9}$$

Unless otherwise stated we have taken ${S_\pm}^i(t = 0) = 0$ and ${S_z}^i(t = 0) = -1$.

5.2 Spectral dynamics when all nodes are interacting with light

In this section we have studied the effect of generation, core-branching and field strength on the absorption spectrum and population inversion spectrum when all nodes are interacting with light.

5.2.1 Effect of generation, core-branching and field strength in overall spectrum

In Fig.5.1 panel A, B, C and D depict the situation when all nodes are interacting with light. In Fig.5.1 panel A predicts the time dependent absorption curve for a 2nd generation dendrimer with core-branching $Z = 3$ with intensity of the field $E_0 = 1.0$ and $g_i = 0.5$. After the initial

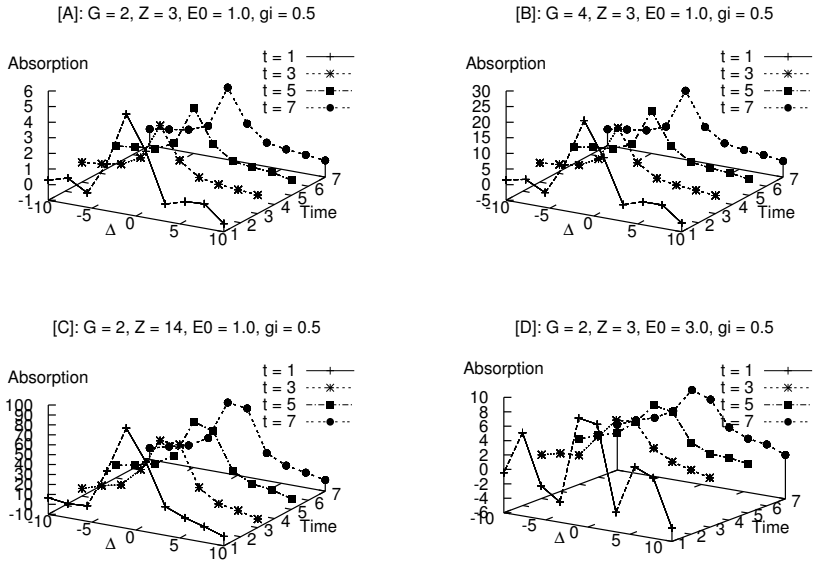

1

[Fig 5.1] Time dependent absorption spectra of [A]: 2nd generation ($G = 2$) dendrimer molecule having core-branching $Z = 3$ with $E_0 = 1.0$ and $g_i = 0.5$, [B]: 4th generation ($G = 4$) dendrimer molecule having core-branching $Z = 3$ with $E_0 = 1.0$ and $g_i = 0.5$, [C]: 2nd generation ($G = 2$) dendrimer molecule having core-branching $Z = 14$ with $E_0 = 1.0$ and $g_i = 0.5$, [D]: 2nd generation dendrimer molecule having core-branching $Z = 3$ with $E_0 = 3.0$ and $g_i = 0.5$.

transients are over, the intensity of absorption oscillates with time and get a steady value after a long time, depending upon the geometry and coupling.

Individual node of a representative generation has been plotted with time in Fig.5.2. The core, 1st generation, 2nd generation of a $G = 2$ dendrimer at $Z = 3, 5$ has been shown here. In Fig.5.2A it is seen that the peripheral nodes absorb light energy maximum. The core node at $Z = 5$ shows gain after certain time. In Fig5.2B the population inversion or excitation of core, 1st and 2nd generation node have been plotted. The peripheral nodes are highly excited in comparison to the other nodes. Core node shows oscilation in population at higher branching.

5.2.2 Higher population inversion at lower field strength with higher branching.

In Fig.5.3 (in panel A, B, C) we want to show how the population inversion at a node of a generation is affected by core-branching and field strength. Population inversion increases with the increase in field strength E_0. It also increases with the core-branching Z. Core and periphery behave differently from the bulk portion. Here we have shown curves with two categories. One curve represent high field ($E_0 = 3.0$) and low branching ($Z = 3$) case (solid line) and the other curve represent low field ($E_0 = 1.0$) and high branching ($Z = 8$) (dashed line). Fig.5.3A shows the behaviour of core node. At initial stage of the time interval solid curve and dashed curve have similar impact. At long time the dashed curve collapses to negative values rapidly. Fig.5.3B shows the nodes of bulk region retain their excitation upto very long time. The behaviour of nodes for solid and dashed curves are the same. This means for a dendrimer with high core-branching, a low field can induce similar impact as a low branched molecule at high field. The networking helps to retain the excitation. In Fig.5.3C we see that the peripheral nodes get saturated to a steady excitation for higher core-branching molecule with very low population inversion (dashed line). Thus the laser field with $E_0 = 3$ with $Z = 3$ or field with $E_0 = 1$ with $Z = 8$ have similar impact on core and bulk nodes (see dotted and dashed line). For the bulk node the similarity of these two curve retains for a long time. For a highly branched dendrimer low intensity of photons can induce a photochemical reaction when the reactant is attached to the core or nearer the core. Aida[2] and co-workers proved it with their experiment.

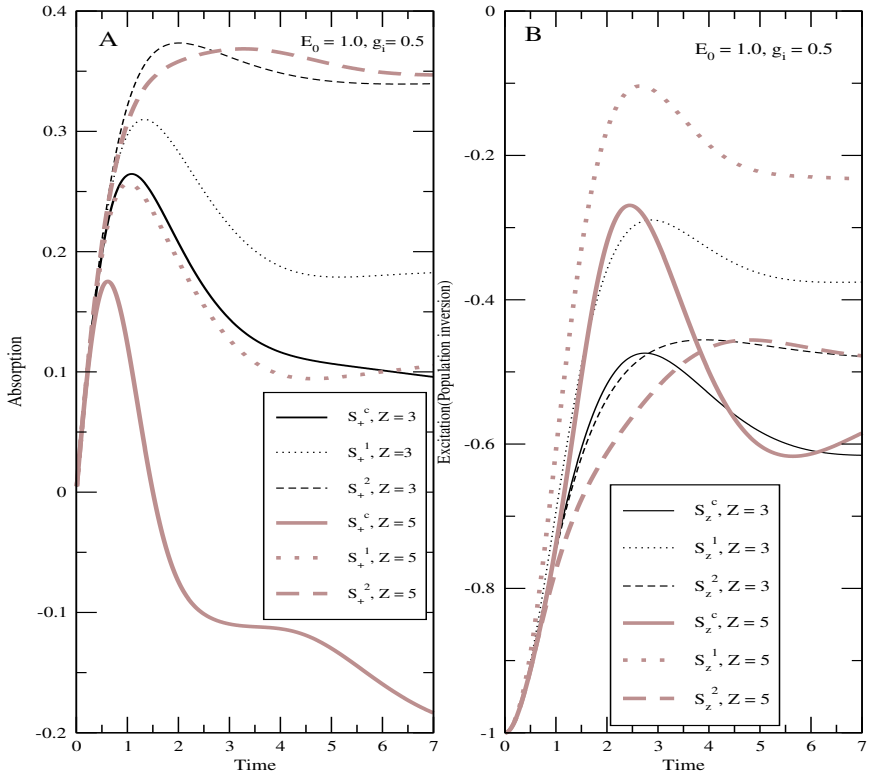

[Fig 5.2] Time dependent absorption spectra (A) and population inversion (B) of representative node in each generation, i.e core, 1st and 2nd generation of a G = 2 dendrimer at Z = 3,5 when all nodes are interacting with light. In (A) it has been seen that absorption intensity of peripheral node is maximum. When branching is high core shows gain after a certain time. In (B) it is the population inversion that has been plotted. The peripheral part is excited more. At $Z = 5$ the core node shows oscilations. The excitation decreases and increases after certain time interval.

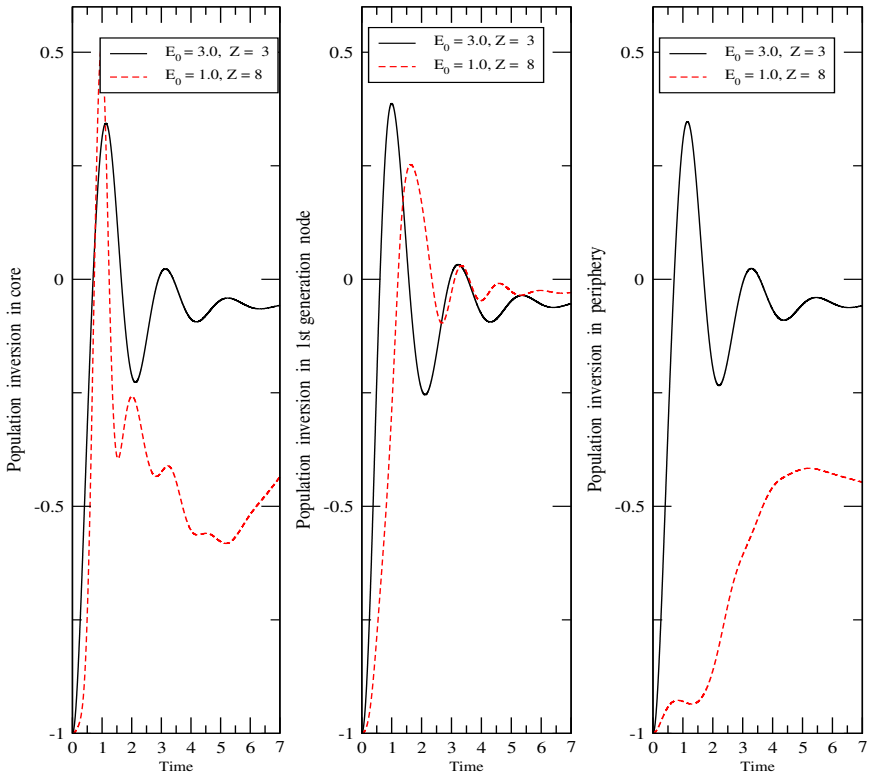

[Fig 5.3] Panel A, B, C are population inversion for core, bulk and periphery. Solid line is for low branched molecule interacting with high field and dashed line is for highly branched molecule interacting with low field. These curves prove that a low energy photon can induce similar changes at core or nearer to the core provided the core-branching (Z) is high.

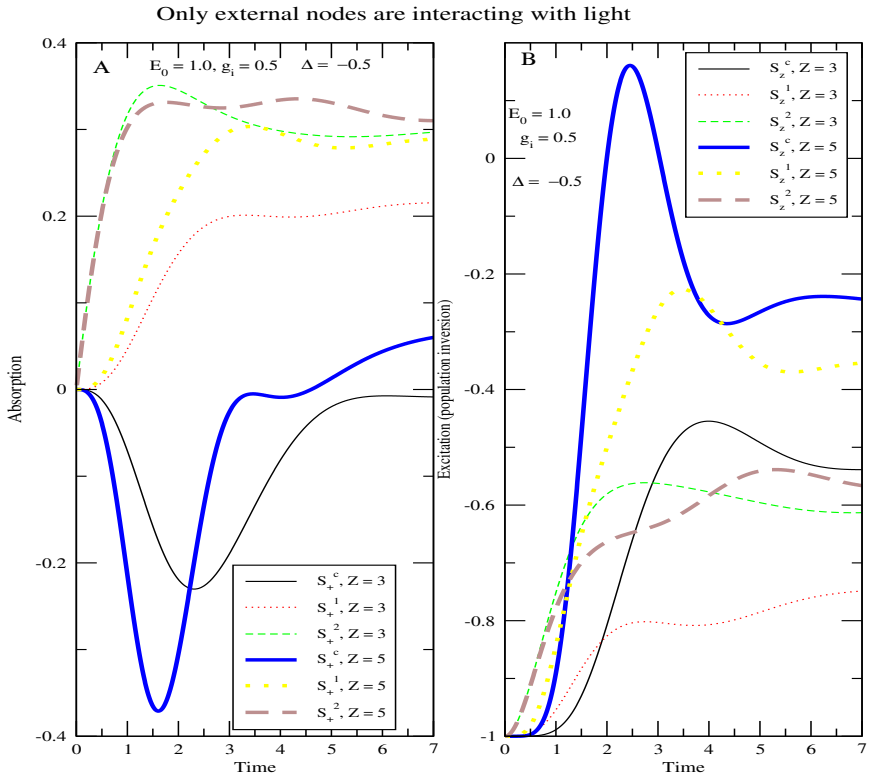

[Fig 5.4] Time dependent absorption spectra(A) and population inversion (B) of representative node in each generation i.e, core, 1st generation, 2nd generation of a $G = 2$ dendrimer at $Z = 3, 5$ when only external nodes are interacting with light. In panel (A) it is being seen that the peripheral nodes have higher absorption intensity and the nodes of next representative generation have to some extent lower absorption intensity. The core node has gain. In panel (B) it is being seen that initially the peripheral nodes have higher population inversion than that of the other nodes. After very short time the population inversion in the core node moves towards more positive values. Higher is the core-branching the more positive is the population inversion values for the core. This part predicts that depending upon time the preferred location of excitation may change although only external nodes are interacting with light.

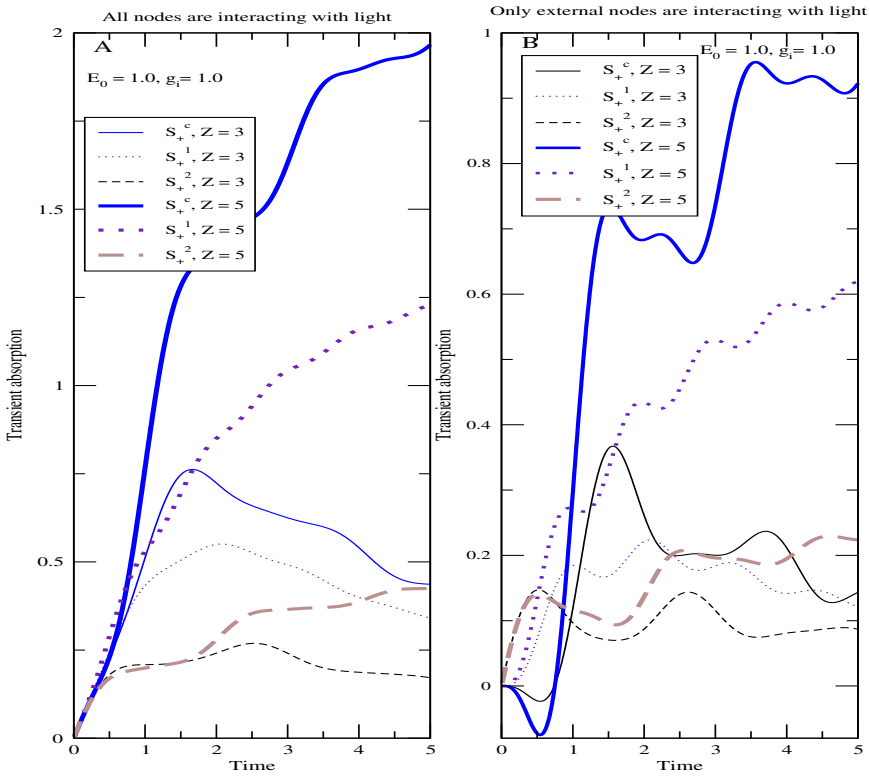

[Fig 5.5] (A) Transient absorption of representative node in each generation i.e, core, 1st generation and 2nd generation of a $G = 2$ dendrimer at $Z = 3, 5$ when all nodes are interacting with light. Here the nodes are in the ground state. at each moment. The intensity of absorption first increases with time and then decreases. The rate of the increase of absorption of the core node is larger than the other nodes. At higher core-branching Z the increase in intensity is much faster. (B) Transient absorption of representative node in each generation i.e, core, 1st generation and 2nd generation of a $G = 2$ dendrimer at $Z = 3, 5$ when only external nodes are interacting with light. In this case the absorption spectra for the core node gets positive values starting from zero through the negative values.

5.3 Spectral dynamics when only external nodes are interacting with light

Fig.5.4A and Fig.5.4B show the situation when only external nodes are exposed light. In Fig.5.4A the absorption spectra of different generation have been shown. Here peripheral nodes have higher absorption intensities and the nodes of next representative generations have to some extent lower absorption intensity. The core node has gain. In Fig.5.4B the population inversion of different generations have been shown. The population inversion curves for peripheral nodes are featureless at low or high core-branching. They dominate at the initial stage of the time interval. The population inversion of the core node initially has lower values but it dominates at long time. The rate of increase is faster for high core-branching. The oscillation of the population inversion with time continues for a long time at higher core-branching. So high branching must transfer the excitation rapidly towards core because we have excited only the peripheral nodes with light. So this study supports our earlier results[35, 37] of effective coupling and damping due to high generation dendrimeric architecture.

5.4 Transient absorption properties

To understand the transient absorption properties we have put ${S_Z}^i = -1$ and at each moment we have calculated the susceptibility of a concerned node at a particular generation. Fig.5.5 to Fig.5.9 are given for the situations when all nodes are interacting with light. Fig.5.10 to Fig.12 are given for the situations when only external nodes are interacting with light.

5.4.1 Transient absorption when all nodes are interacting with light

Fig.5.5A depicts the transient absorption properties when all nodes are interacting with light. The intensity of absorption first increases with time and then decreases. The rate of increase of absorption of the core node is rapid than the other nodes. The core node can retain its absorption for a long time provided the core-branching is high (see two solid lines). Since we have kept population inversion fixed at ground state here the transfer of absorption is solely due to inter-site coupling.

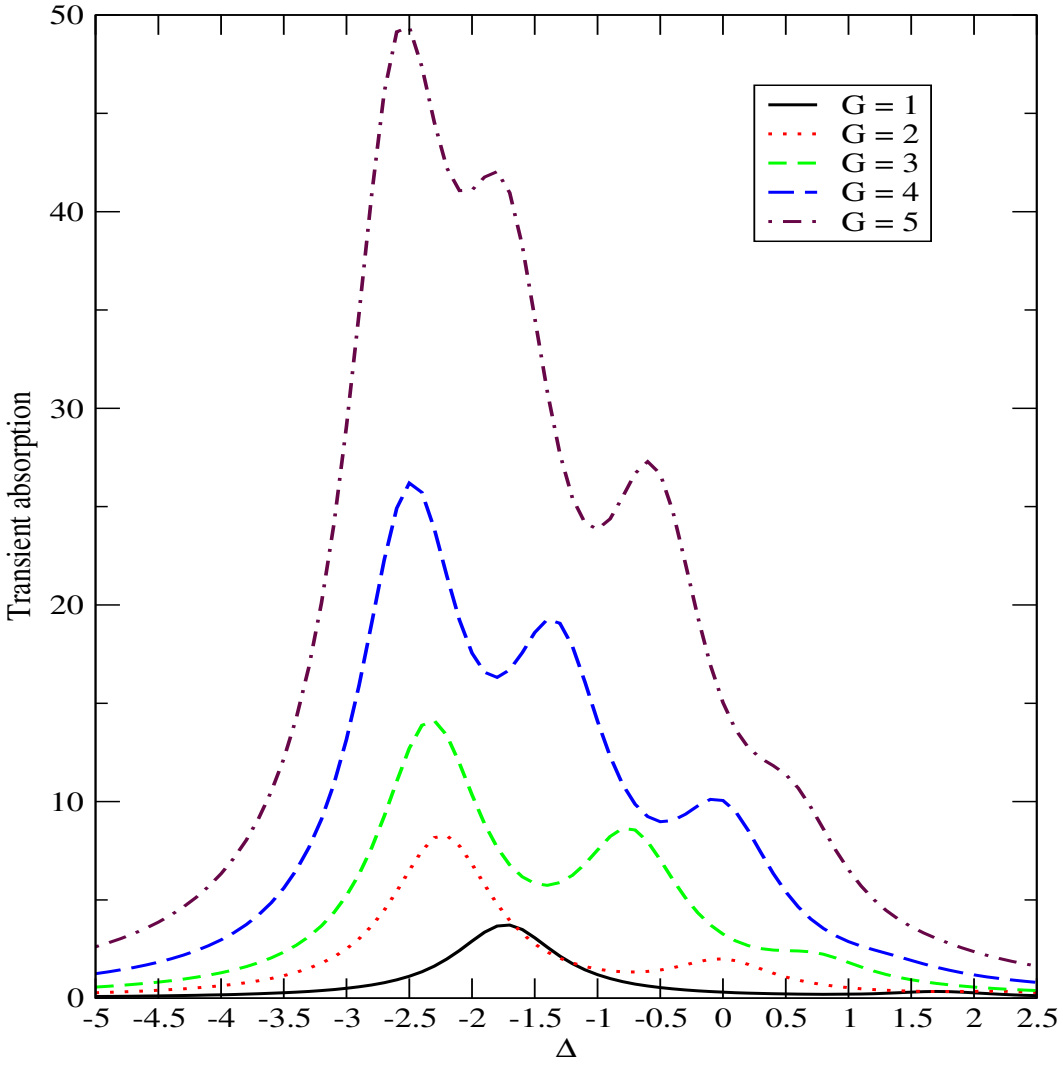

Fig[5.6] Transient absorption spectra for various generations. The intensity of absorption increases with the increase in generation number. There are (n+1) peaks for a dendrimer with n-th generation. The core node absorbs in the higher energy region and peripheral node absorbs in the lower energy region.

Fig.5.5B shows the case when only external nodes are interacting with light. Initially $S_z{}^c$ for $Z = 3$ or $Z = 5$ have negative values as in usual absorption case and as time passes core node gets extra absorption which predominates for longer time for high branching dendrimer. The situation may be considered in the following way. Suppose we are interacting only external nodes with light as shown in Fig.5.4B and suddenly we turn off the field. The situation progresses in a manner as shown and the core node gets positive values (absorption) from the negative value. Here population of individual node is kept fixed in ground state. So from transient absorption spectra we have seen that the geometry and coupling may control the behaviour of core node that can retain its absorbed light for a long time provided the branching around the molecule is high. When only external nodes are interacting with light we have seen that the core node gets maximum absorption after certain time and it dominates for a long time for highly branched molecule.

Fig.5.6 shows absorption plot for dendrimer molecules having various generations. The intensity of absorption increases with the increase in generation number. It has been seen that the the number of peaks arise in the $\Delta = +ve$ region is equal to the number of peaks arise in the $\Delta = -ve$ region. When total number of peaks are odd then a peak (corresponds to G/2) will appear at $\Delta = 0$. These are Autler-Towns splitting due to dipole-dipole interaction. Here a representative dipole of a particular generation interacts nontrivially with its nearest neighbour generations. This study can show distinct peaks for a specific generation. On increasing the coupling strength the splitting become clearly visible. With the increase in generation number the peripheral peaks shift to higher energy region. As the number of nodes in the periphery are the maximum, the most intense blue shifted peak corresponds to peripheral nodes. On the other hand, the peak corresponding to core is shifted to the lower energy region. The inecrease in generation actually increases the separation among the peaks. When the number of peaks are odd then the central peak remains unaffected by the changes in coupling or changes in core-braching. This figure qualitatively matches with the experimental work by Kopelman and co-workers.

We have taken all coupling strength same. The number of peaks blue shifted around $\Delta = 0$ is exactly equal to the number of peaks those are red shifted.

For a PPV dendrimer, the conjugated double bonded system introduces coupling between inter-generation dipoles. Therefore, the dipole-dipole coupling strength scaled with respect to spontaneous decay rate,

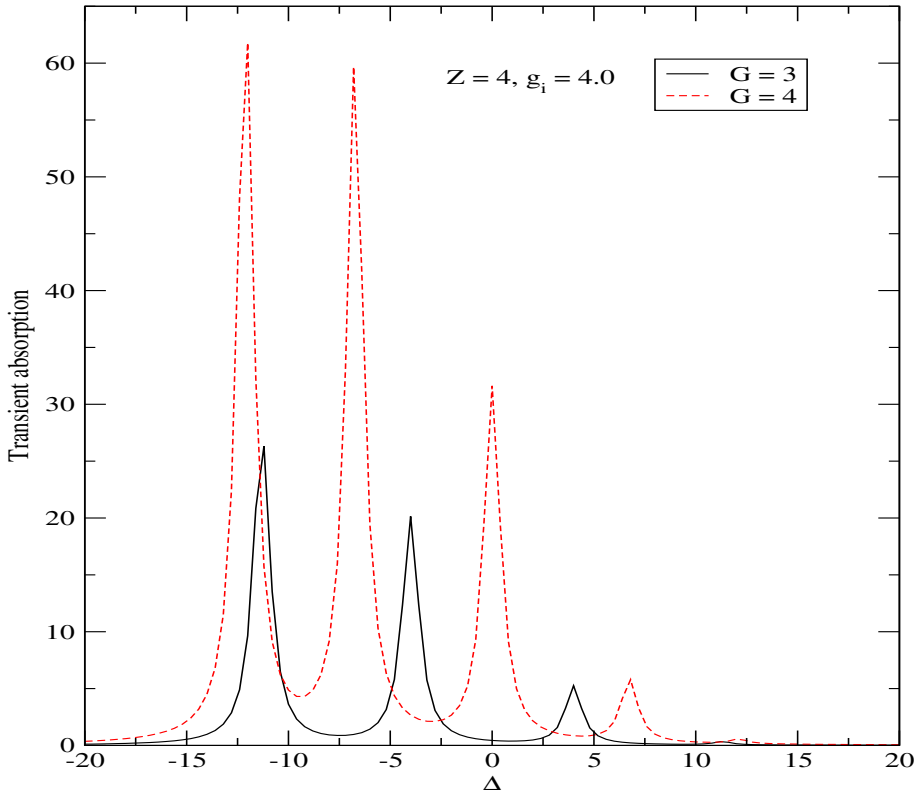

Fig[5.7]Transient absorption spectra for $G = 3$ and $G = 4$ at higher coupling strength. There are four distinct peaks for $G = 3$ and five distinct peaks for $G = 4$.

γ as $\frac{g}{\gamma} \approx 1$ can be estimated as a parameter to get a good fit with the experimental spectral curve of Kopelman. However, for metal containing dendrimer and dendrimer with high electron withdrawing or electron donating group, for example, dendrimer containing N, P and S atoms may be associated with large dipole-dipole coupling strength. For a theoretical understanding about dipole-dipole interaction in dendrimer architecture, we have considered various coupling strength and other parameters of the dendrimeric system.

In the previous figure (Fig.5.6) we have seen the effect of generation. In Fig.5.7 this has been shown more clearly. Solid line is for $G = 3$ and the dotted line is for $G = 4$. There are four distinct peaks for $G = 3$ and five distinct peaks for $G = 4$. The core, 1st and 2nd generation of $G = 4$ molecule is red shifted than the core, 1st and 2nd generation of $G = 3$. We add a peripheral chromophore scaffold around $G = 3$ and all the nodes in the interior start to absorb at low energy. The dendrimeric backbone acts as a solvent in controling the photo-physical properties. This figure predicts that addition of a generation is similar to red shift of absorption spectra.

Now let us have a close look at the distribution of intensities of peaks representing various generations. Intensity decreases from peripheral part to core since number of node absorbing the light decrease on going from periphery to core. There is a significant difference in intensity of 3rd or 2nd generation of large $G = 4$ molecule with the intensity of 3rd or 2nd generation of small $G = 3$ molecule although the number of nodes are same. In the 3rd generation number of nodes is 36 and in the 2nd generation number of node is 12. For larger molecule the peaks in the interior generations are higher in intensity. Since all other parameters are same the higher intensity in the interior peaks are due to the transfer of energy from added peripheral nodes. This transfer occurs through dipole-dipole coupling since all over the time period we have kept ${S_z}^i = -1$.

Fig.5.8 shows the effect of core-branching in the transient absorption spectra. With the increase in core-branching the peripheral peaks shift to higher energy region. Thus the peripheral one shows a blue shift. On the other hand the peak corresponding to core is shifted to the lower energy region. Thus this shows a red shift. Here the total number of peaks is odd. The peak corresponding to 2nd generation is unaffected by the increase in core-branching.

Fig.5.9 shows the effect of coupling strength on the transient ab-

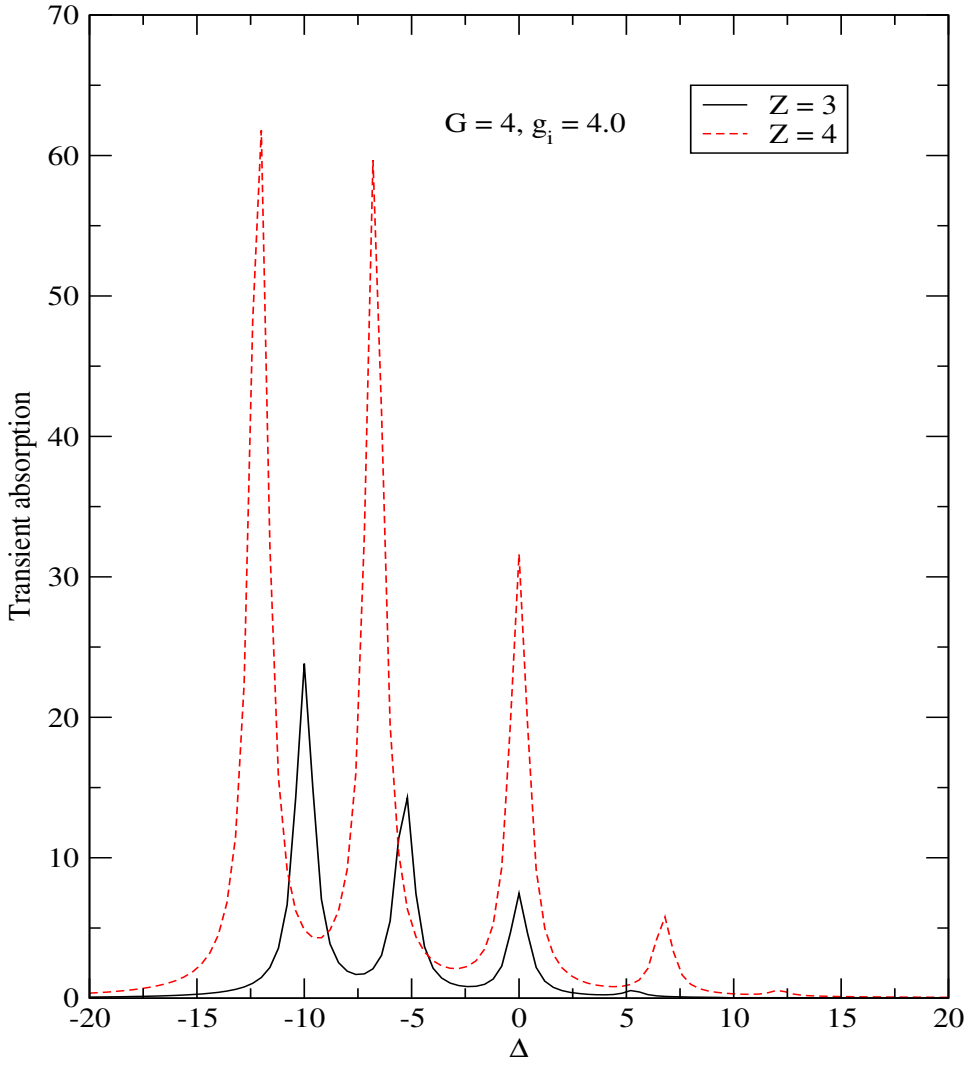

Fig[5.8]Transient absorption spectra at different core-branching. With the increase in core-branching the peripheral peaks shift to higher energy region. Thus the peripheral one shows a blue shift. On the other hand the peak corresponding to core is shifted to the lower energy region.

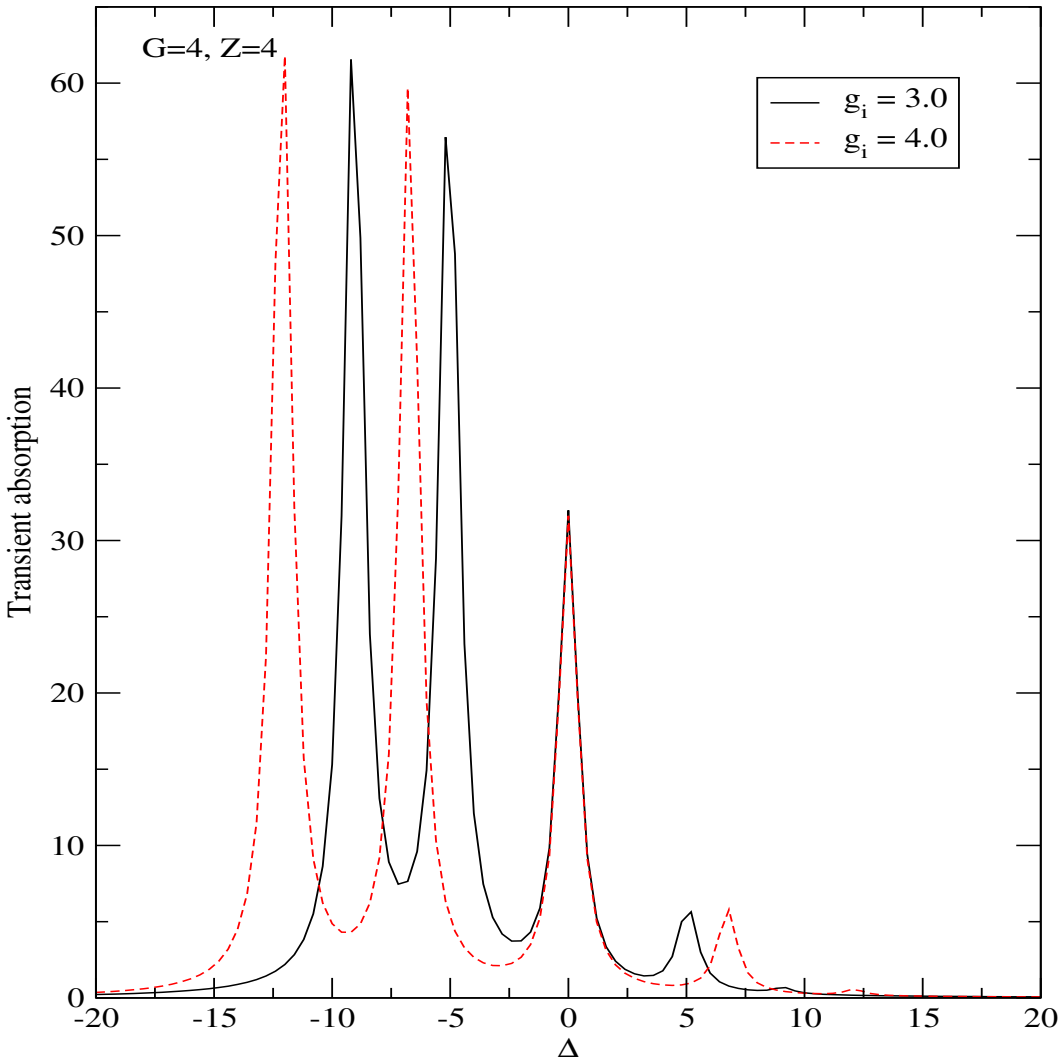

Fig[5.9]Transient absorption spectra at different coupling strengh. The peripheral peaks are blue shifted and the core peak is red shifted. The splitting value is proportional to the coupling strenth.

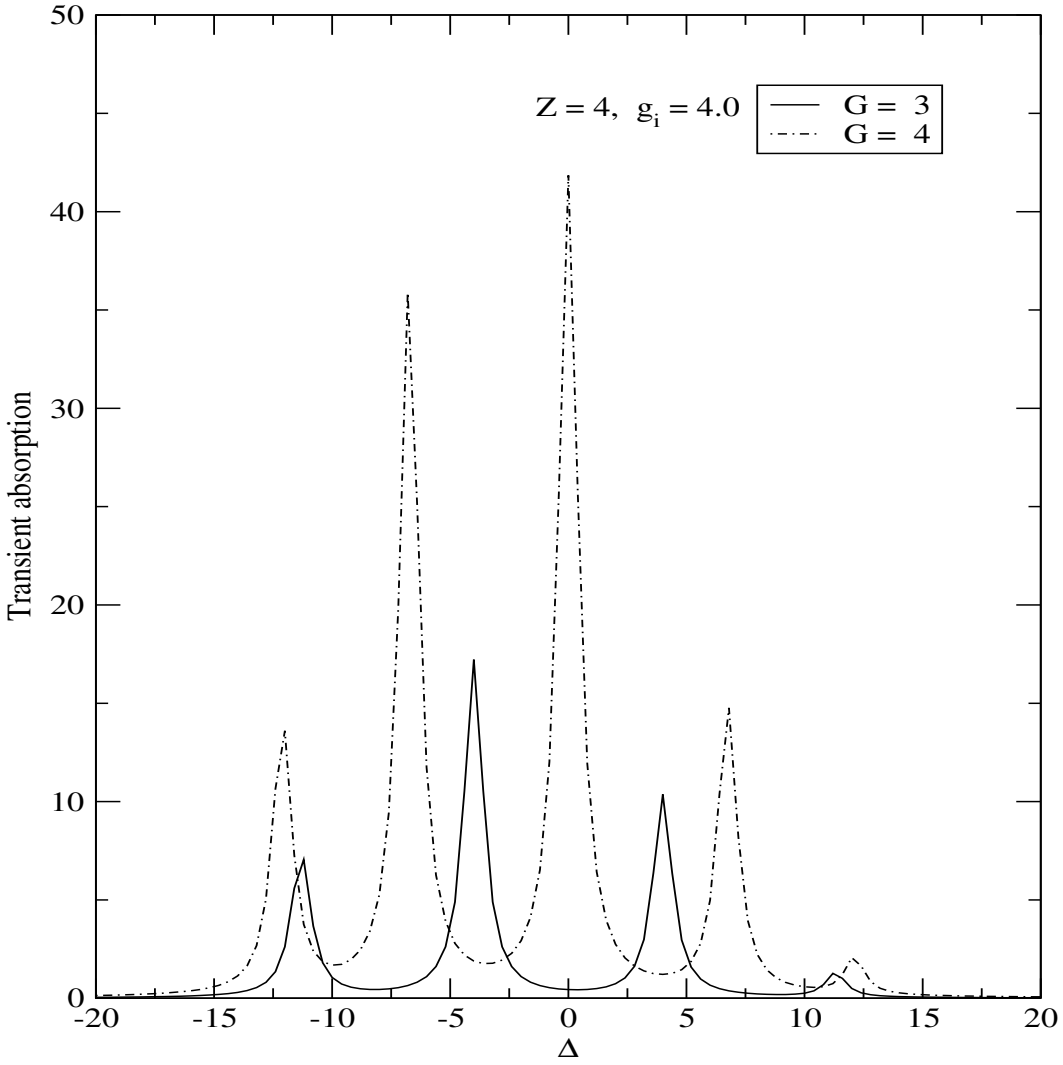

Fig[5.10]Transient absorption spectra for $G = 3$ and $G = 4$ when only external nodes are interacting with light. The positions of peaks remain fixed as it is shown in Fig.5.7. The peak for the intermediate generation is higher than the periphery.

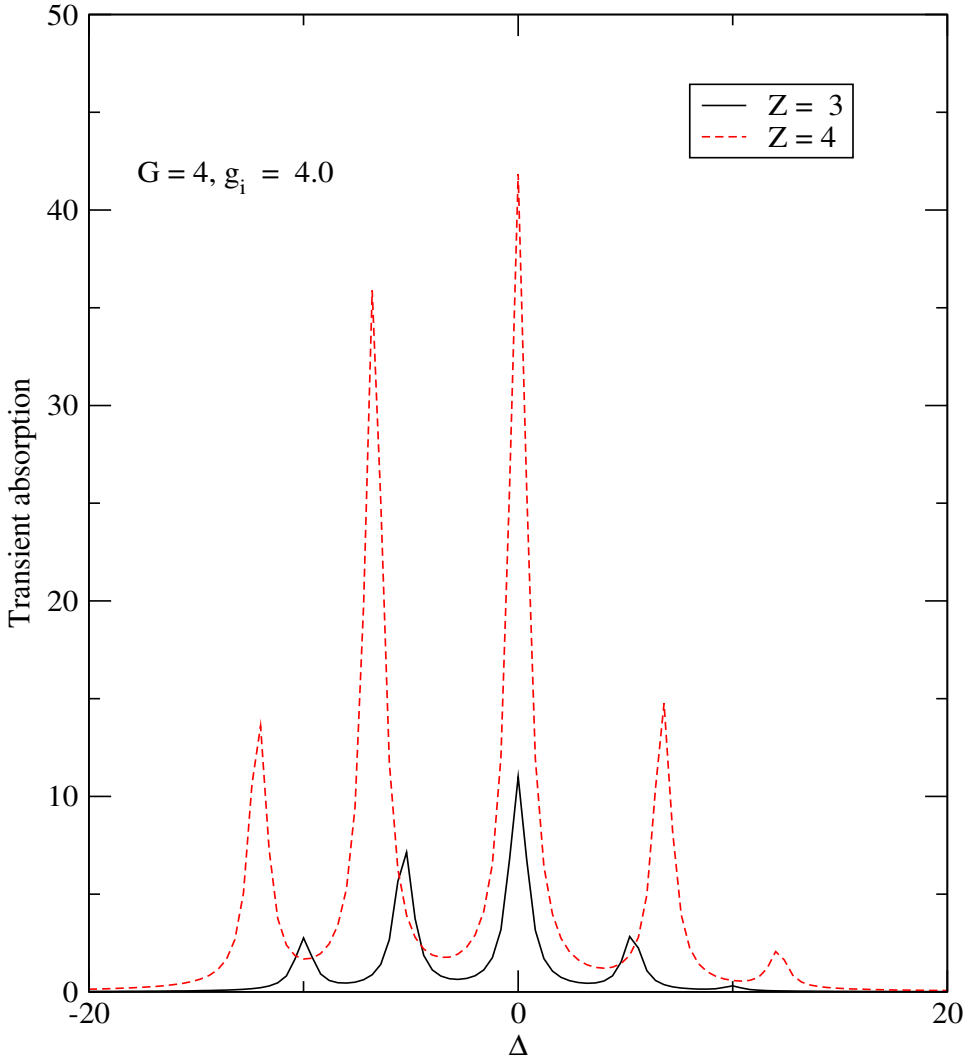

Fig[5.11]Transient absorption spectra for $Z = 3$ and $Z = 4$ when only external nodes are interacting with lighlt. The positions of peaks remain fixed as it is shown in Fig.5.8. The total peaks are splitted symmetrically around central peak of 2nd generation.

sorption spectra. The peripheral peaks are blue shifted and the core peak is red shifted. The splitting value is proportional to the coupling strength. From two figures Fig.5.8 and Fig.5.9 it is seen that the nature of shifts in these figures are same. In Fig.5.8 intensity of the peaks increase with core-branching of the dendrimer molecule as the number of nodes changes with the change in core-branching. In Fig.5.9 the intensities of different peaks of a specific generation are the same. Coupling strength changes the shifts only. Width of the spectrum remain constant with the changes in the system parameters.

5.4.2 Transient absorption when only external nodes are interacting with light

Fig.5.10, Fig.5.11 and Fig.5.12 show the effect of generation, core-branching and coupling strength when only external nodes are interacting with light. It has been seen that the positions of the peaks remain the same as in previous figures (Fig.5.7, Fig.5.8 and Fig.5.9). The intensity of the peaks follow different order. The peak in the bulk region shows higher intensity. Again the intensity that corresponds to the core node is larger than it is when all nodes are interacting with light. The higher intensity in the bulk region proves that the excitation remains in the bulk.

5.5 Summary and conclusions

To identify the effect of branching we have perturbed the dendrimeric molecule in two distinct ways: (i) by interacting the highly branched molecule with light of low intensity and (ii) by interacting low branched molecule with light of high intensity. We have seen that the population inversion curve for generation in the bulk or nearer to the core oscillate with time in both situation in the same way. The excitation retains in the bulk region for branching effect. This proves that the low intensity of photon can impact equally as a high intensity does provided the intermediate branching is higher. High branching can retain the excitation upto a longer time that can lead to transform some photochemical changes even with very low intensity of laser light as shown in his experiment by Aida[2]. A recent study of enhanced rate of valence isomerization of norbornadiene group attached to the core, the quadricyclane group at highly branched dendrimer supports our views regarding the behaviour of the core group[55]. We have seen this excitation in the dendrimer backbone even when only external nodes are interacting with light for some long

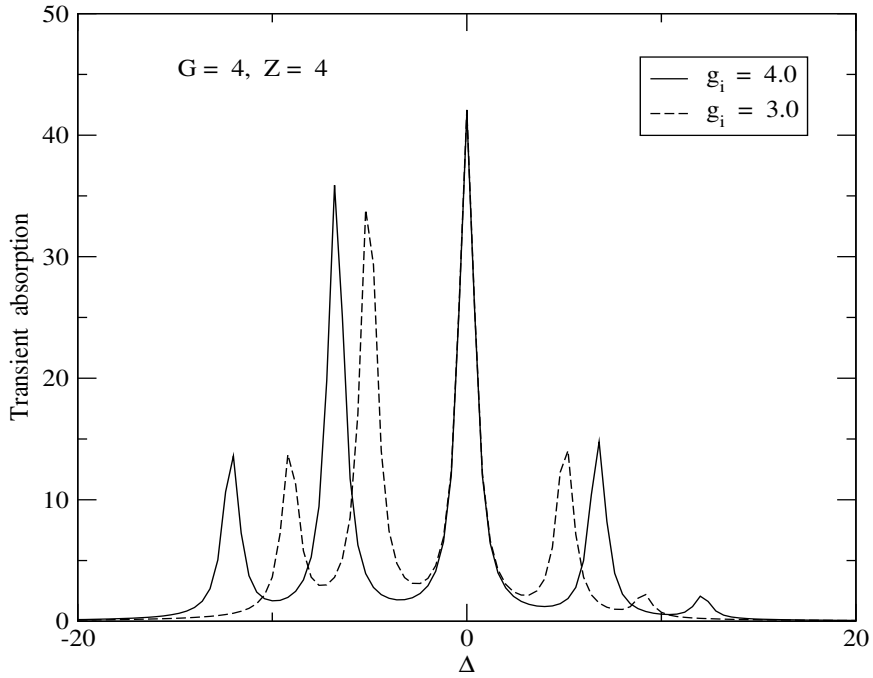

Fig[5.12] Transient absorption spectra at different coupling strength when only external nodes are interacting with light The positions of peaks remain fixed as it is in Fig.5.9. The intensity of intermediate generation is higher than the peripheral generation.

time. In that case the population inversion of the core become higher which is an example of a gained medium in the core.

The appearance of total absorption plot in transient study with generation shows that for n-th generation dendrimer there will be (n+1) peaks. The peak representing core appears at extreme right and peak representing periphery appears at extreme left. The intensity of absorption increases with increase in generation. The number of peaks appear in $\Delta = +ve$ and number of peaks appear in the $\Delta = -ve$ region are equal. Splitting occurs when coupling strength is higher. Kopelman and co-workers have shown experimentally that the lowest energy peak in the extended dendrimer blue shifted on increasing the generation. Here we have seen the blue shifting of core absorption that appears in the lower energy region. In chapter 4 we have given a heuristic arguments to show enhance energy funneling by modifying the coupling strength among the intermediate nodes.

The intensity of absorption of intermediate generation of a larger dendrimer molecule is higher than the intensity of absorption of some interior generation of a smaller dendrimer molecule. The normal distributions of intensities of peaks are decreasing from peripheral generation to core generation. This ordering is according to the number of absorbing nodes present. This distribution changes when only external nodes are interacting with light. The intermediate i.e, the n/2 -th generation got the maximum intensity inspite of the fact that the number of intermediate nodes are lower than those present in the peripheral generation. This study also supports that the energy transfer must occur via the dendrimeric backbone through dipole-dipole coupling. The Autler-Townes splitting due to inter-generation dipole-dipole interaction of the absorption curve is very important to show the effect of geometry. These are intensified when dipole-dipole coupling strength is larger. The large dipolar strength may be associated with dendrimers containing hetero atoms. This feature is also unique due to branched structure which is not observed in the linear chain when all other parameters remain the same.

Chapter 6

6 Electron Transfer Through Dendrimeric Architecture

In this chapter we have discussed our work on the steady state quantum mechanical theory of electron transfer rate in dendrimeric architecture. In section 5.2 we have described the model and the required steady state equations for linear and dendrimer systems. In section 5.3, we have provided the results and discussion to elucidate the distance dependence of electron transfer rate on linear chain and dendrimer case, the effects of dephasing of the bridge elements, influence of coupling strength and the effect of various energy gaps between the donor-acceptor and bridge levels. Finally the paper is concluded in section 5.4.

6.1 Introduction

Long range electron transfer[144, 137] through bridging molecular structure between a donor and an acceptor has been reviewed repeatedly both theoretically [138, 139, 140] and experimentally[141, 142]. Electron transfer is the fundamental process in photosynthesis, mitochondrial transport, protein,[143] and DNA[145, 200]. The distance dependence of bridge mediated electron transfer between donor and acceptor have attracted several groups[201, 202, 203, 204, 205, 206, 207] with several bridging media that contain synthetic peptides, [146, 147, 148] modified proteins,[149, 150] protein-protein complexes,[151] saturated and unsaturated chains[152, 153, 154, 155]. Again recent advances in nanotechnology involves installment of preassigned electronic function into a molecule acting as a nanomaterial in metal-molecule-metal junction[156]. Molecular electronics is a field of studies that proposes the use of single or small packets of molecule to function as the key components in future computational devices where use of a single molecule reduces the area 10^6 times than current silicon chips. There are single, two, three and four terminated molecular wires[157]. Several synthetic routes[157, 158, 159] towards conjugated oligo(phenylene ethynylene)s are producing molecular devices possessing donor groups, acceptor groups, porphyrin interiors, other heterocyclic interiors or in some instances devoid of any group. The nano science experimental technique has been able to demonstrate long

range through-bond electron transfer process[160]. The electronic transparency of a molecule is being determined by coulomb-blockade,[161] nanopore,[162] break-junction,[163] electro-deposition,[164] and nanolithography[165]. Theoretical and experimental studies on I-V characteristic reveals that the resistance on such metal-molecule-metal junction depends very much on the chemical structure of the molecule, its conformation at the junction and its chemical binding to the nano electrode[166, 167, 168, 169]. The electron transfer process through the molecule and the rate at which the junction electrodes deliver electron to the molecule is the determining factor of this metal-molecule-metal nanojunction[170]. Again in natural photosynthesis the chlorophyll moiety surrounds a single reaction center to harvest light and transfer their energy to the reaction center[171, 172]. Long assembly of chromophores transfer their energy with greater efficiency over a nanometer distance[173] and this phenomenon has motivated to study artificial light harvesting system[174]. A wide variety of organic,[175, 176] organometallic,[177, 178] supra-molecular,[179] polymeric[180, 181] and dendritic[183, 184, 185, 186] chromophore assemblies have been developed to mimic natural light harvesting process. An electron tunnelling through a barrier has effective electronic interaction between two center(DA) $\mid H_{DA} \mid^2 = exp(\frac{2(2mL)^{\frac{1}{2}}}{\hbar}) = exp(-\beta R_{DA})$ where L is the tunnelling height and β is the decay rate of coupling with R_{DA} is the distance between the centers[187]. Again Fermi's Golden Rule gives kinetics of electron transfer according to rate equation $k_{ET} = \frac{2\pi}{\hbar} \mid H_{DA} \mid^2 (FC)$ where FC is the Franck Condon factor. This FC is the sum of the products of overlap integrals of the vibrational and solvent wave functions of the reactant/donor to those of the product/acceptor. For an intra-molecular electron transfer, molecular modes are treated quantum mechanically but solvent effects are treated classically. Marcus has shown that $k_{ET} = (\frac{2\pi}{\hbar}) \mid H_{DA} \mid^2 (\frac{1}{4\pi\lambda k_B T})^{(\frac{1}{2})} \ exp[-\frac{(\Delta G^0 + \lambda)^2}{4\lambda k_B T)}]$ where λ is total nuclear re-organizational energy, ΔG^0 is the free energy of the reaction[188]. Most experiments have shown long range electron transfer through bridge using empirical relation $k_{ET} = A(T)exp(-\beta R_{DA})$ where A(T) is the temperature dependent prefactor and β is a constant for fixed bridge D-A setup.

Dendrimeric architecture [182, 183, 184, 185, 186, 189, 190, 191, 192, 193, 194, 195, 196, 93, 219, 220, 221, 35, 223, 224, 225, 226, 227, 231] reveals that they have extreme efficiency of transfer even at higher generation. So these dendrimeric architecture may be used for electron transfer at nanometer range molecular electronic devices.

Aida group have shown fluorescence quenching of dendritic Zn Phorphyrins with methyl viologen(MV^{2+}, an electron acceptor) is obviously

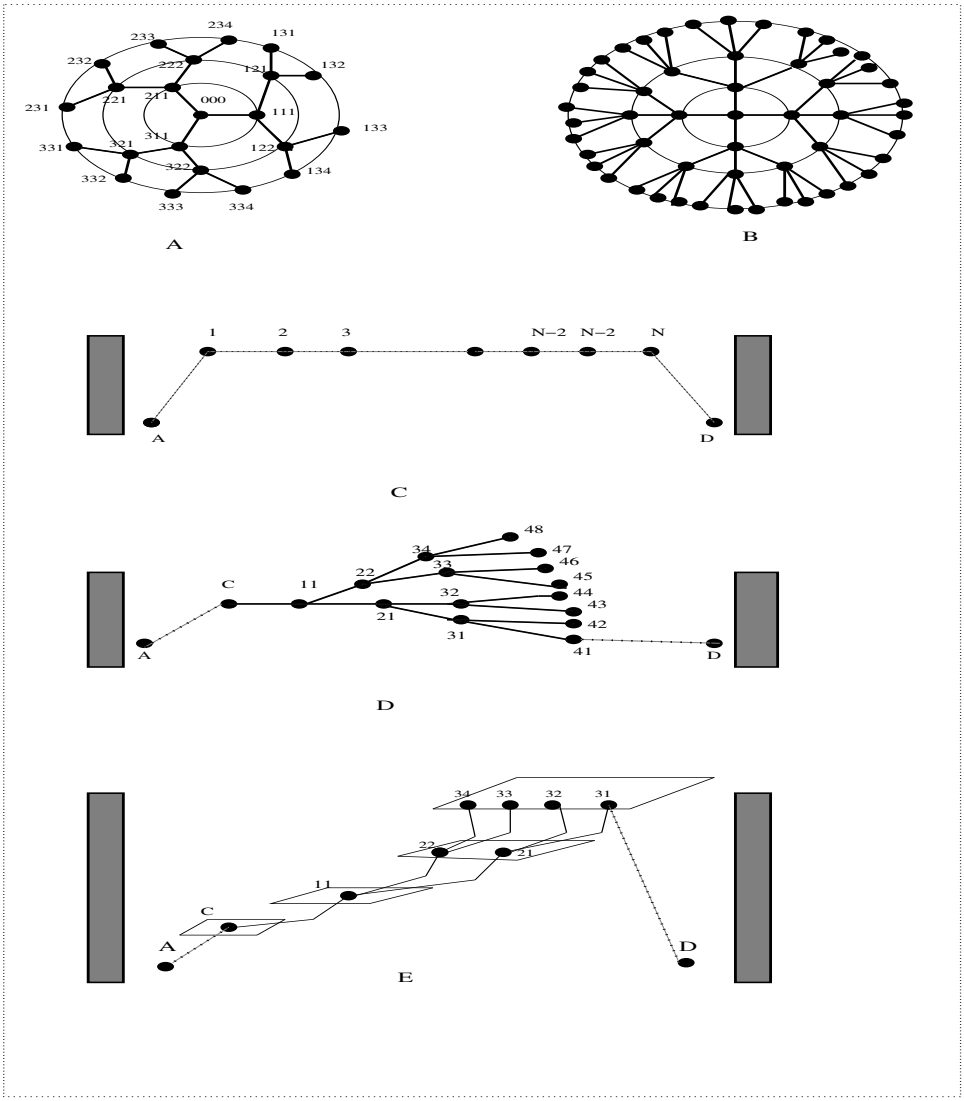

[Fig 6.1] (A): A schematic diagram for dendrimer super-molecule of third generation with core branching C=3. (B): A schematic diagram for dendrimer super-molecule of third generation with core branching C=4. (C): Model for linear one level molecular bridge with N sites for electron transfer between donor and acceptor: A is the acceptor state, D is the donor state, left and right rectangles are the continuum for metal menifolds. (D): A single dendritic branch is taken as a bridging medium between a donor which is connected to a single node at periphery and an acceptor which is connected to the core. Each node is acting as one level site for electron transfer. Here all bridging nodes including the core are assumed to be degenerate. (E): A single dendritic branch is taken as bridging medium between donor which is connected to a single node at the periphery and the acceptor which is connected to the core where the nodes of a fixed generation have the same energy with a superimposed energy funnel from the periphery to the core.

the result of long range photoinduced electron transfer through the dendrimeric architecture[190]. Ghaddar et al [191] have shown that on excitation of a donor unit (benzyleether /naphthalein) at periphery of the dendrimer first and second electron transfer can occur in a stepwise manner to produce monoreduced(MV^+) and doubly reduced (MV) at the core of the dendrimer. According to them dendrimer can be used as synthetic model where only one photon can produce only one electron that reduces the core in a stepwise manner which mimics natural light harvesting antenna system. There are several studies considering DNA as molecular wire. Recent experiment[192] on electron transfer between $[Ru(NH_3)_5pz]^{2+}$ and $[Co(C_2O_4)_3]^{3-}$ in presence of dendrimer reveals that dendrimer and DNA behave similarly in a particular molecular level of functionality. So dendrimeric architecture may play an important role as molecular conductor as DNA does. Again recently dendrimers are being used as organic light emitting diodes[193, 194, 195, 196](OLED) for various purposes. This electro-luminescence property are also related to the intrinsic property of mobility of electronic charges along the dendrimeric structure.

From the extensive studies of electron transfer from donor to acceptor[197, 198, 199] it has been concluded that there are two pathways. One is the superexchange mechanism and other is the sequential hopping. Ratner[200] explained that if the bridging states differ in energy than the initial and final states then a coherent exchange takes place which is generally called superexcahnge mechanism. This coherent/super-exchange/tunnelling mechanism is not operative when the intervening bridging media is of longer distance due to poorer overlap of orbitals in which electronic density is found. In a sequential hopping mechanism the electron actually occupy the bridge state. Some used perturbation theory like McConnel[201, 202, 203] to explain super-exchange mechanism leading to mixing of intervening orbitals with donor and acceptor.

A complete quantum mechanical treatment of electron transfer must include all possible vibrations for donor, acceptor, bridge and surrounding medium. The complexity of the problem increases as a consequence of this. Again the exponential dependence of electron transfer rate is not followed by conducting polymer poly(p- phenylene vinylene)[160]. They show ohmic behaviour($k_{ET} \approx \frac{1}{N}$). Felts, Pollard and Friesner gave plausible mechanism for anomalous distance dependence[197]. Nitzan and co-workers[208] have seen the effect of dephasing and relaxation in bridge mediated electron transfer. [209] Density matrix[209, 210, 211, 212, 213, 214, 215, 216, 217] formalism for dissipative quantum dynamics is the major part for the methodology of this type of bridge mediated

electron transfer study.

With this background we can think of a quasi steady state or a steady state electron transfer process far away from equilibrium in those complex architectures. The natural question is that how an electron transfer process through a dendrimeric architecture can differ from an electron transfer process through a linear chain with similar repeating units. We want to see how complex dendrimeric architecture affects electron transfer rate from a donor to an acceptor. Assigning separate acceptor at the core and a separate donor at the periphery we have studied electron transfer through dendrimeric bridge. The donor and accptor may be any chemically or photochemically active species for example, in their reduced and oxidized state, respectively. They may be metal leads in case of metal-molecule-metal junction for a molecular conductor or a molecular wire. The interplay of donor, acceptor and bridge energy gaps on the electron transfer have been considered. The effect of donor acceptor distance in terms of the number of bridging site and dendrimeric generation have also been studied. In this paper our simplified approach involves reduced density matrix formalism and Liouville equation assigning each bridge level as an eigenstate of the Hamiltonian in local basis where interaction of the bath has been considered phenomenologically as studied by Davis et al.[229] in the backbone of a Cayley tree. This phenomenological damping theory was used by Nitzan and co -workers to relate resonance Raman scattering with resonance fluorescence.[228] Our main aim is to study the signature of the cayley tree architecture into the electron transfer rate using reduced density matrix technique. We would like to see how one can control coherent and incoherent regime of electron transfer by changing system parameters, like number of bridging sites, coupling between bridging sites, dephasing parameters and energy differences between donor/acceptor and bridging media. We shall investigate the effect of these considering linear and dendrimeric architecture.

6.2 Model and steady state equations

In figure 6.1A for linear system A is the acceptor state which is defined as site 0 and D is the donor state which is defined as the $N+1$ site and the sites of the bridge groups are extended from 1 to N. i is the ket vector, $\mid i\rangle$ corresponding to i-th site of the bridging media where i runs from 1 to N. When the intermediate bridges are not linear specifically dendrimeric one, we assume the nodes or sites for a specific generation are degenerate. We assign for example, core = C, node for 1st generation is

11, two degenerate nodes for second generation are 21 and 22 respectively and so on. For this dendrimeric architecture $\mid ij\rangle$ corresponds to the ket vector of a node of ith generation and j is the index of degenerate nodes where j runs from 1 to 2^{i-1} and i runs from 1 to G where G is the size of the dendrimeric bridge. We construct the reduced density matrix defined in the Hilbert space of local basis composed of node or site of linear or dendrimeric bridge and vectors corresponding to acceptor and donor. The Hamiltonian for quantum mechanical system interacting with a bath can be expressed as in the similar way as studied by Davis et al[229]

$$H = H_S + H_B + H_{SB} \tag{6.1}$$

where the three terms on the right hand side of equation(1) are the system, bath and system-bath interaction Hamiltonians, respectively.

6.3 Steady state rate for linear system

In a bridging media where N bridge sites are present with donor and acceptor then H_S may be given as

$$H_S = \omega_A \mid A\rangle\langle A \mid + \omega_D \mid D\rangle\langle D \mid + \sum_{i=1}^{N} \omega_i \mid i\rangle\langle i \mid + V_{A1} \mid A\rangle\langle 1 \mid + V_{1A} \mid 1\rangle\langle A \mid + V_{DN} \mid D\rangle\langle N \mid +$$

$$V_{ND} \mid N\rangle\langle D \mid + \sum_{i=1}^{N-1} (V_{i,i+1} \mid i\rangle\langle i+1 \mid + V_{i+1,i} \mid i+1\rangle\langle i \mid). \tag{6.2}$$

where $\mid A\rangle, \mid D\rangle$ are the acceptor and donor state respectively and bridge states are from $\mid 1\rangle$ to $\mid N\rangle$. The Liouville equation for the density operator ρ of the overall molecule bath system is

$$\dot{\rho} = -i\,[H, \rho]\,(\hbar = 1) \tag{6.3}$$

Using notation for the reduced molecular density operator $\sigma = Tr_B \rho$ under the assumption that V and interaction with bath is small. Then the reduced equation of motion is of the form

$$\dot{\sigma}_{jk} = -i\omega_{jk}\sigma_{jk} - i\,[V, \sigma]_{jk} + L_D \tag{6.4}$$

where L_D includes the dynamical influences of the last two terms of the equation(1).

The equation for linear system may be given as with simple phenomenological damping[229]

$$\dot{\sigma}_{AA} = -iV_{1A}\sigma_{A1} + iV_{A1}\sigma_{1A} - \kappa\sigma_{AA},$$

$$\dot{\sigma}_{11} = -iV_{1A}\sigma_{A1} + iV_{A1}\sigma_{1A} - iV_{12}\sigma_{21} + iV_{21}\sigma_{12},$$
$$\dot{\sigma}_{22} = -iV_{21}\sigma_{12} + iV_{12}\sigma_{21} - iV_{2D}\sigma_{D2} + iV_{D2}\sigma_{2D},$$
$$\dot{\sigma}_{DD} = -iV_{D2}\sigma_{2D} + iV_{2D}\sigma_{D2} + J,$$

$$\dot{\sigma}_{A1} = iV_{A1}\sigma_{AA} - i\omega_{A1}\sigma_{A1} + iV_{21}\sigma_{A2} - iV_{A1}\sigma_{11} - \frac{(\kappa+\gamma)}{2}\sigma_{A1},$$

$$\dot{\sigma}_{A2} = iV_{12}\sigma_{A1} - i\omega_{A2}\sigma_{A2} + iV_{D2}\sigma_{AD} - iV_{A1}\sigma_{12} - \frac{(\kappa+\gamma)}{2}\sigma_{A2},$$

$$\dot{\sigma}_{AD} = iV_{D2}\sigma_{2A} + iV_{1A}\sigma_{D1} + i\omega_{DA}\sigma_{DA} - \frac{\kappa}{2}\sigma_{DA},$$
$$\dot{\sigma}_{12} = -iV_{1A}\sigma_{A2} - iV_{12}\sigma_{22} + iV_{12}\sigma_{11} + iV_{D2}\sigma_{1D} - i\omega_{12}\sigma_{12} - \gamma\sigma_{12},$$

$$\dot{\sigma}_{1D} = -i\omega_{1D}\sigma_{1D} - iV_{12}\sigma_{2D} - iV_{1A}\sigma_{AD} + iV_{2D}\sigma_{12} - \frac{\gamma}{2}\sigma_{1D},$$

$$\dot{\sigma}_{2D} = -i\omega_{2D}\sigma_{2D} - iV_{2D}\sigma_{DD} - iV_{21}\sigma_{1D} + iV_{1D}\sigma_{21} - \frac{\gamma}{2}\sigma_{2D}. \qquad (6.5)$$

with $\sigma_{ij} = \sigma_{ji}{}^*$, $V_{ij} = V_{ji}{}^*$ and $\omega_{ij} = \omega_i - \omega_j$. The donor site is connected with an unspecified source. Electronic population is entering through this site to maintain a constant population flux J. Acceptor site is coupled to a sink with decay rate κ. γ is the thermal dephasing rate in the bridge appears only in the relaxation of all non-diagonal elements of the density matrix associated with the bridge levels.

In matrix notation the equation of motion is

$$\dot{\sigma} = \hat{A}.\sigma + \hat{J} \qquad (6.6)$$

At steady state one can have $\dot{\sigma}_{ij} = 0$. The electron transfer can be calculated as the ratio between the steady state flux[229] through the system J and the population of the donor level, ${\sigma_{DD}}^{SS}$, at steady state

$$k_{ET} = \frac{J}{\sigma_{DD}^{SS}}. \tag{6.7}$$

This steady state rate wiil be equivalent to transient dynamical rate at long time k_{LT} if a quasi-steady state is reached such that most of the populations are in the donor state i.e. $\sigma_{DD} \approx 1$ and $\sigma_{ij} \ll 1$.

6.4 Steady state rate at dendrimeric architecture

For simplicity dendrimeric architecture with a single branch has been considered. Hamiltonian for dendrimeric architecture with nearest neighbour interaction is given by

$$H_S = \omega_A \mid A\rangle\langle A \mid + \omega_C \mid C\rangle\langle C \mid + \omega_D \mid D\rangle\langle D \mid$$

$$+ \sum_{i=1}^{G} \sum_{j=1}^{2^{i-1}} \omega_{ij} \mid ij\rangle\langle ij \mid + V_{AC} \mid A\rangle\langle C \mid + V_{CA} \mid C\rangle\langle A \mid$$

$$+ V_{C,11} \mid C\rangle\langle 11 \mid + V_{11,C} \mid 11\rangle\langle C \mid + V_{G1,D} \mid G1\rangle\langle D \mid + V_{D,G1} \mid D\rangle\langle G1 \mid$$

$$+ \sum_{i=1}^{G} \sum_{j=1}^{2^{i-1}} \sum_{m=2j-1}^{2j} (V_{ij,i+1\,m} \mid ij\rangle\langle i+1\,m \mid + V_{i+1m,ij} \mid i+1\,m\rangle\langle ij \mid) \tag{6.8}$$

where G is the size of the branch i.e. the generation number, C is the core of the dendrimer. Here the acceptor node is connected to the core node C and the donor $\mid D\rangle$ is attached to one of the peripheral nodes. In a similar way reduced equation of motion of a node that is behaving as one level bridge site can be given as follows. For node at the acceptor and core the equations are

$$\dot{\sigma}_{AA} = -iV_{AC}\sigma_{CA} + iV_{CA}\sigma_{AC} - \kappa\sigma_{AA}$$

$$\dot{\sigma}_{AC} = -i\omega_{AC}\sigma_{AC} - iV_{AC}\sigma_{CC} + iV_{AC}\sigma_{AA} + iV_{11,C}\sigma_{A,11} - \frac{\gamma+\kappa}{2}\sigma_{AC}$$

For nodes at the bulk the equations are

$$\dot{\sigma}_{ij,\,lm} \quad = \quad -i\omega_{ij,\,lm}\sigma_{ij,\,lm}$$

$$-iV_{ij,\,i-1k}\sigma_{i-1k,\,lm}(\,k=\frac{j}{2}\text{or}\frac{j+1}{2}\text{for j even or odd}) - i\sum_{k=2j-1}^{2j} V_{ij,i+1k}\sigma_{i+1k,lm}$$

$$+iV_{l-1k,lm}\sigma_{ij,l-1k}(\,k=\frac{m}{2}or\frac{m+1}{2}\text{for m even or odd}) + i\sum_{k=2m-1}^{2m} V_{l+1k,lm}\sigma_{ij,l+1k}$$

$$\dot{\sigma}_{ij,ij} = -iV_{ij,i-1k}\sigma i-1k,ij(k=\frac{j}{2}or\frac{j+1}{2}\text{for j even or odd}) - i\sum_{k=2j-1}^{2j} V_{ij,i+1k}\sigma_{i+1k,ij}$$

$$+iV_{i-1k,ij}\sigma ij,i-1k(k=\frac{j}{2}or\frac{j+1}{2}\text{for j even or odd}) + i\sum_{k=2j-1}^{2j} V_{i+1k,ij}\sigma_{ij,i+1k} - R_{ij,\,lm}\sigma_{ij,\,lm}$$

For peripheral nodes the term containing V_{i+1} become zero, where i is the index of generation.

$$R_{ij,lm} = \gamma\sigma_{ij,\,lm} \text{ for } ij \text{ or } lm \;\neq A \text{ or } D \text{ and } ij \;\neq\; lm$$

$$R_{ij,A} = \frac{\gamma+\kappa}{2}\sigma_{ij,\,A} \text{ for } lm \;=\; A \text{ and } ij \;\neq\; D$$

$$R_{ij,D} = \frac{\gamma}{2}\sigma_{ij,\,D} \;\text{ for } lm \;=\; D \text{ and } \;ij \;\neq\; A$$

$$R_{A,D} = \frac{\kappa}{2}\sigma_{ij,\,lm} \text{ for } lm \;= D \text{ and } ij \;=\; A$$

$$R_{ij,\,ij} = 0 \;\;.$$

The equations corresponding to the donor group that is connected with the first node of G th generation (see Fig.6.1D) are

$$\dot{\sigma}_{DD} = -iV_{D,G1}\sigma_{G1,G1} + iV_{G1,D}\sigma_{D,G1} + J$$

$$\dot{\sigma}_{D,G1} = -i\omega_{D,G1}\sigma_{D,G1} - iV_{D,G1}\sigma_{G1,G1} + iV_{G-11,G1}\sigma_{D,G1} + iV_{D,G1}\sigma_{DD} - \frac{\gamma}{2}\sigma_{D,G1} \tag{6.9}$$

The above equations constitute a set of $(2^G+2)^2$ linear algebraic equation for a dendrimeric architecture of generation G. Here the steady state rate are calculated in the similar way followed for linear case.

6.5 Results and Discussions

We want to show various parametric dependence of electron transfer rate for linear and dendrimeric cases in coherent, intermediate and incoherent regime on the basis of equations (6.8) and equations (6.9). The rate of electron transfer in both linear and dendrimeric cases depend largely on the distance between the donor and acceptor, solvent dephasing, coupling strength between the sites, bridge energy levels. Here our main epmhasis is on the difference in behaviour of ET when the bridge groups are disposed on the linear as well as on a dendrimeric architecture.

Then we want to show the dependence of electron transfer rate on γ, V and ω_B and ω_D where the energy level of the donor site is ω_D . Here κ is the decay rate of the acceptor, ω_A is the energy level of the acceptor. In all cases we have taken all bridge sites are degenerate and have taken $\kappa = 400\ \mathrm{cm}^{-1}$, $\omega_A = \omega_D = 0$ and $\omega_B = 1000\ \mathrm{cm}^{-1}$ and $V = 400\,\mathrm{cm}^{-1}$ unless stated otherwise.

We have solved the equation $\dot{\sigma} = \hat{A}\sigma + \hat{J} = 0$ numerically with proper boundary condition studied earlier[229] for steady state solution. Here only damping mechanism is the dephasing of off-diagonal elements of the density matrix. The donor site has a constant population J and the acceptor site has a decay rate κ. σ is a column vector having N^2 number of elements where N is the total number of sites including the donor and acceptor. To obtain the matrix elements of $\hat{A}$ we have assigned an index variable S(I) for every σ_{ij} element of the vector σ. This S(I) will indicate the row elements of $\hat{A}$. The column elements will be obtained from individual equation of $\dot{\sigma_{ij}}$ with proper identification of index variable S(I). $\hat{J}$ has only one nonzero element corresponding to the equation of $\dot{\sigma}_{DD}$. For dendrimeric architecture we have assigned similar index variable S(I) for every $\sigma_{ij,kl}$ element and rows and columns of $\hat{A}$ are calculated subsequently. Then we have used standard matrix inversion technique to obtain σ_{ij} for linear case and $\sigma_{ij,kl}$ for dendrimeric case. Here all parameters have been taken in cm^{-1} unit. Rate evaluated in all cases are also in the same unit($1\ \mathrm{cm}^{-1} = 3 \times 10^{10}\ \mathrm{Sec}^{-1}$).

6.6 Distance dependence of electron transfer rate

Here we want to show the dependence of electron transfer rate on the number of bridge sites for the linear and dendrimeric case. Distance between the donor and acceptor depends on the number of intervening

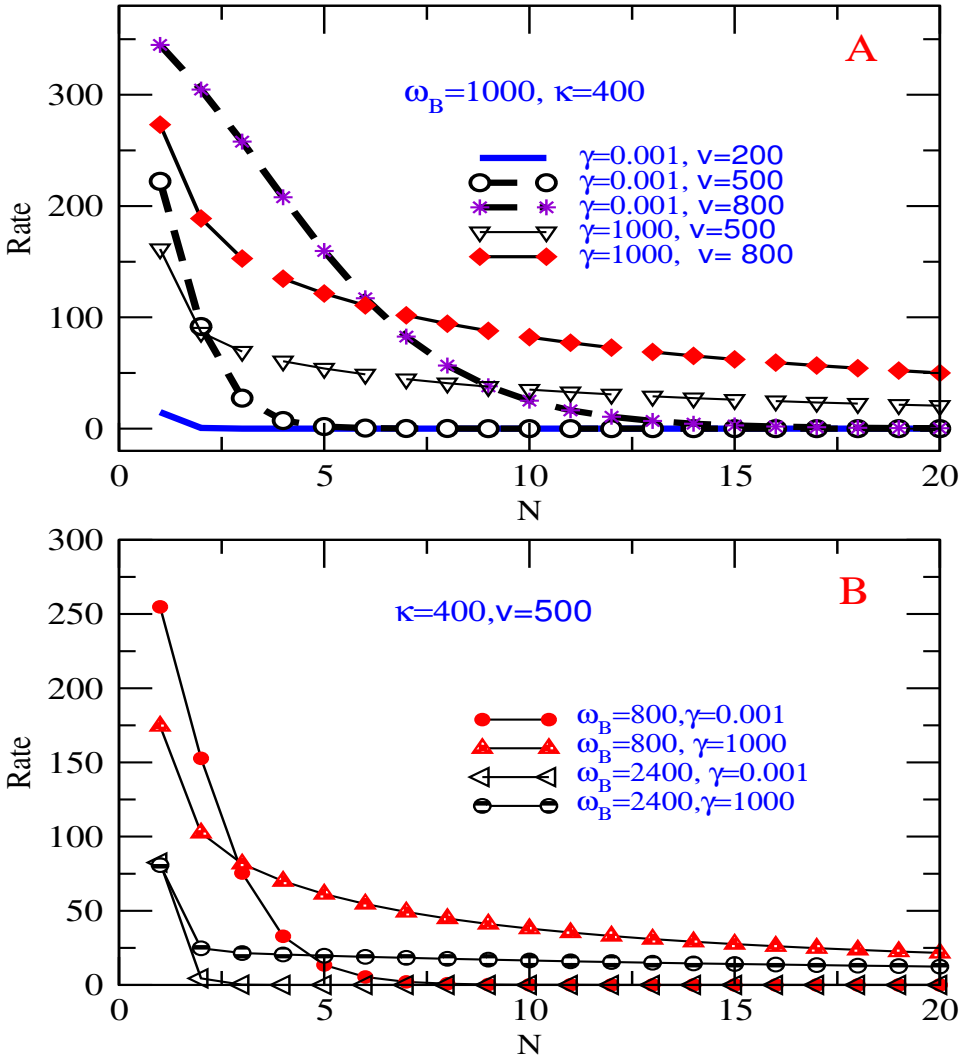

[Fig 6.2] Distance dependence of electron transfer rate is shown for various system parameters for linear bridge. In all cases, unless otherwise stated, we consider $\omega_A = \omega_D = 0\,\mathrm{cm}^{-1}$, $\omega_B = 1000\,\mathrm{cm}^{-1}$, $\kappa = 400\,\mathrm{cm}^{-1}$ and $V = 400\,\mathrm{cm}^{-1}$.

bridge sites between them. In case of dendrimeric architecture distance can also be measured in terms of the number of generations between the donor and acceptor. The distance dependence is very much sensitive on the bridge energy level ω_B , the dephasing parameter γ , the coupling strength V and the number of sites N, for linear bridge and number of generations G, for dendrimeric bridge. To compare the ET for the linear bridge and dendrimeric bridge having equal number of intermediate sites, we have separately discussed at the end of this subsection.

6.6.1 For linear bridge

Previous studies[137, 208] on electron transfer rate in linear system by Nitzan and co-workers showed the bridge length dependence as follows. (i)$\mathrm{k_{ET}} = \exp(-\beta' \mathrm{N})$ corresponds to a superexchange transport for small N, large $\frac{\Delta E_B}{V_B}$ and large $\frac{\Delta E_B}{k_B T}$. (ii) $\mathrm{k_{ET}} = \frac{1}{\mathrm{N}}$ means a steady state hopping of population for large N, small $\frac{\Delta E_B}{V_B}$ and small $\frac{\Delta E_B}{k_B T}$. (iii) $\mathrm{k_{ET}} = \frac{1}{\mathrm{N}^2}$ corresponds to a non-directional hopping mechanism for large N, small $\frac{\Delta E_B}{V_B}$ and small $\frac{\Delta E_B}{k_B T}$. (iv)$\mathrm{k_{ET}} = (\mathrm{k_{up}^{-1}} + \mathrm{k_{diff}^{-1}N})^{-1}$ behaves as an intermediate range for small $\frac{\Delta E_B}{k_B T}$, (v) $\mathrm{k_{ET}} = \mathrm{e}^{-\alpha \mathrm{N}}$ corresponds to a steady state hopping with competing loss at every bridge site. Here we have reviewed the above features along with a detailed study of the nature of dependence of the interplay of various parameters like dephasing γ, coupling V, N, position of energy levels of the donor, acceptor and bridge ω_D, ω_A and ω_B, respectively.

We have studied various parametric dependence of electron transfer rate from lower γ to higher γ and at various coupling strength V. Inspecting the nature of the rate versus N curves we have fitted those curves with equation $\mathrm{k_{ET}} = \mathrm{A_0 exp(-A_1 N)} + \mathrm{A_2}$ or $\mathrm{k_{ET}} = \frac{\mathrm{A_0}}{\mathrm{N^{A_1}}} + \mathrm{A_2}$ or $\mathrm{k_{ET}} = \frac{\mathrm{A_0}}{\mathrm{N}} + \mathrm{A_1}$ or $\mathrm{k_{ET}} = \frac{1}{\mathrm{A_0 + A_1 N}}$ using non-linear curve fitting in XMGRACE software package.

The distance dependence of electron transfer rate in terms of the number of sites at various regimes have been shown in Fig.6.2A and Fig6.2B. Here the electron transfer rate decreases with increase in the number of sites and after some sites it approaches to a saturated value or minimum value. From these plots we shall see the nature of dependence (exponential, ohmic or peculier) of rate on N which is very much sensitive to the change in coupling strength, V and bridge energy level, ω_B in the coherent (low γ), intermediate (intermediate γ) and incoherent (high γ) regime.

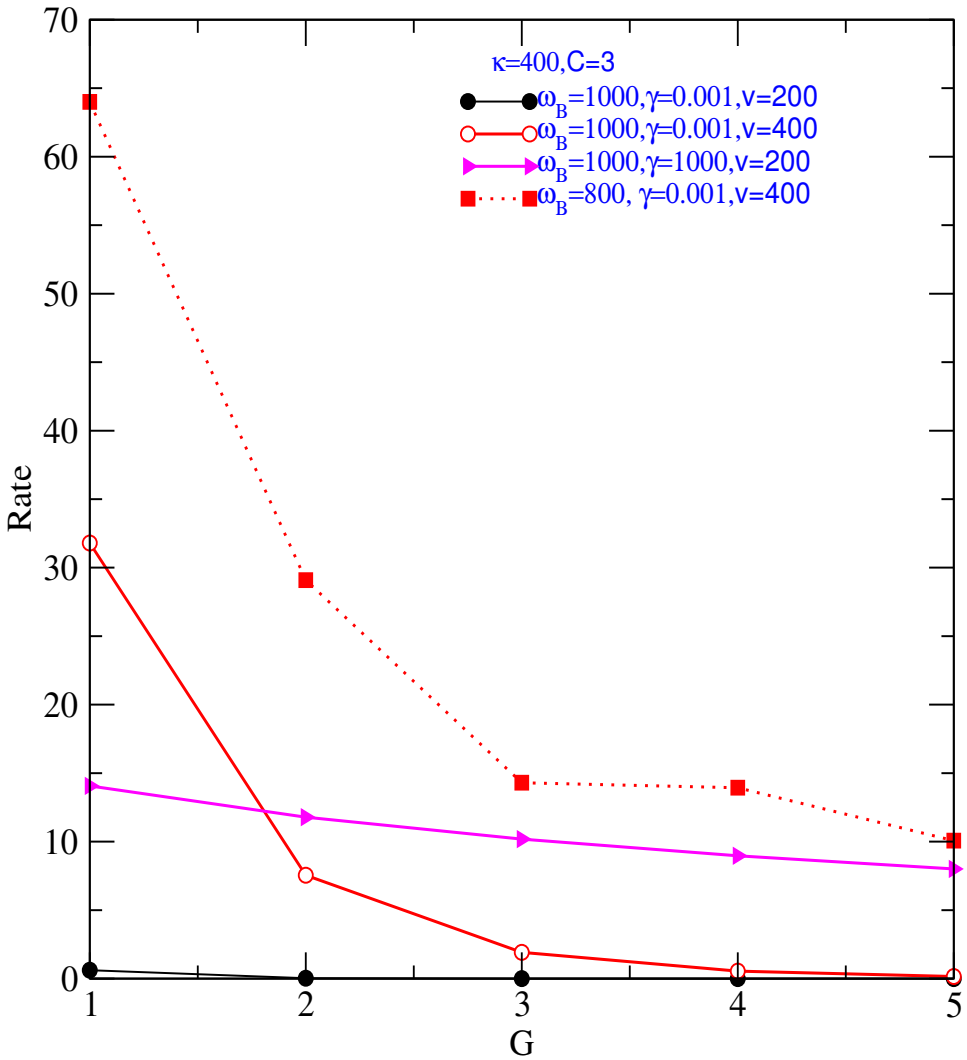

[Fig 6.3] Generation dependence of electron transfer rate for various system parameters for dendrimeric bridge: In all cases, unless otherwise stated, $\omega_A = \omega_D = 0\,\mathrm{cm}^{-1}$, $\omega_B = 1000\,\mathrm{cm}^{-1}$, $\kappa = 400\,\mathrm{cm}^{-1}$ and $V = 400\,\mathrm{cm}^{-1}$.

The distance dependence of electron transfer rate at low, intermediate and high dephasing limit has been studied with the gradual change of V. We have seen as N increases overall transfer rate decreases. In the low γ regime curves follow $k_{ET} = A_0 exp(-A_1 N) + A_2$ with $A_2 \approx 0$ and at intermediate γ regime curves follow $k_{ET} = \frac{A_0}{N^{A_1}} + A_2$ and at high γ regime the curves follow $k_{ET} = \frac{A_0}{N} + A_1$. Here A_0, A_1, A_2 are constants dependent on V, γ, ω_B, and N. As γ increases the nature of the curve loose its exponential character. For longer bridge, the change of rate due to increase in V is significant only in the intermediate and incoherent γ regime.

Distance dependence of electron transfer rate for linear system at low V, intermediate V and high V have been studied with gradual change of solvent dephasing γ. We have seen curves having $\gamma = 0.001$ and $\gamma = 100$ (with $\omega_B = 1000$ cm^{-1} and $V = 200$) follow $k_{ET} = \frac{A_0}{N^{A1}} + A_2$, the curve having $\gamma = 1000$ (with $\omega_B = 1000$ cm^{-1} and $V = 200$) follows $k_{ET} = \frac{1}{A_0 + A_1 N}$ and the curve having $\gamma = 5000$(with $\omega_B = 1000$ cm^{-1} and $V = 200$) follows $k_{ET} = \frac{A_0}{N} + A_1$. At intermediate coupling strength $V(= 500)$ the curves having $\gamma = 0.001$ (with $\omega_B = 1000$) and $\gamma = 100$ follow $k_{ET} = \frac{A_0}{N^2} + A_1$, the curve having $\gamma = 1000$ (with $\omega_B = 1000$) follows $k_{ET} = \frac{1}{A_0 + A_1 N}$ and the curve having $\gamma = 5000$(with $\omega_B = 1000$) follows $k_{ET} = \frac{A_0}{N} + A_1$. At higher coupling stength $V(= 800)$ (with $\omega_B = 1000$) the curve having $\gamma = 0.001$ follows $k_{ET} = \frac{exp(-A_0 N)}{A_1 + A_2 N}$ and curves having $\gamma = 100$, $\gamma = 1000$, $\gamma = 5000$ follow $k_{ET} = \frac{A_0}{N^{A_1}} + A_2$.

Dependence of rate on N is shown at various ω_B keeping other parameters fixed at various dephasing regimes(Fig6.2B). Here most of the curves follow $k_{ET} = \frac{A_0}{N^{A_1}} + A_2$ except the curve with $\omega_B = 2400$ and $\gamma = 1000$ which follows $k_{ET} = A_0 exp(-A_1 N) + A_2$ exactly.

For smaller bridge-length (small N), the number of coherence terms is small and donor is nearer to acceptor. So super-exchange mechanism is operative with high rate and electron can not reside or spend time on the bridge. For higher N the higher number of coherence among nodes exist. Higher number of such intermediate sites make the transfer process low. At higher ω_B rate decreases because of higher energy difference between bridge and donor-aceptor.

Coherent or super-exchange mechanism is operative when γ, N are low and ω_B and V are large. In this regime we have seen the distance dependence is $k_{ET} = A_0 exp(-A_1 N) + A_2$ with $A_1 \rangle 0.3$ and $k_{ET} = \frac{A_0}{N^{A_1}} + A_2$ with $A_1 \rangle 1.0$. At this moment it may be apparent that A_1 - value in exponential dependence may have some similarity with β value of a

specific bridge molecule studied by different groups[146, 147, 148, 149]. At dephasing rate $\gamma = 1000$ or higher the dependence become $k_{ET} \approx (A_0 + A_1 N)^{-1}$ or $k_{ET} \approx \frac{A_0}{N} + A_2$.

So from our simplified model for the linear chain we have been able to see the exponential, $\frac{1}{N}$ and a peculiar distance dependence of electron transfer rate depending upon the system parameters. This supports previous studies [146, 147, 148, 149]. We have given special emphasis on the dependence on dephasing γ and coupling V. The nature of the curves not only depend upon N but also on ω_B, γ and V. These parameters are highly specific for different molecules.

6.6.2 For dendrimeric architecture

For studying the distance dependence of dendrimeric architecture as bridge when all other parameters are fixed at various ranges of consideration we assume all bridging nodes including the core of the dendrimeric architecture are of the same energies. It is generally found that in most of the parameter ranges when the number of sites between the donor and acceptor are the same as in linear structure the rate is higher for dendrimeric case. From the studies of rate versus generation curves we have seen special features mainly in the coherent regime for dendrimeric architecture. We have shown these effects in two ways: firstly, gradually changing γ, V and ω_B for bridge with fixed core branching $C = 3$. Secondly, we have seen the generation dependence of electron transfer rate of dendrimeric bridge having diferent core branching C at low γ, intermediate γ and high γ regimes.

When the curves are fitted with $k_{ET} = A_0 \exp(-A_1 N) + A_2$ or $k_{ET} = \frac{A_0}{N^{A_1}} + A_2$ we have obtained all nonzero A_2 values at higher γ. In linear system this value is zero indicating that with an increase in intermediate nodes the lowest approachable value of ET rate for dendrimeric bridge is greater than that of the linear bridge.

In Fig.6.3 we have shown the effect of dephasing γ, coupling strength V, bridge energy level ω_B. The effect of core branching on ET rate has been shown in Fig.6.4. In Fig.6.3 effect of change of γ on rate profile has been shown. The rate versus G plots for dendrimers are much more horizontal than those for linear curves. The curves become steeper at higher γ values. Although only two curves have been shown, from extensive plots we have seen all curves (upto $V \approx 500$ and $\gamma = 0$ to 1000) fit well with $k_{ET} = A_0 \exp(-A_1 G) + A_2$. Fig.6.3 also shows at coherent

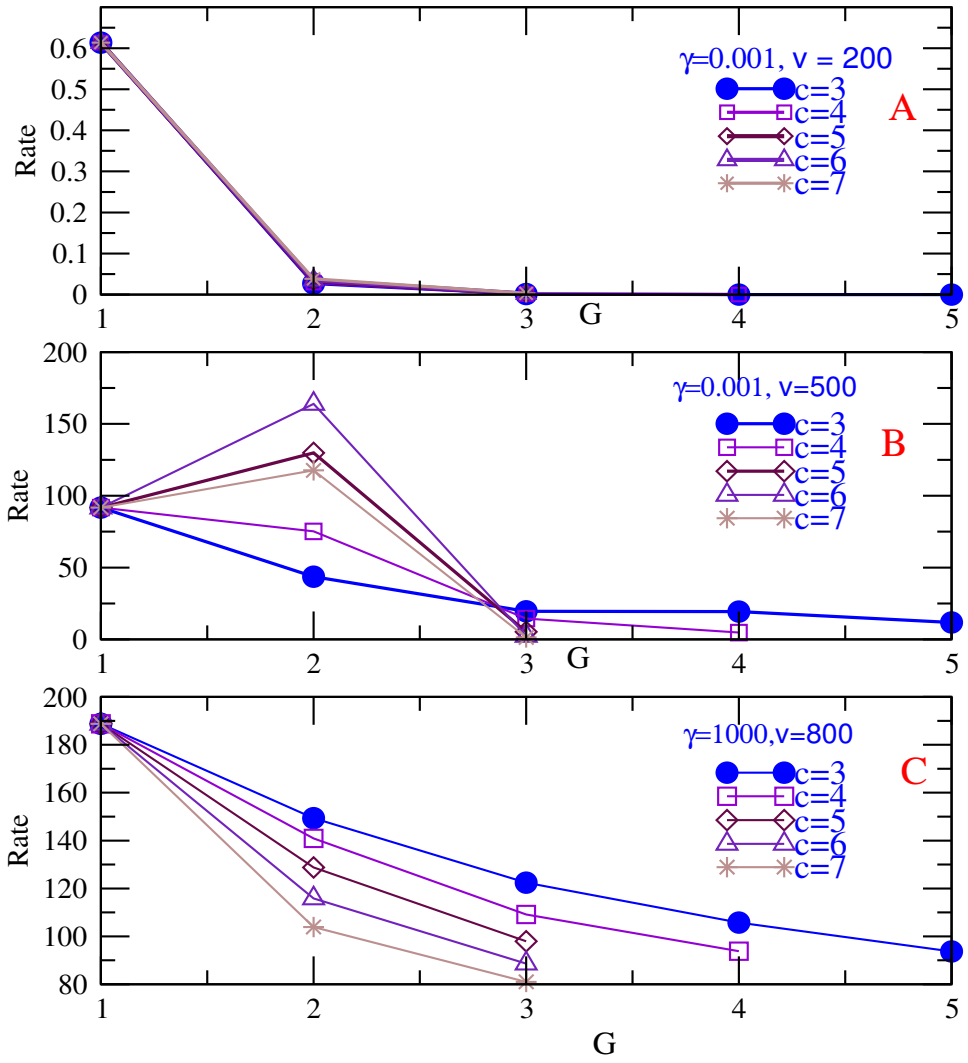

[Fig 6.4] Variation of electron transfer rate with generation where G is the size of the bridge and C is the core branching.

regime the effect of gradual change of V and ω_B at low γ. Here the rate increases as V increases and ω_B decreases. On shifting from $G = 3$ to $G = 4$ the change of rate is almost nil. Here with increase in distance between D and A the rate decreases and increase in branching causes an increase in rate due to coherence effect—an effective increase in coupling strength. At $G = 5$ the rate decreases for large distance and for excessive branching. At high V near generation $G = 4$ and $G = 5$ the exponential dependence is not properly followed.

Nature of curves in Fig.6.3 motivates us to study effect of core branching at coherent (low γ), intermediate γ and incoherent (high γ) regime with gradual changes of V in those regimes and we have seen at

higher core branching, the rate versus generation plot passes through a maximum which depends very much on V and γ. The maxima in those curves disappear as γ increases.

In all the three regimes curves follow $k_{ET} = A_0 exp(-A_1 G) + A_2$. The ET rate is very low at lower coupling strength. We represent here only three of all possible range of parameters in Fig.6.4A, Fig.6.4B and Fig.6.4C. At low V, the rate is very low and all curves fall on each other (Fig.6.4A). Fig.6.4B show the effect of core branching(C) with moderate coupling strength, $V = 500$. Here each of the four curves ($C = 4$, $C = 5$, $C = 6$, $C = 7$), passes through a maximum at second generation. They follow $k_{ET} = A_0\{exp(-A_{-1}G^m)\}G + A_2$. The effect of core branching is minimum at higher generation where equivalent environment is achieved due to the presence of higher number of nodes. The appearance of maxima and different dispositions of rate versus G curves at $G = 2$ and $G = 3$ for different C is the results of interplay of geometry, coherences among nodes, coupling and dephasing. At high $\gamma = 1000$ and high $V = 800$ all curves follow $A_0 exp(-A_1 G) + A_2$ (see Fig.6.4C).

In brief we oberve at lower V, rate versus G plot is exponential at low, intermediate or high γ regime. The exponential dependence is also obvious in high γ regime. Effect of branching is maximum at low γ-intermediate V (Fig.6.4B), low γ-high V (not shown in Fig) and intermediate γ-high V (not shown in Fig). Nature of rate profiles in these regime are significantly different from linear systems.

For coherence effect at a fixed generation order of rate-profiles (their position along vertical axis) with respect to core branching differs for same generation but with different V and or γ. With change in core branching of dendrimeric bridge the process of ET modifies as bridging network changes. For coherent case, the order of curves(their disposition along vertical axis) with respect to core branching depends largely on the size of the dendrimer, V and or γ. Different orders of electron transfer rate for different network supports the existence of superexchange mechanism. At higher γ, i.e, in the incoherent regime, the above variation due to various core branching is abolished. Increase in core branching simply reduces the rate in a regular way due to increase of effective damping.

Here we have seen that at some ranges of parameters steady-state electron transfer rate decreases with increase in generation of the dendrimer. In an experiment on electroluminescence properties of Ruthenium dendrimers Barron[195] et al have shown that the steady-state current in OLED (organic light emitting diode)device decreases with increase

in generation. They have shown that as the barrier for charge injection decreases the ohmic nature of interface contact increases which does not depend so much on the dendrimer generation. The decrease in steady state current in their experiment was attributed to the decrease in intrinsic mobility of electronic carriers as the dendrimer grows larger in size. The actual experimental context may be different from our scheme of calculation. We have taken the effect of solvent phenomenologically. If the bridge structure, donor-bridge and acceptor-bridge bindings are not so different in nature in solid or adsorbed condition which are used for molecular devices than in the solution phase then our simple scheme of ET through the dendrimeric architecture will have some qualitative similiarity to the intrinsic mobility of electronic carriers moving through dendrimeric structure mentioned in their experiment. In our study incoherent transport through bridging sites is responsible for that decrease in rate. For a specific dendrimeric architecture we may assign an effective intrinsic damping due to large number of nodes between the donor and acceptor.

6.6.3 Comparison between dendrimeric bridge and linear bridge

To compare the electron transfer rate we have plotted rate versus number of nodes, N between donor and acceptor in both cases. At low coupling strength, V with low dephasing rate, γ the difference in electron transfer rate between linear and dendrimeric bridge is almost nil (see Fig.6.5A). At very high V and moderate γ the difference in rate between linear and dendrimeric bridge is small (see Fig.6.5C). Significant difference in rate between dendrimeric architecture and linear bridge is obtained at moderate V in the coherent regime(see Fig6.5B) for smaller generation and in the incoherent (high γ) regime for larger generation (not shown). In Fig6.5B it is clear that for $G = 2$ at higher core branching($C = 5, 6, 7$) the electron transfer rate decreases after passing through a maximum to coincide with linear bridge case signifying incoherent motion of electron. At higher core branching the effective damping of the system increases which is not available in the linear system. Fig6.8C shows the rate is higher even at large N due to strong coupling strength.

In the incoherent regime ($\gamma = 400$ or more) the rate in the dendrimeric cases are higher for a fixed number of intermediate bridge sites and the effect of dendrimeric network is not very relevant since rates of dendrimeric network having different core branching fall in the same region whereas in the coherent regime, the dependence of the rate on the number of sites in the bridge for the dendrimer network is very different

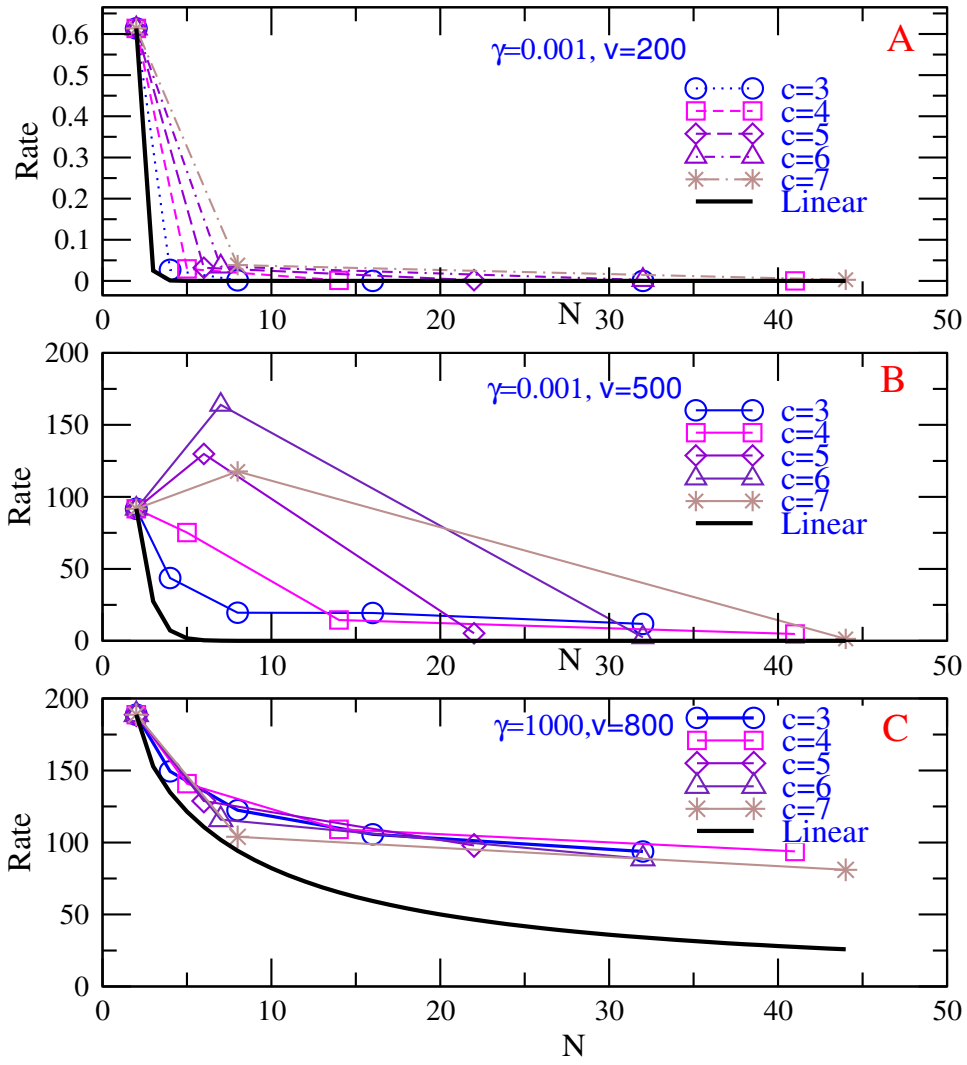

[Fig 6.5] Comparison of electron transfer rate for linear and dendrimeric bridge having equal number of nodes between donor and acceptor.

from the linear case. However, for the interplay of various parameters in the dendrimer, V, γ, ω_B and core branching, it is difficult to find a general trend unless in the case of highly coherent regime.

6.7 Influence of solvent dephasing for linear and dendrimeric case

In both linear and dendrimeric cases the electron transfer rate first increases with dephasing rate (γ), attains a maximum and then decreases with dephasing (γ). This kind of behaviour reminds Kramers' rate theory[229, 230]. When depasing rate is low we can call the region as quantum regime and when γ is high we call it as classical regime. Main point to be noted here is that in dendrimeric system coherent or quantum regime is more stable in large γ value than in the case of linear counterpart. This is depicted by the position of maximum of each curve in the linear and dendrimer cases. The position of the maximum for dendrimeric case depends on the parameters, (i) generation or size of the dendrimer, (ii) bridge energy levels, (iii) core branching and (iv) coupling strength.

Dependence of electron transfer rate with dephasing parameter γ for linear bridge is sensitive towards the change in N and ω_B. Maximum occurs at high γ for low N and high ω_B as depicted in Fig.6.6A. So low N and high ω_B are favourable for quantum regime. At very low γ, rate is almost linear with γ and $N = 4$ and $N = 16$ have the same electron transfer rate. With increasing γ the rate falls off rapidly, see for example in Fig.6.6A, $N = 16$ system. The hopping or classical regime comes at lower γ. At steady state, population transfer from donor state becomes less. Since with the increase in the number of sites between donor and acceptor the coherence between the nodes decreases, it makes a low transfer of population. The increased number of sites between the donor and acceptor increases the inherent damping of bridge sites which facilitates the occurence of the faster classical limit. When ω_B is increased by a value of 500 cm^{-1} the rate versus γ plot shows that the quantum regime dominates over a large range of γ (see unfilled diamond symbol). So we may conclude that the quantum regime prevails upto higher dephasing rate with higher energy gaps between the bridge and the donor-acceptor.

Next we have compared the electron transfer rate with branched architecture i.e, with dendrimeric architecture having core branching $C =$

3. Overall features are more or less similar as in the linear case. In the curve with $G = 4(16$ nodes), $C = 3$ the quantum regime retains upto $\gamma \approx 750 - 800 \ \ cm^{-1}$ (see Fig.6.6B). This value of γ is higher than in the case of linear system. The change in energy gap between bridge and donor-acceptor (see diamond and circle symbols) has similar effect except the fact that the rates are higher for branched or dendrimeric case than in the linear chain.

6.8 Influence of coupling strength for linear and dendrimeric case

In both the linear and branched cases we have shown the effect of electronic coupling between the sites in the electron transfer rate. We have seen that for $V < \omega_B$ the electron transfer rate changes very slowly with increase in V and after certain value of V, rate increases rapidly. Again before that rapid changes to occur an increase of V or an increase in γ have similar effect on the rate. At dephasing rate $\gamma = 1000$ cm^{-1} or higher (in the incoherent regime) there is a monotonic increase of rate with V in all cases. Linear system shows monotonic increase of rate with V in both coherent and incoherent regime. For dendrimeic case monotonic increase of rate with V occurs at incoherent regime i.e. at high γ and low V. Dissimilarity between linear and dendrimeric cases is observed at coherent regime i.e, at low γ and high V. Here an inversion of rate is observed in the rate versus V plot for the branched structure which is discussed in details below.

Effect of V on electron transfer rate for linear bridge with small N and large N are different at coherent or low γ regime (see Fig6.7A). In Fig6.7A we see $\gamma = 10$ cm^{-1} curve and $\gamma = 100$ cm^{-1} curve crosses $\gamma = 1000$ cm^{-1} curve after $V = 600$ cm^{-1}. Around $V(\approx 700$ cm$^{-1})$ rate is maximum for $\gamma = 10$ cm^{-1} curve. For smaller bridge length coherent transfer is favourable. For this reason coherent transfer (here with low γ curve) increases with increase in V. The behaviour is different due to longer chain ($N = 16$). At this bridge length incoherent transfer is operative. So we see the curve with intermediate $\gamma = 100$ cm^{-1} dominates around $V \approx 500$ cm^{-1}. Basically these are an interplay of V and γ. So for linear system low γ regime will be favourable for fast transfer rate provided V is very large.

Fig6.7B-7D show variation of electron transfer rate with coupling constant V for dendrimeric system. Fig6.7B is for dendrimeric bridge

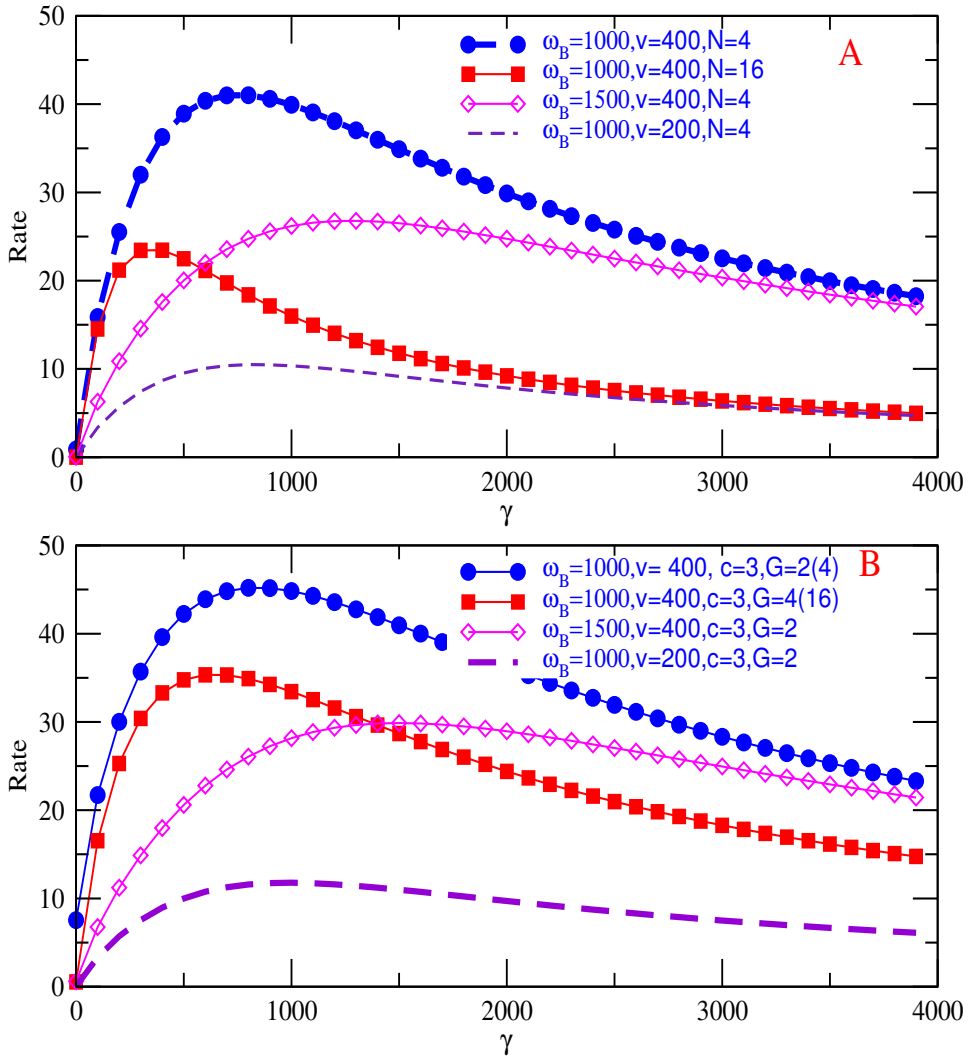

[Fig 6.6] Variation of electron transfer rate with dephasing parameters which describe an increase in γ, the rate profile transfer from quantum to classical regime: (A) is for linear system. (B) is for bridge having dendrimeric architecture. G is the size of the bridge and C is the core branching.

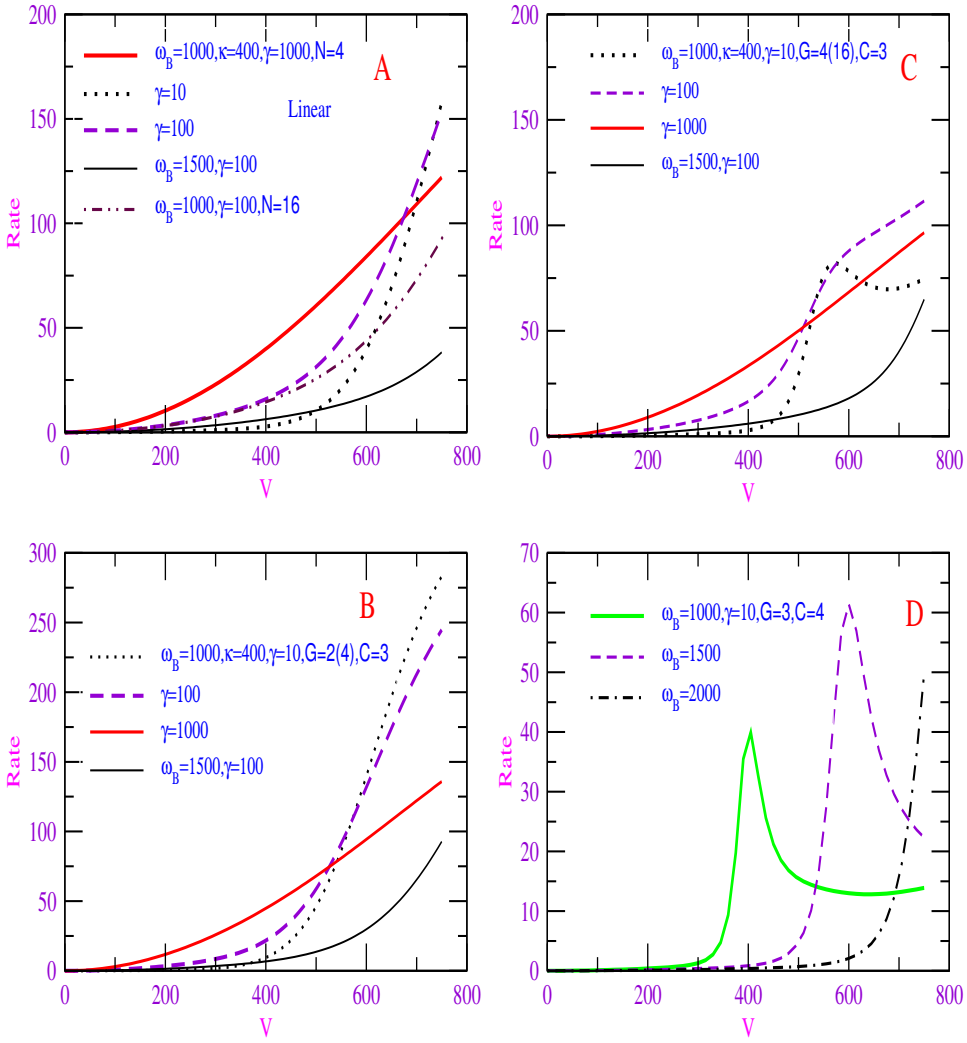

[Fig 6.7] Plot of electron transfer rate with coupling strength V. (A) is for linear system where rate saturates at much higher V. (B)-(D) are for bridge having dendrimeric architecture where at coherent regime saturation of rate appears after inversion at high V. G is the size of the bridge and C is the core branching.

with generation $G = 2$ having core branching $C = 3$. Comparing Fig6.7A(linear) and Fig6.7B(dendrimer) we see that for $\gamma = 10$ cm^{-1} and $\gamma = 100$ cm^{-1} curves dominate over the other curves at low V values for branched structure. Branching makes the coherent transfer easier at lower V than the corresponding linear case. In Fig6.7C, $\gamma = 10$ cm^{-1} curve shows that there is a maximum and after some high V, rate becomes saturated. Here the curve with $\gamma = 100$ cm^{-1} shows a kink for V (around $v \approx 550$ cm^{-1}). This kind of deviation from linear system is special for branched structure in the low γ regime. This is due to the existence of coherence among the sites. It is seen that there is a saturation of rate after deflection point. This is a critical situation when the rate is not affected by V. More is the core branching(C) the deflection points occurs at lower V. The $\gamma = 1000$ cm^{-1} curve dominates over the other curves, indicating that at higher dephasing rate linear like behaviour is obtained due to the existance of incoherent mechanism of transfer. Increase of coupling strength, V is related to the increase of adiabaticity[144] of the process. We know adiabatic ET rate is solvent controlled. Here we have observed that dephasing rate, γ has prominent effect at higher coupling strength, V. In Fig6.7D we have seen that the inversion point comes at higher V as ω_B becomes larger. However, a detailed analysis of the contribution of adiabatic and non-adiabatic rate in the various parameter regime is not provided here.

In the coherent regime (with high V and low γ) timescale associated with the coupling becomes much smaller than the timescale associated with dephasing rate ($\frac{1}{\gamma}$). For branched structure with high V, the population transfer between the sites occurs at much faster rate than the relaxation of coherences. In this situation further increase in coupling V may introduce incoherent mechanism of transfer or some other scattering channel of transfer process become operative which is analogous to the power brodening in coherent spectroscopy[233]. This process makes the overall transfer rate to decrease with increase in V after passing through the maxima at coherent regime.

6.9 Effect of energy levels of the bridge, donor and acceptor

Unlike the ordinary electron transfer process with one energy gap between the donor and acceptor here the bridge energy levels can be different from the donor and acceptor. First we have considered the donor and acceptor are at the same energy level. In Fig6.8 the maximum in rate occurs at

$\omega_B = 0$ for both in linear and dendrimeric cases. The position of the maximum depends upon the values of γ, V and N or G as applicable. In the coherent regime multiple peaks are obtained for dendrimeric architecture. In the linear system this behaviour is obtained at the parameter range that are drastically different from these results and that have only of parametric significance and are not shown in figures. For dendrimers at incoherent regime these multiple peaks vanish and only a single peak is obtained like the linear case. Single peak is also obtained at the same parameter range (at coherent regime) for dendrimeric bridge on neglecting higher order coherence terms in the calculation of electron transfer rate. This shows that the multiple peaks are the consequence of coherence effect due to branching network in the dendrimer with a suitable size and core branching.

Fig6.8A shows the effect of energy spacing between bridge and donor-acceptor in electron transfer rate for $N = 4$ and $N = 16$ for linear bridge. Here we have considered $V = 400$ cm^{-1}, $\kappa = 400$ cm^{-1} and $\gamma = 5$ cm^{-1}. The figure shows that the rate is maximum when energy difference between bridge level and donor-aceptor is nil. This is the resonance condition. The effect of electronic coupling V for linear $N = 4$ system has been shown. Rate is lower for $N = 8$ in this region of ω_B. Fig6.8B shows the effect of energy gap between dendrimeric bridge with core branching $C = 3$ for generation $G = 2$(4 nodes), $G = 3$(8 nodes) and $G = 4$(16 nodes). Instead of getting single peak, multiple peaks are obtained depending upon the branching. Here around $\omega_B \approx 0$ rate is higher for $G = 4$ than $G = 3$. As generation increases D-A separation increases. High branching may introduce an effective damping that in turn can introduce incoherent motion. At low ω_B, hopping or incoherent transport dominates. All these effects make the ET rate for $G = 4$ higher than $G = 3$ at around $\omega_B \approx 0$. This kind of maxima or minima reflects an effect of geometry of the system as a consequence of coherences at low γ regime. When γ is high this multiple peaks converge to a single peak as shown in Fig.8C. In Fig6.8B we have plotted the same for dendrimeric architecture neglecting higher order coherence terms (NHC curve). Here all $\sigma_{ij,kl}$ with $\mid i - k \mid \neq 1$ are zero and multiple peaks disappear. So those peaks arise due to higher order coherence effect at low γ regime reflecting geometry effect. The effect of electronic coupling on splitting of peaks for generation $G = 3$ has been shown in Fig6.8C. We have seen that the splitting is nearly proportional to $\frac{V}{\omega_B}$ ratio. The proportionality constant depends upon the specific generation of the dendrimer. For a specific generation we have increased the core branching and in those cases we have seen that an increase in core branching is similar to that of increase of effective damping. In our study[93] we have seen that the

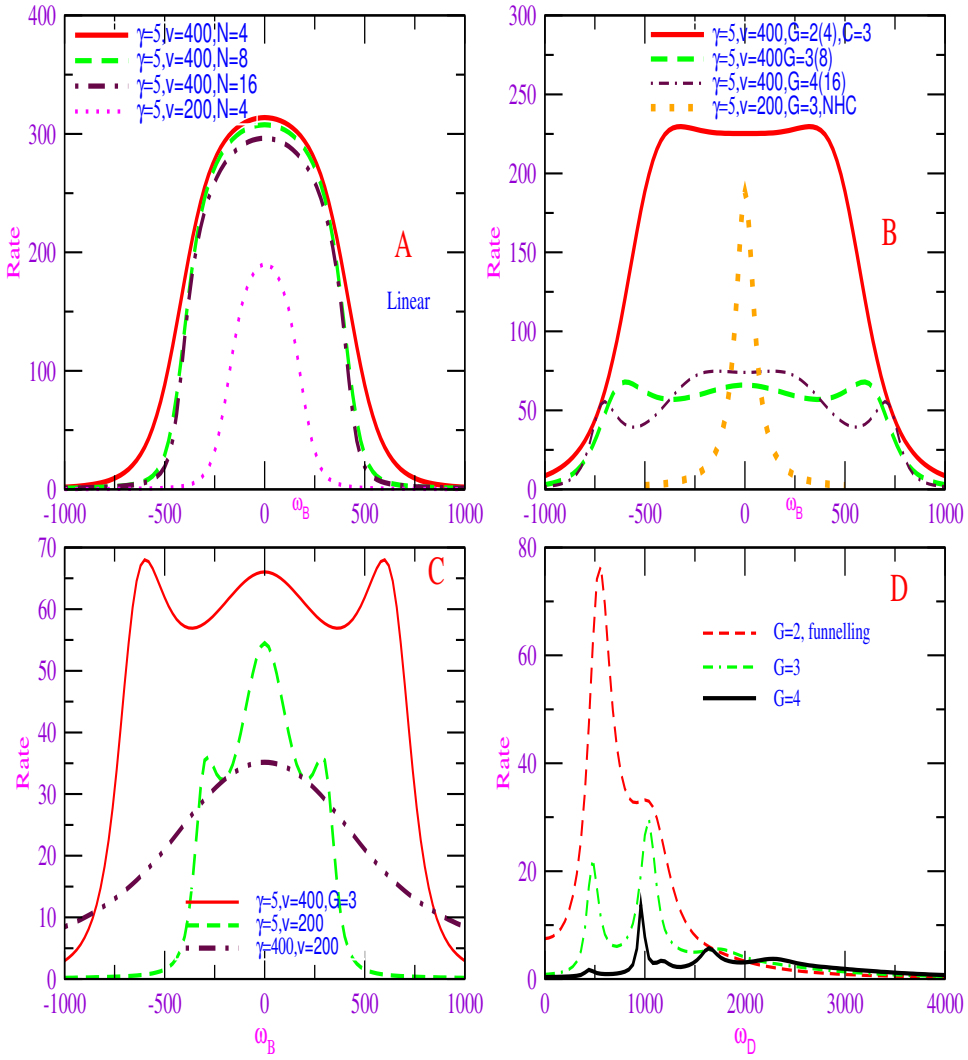

[Fig 6.8] Plot of electron transfer rate with energy gap between the bridge and the donor or acceptor for $\omega_B - \omega_{A/D}$ where $\omega_{\rm A} = \omega_{\rm D} = 0$: (A) for linear, (B) and (C) for dendrimer. In (B) NHC means neglecting higher order coherence, shows no splitting in the rate profile for generation 3. (D) Plot of electron transfer rate versus energy of donor ω_D for energy biased dendrimeric network: Here an energy funnel has been imposed with $\omega_A = 0 = \omega_D$ and each successive bridge site(or degenerate sites of specific generation) is 500 $\rm cm^{-1}$ higher from the previous site with core site energy $\omega_C = 500$ $\rm cm^{-1}$(see Fig.1E).

dendrimeric nodes act as a bath for highly branched sructure where all individual node feels equivalent electrochemical environment. Here for a special branching there should also be an effective inherent damping discussed in the context of Fig6.5A, Fig6.5B and Fig6.5C. This multiple peaks arise due to the interplay of effective inherent damping for geometry effect and coherence effect at the low γ regime. We feel that the role played by entropy effect [220, 219] arising due to the geometry or branching in dendreimeric structure in the classical studies of energy transfer is a similar special effect that is precisely played here by quantum coherence. Fig6.8D shows the variation of electron transfer rate with ω_D when there is a fixed energy gardient along dendrimeric architecture from periphery to the core. In this case $\omega_A = 0$, $\omega_C = 500$ cm^{-1} and $\omega_{ij} = (500 \times i)$ cm^{-1} where $i = 1, 2, 3, ...G$. Here all higher generation nodes are 500 cm^{-1} above the nodes of previous generation. In this case ω_D is variable. Here we observe two peaks for generation $G = 2$, three peaks for generation $G = 3$ and four peaks for generation $G = 4$. In this case energy difference between donor state and acceptor state $= \Delta = \omega_A - \omega_D = -\omega_D$ since $\omega_A = 0$. So higher is the value of ω_D more negative is the value of Δ.

6.10 Summary and Conclusions

We have studied electron transfer from the donor to the acceptor through linear bridge and branched dendrimeric network as dendrimers are recently becoming an important class of macromolecules with exciting photo-physical and electrochemical properties suitable for molecular electronics devices. Nitzan and co-workers have studied steady state electron transfer rate for a linear bridge. They have shown how the electron transfer rate through a bridge may be modified by dephasing and coupling strength. Their studies have now become a standard methodology for investigating electron transfer through these systems. We adopt the same formalism to study electron transfer rate through dendrimeric architecture. Here the core site is connected to a trap and a peripheral node is connected to a donor where a constant population is maintained externally. We have taken a single dendrimeric branch for our investigation. Actually in a whole molecule the accessibility of the core is limitted to engage any chemical process due to the spherical shape of the overall molecule.

We have numerically solved the steady state equation for linear and dendrimeric cases. First of all we have studied the linear system as

studied by Davis et al[229] along with additional detailed investigation on the dependence of bridge energy levels, dephasing, coupling strength and other parameters of the system. This study facilitates the comparison between the network system with the linear bridge.

From the studies of distance dependence of electron transfer rate we have seen that for linear system the superexhange mechanism is operative with small dephasing rate, γ. Higher values of energy gap between the acceptor or donor and the bridge $\omega_B - \omega_{A/D}$ can facilitate the coherent process. As the bridge length increases the incoherent mechanism increases. Distance dependence of the electron transfer rate has been depicted for linear and dendrimeric case in terms of N or G. For linear system at low γ and wide range of V, exponential dependence on the number of sites is observed. Depending upon the system parameters it changes to ohmic (high γ) and intermediate (intermediate γ and V) dependence which are more or less as observed by Nitzan and co-workers. In the coherent regime with moderate coupling strength, V dendrimeric architecture shows a maximum at some generation in the rate versus G plot. This behaviour is not observed in linear case in the similar condition. The arrangement of rate versus G curve at various core branching is a result of interplay between the core branching(C), V, γ, and generation G. At coherent or incoherent regime the rate versus N curve approaches a minimum value(A_2) which is larger than linear chain. In the incoherent regime dendrimer bridges with various core branching C show regular decrease of ET rate with increase of generation.

We have studied the effect of solvent dephasing on electron transfer rate for linear as well as branched structure. In both cases we have found that the rate increases with γ at low γ regime, attains a maximum and then decreases with γ. Around the maximum the low γ regime is quantum or coherent regime and with the higher values of γ we found it as a classical or incoherent regime.

From the study of electron transfer rate versus coupling strength we have seen that for linear system with smaller bridge length, curve with low γ (coherent) dominates at higher V. For dendrimeric architecture at low γ regime, rate passes through a maximum. After an optimum value of V, an inversion in the rate is obtained. At higher V regime with high branching the coherence is extended over many nodes which affect the situation in such a way that within the limit of relaxation time of coherences population transfer between nodes occurs many times through coupling (since in this case $\gamma\frac{1}{\gamma} \rangle \frac{1}{\mathrm{V}}$) and the overall transfer from donor to the acceptor decreases. When ω_B becomes higher then the inversion

of rate occurs at higher V.

We have seen that the electron transfer rate is maximum when the bridge energy levels are in resonance with the donor and acceptor. In case of dendrimeric branch we have obtained multiple maxima of rate for different values of ω_B for low γ regime. This multiple peaks on the profile of rate versus ω_B is a direct consequence of coherence effect. When all higher order coherence terms are neglected in the steady state equations then this multiple peaks converge to a single peak. On imposing an energy funnelling from the periphery to the core and by changing the on-site energy of the donor state different from the acceptor we observe that the generation of multiple peaks are sharper and peaks are assymmetric around $\omega_B = 0$. We feel that in this treatment the branching generates a coherence effect which is reminiscent to the entropy effect introduced by geometry in classical treatment of energy transfer in dendrimer[220]. So with proper manipulation of on-site energy of bridge or donor or acceptor many interesting changes in electron transfer rate is possible which is essential for molecular switch[232] property.

From all these studies on linear and dendrimeric cases of electron transfer, there appears two sharply defined regimes characterizing the interactions between the bridging sites, which are connected through an intermediate regime. In both linear and branched structure, in the coherent regime where superexchange transfer is operative, the parameters of the system are like, low dephasing rate, high coupling strength and small number of intermediate sites between the donor and acceptor. For the incoherent regime where the transfer is through hopping of population the parameters are for high dephasing, low coupling and a large number of intermediate sites between the donor and acceptor. When a linear system shows an incoherent transfer, in the same parameters regime dendrimer case shows a coherent transfer as if an extra coherence contribution is generated induced by branching. This can be rationalized as due to larger number of nearest neighbour nodes dynamics of off-diagonal elements of the density matrix are very different from the linear case even if the total number of intermediate nodes between D and A are the same. The energy levels of the bridge also induces more coherent behaviour in the case of dendrimer than in the linear chain. For large size and high core branching, an increase in incoherent behaviour appears in the dendrimer which is due to increased effective dephasing (due to larger number of neighbouring nodes) of the system. This is also the reason for obtaining multiple peaks on the profile of dendrimer due to the extra coherence in the small dendrimer than in the case of linear chain. However, with the large increase in the number of generation or

core branching, the rate profile flattens like increase in total dephasing of the system in spectroscopy. In the case of coherent and incoherent regime the dendrimeric structure has always higher rate than a linear bridge with the comparable number of intermediate sites.

We have used a tight binding Hamiltonian. This procedure may be useful for many other molecules and for other mesoscopic systems. In molecular conduction problem, the nature of a single molecule or a layer of those molecules between metal leads is significant as the electron is passing through. Recent experiment on electroluminescence property of Ruthenium dendrimers Barron et al[195] have shown that the steady state current in OLED (organic light emmitting diode) decreases with the increase in size of the dendrimer which is due to the decrease of intrinsic mobility of electronic carriers as the dendrimer generation becomes larger. Here also we have found that the electron transfer rate decreases with the increase in generation of dendrimeric architecture. So there must be an effective inherent damping with a specific branching arising out of the involvement of neighbouring nodes which collectively acts like a bath in accordance with our earlier studies[35]. We hope this study provides a way to show the effectiveness of dendrimeric branching on electron transfer process where the bridge is used as a molecular wire, molecular switch or molecular rectifier.

References

[1] A.L. Lehninger; D.L. Nelson; M.M. Cox; Principle of Biochemistry;Worth Inc; New York 1993.

[2] D. L. Jiang, T. Aida, *Nature*, **388**, 454,(1997)

[3] S. Mukamel, *Nature*, **388**, 425, (1997).

[4] D.K.Smith, L. Müller, *Chem.Commun.*, 1915, (1999)

[5] R.H. Jin, T.Aida, S.Inoue, *J.Chem.Soc.Chem.Commun.*,1260,(1993)

[6] J.Issberner, F. Vogtle, L.De Cola, V. Balzani, *Chem.Eur.J.*,**3**, 706, (1997)

[7] D.Tzalis, Y.Tor, *Tetrahedron Lett.*, **37**, 8293, (1996)

[8] P.Ceroni, G.Bergamini, F. Marchioni, V. Balzani, *Prog. Polym.Sci.*, **30**, 453, (2005)

[9] G.Accorsi, N. Armaroli, J.F. Eckert, J.F. Nierengarten, *Tetrahedron Lett.*, **43**, 65, (2002)

[10] M.Mous, R.De, M. Lor, T. Weil, S. Mitra, Uwe-M. Wiesler, A. Herrmann, J. Hofkens, T. Vosch, K. Mullen, F.C. De Schryver, *J.Am.Chem.Soc.*, **123**, 7668, (2001)

[11] M.Mous, M. Lor, J. Hofkens, T. Weil, A. Herrmann, K. Mullen, F.C. De Schryver, *J.Phys.Chem.A*, **105**, 3961, (2001)

[12] M. Lor, R. De, S. Jordens, G. De Belder, G. Schweitzer, M. Cotlet, J. Hofkens, T. Weil, A. Herrmann, K. Mullen, M. Van Der Auweraer, F.C. De Schryver, *J. Phys. Chem. A*, **106**, 2083, (2002)

[13] A. Herrmann, T. Weil, V. Sinigersky, U. M. Weisler, T. Vosch, J. Hofkens, F.C. De Schryver, K. Mullen, *Chem.-Eur.J.*, **7**, 4844, (2001)

[14] T. Weil, U.M. Weisler, A. Herrmann, R. Bauer, J. Hofkens, F.C. De Schryver, K. Mullen, *J. Am. Chem. Soc.*, **123**, 8101, (2001)

[15] T. Weil, E. Reuther, K. Mullen, *Angew. Chem. Int. Ed.*, **41**, 1900, (2002)

[16] J. M. Serin, D.W. Brousmiche, J.M.J. Frechet, *J. Am. Chem. Soc.*, **124**, 11848, (2002)

[17] G. De Belder, S. Jordens, M. Lor, G. Schweitzer, R. De, T. Weil, A Hermann, U.K. Weisler, K. Mullen, F. C. De Schryver, *J. Photochem. Photobiol. A : Chem.*, **145**, 61, (2001)

[18] G. De Belder, G. Schweitzer, S. Jordens, M. Lor, S. Mitra, J. Hofkens, S. De Feyter, M. Van der Auweraer, A. Hermann, T. Weil, K. Mullen, F.C. De Schryver, *ChemPhysChem*, **No1**, 49, (2001)

[19] S. Jordens, G. De Belder, M. Lor, G. Schweitzer, M Van der Auweraer, T. Weil, E. Reuther, K. Mullen, F. C. De Schryver, *Photochem. Photobiol. Sci.*, **2**, 177, (2003)

[20] D. Liu, S. De Feyter, M. Cotlet, A. Stefan, U. M. Wiesler, A. Herrmann, D. G. Koehler, J. Qu, K. Mullen, F. C. De Schryver, *Macromolecules*, **36**, 5918, (2003)

[21] R. Sadamoto, N. Tomioka, T.Aida, *J. Am. Chem. Soc.*, **118**, 3978, (1996)

[22] V. Sundstrom, T. Pullerits, R. Van Grondelle, *J. Phys. Chem. B*, **103**, 2327, (1999)

[23] A. Bar-Haim, J. Klafter, R. J. Kopelman, *J.Am.Chem.Soc.*, 119, 6197, (1997)

[24] R. Kopelman, M. Shortreed, Z. Y Shi, W. Tan, Z. Xu, J. S. Moore, A. Bar-Haim, J. Klafter, *Phys.Rev.Lett.*, **78**, 1239, (1997)

[25] J.S. Melinger, Y. Pan, V. D. Kleiman, Z. Peng, B. L. Davis, D. Me Morrow, M. Lu, *J. Am. Chem. Soc.*, **124**, 12002, (2002)

[26] A. Bar-Haim, J. Klafter, *J.Phys.Chem.B*, **102**, 1662-1664, (1998)

[27] A. Bar-Haim, J. Klafter, *J.Chem. Phys.*, **109**, 5187-5193, (1998)

[28] S. Tretiak, V. Chernyak, S. Mukamel, *J.Phys.Chem.B*, **102**, 3310-3315, (1998)

[29] K. Hariagaya, *Int.J.Mod.Phys.*, **13**, 2531-2543, (1999)

[30] K. Hariagaya, *PCCP*, **1**, 1687-1699, (1999)

[31] Z.Xu, M. Kahr, L. Kathleen, C.L.Wilkins, J.S.Moore, *J.Am.Chem.Soc.*,**116**, 4537-4550, (1994)

[32] Y. Poliakov et.al, *J.Chem. Phys.*, **110**, 8161-8175, (1999)

[33] M.R. Shortreed, Stephan F. Swallen, Z.Y.Shi, W. Tan, Z. Xu, C.Devadas, J.S. Moore, R Kopelman, *J.Phys.Chem.B*, **101**, 6318-6322, (1997)

[34] Samantha Glazier, B.A.Jasson, P.L.Huston, H.D.Abruna, *J. Phys. Chem. B*, **106**, 9993, (2002)

[35] D. Rana, G. Gangopadhyay, *Chem. Phys. Letts.*, **334**, 314, (2001).

[36] D. Rana, G. Gangopadhyay, *J. Chem. Phys.*, **118**, 434, (2003).

[37] D. Rana, G. Gangopadhyay, *J. Chem. Phys.*, **124**,044909,(2006).

[38] J.Cornil, D.A. dos Santos, D. Beljonne and J.L. Bredas, *J. Phys. Chem.*, **99**, 5604, (1995)

[39] J.F. Eckert, J.F. Nicoud, J.F Nierengarten, S.G. Liu, L. Echegoyen, F. Barigelletti, N. Armaroli, L, Ouali, V. Krasnikov, G. Hadziioannou, *J. Am. Chem. Soc.*, **122**, 7467, (2000)

[40] J.F. Nierengarten, J.F. Eckert, J.F. Nicoud, L. Ouali, V. Krasnikov, G. Hadziioannou, *Chem. Comm.*,, 617,(1999)

[41] C.M. Heller, I.H. Campbell, B.K. Laurich, D.L. Smith, D.D.C. Bradley, P.L. Burn, J.P. Ferraris, K. Mullen, *Phys. Rev. B*, **54**, 5516, (1996)

[42] A. Adronov, S.L. Gilat, J.M.J. Frechet, K. Ohta, F.V.R. Neuwahl, G.R. Fleming, *J. Am. Chem. Soc.*, **122**,1175,(2000)

[43] J.P. Majoral, A.M. Caminade, *Macromolecules*, **99**, 845, (1999)

[44] A. Dirksen, E.Zuidema, R. M. Williams, L.De Cola, C. Kauffmann, F. Vogtle, A. Roque, F. Pina, *Macromolecules*, **35**, 2743, (2002)

[45] T. Basche, W. E. Moerner, M. Orrit, U.P. Wild, *Single Molecule Optical Detection, Imaging and Spectroscopy*, Wiley VCH, Weinheim: Munich, 1997

[46] M. Lor, J. Thielemans, L. Viaene, M. Cotlet, J. Hofkens, T. Weil, C. Hampel, K. Mullen, J. W. Verhoeven, M. Van der Auweraer, F.C. De Schryver, *J. Am. Chem. Soc.*, **124**, 9918, (2002)

[47] T. Vosch, J. Hofkens, M. Cotlet, F. Kohn, H. Fujiwara, R. Gronheid, K. Van der Biest, T. Weil, A. Hermann, K. Mullen, S. Mukamel, M. Van der Auweraer, F. C. De Schryver, *Angew. Chem. Int. Ed.*, **40**, 4643, (2001)

[48] J. Hofkens, W. Schroeyers, D. Loos, M. Cotlet, F. Kohn, T. Vosch, M. Maus, A. Herrmann, K. Mullen, T. Gensch, F. C. De Schryver, *Spectroc. Acta Pt. A-mol. Biomol. Spectrosc*, **57**, 2093, (2001)

[49] J. Hofkens, T. Vosch, S. De Feyter, F. C. De Schryver, *Macromol. Symp*, **178**, 1, (2002)

[50] R. Gronheid, J. Hofkens, F. Kohn, T. Weil, E. Reuther, K. Mullen, F. C. De Schryver, M. Sauer, *J. Am. Chem. Soc.*, **124**, 2418, (2002)

[51] P. Tinnefeld, K. D. Weston, T. Vosch, M. Cotlet, T. Weil, J. Hofkens, K. Mullen, F. C. De Schryver, M Sauer, *J. Am. Chem. Soc.*, **124**, 14310, (2002)

[52] M. Cotlet, R. Gronheid, S. Habuchi, A. Stefan, A. Barbafina, K. Mullen, J. Hofkens, F. C. De Schryver, *J. Am. Chem. Soc.*, **125**, 13609, (2003)

[53] R. Metivier, F. Kulzer, T. Weil, K. Mullen, T. Basche, *J. Am. Chem. Soc.*, **126**, 14364, (2004)

[54] R. Gronheid, A. Stefan, M. Cotlet, J. Hofkens, J. Qu, K. Mullen, M. Van der Auweraer, J. W. Verhoeven, F. C. De Schryver, *Angew. Chem. Int. Ed.*, **42**, 4209, (2003)

[55] J. Chen, L. Zhang, S. Li, Y. Y. Li, J. Chen, G. Yang, Y. Li; *J. Photochem. Photobiol. A*, **185**, 67, (2007)

[56] A. Szabo, K. Schulten, Z. Schulten, *J. Chem. Phys.*, **72** , 4350, (1980)

[57] Rohatgi-Mukherjee, K.K.; *Fundamentals of Photochemistry*, New Age International (P) Limitted, Publishers (1997)

[58] Robinson, G.W. and Frosch R.P. *J. Chem. Phys.*, **37**, 1962, (1962)

[59] Robinson, G.W. and Frosch R.P. *J. Chem. Phys.*, **38**, 1187, (1963)

[60] Förster, Th. In *Modern Quantum Chemistry*, Sinanoglu, O., Ed. Academic Press: New York, Vol 3, p 93

[61] Dexter, D. L. *J. Chem. Phys.*, **21**, 836,(1953)

[62] Lin, S. H. *Mol. Phys.* **21** 853, (1971)

[63] Lin, S. H. *Proc. R. Soc. London A*, **335** 51, (1973)

[64] Lin, S. H. *Phys. Rev. E* **47**, 3698, (1993)

[65] M. Cotlet, R. Gronheid, S. Habuchi, A. Stefan, A. Barbafina, K. Mullen, J. Hofkens, F. C. De Schryver, *J. Am. Chem. Soc.*, **125**, 13609, (2003)

[66] Lin, S.H. *J. Chem. Phys.*, **44**, 3759, (1966)

[67] Schole, G.D.; Clayton, A.H.A.; Ghiggino, K.P. *J. Chem. Phys.*, **97**, 7405, (1992)

[68] Islampour, R.; Alden, R.G.; Wu, G.Y.C.; Lin, S.H. *J. Phys. Chem.*, **97**, 6793, (1993)

[69] A.Nitzan *Chemical Dynamics in Condensed Phases* ,Oxford University Press Inc. New York (2006)

[70] A.Nitzan *Annu. Rev. Phys. Chem.*, **52**, 681, (2001)

[71] V. Sundstrom, T. Pullerits, R. van Grondelle, *J. Phys. Chem. B*, **103**, 2327, (1999)

[72] H. Sumi, *J. Phys. Chem. B*, **103**, 252, (1999)

[73] Buhleier, E W; Wehner, W; Vögtle, F; *Synthesis*, **155**, (1978)

[74] Jiang D.L;Aida,T.,*Nature***388**,454,(1997)

[75] Mukamel,S*Nature***388**,425,(1997).

[76] Bar-Haim,A; Klafter J; Kopelman,R.J; *J.Am.Chem.Soc.*, **119**,6197,(1997)

[77] Kopelman R; Shortreed M; Shi Z. Y; Tan W; Xu Z; Moore, J. S; Bar-Haim A;Klafter J;*Phys.Rev.Lett.***78**,1239,(1997)

[78] Bar-Haim,A; Klafter J;*J.Phys.Chem.B***102**, 1662-1664,(1998)

[79] Sergei
Tretiak; Vladimir Chernyak; Shaul Mukamel; *J.Phys.Chem.B***102**, 3310-3315, (1998)

[80] Kikuo Hariagaya*Int.J.Mod.Phys.*,**13**,2531-2543(1999)

[81] Kikuo Hariagaya*pccp*,**1**,1687-1699,(1999)

[82] Z Xu, M
Kahr, L Kathleen, C.L.Wilkins, J.S.Moore; *J.Am.Chem.Soc.***116**, 4537-4550, (1994)

[83] Tomalia, D A; Baker, H; Dewald, J; Hall, M; Kallos, C; Martin, S; Roeck, J; Ryder J; Smith P; *Polym. J.*, **17**, 117, (1985)

[84] Tomalia, D A; Baker, H; Dewald, J; Hall, M; Kallos, C; Martin, S; Roeck, J; Ryder J; Smith P; *Macromolecules*, **19**, 2466, (1986)

[85] Newkome, G R; Yao, Z; Baker, G R; Gupta, V K; *J. Org. Chem.*, **50**, 2003, (1985)

[86] Hawker, C J; Frechet J. M. J. *J. Am. Chem. Soc.*, **112**, 7638, (1990)

[87] Y.Poliakov et.al *J.Chem. Phys.***110**,8161-8175,(1999)

[88] Bar-Haim,A; Klafter J; *J.Chem. Phys.*,**109**,5187-5193,(1998)

[89] M.R.Shortreed;Stephan .F. Swallen ; Z.Y.Shi; W. Tan; Z. Xu; C.Devadas, J.S. Moore;R Kopelman*J.Phys.Chem.B* **101**, 6318-6322,(1997)

[90] J.S. Moore, *Acc. Chem. Res.*, **30**, 402, (1997).

[91] Arie Bar-Haim and Joseph Klafter, *J. Chem. Phys.*, **109**, 5187, (1997)

[92] S. Raychoudhury, Y.Shapir, V. Chernyak and S. Mukamel, *Phys.Rev.Lett.*, **85**, 282, (2000).

[93] D. Rana and G. Gangopadhyay, *submitted*.

[94] S.Roychoudhury, Y.Shapir and S.Mukamel,*Phys.Rev.E*, **65**, 021803,(2002).

[95] Peter Hanggi; Peter Talkner; Michal Borkovec, *Rev. Mod. Phys.*, **62**, 251, (1990).

[96] N.Lakshminarayanaiah, *Equation of membrane biophysics*, Academic Press Inc.(London) Ltd.,1984.

[97] E.W. Meijer, *Science*, **266**, 1226, (1994)

[98] D.M. Watkins, Y.S. Sweet, J.W. Kimash, N.S. Turro, D.A. Tomalia, *Langmuir*, **13**, 3136, (1997).

[99] Christopher Gorman, *Nature*, **415**, 487, (2002)

[100] K. Yamamoto, M. Higuchi, S. Shiki, M. Tsuruta, H. Chiba, *Nature*, **415**, 509, (1999).

[101] J.M.J. Fre′chet et al; *J. Am. Chem. Soc.*, **121**, 9471, (1999).

[102] A.W. Bosman, H.M. Janssen, E.W. Meijer, *Chem. Rev.*, **xxx**, 1665, (1999).

[103] J.W.J. Knepen, A.W. van der Made, J.C. de Wilde, P.W.N.M. van Leeuwen, P. Wijkens, D. M. Grove, G. van Koten, *Nature(London)*, **372**, 659, (1994).

[104] H. Brunner, *J. Organomet. Chem.*, **500**, 39, (1995),

[105] A. Miedaner, C.J. Curtis, R.M. Barkley, D.L. DuBios, *Inorg. Chem.*, **33**, 5482, (1994).

[106] D. Seebach, R.E. Marti, T. Hintermann, *Helv. Chim. Acta*, **79**, 1710, (1996).

[107] M.T. Reetz, G. Lohmer, R. Schwickardi, *Angew. Chem.*, **109**, 1559, (1997).

[108] M.T. Reetz, G. Lohmer, R. Schwickardi, *Angew. Chem. Int. Ed. Engl.*, **36**, 1526, (1997).

[109] P. Bhyrappa, J.K. Young, J.S. Moore, K.S. Suslick, *J. Am. Chem. Soc.*, **118**, 5708, (1996).

[110] I. Morao, F.P. Cassio, *Tetrahedron Lett.*, **38**, 6461, (1997).

[111] C.C. Mak, H. F. Chow, *Macromolecules*, **30**, 1228, (1997).

[112] H.F. Chow, C.C. Mak, *J. Org. Chem.*, **62**, 5116, (1997).

[113] K.R. Stickley, S.C. Blackstock, *J. Am. Chem. Soc.*, **116**, 11576, (1994).

[114] V. Balzani et al, *Acc. Chem. Res.*, **31**, 26, (1998).

[115] P.J. Dandliker, F. Diederich, M. Gross, C.B. Knobler, A. Louati, E.M. Sanford, *Angew. Chem. Int. Ed. Engl.*, **33**, 1739, (1994).

[116] P.J. Dandliker, F. Diederich, J.P. Gisselbrecht, A. Louati, M. Gross *Angew. Chem. Int. Ed. Engl.*, **34**, 2725, (1995).

[117] P. Weyermann, J.P. Gisselbrecht, C. Boudon, F. Diederich, M. Gross *Angew. Chem. Int. Ed. Engl.*, **38**, 3215, (1999).

[118] C.B. Gorman, B.L Parkhurst, W.Y. Su, K. Y. Chen, *J. Am. Chem. Soc*, **119**, 1141, (1997).

[119] K. Y. Chen, C.B. Gorman, *J. Org. Chem.*, **61**, 9229, (1996).

[120] K. W. Pollak, J. W. Leon, J.M.J. Fre′chet, M, Maskus, H.D Abruna, *Chem. Mater.*, **10**, 30, (1998)

[121] Cameron et al, *J.Am. Chem. Soc.*, **118**, 12925, (1996)

[122] T.D. Selby, S.C. Blackstock, *J.Am. Chem. Soc.*, **120**, 12155, (1998).

[123] T.D. Selby, K.R. Stickley, S.C. Blackstock, *Org. Lett.*, **2**, 171 (2000).

[124] M. Wells, R. M. Gooks, *J. Am. Chem. Soc.*, **16**, 3988, (1996).

[125] P.W. Wang, Y.J. Liu, C. Devadoss, P. Bharathi, J.S. Moore, *Adv. Mater*, **8**, 237, (1996).

[126] J.M. Lupton, I.D.W. Samuel, R. Beavington, P.L. Burn, H. Bassler, *Adv. Mater*, **13**, 258, (2001).

[127] M. Halim, I.D.W. Samuel, J.N.G. Pillow, P.L. Burn, *Synth. Met.*, **102**, 1113, (1999).

[128] M. Halim, J.N.G. Pillow, I.D.W. Samuel, P.L. Burn, *Adv. Mater.*, **11**, 371, (1999).

[129] J.M. Lupton, I.D.W. Samuel, R. Beavington, M.J. Frampton, P.L. Burn, H. Bassler, *Phys. Rev. B*, **63**, 155206, (2001).

[130] V. Balzani, S. Campanga, G. Denti, A. Juris, S. Serroni, M.Venturi, *Acc. Chem. Res.*, **31**, 26, (1998).

[131] F. Li, S.I. Yang, Y. Ciringh, J. Seth, C.H. Martin, D.L. Singh, D. Kim, R.R. Birge, D.F. Bocian, D. Holtan, J.S. Lindsey, *J. Am. Chem. Soc.*, **120**, 10001, (1998).

[132] J.C. Goedheer, *Biochim. Biophys. Acta.*, **172**, 252, (1969).

[133] B. Demming-Adams, *Biochim. Biophys. Acta.*, **1020**, 1,(1990).

[134] S. Campanga, G. Denti, S. Serroni, M. Ciano, A. Juris, V. Balzani, *Inorg. Chem.*, **31**, 2982, (1992).

[135] S. Serroni, A. Juris, M. Venturi, S. Campanga, I.R. Resino, G. Denti, A. Credi, V. Balzani, *J. Mater. Chem.*, **7**, 1227, (1997).

[136] E.C. Constable, P. Harverson, *Chem. Commun.*, 33-34, (1996).

[137] A.Nitzan,*Annu. Rev. Phys. Chem.* **52**, 681, (2001).

[138] M.D. Newton; N. Sutin, *Annu. Rev. Phys. Chem.* **35**, 437, (1984).

[139] M.D. Newton, *Chem. Rev.*, **91**, 767, (1991).

[140] K.D. Jordan; M.N. Paddon-Row, *Chem. Rev.* **92**, 395, (1992).

[141] S.S.Isied; M.Y. Ogawa; J.F. Wishart, *Chem. Rev.* **92**, 381, (1992).

[142] P.Chen; T.J. Meyer, *Chem. Rev.* **98**, 1439, (1998).

[143] D.N. Beratan; J.N. Betts; J.N. Onuchic; *Science* **252**, 1285, (1991).

[144] J. Jortner and M. Bixon, *Adv. Chem. Phys.*, **106**, 107,, (1999)

[145] J.Jortner; M.Bixon; T. Langenbacher; M.E. Michel-Beyerle, *Proc. Natl. Acad. Sci. USA.* **95**, 12759, (1998).

[146] S.S.Isied; A.Vassilian,*J. Am. Chem. Soc* **106**, 1726, (1984)

[147] S.S.Isied; A.Vassilian,*J. Am. Chem. Soc* **106**, 1732, (1984)

[148] G.Basu; M.Kubasik; D. Angios; B. Secor; A. Kuki, *J. Am. Chem. Soc.* **112**, 9410, (1990)

[149] S.S.Isied; G. Worosila; S.J. Artherton, *J. Am. Chem. Soc* **104**, 7659, (1982)

[150] S.L. Mayo, *Science* **233**, 948, (1986)

[151] N.Liang et al. *Proc. Natl. Acad. Sci. USA* **84**, 1249, (1987)

[152] H. Overing et al *J. Am. Chem. Soc.* **109**, 3258, (1987)

[153] M.D. Johnson; *J. Phys. Chem.* **93**, 1173, (1989)

[154] C.A.Stein; *J. Am. Chem. Soc.* **104**, 2596, (1982);

[155] M.R.Wesielewski; *Tetrahedron* **45**, 4785, (1989)

[156] C. Joachim; J.K. Gimzewski, R.R. Schlittler; C. Chavy, *Phys. Rev. Lett.* **74**, 2102, (1995)

[157] J.M. Tour; A.M. Rawlett; Masatoshi Kozaki; Y. Yao; R.C. Jagessar; S.M. Dirk; D.W. Price; M.A. Reed; C.W. Zhou; J.Chen; W. Wang; I. Campbell, *Chem. Eur. J.* **7**, (2001)

[158] J.M. Tour, *Acc. Chem. Res.* **33**, 791, (2000)

[159] M.A. Reed; J.M. Tour, *Sci. Am.* **282(6)**, 86, (2000)

[160] W.B. Davis; W.A. Svec; M.A. Ratner; M.R. Wasielewski, *Nature* **396**, 60, (1998)

[161] M. Dorogi; J. Gomez; R. Osifchin; R.P. Andres; R. Reifenberger, *Phys. Rev.B* **52**, 9071, (1995)

[162] M.A. Reed et al, *Ann.N Y Acad. Sci.* **852**, 133, (1998)

[163] M.A. Reed; C. Zhou; C.J. Miller; T.P. Burgin; J.M. Tour, *Science* **278**, 252, (1997)

[164] A. Bezryadin; C. Dekker; G. Schmid, *App. Phys. Lett.* **71**, 1273, (1997)

[165] E. Di Fabrizio, *Jpn. J. Appl. Phys* **36**, L70, (1997)

[166] M. Magoga; C. Joachim; *Phys. Rev.B* **56**, 4722, (1997)

[167] C.P. Kubiak; I.J. Henderson; S. Datta; W.Tian; M.P. Samanta, *Phys. Rev. B* **53**, 7626, (1996)

[168] M.Olson et al. *J. Phys. Chem. B* **102**, 941, (1998)

[169] S.N. Yaliraki; M. Kemp; M.A. Ratner, *J. Am. Chem. Soc.* **121**, 3428, (1999)

[170] H.Ness; A.J. Fischer, *Phys. Rev. B* **56**, 12462, (1997)

[171] G. McDermott; S.M. Prince; A.A. Freer; A.M. Hawthornth-Lawless; M.Z. Papiz; R.J. Cogdell;W.N. Isaacs, *Nature* **374**, 517, (1995)

[172] W. Kuhl Brandt; D.N Wang,*Nature* **350**, 130, (1991)

[173] A.N. Glazer,*Annu. Rev. Biophys. Biophys. Chem.* **14**, 47, (1995)

[174] M.Ed. Gratzel, *Energy Resources through photochemistry and catalysis*, Academic Press: New York 1983

[175] G.Steinberg-Yfrach; P.A.Liddell; S.C.Hung; A.L. Moore; D.Gust; T.A. Moore, *Nature* **385**, 293, (1997)

[176] M.Beggren; A. Dodabalapur; R.E. Slusher; Z.Bao,*Nature* **389**, 466, (1997)

[177] A.Nakano; A.Osuka; I.Yamazaki; T.Yamazaki; Y.Nishimura, *Angew. Chem. Int. Ed. Engl.* **37**, 3023, 1998

[178] F.Li; S.I. Yang; Y.Ciringh;J.Seth;C.H.Martin III; D.L.Singh; D.Kim;R.R.Birge; D.F. Bocian; D.Holten; S.J. Lindsey, *J. Am. Chem. Soc.* **120**, 10001, (1998)

[179] P. Belser; A. VonZelewsky; M. Frank; C. Seal; F. Vogtle; L.De Cola; F. Barigelletti; V. Balzani, *J. Am. Chem. Soc.* **115**, 4076, (1993)

[180] S.E. Webber, *Chem. Rev.* **90**, 1469, (1990)

[181] G. Jones II; A.M. Rahman, *Chem. Phys. Lett.* **200**, 241, (1992)

[182] S.M. Risser; D.N. Beratan; J.N. Onuchic, *J. Phys. Chem.* **97**, 4523, (1993)

[183] C. Devadoss; P.Bharati; J.S. Moore, *J. Am. Chem. Soc.* **118**, 9635, (1996)

[184] M.R. Shortreed; S.F. Swallen; Z.Y. Shi; W. Tan; Z. Xu; C. Devadoss; J.S. Moore; R.Kopelman, *J. Phys. Chem. B* **101**, 6318, (1997)

[185] T.Aida; D.L. Jiang, *Nature* **388**, 454, (1997)

[186] T.Aida; D.L. Jiang, *J. Am. Chem. Soc.* **120**, 10895, (1998)

[187] G.Z. Gamow, *Z. Phys.* **51**, 204, (1928)

[188] R.A. Marcus, *Rev. Mod. Phys.* **65(3)**, 599, (1993)

[189] A. Jouris,*Annu. Rep. Prog. Chem. Sect. C* **99**, 177-241, (2003)

[190] R. Sadamoto; N. Tomioka; T.Aida, *J. Am. Chem. Soc.* **118**, 3978, (1996)

[191] T.H. Ghaddar; J.F. Wishart; D.W. Thompson; J.K. Whitesell; M.A. Fox, *J. Am. Chem. Soc.* **124**, 8285, (2002)

[192] Reyes De la Vega; Pilar Prez-Tejeda; R. Prado-Gotor; P. Lpez-Cornejo; R. Jimnez; Francisco Prez and Francisco Snchez, *Chem. Phys. Lett* **398**, 82, (2004)

[193] M.Halim; N.G. Pillow; I.D.W. Samuel; P.L. Burn, *Adv. Mater* **11**, 371, (1999)

[194] J.M. Lupton; I.D.W. Samuel; M.J. Frampton; R. Beavington; P.L. Burn, *Adv. Funct. Mater.* **11**, 287, (2001)

[195] J.A.Barron; S.Bernhard; P.L. Houston; H.D. Abruna, J.L Ruglovsky; G.G. Milliaras, *J. Phys. Chem. A* **107**, 8130, (2003)

[196] S. Glazier; J.A. Barron; N. Morales; A.M. Ruschak, P.L. Houston; H.D. Abruna, *Macromolecules* **36**, 1272, (2003)

[197] M.Y.Ogawa; I. Moreira; J.F. Wishart; S.S.Isied, *J. Phys. Chem.* **97**, 11456, (1993)

[198] R.Abdel Malak; Z. Gao; J.F. Wishart; S.S. Isied, *J. Am. Chem. Soc.* **126**, 13888, (2004)

[199] A.K.Felt; W.T. Pollard; R.A. Friesner, *J. Phys. Chem.* **99**, 2929, (1995)

[200] M.A. Ratner, *Nature* **397**, 480, (1999)

[201] H.M. McConnell, *J. Chem. Phys.* **35**, 308, (1961)

[202] J.R. Miller; J.V. Beitz, *J. Chem. Phys.* **74**, 6746, (1981)

[203] M.A. Ratner, *J. Phys. Chem.* **94**, 4877, (1990)

[204] K.V. Mikkelsen; M.A. Ratner, *Chem. Rev.* **87**, 113, (1987)

[205] G.L.Closs; J.R. Miller, *Science* **240**, 440, (1988)

[206] H.M. Chou; C. Creutz; N.Sutin, *Inorg. Chem.* **11**, 2318, (1992)

[207] D.N. Beratan, J.N. Onuchic; J.J. Hopefield, *J. Chem. Phys.* **86**, 4488, (1987)

[208] D.Segal; A.Nitzan; W.B. Davis; M.R. Wasielewski; M.A. Ratner, *J. Phys. Chem. B* **104**, 3817, (2000)

[209] A.Okada; V.Chernyak; S.Mukamel, *J. Phys. Chem. A* **102**, 1241, (1998)

[210] U. Fano, *Rev. Mod. Phys.* **29**, 74, (1957)

[211] K.Blum, *Density matrix theory and application*; Plenum Press; New York, (1981)

[212] A.Nizan, *Chem.Phys.* **41**, 163, (1979)

[213] W.T. Pollard; R.A. Friesner, *J. Chem. Phys.* **100**, 5054, (1994)

[214] D.Egorova; A.Kuhl; W.Domcke, *Chem. Phys.* **268**, 105, (2001)

[215] E.G.Petrov; Y.V.Schevchenko; V.T. Teslenko, *J. Chem. Phys.* **115**, 7107, (2001)

[216] D.Segal; A.Nitzan, *Chem. Phys.* **268**, 315, (2001)

[217] D.Segal; A.Nitzan, *Chem. Phys.* **281**, 235, (2002)

[218] D. Rana; G. Gangopadhyay, *in preparation.*

[219] A.Bar Haim; J.Klafter; R.Kopelman, *J. Am. Chem. Soc* **119**, 6197, (1997)

[220] A.Bar Haim; J.Klafter, *J.Lumin.* **77**,197,(1998), *J. Phys. Chem. B*, **102**, 1662, (1998)

[221] A.Bar Haim; J.Klafter, *J. Chem. Phys* **109**, 5187, (1998)

[222] D. Rana; G. Gangopadhyay, *in preparation.*

[223] S. Tretiak; V. Chernyak; S. Mukamel, *J. Phys. Chem. B* **102**, 3310, (1998)

[224] O. Varnavski; I.D.W. Samuel; L.O. Palsson; R. Beavington; P.L.Burn;T.Goodson III, *J. Chem. Phys.* **116**, 8893, (2002)

[225] O.P.Varnavski; J.C. Ostrowski; L.Sukhomlinova;R.T. Twieg; G.C.Bazan; T.GoodsonIII, *J. Am. Chem. Soc.* **124**, 1736, (2002)

[226] M.I. Ranasinghe; O.P.Varnavski; J. Pawlas; S.I. Hank;J.Louie; J.F. Hartwig; T.GoodsonIII, *J. Am. Chem. Soc.* **124**, 6520, (2002)

[227] M.I.Ranasinghe; Y.Wang; T.GoodsonIII; *J. Am. Chem. Soc.* **125**, 5258, (2003)

[228] D.A. Weitz; S.Garoff et al., *J. Chem. Phys.* **78**, 5324, (1983)

[229] W.B. Davis; M.R.Waseielewski; M.A.Ratner; V.Mujica; A.Nitzan, *J. Phys. Chem. A* **101**, 6158, (1997)

[230] H.A. Kramers, *Physica*(Amsterdam) **4**, 284, (1940)

[231] Samantha Glazier; B.A.Jasson; P.L.Huston; H.D.Abruna, *J. Phys. Chem. B* **106**, 9993, (2002)

[232] *Molecular Switches* (Ed: B.L. Feringa), Wiley-VCH , Weinheim, (2001)

[233] B.W. Shore, *Theory of Coherent Atomic Excitation*, Wiley,(New York, 1990)